DEPARTMENT OF PHYSICS
UNIVERSITY OF JYVÄSKYLÄ
RESEARCH REPORT No. 6/2016

TIME-DEPENDENT QUANTUM TRANSPORT IN NANOSYSTEMS: A NONEQUILIBRIUM GREEN'S FUNCTION APPROACH

BY
RIKU TUOVINEN

Academic Dissertation
for the Degree of
Doctor of Philosophy

To be presented, by permission of the
Faculty of Mathematics and Natural Sciences
of the University of Jyväskylä,
for public examination in Auditorium YAA303 of the
University of Jyväskylä on June 8th, 2016
at 12 o'clock noon

Jyväskylä, Finland
June 2016

ISBN 978-951-39-6593-8 (paper copy)
ISBN 978-951-39-6594-5 (pdf)
ISSN 0075-465X

Author Riku Tuovinen
Department of Physics
Nanoscience Center
University of Jyväskylä
Finland

Supervisor Prof. Robert van Leeuwen
Department of Physics
Nanoscience Center
University of Jyväskylä
Finland

Reviewers Prof. Esa Räsänen
Department of Physics
Tampere University of Technology
Finland

Prof. Lev Kantorovich
Department of Physics
King's College London
United Kingdom

Opponent Prof. Liliana Arrachea
Department of Physics
University of Buenos Aires
Argentina

Preface

This thesis work has been carried out at the Department of Physics and at the Nanoscience Center of the University of Jyväskylä during the years 2011–2016.

I would like to express my deep gratitude for the guidance from my advisor, Prof. Robert van Leeuwen, and for the opportunity to work in his research group starting already on my undergraduate projects. Further thanks for directing me towards this field of research and for the opportunity to work first as an undergraduate and then as a doctoral student go to the departmental and administrative staff. In addition, *many* people deserve credit for giving me the opportunity to take part in teaching and in the development of teaching methods in our department.

In the scientific work, further thanks go to Dr. Adrian Stan and Dr. Petri Myöhänen for introducing me to the research topics and methods in practice. For the overall conversational working atmosphere and daily discussions about studies, research, teaching and whatnot I wish to thank Doc. Pekka Koskinen, Prof. Tero Heikkilä, Dr. Francesco Massel (and their research groups), Dr. Anna-Maija Uimonen, Dr. Daniel Karlsson, Dr. Janne Nevalaita, Dr. Lauri Lehtovaara, Dr. Rosalba Juarez, Mr. Niko Säkkinen, Mr. Topi Korhonen, Mr. Ilkka Mäkinen, Mr. Markku Hyrkäs, Mr. Luis Cort and Mr. Richard Lynn. For programming and computer support in general I am indebted to Dr. Vesa Apaja.

For very fruitful scientific collaborations and for sharing their vast wisdom I am grateful to Dr. Gianluca Stefanucci and Dr. Enrico Perfetto from the University of Rome Tor Vergata and to Dr. Claudia Gomes da Rocha from the Trinity College Dublin.

I also wish to thank Prof. Esa Räsänen and Prof. Lev Kantorovich for thoroughly pre-examining the original manuscript and for providing me with useful comments. I am further grateful to Prof. Liliana Arrachea and I feel humbly honoured to have her as an opponent.

Financial support from the Ellen and Artturi Nyyssönen Foundation and the Vilho, Yrjö and Kalle Väisälä Foundation are gratefully acknowledged.

Perhe ja läheiset ansaitsevat kuitenkin suurimmat kiitokset. Vanhemmilleni olen kiitollinen rohkaisusta ja kannustuksesta opiskeluun sekä eväistä maailman monien ihmeellisten asioiden hämmästelyyn ja kummasteluun; appivanhemmille kiitos tuesta ja avusta niin arjessa kuin vapaallakin. Veeralle erityiskiitos rakkaudesta, ymmärryksestä ja kärsivällisyydestä – varsinkin tämän kirjan kirjoittamisen aikana.

Jyväskylä, June 2016

Riku Tuovinen

Abstract

A time-dependent extension to the Landauer–Büttiker approach to study transient quantum transport in arbitrary junctions composed of leads and conducting devices is developed. The nonequilibrium Green's function approach is employed for describing the charge and heat transport dynamics. The importance of the developed method is that it provides a closed formula for the time-dependent density matrix in both electronic and phononic systems. In the electronic case the nonequilibrium conditions are due to a switch-on of a bias voltage in the leads or a perturbation in the junction whereas in the phononic case the central region of interest is coupled to reservoirs of different temperatures. In both cases the time-dependent density matrices, and furthermore other transport properties such as local charge and heat currents, may be evaluated without the necessity of propagating individual single-particle orbitals or Green's functions

More precisely, an analytic solution to the Kadanoff–Baym equations of motion for both electronic and phononic Green's functions describing an arbitrarily shaped and sized noninteracting lattice connected to an arbitrary number of noninteracting wide-band terminals, also of arbitrary shape and size, is provided. In the electronic case, the initial equilibrium state is properly described by the addition of an imaginary track to the Keldysh time contour, on which the equation of motion is described. From the solution the time-dependent electron and phonon densities and currents within the junction are extracted. The final results are analytic expressions as a function of time, and therefore no time propagation is needed – either in transient or in steady-state regimes.

As the formalism allows for studying time-dependent transport in noninteracting but arbitrary molecular systems coupled to wide band leads, several applications are presented and discussed. Especially, transient charge dynamics in graphene nanoribbons of different geometries is studied. The transient time scales are found to exceed several hundreds of femtoseconds while displaying a long time oscillatory motion related to multiple reflections of the density wave in the nanoribbons at the ribbon–lead interface. This finding strongly vouches for the need for a fully time-dependent description of the quantum transport processes. The time-dependent current through a graphene nanoribbon has a shape that scales with the length of the ribbon and is modulated by fast oscillations described by intra-ribbon and ribbon–lead transitions. Furthermore, time-dependent quantum transport is studied in curved graphene nanoribbons. The curvature is found to trigger temporally and spatially focused electric currents which might prove pivotal for a robust design of graphene sensors and circuitries. Further simulations in a superconducting benzene-like molecule attached to normal metal leads show formation of Cooper pairs within the molecule related to Andreev reflection processes. In addition, transient heat transport in atomic chains is studied where the transient oscillations are found to be related to the transitions between the chain's vibrational modes.

List of Publications

[I] R. Tuovinen, R. van Leeuwen, E. Perfetto, and G. Stefanucci, "Time-dependent Landauer–Büttiker formula for transient dynamics", J. Phys.: Conf. Ser. **427**, 012014 (2013).

[II] R. Tuovinen, E. Perfetto, G. Stefanucci, and R. van Leeuwen, "Time-dependent Landauer–Büttiker formula: Application to transient dynamics in graphene nanoribbons", Phys. Rev. B **89**, 085131 (2014).

[III] C. G. Rocha, R. Tuovinen, R. van Leeuwen, and P. Koskinen, "Curvature in graphene nanoribbons generates temporally and spatially focused electric currents", Nanoscale **7**, 8627 (2015).

[IV] R. Tuovinen, R. van Leeuwen, E. Perfetto, and G. Stefanucci, "Time-dependent Landauer–Büttiker formalism for superconducting junctions at arbitrary temperatures", J. Phys.: Conf. Ser. **696**, 012016 (2016).

[V] R. Tuovinen, N. Säkkinen, D. Karlsson, G. Stefanucci, and R. van Leeuwen, "Phononic heat transport in the transient regime: An analytic solution", Phys. Rev. B, *accepted* (2016), arXiv:1604.02298.

The author has been in a significant role in developing the new theoretical framework in Publications [I, II, IV, V], and in writing these publications. The author has written from scratch the numerical programs and done all the numerical calculations presented in Publications [I, II, IV]. The same programs were also used in some of the numerical calculations presented in Publications [III, V], and the author also participated in writing and performing computations in Publication [III].

Contents

1 Introduction

1.1 Quantum transport and nanoscale electronics

Roughly speaking we can divide a field in physics in two parts: statics and dynamics. Statics, as the Greek word suggests, is concerned with balance and equilibrium of objects. Dynamics, on the other hand, deals with something that is changing in time. We might further separate kinematics from dynamics as a mere mathematical description of motion and leave the cause and the laws of motion under dynamics. In *quantum transport* the key element typically is to describe the dynamics of charge in a studied structure. Charge is a quantity related to electrons so let us start with electronic transport by asking: What is it that the electrons do in a circuit? As already realized, we could put this in a simple way and say that they have an internal property called charge and they move.

Atoms, as the building blocks of materials, contain electrons in a cloud-like shape around the nucleus. This cloud is a collection of electrons trapped in the atomic orbitals whose number and the overall structure depends on the element we are dealing with. Typically it takes a considerable amount of energy for the electrons to escape from their orbitals, especially when the orbital in question is close to the nucleus. Some elements are identified as metals, for which the outer layers of the atomic orbitals are not attached to the nucleus so strongly, and it is possible for individual electrons to move from one atom's outer orbital to another atom's outer orbital. When we have a collection of metal atoms composing a material the outer orbitals behave as a sea of mobile electrons. Just like in regular water, this electron sea can have currents. The difference in gravitational potential causes water to flow in a river whereas electrical potential causes electrons to flow in a metal. This electrical potential could be caused by a battery, setting higher voltage to some part of the metal and lower voltage to another part. If we form a circuit with potential differences as a closed path in the electron sea, we have a continuous current. It is, however, important to notice that applying a voltage on a metal structure, only the electrons in the outmost orbitals are affected since the electrons in orbitals closer to the nucleus would require rather assertive batteries to break them free.

As discussed above, the outer layers are the ones important for electric circuitries, and there also most of the chemistry happens. If neighbouring metal atoms share their outmost orbitals so that there are no vacancies but the electrons completely

occupy the orbitals evenly, the metal is called an *insulator* as there is no possibility for the electrons to move about. Some materials, on the other hand, have free electrons and free space in their outmost orbitals which means the electrons can be moved with very small voltages (fractions of volts), and these materials are called *conductors*. These materials can also be engineered as devices of intermediate forms or combinations of insulators and conductors (called *semi-conductors*) where external forces (e.g., electro-magnetic fields) may be used to move or trap electrons into a particular configuration. This movement may further generate electro-magnetic fields or heat which may, in turn, affect the flow of electrons even more.

One milestone in the development of *molecular electronics*, which studies molecular building blocks as electronic components, was put forward by Aviram and Ratner in 1974 when they proposed a molecular rectifier as a single organic molecule functioning as a one-way conductor of electric current [6]. After this idea and from then onward, experiments have been designed to measure transport properties, like the conductance, in molecular scale [7–9]. Furthermore, based on the measurement of the transmission of electrons through an atomic contact many diagnostic and spectroscopical tools have been developed, e.g., scanning tunneling microscope [10] by Binnig and Rohrer for which they received the Nobel prize in 1986 [11], atomic force microscope [12], point-contact spectroscopy [13], inelastic electron tunneling spectroscopy [14] and resonant inelastic tunneling spectroscopy [15].

However, starting already from the discovery of the transistor in 1948 by Shockley, Bardeen and Brattain (for which they received the Nobel prize in 1956 [16]), the field of electronics was slowly but surely converging towards the atomic scale as the building blocks kept getting smaller and smaller, also famously predicted by Moore in 1965 [17]. Vacuum tubes [18] and diodes [19] were soon after the second world war replaced by transistors, which in turn were soon composed into integrated circuits [20] leading to the early stages of microprocessors [21–24] which we now carry around us in our everyday devices, see Fig. 1.1.

From this development we notice two approaches towards roughly the same destination.

i. The technological approach, ultimately leading to a present day hot topic of nanotechnology [26–28], pushes the existing ideas and technology to their limits towards smaller scale.

To include a few examples, molecular wires, two- and three-terminal transistor-like devices including molecule-electrode contacts and local heating are discussed in Ref. [29] reviewing experimental progress over the past decade. Also, graphene and carbon nanotube based transistors' performance has recently been analyzed thoroughly [30, 31].

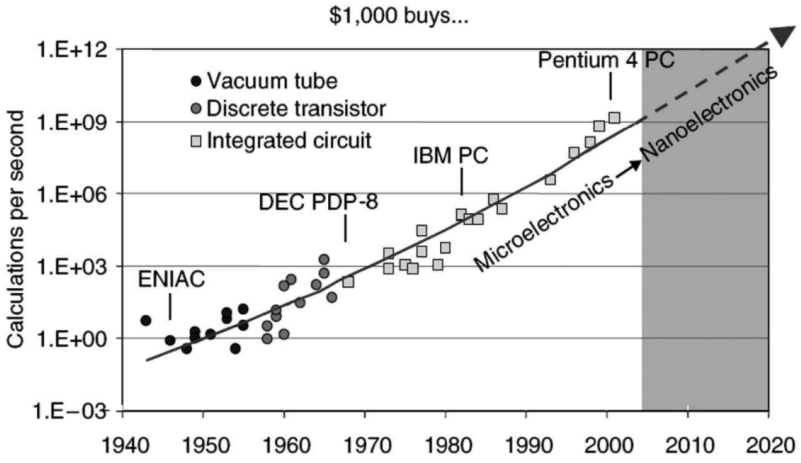

Fig. 1.1: Development of electronic components. Picture from Ref. [25].

ii. The fundamental science approach constructs new ideas from known basic principles of nature ultimately leading to a concrete realization of technological importance.

To include few examples also on the theoretical advances, density-functional theory [32–34], nonequilibrium Green's functions [35–42], density-matrix renormalization group [43, 44], dynamical mean field theory [45–47] and quantum Monte Carlo [48, 49] are amongst the most commonly studied and used methods.

This thesis concentrates on the latter approach: New theoretical methods, particularly in the field of nonequilibrium Green's functions, are studied in order to shed light on various nanoscale and molecular electronics phenomena such as charge and heat transport in a molecular junction.

The quantum transport problems are typically time dependent; there is no guarantee that the system would in an instant relax to a steady-state configuration once the junction is "switched on" (as in connecting different devices or driving them out of equilibrium by an external perturbation). In contrast, there are transient effects depending on, e.g., the system's geometry [50–53], its predisposition to external perturbations [54–57], the physical properties of the transported quanta and their mutual interactions [58–63]. In future applications these nanoscale devices are pursued to operate at very fast switching time scales meaning how fast the device can be switched on and off. This essentially relates to, e.g., microprocessors' operation times and efficiencies to perform floating-point arithmetic operations. If the quantum transport problem was completely solved, we would have specific information about the electron density regarding the studied structure, as in how many electrons there are in a particular configuration within the structure at certain moment in time and, more importantly, how we could control this. This outcome

in determining materials' electronic properties is a key point in modern electronics and nanotechnology, and a logically and consistently formulated theory gives a basis for the development of technological applications. Even though the technological applications are an integral part of science and they steer the ways of research, even more important is the underlying understanding of nature. Without basic understanding of the fundamental mechanisms that dictate, e.g., the electrical conduction in a molecular junction, there is no application.

This discussion, interestingly, is not limited to charge transport and electrons only but there are other possibilities for quantum transport as well. Oscillations and vibrations in a solid stemming from thermal energy may be regarded as mechanical waves or *phonons* traversing along the solid in question. In principle, the transport of phonons relates to heat transfer in a studied structure [64–66]. Also, very recently there have been efforts in manufacturing photonic circuits where the information flow would be handled as photon transport [67]. In addition, in the field of cosmology the fundamental question of asymmetry between the matter and antimatter content in the universe is remotely related to quantum transport. The standard model in cosmology [68] incorporates *inflation* – an early period of very fast expansion of the universe; the dynamical mechanism responsible for creating baryons after inflation is not known but the description of this *baryogenesis* involves setting up transport equations for relativistic quantum systems in out-of-equilibrium conditions [69, 70].

1.2 Quantum physics of many particles

Just like in the field of classical physics, also in quantum physics there are *rules*, cf. Newton's laws of motion. The rules are, however, invented by us, humans, and they should agree with our experience of nature. Naturally, this sets a limitation on how nature can be perceived by us or by the apparatus we build. The rules of quantum physics are typically called *postulates* as they are not something that can be deduced from the knowledge in classical physics. The postulates of quantum physics are stated in almost every textbook on the field (see e.g. [71]); the exact form of the statements is not important here. However, most importantly, once the set of rules is given, the consequences are to be calculated and then compared with experiments. If the calculations do not agree with the experiment, then the underlying set of rules is wrong. (This, of course, applies to any field of science.) The last step is the most important one since the postulates are not similar to, e.g., axioms in mathematics; the postulates can only be justified by comparison with the theory they lead to and our experience of nature.

One of the postulates discussed above is about the time-evolution of a system de-

scribed by a state vector $|\Psi(t)\rangle$ at time t. This is given by the *Schrödinger equation* [72–74] (we use $\hbar = 1$ unless stated otherwise)

$$\mathrm{i}\frac{\mathrm{d}}{\mathrm{d}t}|\Psi(t)\rangle = \hat{H}(t)|\Psi(t)\rangle, \tag{1.1}$$

where the Hamiltonian, which can be time-dependent, $\hat{H} = \hat{T} + \hat{U}$ represents the total energy (kinetic + potential) of the system. This is a first-order linear differential equation which can be solved uniquely with an initial condition $|\Psi(t = 0)\rangle$. Equation (1.1) tells us that the dynamics of the system is completely determined by the Hamiltonian. The actual (physical) properties of the system are encoded into the state vector $|\Psi\rangle$. More explicitly, this is an element of a complex Hilbert space $\mathcal{H}$, and it gives a mathematical representation of the state of the system. (In fact, this is another postulate.) When expressed in a specific basis, this object is also related to *the wave function* or *the probability amplitude* which further relates to the probability of finding the system in a physical state represented by the state vector.

In general, the state vector $|\Psi\rangle$ might include a huge amount of information. When studying systems of atoms, molecules and solids we are typically dealing with electron configurations ranging from $N = 1$ particle to 1 mole of particles ($N \sim 10^{23}$ particles). (This is not limited to electrons only.) The state vectors, or further, wave functions, $\Psi(x_1, x_2, \ldots, x_N, t)$, might include an enormous number of variables for each spatial coordinate of each particle, for instance. In principle, we know the rules that describe the dynamical evolution of the system of interest; we only need to solve the Schrödinger equation (1.1). In practice, however, this is not possible since the number of equations to be solved, even numerically by using highly efficient supercomputers, is simply out of reach. There is, however, a way around this which does not solve the actual problem but helps us in dealing with it. In this field of many-particle quantum physics, a very important observation is that rather many interesting properties of many-particle systems that are observed in experiments involve observables related to only a few particles such as densities and currents. Then, to evaluate these quantities from the underlying theory to be compared with experiments might be possible in terms of a *reduced quantity*. This means, that we do not need the full and complicated state vector or wave function for every particle of the system but we might be able to theoretically describe an observable and predict its properties by looking at less complicated quantities.

The use of reduced quantities is the key in the theory of nonequilibrium Green's functions (NEGF) and in density-functional theory (DFT). In the Green's function approach the state of the system is described in terms of NEGFs, $G(x, t; x', t')$, depending only on two spatial and time coordinates (spin may also be included in the spatial coordinate). We will consider these in more detail in the next Chapter but it should be noted that the time-coordinates t, t' lie on the contour in Fig. 1.2. In DFT the state of the system is described in terms of densities, $n(x, t) =$

$N \int \mathrm{d}x_2 \cdots \int \mathrm{d}x_N |\Psi(x, x_2, \ldots, x_N, t)|^2$, where the remaining (unimportant) coordinates have been integrated out. In fact, the densities and Green's functions are related by $n(x,t) = \pm \mathrm{i} G^<(x,t;x,t)$ ('$<$' denotes the lesser Green's function) where the sign is + for bosons and − for fermions [73]. Even if we discuss the properties of the system in terms of a reduced quantity, such as the NEGF, we should still follow the underlying set of rules. The description therefore is to be completely equivalent to the Schrödinger equation although the dynamical equations of motion might take modified forms, e.g., Kadanoff–Baym equations [38, 73, 75] (the spatial and spin coordinates are suppressed for clarity)

$$[\mathrm{i}\partial_t - \hat{h}(t)]G(t,t') = \delta(t,t') + \int_\gamma \mathrm{d}\bar{t}\Sigma(t,\bar{t})G(\bar{t},t'). \tag{1.2}$$

Instead of the form of a differential equation in Eq. (1.1) for a function $|\Psi(t)\rangle$ of one time variable, in Eq. (1.2) we have an integro–differential equation for a function of two time variables $G(t,t')$. Also, in contrast to the Schrödinger equation, in Eq. (1.2) the Hamiltonian is split so that $\hat{h}$ represents the noninteracting part and the interactions are encoded in the integral kernel or the self-energy Σ on the right-hand side. The self-energy may be thought of as an effective medium (in macroscale) or as a scattering potential (in microscale). Including or excluding particular types of interactions can then be done by approximating this object Σ. In addition, the integrals are performed on a contour γ in a complex time plane, the Keldysh contour [39, 73], see Fig. 1.2. The addition of a complex-time track to the contour is a trick to include equilibrium weight, i.e., initial correlations to the evolution of the Green's function. In DFT, and in time-dependent DFT (TDDFT), the dynamical

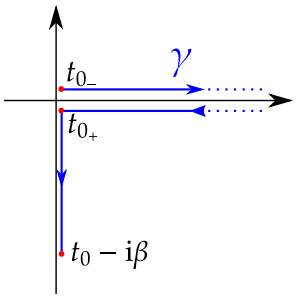

Fig. 1.2: Keldysh contour on the complex time plane has a forward (−) and a backward branch (+) on the real-time axis, $[t_0, \infty[$ and a vertical branch on the imaginary axis, $[t_0, t_0 - \mathrm{i}\beta]$ with inverse temperature β. (The contour is slightly shifted from the axes for clarity.)

equations of motion for the system are given by the Kohn–Sham equations [33, 34, 76]

$$[\hat{T} + \hat{v}_{\mathrm{KS}}(t)]\varphi_j(t) = \mathrm{i}\frac{\mathrm{d}\varphi_j(t)}{\mathrm{d}t}, \tag{1.3}$$

where $\hat{T}$ is the kinetic part of the Hamiltonian, $\varphi_j(t)$ are the (time-dependent) Kohn–Sham orbitals, from which the density is obtained as $n(t) = \sum_{j\in\mathrm{occ}} |\varphi_j(t)|^2$, and $\hat{v}_{\mathrm{KS}}[n(t),t] = \hat{v}_{\mathrm{ext}}(t) + \hat{v}_{\mathrm{H}}[n(t)] + \hat{v}_{\mathrm{xc}}[n(t)]$ is the Kohn–Sham potential composed of the external potential, Hartree potential and the exchange–correlation potential which, in principle, are functionals of the above density. The interacting part of the Hamiltonian, $\hat{U}$, enters the Hartree potential and the exchange–correlation potential in a way similar to the self-energy in the Kadanoff–Baym equation (1.2). In fact, between these objects (typically to be approximated in a practical calculation) there is a connection [77].

The original simplicity and the intuition in the Schrödinger equation for a state vector $|\Psi\rangle$ is unfortunately gone by introducing the Green's functions or the density functionals as the description of the dynamics of the system becomes highly complicated. However, this is the price to pay in order to perform calculations in practice.

1.3 Lattice models for electronic transport studies

In order to model particle transport in a structure of interest we need to construct a quantum description for the movement of the particles in every point of the structure, as in a lattice.

A (many-particle) Hamiltonian representing N particles with coordinates $\boldsymbol{x}_j$, momenta $\boldsymbol{p}_j$ and masses m_j in a potential V, which in general may be time-dependent, is written (in first quantization) as

$$\hat{H}(t) = \sum_{j=1}^{N}\left[\frac{\hat{\boldsymbol{p}}_j^2}{2m_j} + \hat{V}(\boldsymbol{x}_j,t)\right] + \sum_{j<k}\hat{W}(\boldsymbol{x}_j,\boldsymbol{x}_k) =: \sum_{j=1}^{N}\hat{h}(\boldsymbol{x}_j,t) + \sum_{j<k}\hat{W}(\boldsymbol{x}_j,\boldsymbol{x}_k), \tag{1.4}$$

where the inter-particle interactions are given by the function W whose strength typically depends on the distance $|\boldsymbol{x}_j - \boldsymbol{x}_k|$, like in the Coulomb potential. A (many-particle) wave function $\Psi_j(\boldsymbol{x}_1,\ldots,\boldsymbol{x}_N,t)$ satisfies the time-independent Schrödinger equation, $\hat{H}\Psi_j = E_j\Psi_j$, returning the energy E_j corresponding to the j-th eigenstate of the time-independent Hamiltonian. On the other hand, if the Hamiltonian is time-dependent, e.g. consisting of a perturbation $V(t)$, then the dynamics of a many-particle state is given by the time-dependent Schrödinger equation, $\mathrm{i}\partial_t\Psi(t) = \hat{H}(t)\Psi(t)$, with an initial condition arising from the time-independent problem. In addition, the many-particle wave function obeys *the spin–statistics theorem* [78] stating that when interchanging two particles the wave function is either symmetric (bosons) or antisymmetric (fermions), $\Psi(\boldsymbol{x}_1,\ldots,\boldsymbol{x}_j,\ldots,\boldsymbol{x}_k,\ldots,\boldsymbol{x}_N) = \pm\Psi(\boldsymbol{x}_1,\ldots,\boldsymbol{x}_k,\ldots,\boldsymbol{x}_j,\ldots,\boldsymbol{x}_N)$. In this context we consider fermions only.

Instead of quantizing the particles' coordinates and momenta it is often advantageous to quantize the wave function itself. Let us then introduce electronic field operators $\hat{\Psi}^{(\dagger)}(\boldsymbol{x})$ which, when acting to an N-particle state vector $|\boldsymbol{x}_1,\ldots,\boldsymbol{x}_N\rangle$, remove (create) an electron from (to) coordinate $\boldsymbol{x}$. (It is possible to include also a spin degree of freedom by denoting $\boldsymbol{x}=(\boldsymbol{r},\sigma)$.) More explicitly,

$$\hat{\Psi}^\dagger(\boldsymbol{x})|\boldsymbol{x}_1,\ldots,\boldsymbol{x}_N\rangle = |\boldsymbol{x}_1,\ldots,\boldsymbol{x}_N,\boldsymbol{x}\rangle, \tag{1.5}$$

$$\hat{\Psi}(\boldsymbol{x})|\boldsymbol{x}_1,\ldots,\boldsymbol{x}_N\rangle = \sum_{k=1}^{N}(-1)^{N-k}\delta(\boldsymbol{x}-\boldsymbol{x}_k)|\boldsymbol{x}_1,\ldots,\boldsymbol{x}_{k-1},\boldsymbol{x}_{k+1},\ldots,\boldsymbol{x}_N\rangle. \tag{1.6}$$

The structure in the latter equation is a little more involved because it has to take into account all the possibilities on how one of the particles (from 1 to N) could be removed from coordinate $\boldsymbol{x}$. Creating and removing particles by the field operators means that any N-particle state may be constructed by consecutively acting with a creation operator to the vacuum state: $|\boldsymbol{x}_1,\ldots,\boldsymbol{x}_N\rangle = \hat{\Psi}^\dagger(\boldsymbol{x}_N)\cdots\hat{\Psi}^\dagger(\boldsymbol{x}_1)|0\rangle$. On the other hand, trying to remove a particle from the vacuum state yields a null state (zero) $\hat{\Psi}(\boldsymbol{x})|0\rangle = |\emptyset\rangle$. It can, further, be shown [73] that the proper (anti)symmetrization of the N-particle wave function is encoded in the field operators as anticommutation relations

$$\left\{\hat{\Psi}^{(\dagger)}(\boldsymbol{x}),\hat{\Psi}^{(\dagger)}(\boldsymbol{x}')\right\}=0\,,\quad \left\{\hat{\Psi}(\boldsymbol{x}),\hat{\Psi}^\dagger(\boldsymbol{x}')\right\}=\delta(\boldsymbol{x}-\boldsymbol{x}'). \tag{1.7}$$

Using the field operators the N-particle Hamiltonian may then be written (in second quantization) as [73]

$$\hat{H}(t)=\int \mathrm{d}\boldsymbol{x}\hat{\Psi}^\dagger(\boldsymbol{x})\hat{h}(\boldsymbol{x},t)\hat{\Psi}(\boldsymbol{x})+\frac{1}{2}\iint \mathrm{d}\boldsymbol{x}\mathrm{d}\boldsymbol{x}'\hat{\Psi}^\dagger(\boldsymbol{x})\hat{\Psi}^\dagger(\boldsymbol{x}')\hat{W}(\boldsymbol{x},\boldsymbol{x}')\hat{\Psi}(\boldsymbol{x}')\hat{\Psi}(\boldsymbol{x}). \tag{1.8}$$

The next question is: What is a suitable basis for expanding the field operators, and therefore, expressing the many-particle Hamiltonian in Eq. (1.8)? Here we may be very general and choose a one-particle state $|j\sigma'\rangle$ labelling both an orbital index j and a spin orientation σ' along a chosen axis (e.g., the z-direction). We may express this in the position-spin space, $|\boldsymbol{x}\rangle=|\boldsymbol{r}\sigma\rangle$, as a projection $\langle\boldsymbol{r}\sigma|j\sigma'\rangle =: \varphi_{j\sigma'}(\boldsymbol{x})=\varphi_j(\boldsymbol{r})\delta_{\sigma\sigma'}$. Since $\int \mathrm{d}\boldsymbol{x}|\boldsymbol{x}\rangle\langle\boldsymbol{x}|=\hat{\mathbb{1}}$, this relates to the one-particle state $|j\sigma'\rangle$ being created by acting on the vacuum state with a creation operator

$$\hat{d}^\dagger_{j\sigma'} := \int \mathrm{d}\boldsymbol{x}\varphi_{j\sigma'}(\boldsymbol{x})\hat{\Psi}^\dagger(\boldsymbol{x}). \tag{1.9}$$

A similar description applies to the annihilation operator

$$\hat{d}_{j\sigma'} := \int \mathrm{d}\boldsymbol{x}\varphi^*_{j\sigma'}(\boldsymbol{x})\hat{\Psi}(\boldsymbol{x}). \tag{1.10}$$

Now, if the set of the one-particle states, $\{|j\sigma'\rangle\}$, forms an orthonormal basis, we may expand the field operators in this basis by

$$\hat{\Psi}^{(\dagger)}(\boldsymbol{x}) = \sum_{j\sigma'} \varphi^{(*)}_{j\sigma'}(\boldsymbol{x})\hat{d}^{(\dagger)}_{j\sigma'}. \tag{1.11}$$

In practical calculations the basis functions φ are related to the (physical) properties of the studied system. One popular model description, by Pariser, Parr and Pople [79, 80], considers each atomic site j in a lattice being described by one localized orbital, and these orbitals are assumed to be almost perfectly localized, i.e., that the overlap integral is [73]

$$\int \mathrm{d}\boldsymbol{x}\varphi^*_{j\sigma'}(\boldsymbol{x})\varphi_{k\sigma'}(\boldsymbol{x}) = \begin{cases} 1 & \text{when } j = k, \\ \delta & \text{when } j,k \text{ nearest neighbours.} \end{cases} \tag{1.12}$$

However, when the overlap between neighbouring sites is nonzero, the orbitals do not form an orthonormal basis. It is still possible to construct one by expanding in small δ

$$\Phi_{j\sigma'}(\boldsymbol{x}) \coloneqq \varphi_{j\sigma'}(\boldsymbol{x}) - \frac{\delta}{2}\varphi_{(j+1)\sigma'}(\boldsymbol{x}) - \frac{\delta}{2}\varphi_{(j-1)\sigma'}(\boldsymbol{x}), \tag{1.13}$$

and use this finite basis to expand the field operators. As the field operators would in this case be expressed in terms of the localized orbitals, the corresponding operators $\hat{d}^{(\dagger)}_{j\sigma'}$ remove (create) an electron from (at) the atomic site j with spin orientation σ'.

Inserting the field operators from Eq. (1.11) into Eq. (1.8) leads to a representation for the Hamiltonian

$$\hat{H}(t) = \sum_{jk,\sigma} T_{jk}(t)\hat{d}^\dagger_{j\sigma}\hat{d}_{k\sigma} + \frac{1}{2}\sum_{jklm,\sigma\sigma'} U_{jklm}\hat{d}^\dagger_{j\sigma}\hat{d}^\dagger_{k\sigma'}\hat{d}_{l\sigma'}\hat{d}_{m\sigma}\ , \tag{1.14}$$

where we defined *the hopping and Coulomb integrals*

$$T_{jk}(t) = \int \mathrm{d}\boldsymbol{r}\varphi^*_j(\boldsymbol{r})\hat{h}(\boldsymbol{r},t)\varphi_k(\boldsymbol{r}), \tag{1.15}$$

$$U_{jklm} = \iint \mathrm{d}\boldsymbol{r}\mathrm{d}\boldsymbol{r}'\varphi^*_j(\boldsymbol{r})\varphi^*_k(\boldsymbol{r}')\hat{W}(\boldsymbol{r},\boldsymbol{r}')\varphi_l(\boldsymbol{r}')\varphi_m(\boldsymbol{r}). \tag{1.16}$$

Even though U is called the Coulomb integral, any type of interaction, say Yukawa, is possible to include as a different form for the function W. Also, in the hopping integral, technically only the off-diagonal terms ($j \neq k$) may be regarded as *hoppings*. In principle, these integrals need to be evaluated in order to accurately model a realistic system by the Hamiltonian in Eq. (1.14) but it is also possible to regard them as parameters. By choosing a proper parameter set, the full Hamiltonian

matrix with the hopping and interaction matrices can be constructed. For instance, in *the tight-binding approximation*, we would assume the matrix T in Eq. (1.15) to be very close to a diagonal one; the diagonal elements would represent the lattice's on-site energies and the first off-diagonal elements the hopping probabilities between the neighbouring lattice sites.

Even though the above formulations can incorporate electronic interactions by the Coulomb integrals, in practice (computationally) this inclusion can be a very demanding task. However, many nanosystems of general interest may be grown to be perfect conductors meaning that the electrons can travel considerable distances without encountering any obstacles; these sort of systems are typically referred to as *ballistic conductors* [81, 82]. With this in mind, in many of the example simulations presented in this thesis we will be concentrating on *graphene* structures. Graphene, a thin carbon film of hexagonal (or honeycomb) geometry, can be regarded as a two-dimensional material as one dimension is highly suppressed to be only one atomic layer thick, see Fig. 1.3. Graphene holds promise for technological advances due to its beneficial properties such as conductivity, mechanical strength and transparency for light [83].

Although in realistic configurations the tight-binding approximation might be too crude, in the field of ultracold atom gases it is common practice to construct so-called *optical lattice* structures by using laser grids [84–86]. The lasers are used to create trapping potentials in a way similar to periodic potentials in a crystal structure. The cold atoms in a gas trapped by the lasers further act as generic particles which can further be used as a model for electrons in a transport setup. Because of the recent progress in the laser technology, the applicability and control in these arbitrary lattice systems is very exceptional and novel. It is therefore possible to relate our tight-binding model systems to an experimental setup.

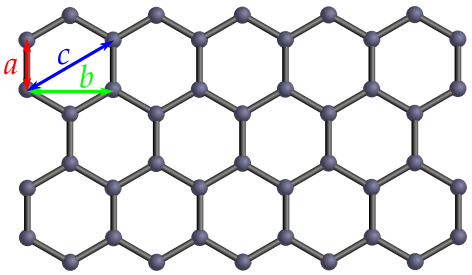

Fig. 1.3: Graphene is a two-dimensional monoatomic thick building block of a carbon allotrope. The nearest-, the second-nearest- and the third-nearest-neighbour distances are, respectively, $a = 1.42$ Å, $b = 2.46$ Å and $c = 2.84$ Å [87].

In many computational tools, such as the Atomic Simulation Environment (ASE) [88], graphene structures (among others) can be tailored and the (x, y, z)-coordinates of

the atomic configuration can be extracted. The (nonzero) elements of the hopping matrix for a graphene structure can therefore be constructed from known parameters [89] by

$$T_{jk} = \begin{cases} \gamma_1 = 2.70 \text{ eV} & \text{if } d_{jk} = a \\ \gamma_2 = 0.20 \text{ eV} & \text{if } d_{jk} = b \\ \gamma_3 = 0.18 \text{ eV} & \text{if } d_{jk} = c, \end{cases} \tag{1.17}$$

where the distance is evaluated by $d_{jk} = \sqrt{(x_j - x_k)^2 + (y_j - y_k)^2 + (z_j - z_k)^2}$. Other models for, e.g., hydrogen passivation and impurities can be implemented in a similar fashion [90].

1.4 A brief overview on (time-dependent) quantum transport studies

The formalism developed by Landauer in 1957 [91] and later complemented by Büttiker in 1986 [92] provides an intuitive physical framework of the current flowing in a junction composed of leads and a central conducting device, i.e., a molecule. First, the current $I_{\alpha\beta}$ in lead β, carried by the scattering states originating from lead $\alpha \neq \beta$, is calculated. In this calculation, the current $I_{\alpha\beta}$ is essentially given by an integral of the transmission probability for an electron to go from lead α to lead β. Then, the difference $I_{\alpha\beta} - I_{\beta\alpha}$ between the currents flowing into and out of the lead β over all terminals $\alpha \neq \beta$ is calculated. This gives the current I_β in terminal β in *steady-state regime*.

Based on the time-dependent Schrödinger equation (1.1), Caroli et al. presented in 1971 a microscopic derivation of a tunneling current in a transport setup (which would nowadays be called a Landauer–Büttiker formula) [93, 94]. In these works, the leads are considered to be initially uncontacted from the central conducting device so that they are in equilibrium at different chemical potentials. Then the contact is switched on suddenly, and the Landauer–Büttiker formula is recovered as the long-time limit $t \to \infty$ of the expectation value of the current operator. As this approach of suddenly switching on a contact in a junction might not have resembled the way the experiments are typically carried out, Cini proposed in 1980 an alternative approach [95]. In this work the whole system is considered to be initially contacted and in equilibrium at a unique chemical potential. Then the system is driven out of equilibrium by an applied bias voltage to the leads. Even though the initial setups in these works are different, the same Landauer–Büttiker formula is recovered since the way the system is prepared does not affect the steady-state properties as was shown later in 2004 by Stefanucci and Almbladh [96].

The formalism of Landauer's and Büttiker's may also be derived using NEGFs as studied by Meir and Wingreen in 1992 [97]. This mathematical tool when applied to quantum transport in multi-terminal junctions provides a natural framework to calculate the current at *all times*, and it is not limited to the steady state. This leads to several studies of generalizing the Landauer–Büttiker formula to *transient regime*. Around the same time as the work of Meir and Wingreen, in 1991, Pastawski derived a formula using NEGFs for $I_\beta(t)$ using the approach of Caroli's (in partitioning the transport setup) in the linear response and adiabatic regime [98]. Also, in 1994 a calculation of $I_\beta(t)$ was done by Jauho et al. where the same (partitioned) approach was used to write $I_\beta(t)$ as a double integral over time and energy; the corresponding integrand consists of a combination of Green's functions in the central region [99]. Later, in 2004, Stefanucci and Almbladh further realized that when the leads are described within wide-band approximation and when the central conducting device consists of only a single level, it is possible to perform the time integral analytically and obtain a time-dependent extension to the Landauer–Büttiker formula [96]. In addition, they used the approach of Cini's (without partitioning the transport setup), and thus confirmed the loss of memory of the initial preparation in the steady state. A step forward in deriving a time-dependent Landauer–Büttiker formula for arbitrary junctions was done by Perfetto et al. in 2008 where also the spin was added to the single-level junction [100].

As a part of this thesis, the results of Ref. [100] are further generalized to junctions of any shape and dimensions within the wide-band approximation for the leads and noninteracting electrons; see Sec. 2.2, Pub. [I] and Ref. [73]. An extension to time-dependent bias profiles was derived by Ridley et al. in Ref. [101]; here this is briefly discussed in Sec. 2.4.3. Furthermore, also an analytic formula for the time-dependent one-particle density matrix is derived separately at zero and arbitrary temperatures and for perturbed and superconducting central regions; see Secs. 2.3 and 2.4 and Pubs. [II, IV]. The result for the density matrix can be used to calculate the local density and current density in the central region, e.g., in graphene samples; see Chap. 3 and Pubs. [II, III]. Similar to the discussion of electronic transport in the framework of Landauer and Büttiker, also a derivation in the case of phononic transport for the time-dependent one-particle density matrix is presented in Sec. 2.5 and in Pub. [V]. This result can further be used to study local heat currents within the central region in the transient regime.

2 Theoretical background

2.1 Introduction to quantum transport problems

In this section the basic concepts of Green's functions stemming from the time-dependent Schrödinger equation will shortly be introduced, and we will briefly consider the applicability of the Green's functions in a two-terminal transport problem.

2.1.1 Green's functions as propagators

Let us start with a consideration of a system whose properties are determined by a time-independent Hamiltonian $\hat{H}$. In the Schrödinger picture a state Ψ evolves by a unitary operator $\hat{U}$ so that

$$|\Psi(t)\rangle = \hat{U}(t, t_0)|\Psi(t_0)\rangle. \tag{2.1}$$

The time evolution operator $\hat{U}$ itself satisfies the equation of motion due to the Schrödinger equation (1.1)

$$\mathrm{i}\frac{\mathrm{d}}{\mathrm{d}t}\hat{U}(t, t_0) - \hat{H}\hat{U}(t, t_0) = 0 \tag{2.2}$$

which is a homogeneous, first order, ordinary differential equation. To solve the equation we need an initial condition which is provided by the nature of a time-evolution operator; it must be $\hat{U}(t_0, t_0) = \hat{\mathbb{1}}$, i.e., propagating a state from t_0 to t_0 is a unit operator. The solution to Eq. (2.2) reads simply

$$\hat{U}(t, t_0) = \mathrm{e}^{-\mathrm{i}\hat{H}(t-t_0)}. \tag{2.3}$$

We can use this expression also for propagating backwards in time since it is valid for $t < t_0$ also. The above discussion could also be performed for time-dependent Hamiltonians $\hat{H}(t)$ by using chronological and anti-chronological time-ordering operators [73] but here we would like to make an introduction to the use of NEGF formalism in a transport setup with as little complexity as possible.

From the solution for the time-evolution operator we may define two new operators depending on the propagation direction in time by employing a step function representation:

$$\hat{G}^{\mathrm{R/A}}(t,t_0) = \mp \mathrm{i}\theta(\pm(t-t_0))\hat{U}(t,t_0). \tag{2.4}$$

Because the time-evolution operator $\hat{U}$ is unitary, we have a relation between the two operators defined in Eq. (2.4)

$$[\hat{G}^{\mathrm{R}}(t,t_0)]^\dagger = \hat{G}^{\mathrm{A}}(t_0,t). \tag{2.5}$$

By direct differentiation and using the equation of motion for the time-evolution operator we may also write the following equation of motion for $\hat{G}^{\mathrm{R/A}}$

$$\mathrm{i}\frac{\mathrm{d}}{\mathrm{d}t}\hat{G}^{\mathrm{R/A}}(t,t_0) - \hat{H}\hat{G}^{\mathrm{R/A}}(t,t_0) = \delta(t-t_0). \tag{2.6}$$

In contrast to Eq. (2.2) this is a non-homogeneous differential equation. If the source term (on the right-hand side) is of the form of a delta function, the functions satisfying this type of equation are typically called *Green's functions* or *propagators*. The distinction between the propagation direction in time, denoted by R/A, is then called either *retarded* or *advanced* Green's function.

By looking at Eqs. (2.3) and (2.4) we also see how the retarded and advanced Green's functions depend only on the time difference $t - t_0$. Using this property it is often useful to express these quantities in the frequency space. Using an integral representation for the step function in Eq. (2.4)

$$\theta(t-t_0) = \lim_{\eta\to 0^+}\frac{-1}{2\pi\mathrm{i}}\int_{-\infty}^{\infty}\mathrm{d}\omega\frac{\mathrm{e}^{-\mathrm{i}\omega(t-t_0)}}{\omega+\mathrm{i}\eta}, \tag{2.7}$$

which can be proven using the residue theorem, we get for the retarded Green's function

$$\begin{aligned}\hat{G}^{\mathrm{R}}(t-t_0) &= -\mathrm{i}\lim_{\eta\to 0^+}\left(\frac{-1}{2\pi\mathrm{i}}\right)\int_{-\infty}^{\infty}\mathrm{d}\omega\frac{\mathrm{e}^{-\mathrm{i}\omega(t-t_0)}}{\omega+\mathrm{i}\eta}\mathrm{e}^{-\mathrm{i}\hat{H}(t-t_0)} \\ &= \lim_{\eta\to 0^+}\int_{-\infty}^{\infty}\frac{\mathrm{d}\omega}{2\pi}\frac{\mathrm{e}^{-\mathrm{i}(\omega+\hat{H})(t-t_0)}}{\omega+\mathrm{i}\eta}.\end{aligned} \tag{2.8}$$

Changing the integration variable as $\omega' = \omega + \hat{H}$ we may manipulate this to take the form of the Fourier transform

$$\hat{G}^{\mathrm{R}}(t-t_0) = \int_{-\infty}^{\infty}\frac{\mathrm{d}\omega'}{2\pi}\mathrm{e}^{-\mathrm{i}\omega'(t-t_0)}\hat{G}^{\mathrm{R}}(\omega') \qquad (\eta\to 0^+), \tag{2.9}$$

where $\hat{G}^{\mathrm{R}}(\omega) \coloneqq [\omega - \hat{H} + \mathrm{i}\eta]^{-1}$. It is worth noticing that above we have operator identities for which a spectral representation can be written in terms of the eigenstates of $\hat{H}$. As in the time domain, also here a symmetry relation holds

$$[\hat{G}^{\mathrm{R}}(\omega)]^\dagger = \hat{G}^{\mathrm{A}}(\omega), \tag{2.10}$$

and then we may formally express the propagators as

$$\hat{G}^{\mathrm{R/A}}(\omega) = [(\omega \pm \mathrm{i}\eta)\hat{\mathbb{1}} - \hat{H}]^{-1} \tag{2.11}$$

or, equivalently, the equation of motion (2.6) in frequency domain as

$$[(\omega \pm \mathrm{i}\eta)\hat{\mathbb{1}} - \hat{H}]\hat{G}^{\mathrm{R/A}}(\omega) = \hat{\mathbb{1}}. \tag{2.12}$$

The positive infinitesimal η accounts for proper causal structure in the retarded and advanced Green's functions; $\hat{G}^{\mathrm{R}}$ is analytic in the upper-half plane whereas $\hat{G}^{\mathrm{A}}$ is analytic in the lower-half plane. In the above discussion essentially nothing more than the Schrödinger equation was used to introduce the concept of propagators. The interpretation of the system's properties in terms of these propagators [based on the system's Hamiltonian in Eq. (2.11)] is therefore completely equivalent to the Schrödinger equation.

All the above discussion is very general. The retarded and advanced Green's functions follow, in this case, from the time-evolution operator in Eq. (2.3) for a time-independent Hamiltonian. Had we included time-dependency in the Hamiltonian, the time-evolution operator would only take a little more intricate form due to the chronological time-orderings [73]. As was briefly discussed in Eq. (1.2) with Fig. 1.2, it is possible to include the system's properties at equilibrium to the time-evolution by adding an imaginary-time propagation, i.e., the vertical track in the Keldysh contour. In addition to the retarded and advanced Green's functions, we will encounter other *Keldysh components* of the Green's functions depending on the time arguments; we will see these forms more explicitly in the next section.

2.1.2 Nonequilibrium density matrix in a two-terminal setup

Let us then apply the Green's function description to a more explicit calculation in an atomic-scale junction. We look at a specific setup of partitioning the system of interest in a transport sense into left (L) and right (R) leads and to a central conducting device (C), see Fig. 2.1. We wish to see what the Green's functions look like for these sort of setups, and how the corresponding components are evaluated. We assume that the basis of the studied LCR system can indeed be divided accordingly. We let the Hamiltonian be of the form (we drop the hats in the notation for now)

$$H = \begin{pmatrix} H_{LL} & H_{LC} & 0 \\ H_{CL} & H_{CC} & H_{CR} \\ 0 & H_{RC} & H_{RR} \end{pmatrix}. \tag{2.13}$$

This means the leads are coupled only through the central region as the direct couplings between them are zero. Now, we project the equation of motion (2.12)

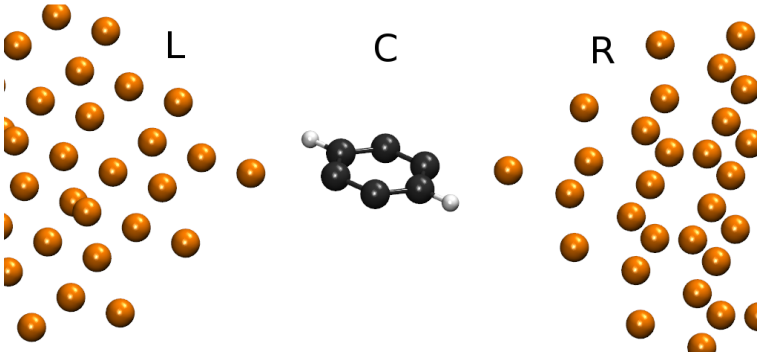

Fig. 2.1: Division of the transport system basis into three blocks. Each atom can be described with several basis functions for different orbitals.

for the retarded Green's function onto the CC subspace to extract an expression for the propagator on the central region embedded into the lead environment. The CC and αC elements of Eq. (2.12) read (where $\alpha \in \{L, R\}$)

$$(\omega \pm \mathrm{i}\eta) G^{\mathrm{R/A}}_{CC}(\omega) - H_{CC} G^{\mathrm{R/A}}_{CC}(\omega) - \sum_{\alpha} H_{C\alpha} G^{\mathrm{R/A}}_{\alpha C}(\omega) = \mathbb{1}, \tag{2.14}$$

$$(\omega \pm \mathrm{i}\eta) G^{\mathrm{R/A}}_{\alpha C}(\omega) - H_{\alpha C} G^{\mathrm{R/A}}_{CC}(\omega) - H_{\alpha\alpha} G^{\mathrm{R/A}}_{\alpha C}(\omega) = 0. \tag{2.15}$$

Here we may multiply the second row from left by the propagator in the lead α (denoted by a lower-case g), and then use the corresponding equation of motion $g^{\mathrm{R/A}}_{\alpha\alpha}(\omega)[(\omega \pm \mathrm{i}\eta) - H_{\alpha\alpha}] = \mathbb{1}$ to extract an expression for the coupling propagator $G^{\mathrm{R/A}}_{\alpha C}$

$$G^{\mathrm{R/A}}_{\alpha C}(\omega) = g^{\mathrm{R/A}}_{\alpha\alpha}(\omega) H_{\alpha C} G^{\mathrm{R/A}}_{CC}(\omega). \tag{2.16}$$

Inserting this back into the first row closes the equation for $G^{\mathrm{R/A}}_{CC}(\omega)$ and we may write the solution as

$$G^{\mathrm{R/A}}_{CC}(\omega) = [(\omega \pm \mathrm{i}\eta) - H_{CC} - (\Sigma_{\mathrm{em},L})^{\mathrm{R/A}}_{CC}(\omega) - (\Sigma_{\mathrm{em},R})^{\mathrm{R/A}}_{CC}(\omega)]^{-1}, \tag{2.17}$$

where we defined *the embedding self-energy* as

$$(\Sigma_{\mathrm{em},\alpha})^{\mathrm{R/A}}_{CC}(\omega) = H_{C\alpha} g^{\mathrm{R/A}}_{\alpha\alpha}(\omega) H_{\alpha C}. \tag{2.18}$$

[Hopefully, the lead index R (cursive symbol) will not be confused with the retarded component R (upright symbol).] It is to be noted, as can be seen from the definition, that the embedding self-energy is a matrix defined on the CC subspace. Even though in the subscript there also is a lead index α, it is not to be confused with objects in the lead subspace. We call this quantity an *embedding* self-energy as it stems from the coupling between the central region and the lead environment. Later we will also encounter many-body self-energies taking into account the interactions within

the studied system. A common definition together with the embedding self-energy is *the level-width function*

$$(\Gamma_\alpha)_{CC}(\omega) = \mathrm{i}[(\Sigma_{\mathrm{em},\alpha})^{\mathrm{R}}_{CC}(\omega) - (\Sigma_{\mathrm{em},\alpha})^{\mathrm{A}}_{CC}(\omega)] = -2\,\mathrm{Im}[(\Sigma_{\mathrm{em},\alpha})^{\mathrm{R}}_{CC}(\omega)] \tag{2.19}$$

for which we have the same notation as for the embedding self-energy; also this is a matrix defined on the CC subspace. Similarly, we very often encounter a difference of the retarded and advanced Green's functions, called *the spectral function*, as

$$A_{CC}(\omega) = \mathrm{i}[G^{\mathrm{R}}_{CC}(\omega) - G^{\mathrm{A}}_{CC}(\omega)]. \tag{2.20}$$

As the Green's functions depend on the self-energies originating from the lead environment, we get a contribution from both leads by manipulating Eq. (2.20) as

$$\begin{aligned} A_{CC}(\omega) &= \mathrm{i}G^{\mathrm{R}}_{CC}(\omega)[(G^{\mathrm{A}}_{CC}(\omega))^{-1} - (G^{\mathrm{R}}_{CC}(\omega))^{-1}]G^{\mathrm{A}}_{CC}(\omega) \\ &= \mathrm{i}G^{\mathrm{R}}_{CC}(\omega)[-\mathrm{i}(\Gamma_L)_{CC}(\omega) - \mathrm{i}(\Gamma_R)_{CC}(\omega)]G^{\mathrm{A}}_{CC}(\omega) \\ &= G^{\mathrm{R}}_{CC}(\omega)[(\Gamma_L)_{CC}(\omega) + (\Gamma_R)_{CC}(\omega)]G^{\mathrm{A}}_{CC}(\omega) = (A_L)_{CC}(\omega) + (A_R)_{CC}(\omega), \end{aligned} \tag{2.21}$$

where we inserted Eqs. (2.17) and (2.19). Also, we notice from Eq. (2.19) that the imaginary part of the embedding self-energy function gives rise to the broadening of the band. This is intuitively understood by looking at Eq. (2.17): the real part of the embedding self-energy could be absorbed into the Hamiltonian H_{CC}, thus, only shifting the poles of the Green's function, whereas the imaginary part of the embedding self-energy gives the width of the peaks.

Granted the simplicity of Eq. (2.21), it leads to a very important result. As it describes the spectral density in the central region due to the lead self-energy, we may weigh this function by the occupation probability (given by the Fermi distribution) and integrate over the frequency to obtain

$$\rho_{CC} = \int_{-\infty}^{\infty} \frac{\mathrm{d}\omega}{2\pi} f(\omega)[(A_L)_{CC}(\omega) + (A_R)_{CC}(\omega)], \tag{2.22}$$

where $f(\omega) = [\mathrm{e}^{\beta(\omega-\mu)} + 1]^{-1}$ is the Fermi function with chemical potential μ and inverse temperature $\beta = (k_{\mathrm{B}}T)^{-1}$. This is the nonequilibrium density matrix for the central region C, and it could readily be generalized to an arbitrary number of leads. We will look at an example calculation in the next section, after deriving also a current formula of the similar form of Eq. (2.22).

2.2 Time-dependent quantum transport

So far we have discussed only time-independent or stationary transport. There is, however, no guarantee that this steady-state description would capture the essential

physics in, say, atomic-scale junction operating at high-frequency regime where bits are being switched from zeros to ones at an appreciable pace. Therefore, we need an accurate theory for describing the full time-dependence.

Before diving into the formal development of the time-dependent quantum transport in terms of the nonequilibrium Green's functions in Pub. [I], let us briefly look at other theoretical approaches and computational methods for this task. As briefly touched upon in Chap. 1 the time-dependent density in a system of interest may be evaluated from Eq. (1.3) (according to the Runge–Gross theorem [34]). From the Kohn–Sham orbitals it is possible to define a (Kohn–Sham) current density which is equivalent to the *true* current density when considered via a surface integral relating to the system's geometry [102–104]. This is the essential starting point for a (partition-free) scheme based on TDDFT to treat the time-dependent current response, even in fully interacting systems. Another widely used method, which was also briefly mentioned in Chap. 1, is the density matrix renormalization group (DMRG). DMRG is, also in the context of time-dependent problems, a powerful technique especially in case of one-dimensional interacting quantum systems. It has been successfully used in the study of real-time dynamics (as in time-dependent quantum transport) where a certain hierarchy of equations for the time-evolution operator and the density matrix is solved using specific approximations [105–108]. In one-dimensional systems the matrices describing the transport setup are sparse as there are fewer connections between the relevant basis states, and together with DMRG a *time-evolving block decimation* algorithm is often used [109–111]. However, arguably the most used technique in time-dependent quantum transport is the NEGF formalism with its natural connection to the traditional Landauer approach as we will see in the following.

Next, in this section, we introduce a multi-terminal quantum transport model for which the dynamical equations of motion for the Green's function can be solved analytically. We first have a look at the Hamiltonian, Green's functions, and the equations connecting them, and we derive in a steady-state limit important results known as the Meir–Wingreen [97] and the Landauer–Büttiker [91, 92] formulae. Furthermore, an analytically solvable time-dependent quantum transport model will be discussed, for which the full solution to the equations of motion in transient regime will be presented in the next section, thus extending the traditional Landauer–Büttiker formalism into time domain without losing the intuitive interpretation or increasing the computational cost. The presented derivations follow the theoretical framework set forward in Pubs. [I, II].

2.2.1 Hamiltonian, Green's functions, and the equations connecting them

We start by describing the system's Hamiltonian $\hat{H} = \hat{H}_0 + \hat{H}_{\text{int}}$, where the noninteracting part is in second quantization [see Eq. (1.14)]

$$\hat{H}_0 = \sum_{k\alpha,\sigma} \epsilon_{k\alpha} \hat{d}^\dagger_{k\alpha,\sigma} \hat{d}_{k\alpha,\sigma} + \sum_{m,n,\sigma} T_{mn} \hat{d}^\dagger_{m,\sigma} \hat{d}_{n,\sigma} + \sum_{m,k\alpha,\sigma} \left[T_{mk\alpha} \hat{d}^\dagger_{m,\sigma} \hat{d}_{k\alpha,\sigma} + T_{k\alpha m} \hat{d}^\dagger_{k\alpha,\sigma} \hat{d}_{m,\sigma} \right]. \quad (2.23)$$

The first term accounts for the α-th lead with $k\alpha$ being the k-th basis function of the α-th lead, the second term is for the central molecule, and the last term is for the coupling between the central part and the α-th lead. The corresponding annihilation (creation) operators for these states are denoted in Eq. (2.23) by $\hat{d}^{(\dagger)}$ obeying the fermionic anticommutation rules $\{\hat{d}_{x\sigma}, \hat{d}^\dagger_{y\sigma'}\} = \delta_{xy}\delta_{\sigma\sigma'}$. The interacting part can be written in terms of the Coulomb integrals v_{ijmn} as [see Eq. (1.14)]

$$\hat{H}_{\text{int}} = \frac{1}{2} \sum_{ijmn,\sigma\sigma'} v_{ijmn} \hat{d}^\dagger_{i,\sigma} \hat{d}^\dagger_{j,\sigma'} \hat{d}_{m,\sigma'} \hat{d}_{n,\sigma}. \quad (2.24)$$

This sum is restricted to molecular indices only, i.e., the interactions are described only between the electrons within the central molecule. It is worth noticing that we may still keep the interacting Hamiltonian in our derivation even if, later in this thesis, we consider only free electrons occupying the lattice system without interacting with each other. The setup is depicted in Fig. 2.2.

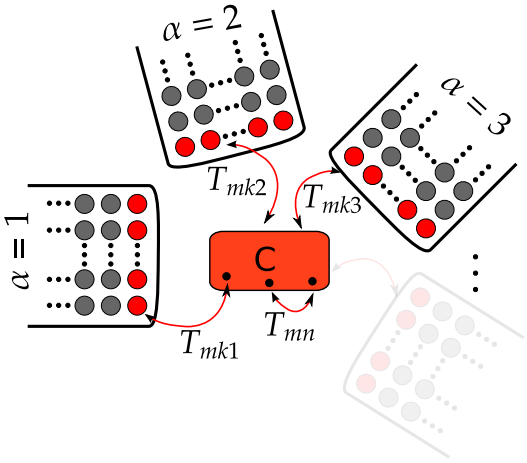

Fig. 2.2: Transport model corresponding to Eq. (2.23) where a central molecule (C) of arbitrary shape and size is connected to arbitrary number of leads, also of arbitrary shape and size (the structure is for illustration only.)

The transport and nonequilibrium conditions are as follows:

1. The system is initially ($t < t_0$) in thermal equilibrium at inverse temperature β and in chemical potential μ, when the density matrix is of the form $\hat{\rho} = \frac{1}{\mathcal{Z}} \mathrm{e}^{-\beta(\hat{H}-\mu\hat{N})}$ with $\hat{N}$ and $\mathcal{Z}$ being the particle number operator and the grand-canonical partition function, respectively.
2. At times $t > t_0$ the system is driven out of equilibrium with an external field by raising suddenly the energy levels of every lead $\epsilon_{k\alpha} \to \epsilon_{k\alpha} + V_\alpha$.

From the nonequilibrium conditions we get that after $t = t_0$ charge carriers start to flow through the central molecule. To calculate time-dependent nonequilibrium quantities we use the equations of motion for the one-particle Green's function on the Keldysh contour γ. This quantity is defined as the ensemble average of the contour-ordered product of particle creation and annihilation operators in the Heisenberg picture [73]

$$G_{rs}(z, z') = -\mathrm{i}\langle \mathcal{T}_\gamma [\hat{d}_{r,\mathrm{H}}(z) \hat{d}^\dagger_{s,\mathrm{H}}(z')] \rangle, \tag{2.25}$$

where the indices r, s can be either indices in the leads or in the central region and the variables z, z' run on the contour. The contour has a forward and a backward branch on the real-time axis, $[t_0, \infty[$, and also a vertical branch on the imaginary axis, $[t_0, t_0 - \mathrm{i}\beta]$ with inverse temperature β, see Fig. 1.2 and, e.g., Refs. [73, 112]. For a function $k(z, z')$ on the Keldysh contour the components lesser ($<$), greater ($>$), retarded (R), advanced (A), left ($\ulcorner$), right ($\urcorner$) and Matsubara (M) are defined as [73]

$$\begin{aligned}
k^<(t, t') &= k(t_-, t'_+), && \text{(2.26a)}\\
k^>(t, t') &= k(t_+, t'_-), && \text{(2.26b)}\\
k^\mathrm{R}(t, t') &= +\theta(t - t') \left[k^>(t, t') - k^<(t, t')\right], && \text{(2.26c)}\\
k^\mathrm{A}(t, t') &= -\theta(t' - t) \left[k^>(t, t') - k^<(t, t')\right], && \text{(2.26d)}\\
k^\ulcorner(\tau, t') &= k(t_0 - \mathrm{i}\tau, t'), && \text{(2.26e)}\\
k^\urcorner(t, \tau) &= k(t, t_0 - \mathrm{i}\tau), && \text{(2.26f)}\\
k^\mathrm{M}(\tau, \tau') &= k(t_0 - \mathrm{i}\tau, t_0 - \mathrm{i}\tau'). && \text{(2.26g)}
\end{aligned}$$

The matrix $\boldsymbol{G}$ with matrix elements G_{rs} satisfies the equations of motion [38, 73]

$$\left[\mathrm{i}\frac{\mathrm{d}}{\mathrm{d}z} - \boldsymbol{h}(z)\right] \boldsymbol{G}(z, z') = \delta(z, z')\mathbf{1} + \int_\gamma \mathrm{d}\bar{z}\, \boldsymbol{\Sigma}_\mathrm{mb}(z, \bar{z}) \boldsymbol{G}(\bar{z}, z'), \tag{2.27}$$

$$\boldsymbol{G}(z, z') \left[-\mathrm{i}\frac{\overleftarrow{\mathrm{d}}}{\mathrm{d}z'} - \boldsymbol{h}(z')\right] = \delta(z, z')\mathbf{1} + \int_\gamma \mathrm{d}\bar{z}\, \boldsymbol{G}(z, \bar{z}) \boldsymbol{\Sigma}_\mathrm{mb}(\bar{z}, z'), \tag{2.28}$$

with a boundary condition such that the Green's function is antiperiodic along the contour γ (Kubo–Martin–Schwinger boundary conditions). On the right-hand

side of Eqs. (2.27) and (2.28), *the many-body self-energy* $\Sigma_{\rm mb}$ takes into account the many-body interactions due to Eq. (2.24) [73]. This object is now different from the embedding self-energy defined earlier. Here $\boldsymbol{h}(z)$ is the single-particle Hamiltonian which, in the basis $k\alpha$ and m, has the following block structure

$$\boldsymbol{h} = \begin{pmatrix} h_{11} & 0 & \cdots & h_{1C} \\ 0 & h_{22} & \cdots & h_{2C} \\ \vdots & \vdots & \ddots & \vdots \\ h_{C1} & h_{C2} & \cdots & h_{CC} \end{pmatrix}, \tag{2.29}$$

where $(h_{\alpha\alpha'})_{kk'} = \delta_{\alpha\alpha'}\delta_{kk'}\epsilon_{k\alpha}$ corresponds to the leads, $(h_{\alpha C})_{km} = T_{k\alpha m}$ is the coupling part, and $(h_{CC})_{mn} = T_{mn}$ accounts for the central molecule. Accordingly, the matrix structures for the Green's function and for the many-body self-energy are

$$\boldsymbol{G} = \begin{pmatrix} G_{11} & G_{12} & \cdots & G_{1C} \\ G_{21} & G_{22} & \cdots & G_{2C} \\ \vdots & \vdots & \ddots & \vdots \\ G_{C1} & G_{C2} & \cdots & G_{CC} \end{pmatrix}; \qquad \boldsymbol{\Sigma}_{\rm mb} = \begin{pmatrix} 0 & 0 & \cdots & 0 \\ 0 & 0 & \cdots & 0 \\ \vdots & \vdots & \ddots & \vdots \\ 0 & 0 & \cdots & (\Sigma_{\rm mb})_{CC} \end{pmatrix}, \tag{2.30}$$

where, as mentioned earlier, all the interactions are contained in the component $(\Sigma_{\rm mb})_{CC}$, i.e., the leads are described within a noninteracting framework. This assumption makes $(\Sigma_{\rm mb})_{CC}[G_{CC}]$ to be a functional of G_{CC} only. As we are mainly interested in the dynamical quantities within the central molecule, it is convenient to project the equation of motion in Eq. (2.27) onto states CC and αC. This is a similar procedure we already performed in Sec. 2.1. The projection involves some book-keeping with the matrix products, and this process is outlined as follows:

$$\begin{aligned} & \mathrm{i}\frac{\mathrm{d}}{\mathrm{d}z}G_{CC}(z,z') - \sum_\alpha h_{C\alpha}(z)G_{\alpha C}(z,z') - h_{CC}(z)G_{CC}(z,z') \\ = \;& \delta_{CC}(z,z') + \sum_\alpha \int_\gamma \mathrm{d}\bar{z}(\Sigma_{\rm mb})_{C\alpha}(z,\bar{z})G_{\alpha C}(\bar{z},z') + \int_\gamma \mathrm{d}\bar{z}(\Sigma_{\rm mb})_{CC}(z,\bar{z})G_{CC}(\bar{z},z'), \end{aligned} \tag{2.31}$$

$$\begin{aligned} & \mathrm{i}\frac{\mathrm{d}}{\mathrm{d}z}G_{\alpha C}(z,z') - h_{\alpha\alpha}(z)G_{\alpha C}(z,z') - h_{\alpha C}(z)G_{CC}(z,z') \\ = \;& \delta_{\alpha C}(z,z') + \sum_\beta \int_\gamma \mathrm{d}\bar{z}(\Sigma_{\rm mb})_{\alpha\beta}(z,\bar{z})G_{\beta C}(\bar{z},z') + \int_\gamma \mathrm{d}\bar{z}(\Sigma_{\rm mb})_{\alpha C}(z,\bar{z})G_{CC}(\bar{z},z'), \end{aligned} \tag{2.32}$$

where we may use the facts $(\Sigma_{\rm mb})_{\alpha\beta}, (\Sigma_{\rm mb})_{\alpha C}, \delta_{\alpha C} = 0$ to get

$$\begin{aligned} \left[\mathrm{i}\frac{\mathrm{d}}{\mathrm{d}z} - h_{CC}(z)\right]G_{CC}(z,z') &= \delta(z,z') + \sum_\alpha h_{C\alpha}(z)G_{\alpha C}(z,z') \\ &+ \int_\gamma \mathrm{d}\bar{z}(\Sigma_{\rm mb})_{CC}(z,\bar{z})G_{CC}(\bar{z},z') \end{aligned} \tag{2.33}$$

$$\left[\mathrm{i}\frac{\mathrm{d}}{\mathrm{d}z} - h_{\alpha\alpha}(z)\right]G_{\alpha C} = h_{\alpha C}(z)G_{CC}(z,z'). \tag{2.34}$$

Then we multiply Eq. (2.34) with the Green's function of the isolated α-th reservoir, $g_{\alpha\alpha}(z,z')$, whose equation of motion is $\left[\mathrm{i}\frac{\mathrm{d}}{\mathrm{d}z} - h_{\alpha\alpha}(z)\right] g_{\alpha\alpha}(z,z') = \delta(z,z')$ (due to no interactions in the lead sector), and integrate over the Keldysh contour γ. This way we obtain

$$\int_\gamma \mathrm{d}\bar{z} g_{\alpha\alpha}(z,\bar{z})\left[\mathrm{i}\frac{\mathrm{d}}{\mathrm{d}\bar{z}} - h_{\alpha\alpha}(\bar{z})\right] G_{\alpha C}(\bar{z},z') = \int_\gamma \mathrm{d}\bar{z} g_{\alpha\alpha}(z,\bar{z}) h_{\alpha C}(\bar{z}) G_{CC}(\bar{z},z'). \tag{2.35}$$

Due to the occurring delta function on the left-hand side, the integral readily gives

$$G_{\alpha C}(z,z') = \int_\gamma \mathrm{d}\bar{z} g_{\alpha\alpha}(z,\bar{z}) h_{\alpha C}(\bar{z}) G_{CC}(\bar{z},z'). \tag{2.36}$$

Then, from Eq. (2.36) we may insert $G_{\alpha C}$ into Eq. (2.33) to obtain

$$\begin{aligned}
&\left[\mathrm{i}\frac{\mathrm{d}}{\mathrm{d}z} - h_{CC}(z)\right] G_{CC}(z,z') = \delta(z,z') \\
&+ \sum_\alpha h_{C\alpha}(z) \int_\gamma \mathrm{d}\bar{z} g_{\alpha\alpha}(z,\bar{z}) h_{\alpha C}(\bar{z}) G_{CC}(\bar{z},z') + \int_\gamma \mathrm{d}\bar{z} (\Sigma_{\mathrm{mb}})_{CC}(z,\bar{z}) G_{CC}(\bar{z},z') \\
\Rightarrow \quad &\left[\mathrm{i}\frac{\mathrm{d}}{\mathrm{d}z} - h_{CC}(z)\right] G_{CC}(z,z') = \delta(z,z') \\
&+ \int_\gamma \mathrm{d}\bar{z}\Big[(\Sigma_{\mathrm{mb}})_{CC}(z,\bar{z}) + \sum_\alpha h_{C\alpha}(z) g_{\alpha\alpha}(z,\bar{z}) h_{\alpha C}(\bar{z})\Big] G_{CC}(\bar{z},z').
\end{aligned} \tag{2.37}$$

Here we notice that the second term in the square parentheses on the right-hand side is exactly *the embedding self-energy* Σ_{em} we defined in Sec. 2.1. Then, we obtain the equation of motion for the Green's function projected onto the central molecule

$$\left[\mathrm{i}\frac{\mathrm{d}}{\mathrm{d}z} - h_{CC}(z)\right] G_{CC}(z,z') = \delta(z,z') + \int_\gamma \mathrm{d}\bar{z}\left[(\Sigma_{\mathrm{mb}})_{CC}(z,\bar{z}) + (\Sigma_{\mathrm{em}})_{CC}(z,\bar{z})\right] G_{CC}(\bar{z},z'). \tag{2.38}$$

The adjoint equation of motion can be derived in a similar manner. So far, we did not specify the type of interaction or any explicit form for the self-energy Σ_{mb}. For practical calculations these forms typically need to be approximated; see, e.g., [113, 114]. Otherwise the equations of motion for the Green's function are general integro–differential equations which can be solved numerically using time-stepping schemes [73, 75, 115].

2.2.2 Meir–Wingreen formula

It is worth stressing that everything so far has been very general; we are dealing with a multi-terminal junction with interacting central region, and in addition to the

equation of motion, we have obtained a Green's function in Eq. (2.36) to describe the propagation of a particle from lead α to the central region. This turns out to be a very convenient quantity since we can relate it to the current in the interface between the central region and the lead. Let us consider current in lead α as a rate of change in particle number, $I_\alpha(t) = q\frac{\mathrm{d}}{\mathrm{d}t}N_\alpha(t)$ with q being the charge of the particles. Furthermore, the particle number, $N_\alpha(t)$, is the ensemble average of the number operator in the Heisenberg picture, $\langle\hat{N}_\alpha\rangle = \langle\sum_{k\sigma}\hat{d}^\dagger_{k\alpha,\sigma}\hat{d}_{k\alpha,\sigma}\rangle$, for which we have the equation of motion as [73]

$$\begin{aligned} I_\alpha(t) &= q\Big\langle\frac{\mathrm{d}}{\mathrm{d}t}\hat{N}_\alpha(t)\Big\rangle = -\mathrm{i}q\left\langle\left[\hat{N}_\alpha(t),\hat{H}(t)\right]\right\rangle \\ &= -\mathrm{i}q\Big\langle\sum_{k\sigma,k'\alpha'\sigma'}\left[\hat{d}^\dagger_{k\alpha,\sigma}(t)\hat{d}_{k\alpha,\sigma}(t)\ ,\ \epsilon_{k'\alpha'}\hat{d}^\dagger_{k'\alpha',\sigma'}(t)\hat{d}_{k'\alpha',\sigma'}(t)\right] \\ &\quad+\sum_{k\sigma,mn\sigma'}\left[\hat{d}^\dagger_{k\alpha,\sigma}(t)\hat{d}_{k\alpha,\sigma}(t)\ ,\ T_{mn}\hat{d}^\dagger_{m,\sigma'}(t)\hat{d}_{n,\sigma'}(t)\right] \\ &\quad+\sum_{k\sigma,mk'\alpha'\sigma'}\left[\hat{d}^\dagger_{k\alpha,\sigma}(t)\hat{d}_{k\alpha,\sigma}(t)\ ,\ T_{mk'\alpha'}\hat{d}^\dagger_{m,\sigma'}(t)\hat{d}_{k'\alpha',\sigma'}(t)\right] \\ &\quad+\sum_{k\sigma,mk'\alpha'\sigma'}\left[\hat{d}^\dagger_{k\alpha,\sigma}(t)\hat{d}_{k\alpha,\sigma}(t)\ ,\ T_{k'\alpha'm}\hat{d}^\dagger_{k'\alpha',\sigma'}(t)\hat{d}_{m,\sigma'}(t)\right]\Big\rangle. \end{aligned} \tag{2.39}$$

A nonzero current follows from a voltage shift in the lead Hamiltonian as raised energy level $\epsilon_{k\alpha} \to \epsilon_{k\alpha} + V_\alpha$. Since the number operator commutes with the lead and molecule part of the Hamiltonian, the first two commutators in the above expression give simply zero. The nonzero contribution comes from the coupling terms which we can expand as follows

$$\begin{aligned} I_\alpha(t) &= -\mathrm{i}q\Big\langle\sum_{k\sigma,mk'\alpha'\sigma'}\Big\{T_{mk'\alpha'}\hat{d}^\dagger_{m,\sigma'}\left[\hat{d}^\dagger_{k\alpha,\sigma}(t)\hat{d}_{k\alpha,\sigma}(t)\ ,\ \hat{d}_{k'\alpha',\sigma'}(t)\right] \\ &\qquad+T_{k'\alpha'm}\left[\hat{d}^\dagger_{k\alpha,\sigma}(t)\hat{d}_{k\alpha,\sigma}(t)\ ,\ \hat{d}^\dagger_{k'\alpha',\sigma'}(t)\right]\hat{d}_{m,\sigma'}(t)\Big\}\Big\rangle. \end{aligned} \tag{2.40}$$

Next, using $[AB,C] = A\{B,C\} - \{A,C\}B$ for the commutator and the anticommutation relations for the creation and annihilation operators we further get

$$I_\alpha(t) = -\mathrm{i}q\Big\langle\sum_{mk,\sigma}\Big[-T_{mk\alpha}\hat{d}^\dagger_{m,\sigma}(t)\hat{d}_{k\alpha,\sigma}(t) + T_{k\alpha m}\hat{d}^\dagger_{k\alpha,\sigma}(t)\hat{d}_{m,\sigma}(t)\Big]\Big\rangle. \tag{2.41}$$

Here we may identify the equal-time lesser Green's function [Eqs. (2.25) and (2.26a)] for the αC block in Eq. (2.36) and use the following symmetry relation

$$[G^<(t,t')]^\dagger = \left[-\mathrm{i}\left\langle\hat{d}^\dagger(t')\hat{d}(t)\right\rangle\right]^\dagger = \mathrm{i}\left\langle\hat{d}^\dagger(t)\hat{d}(t')\right\rangle = -G^<(t',t). \tag{2.42}$$

Also, using the fact that the hopping matrix is hermitian, summing over the spin index σ, and using the identity $z + z^* = 2\,\mathrm{Re}\,z$ for a complex number z in Eq. (2.41),

we get

$$I_\alpha(t) = 4q \sum_{mk} \mathrm{Re}\left[T_{mk\alpha} G^<_{k\alpha m}(t,t)\right]. \tag{2.43}$$

The summation in Eq. (2.43) corresponds to a trace over the molecular indices $m \in C$ of the matrix product $h_{C\alpha}G_{\alpha C}$, so we may also write the current as

$$I_\alpha(t) = 4q\,\mathrm{Re}\left\{\mathrm{Tr}_C\left[h_{C\alpha}G^<_{\alpha C}(t,t)\right]\right\}. \tag{2.44}$$

We may expand the product inside the trace using Eq. (2.36) as

$$h_{C\alpha}(z)G_{\alpha C}(z,z') = \int_\gamma \mathrm{d}\bar{z} h_{C\alpha}(z) g_{\alpha\alpha}(z,\bar{z}) h_{\alpha C}(\bar{z}) G_{CC}(\bar{z},z') = \int_\gamma \mathrm{d}\bar{z} (\Sigma_{\mathrm{em},\alpha})_{CC}(z,\bar{z}) G_{CC}(\bar{z},z'), \tag{2.45}$$

where we noticed the definition of the embedding self-energy for lead α, $(\Sigma_{\mathrm{em},\alpha})_{CC}$. Then we should take the lesser component of Eq. (2.45). Different components of the functions on the Keldysh contour, see Eqs. (2.26a)–(2.26g), are related by *the Langreth rules* [73, 116]. Using these rules in Eq. (2.45) and then inserting to Eq. (2.44) we have

$$I_\alpha(t) = 4q\,\mathrm{Re}\left\{\mathrm{Tr}_C\left[(\Sigma_{\mathrm{em},\alpha})^<_{CC} \cdot G^{\mathrm{A}}_{CC} + (\Sigma_{\mathrm{em},\alpha})^{\mathrm{R}}_{CC} \cdot G^<_{CC} + (\Sigma_{\mathrm{em},\alpha})^{\rceil}_{CC} \star G^{\lceil}_{CC}\right](t,t)\right\}, \tag{2.46}$$

where we defined time-convolutions on the Keldysh contour as

$$[f \cdot g](t,t) = \int_{t_0}^{\infty} \mathrm{d}\bar{t} f(t,\bar{t}) g(\bar{t},t); \quad [f \star g](t,t) = -\mathrm{i}\int_0^\beta \mathrm{d}\tau f(t,\tau) g(\tau,t). \tag{2.47}$$

Equation (2.46) is a very general formula for the current through the interface between the central region and the α-th lead since it is already in the transient regime (t-dependency) and it properly takes the vertical track of the Keldysh contour into account (last term). This term is responsible for the initial couplings and correlations in the system. Importantly, if the Green's functions appearing in Eq. (2.46) satisfy the equation of motion (2.38), also the interactions are properly included to the description.

Let us study some limiting cases of Eq. (2.46). First, in the steady-state limit ($t \to \infty$) we may assume that the dependency of the initial state is washed out [96], i.e., we may drop the last term in the square brackets. Furthermore, the functions $(\Sigma_{\mathrm{em},\alpha})_{CC}$ and G_{CC} (of two time variables) become functions of the time difference only and we may employ the Fourier transform. Then, the convolutions become products of the corresponding Fourier transformed functions, and we may obtain an expression for the steady-state current by

$$\begin{aligned} I_\alpha &= \lim_{t\to\infty} I_\alpha(t) \\ &= 2\mathrm{i}q \int \frac{\mathrm{d}\omega}{2\pi} \mathrm{Tr}_C\Big\{(\Sigma_{\mathrm{em},\alpha})^<_{CC}(\omega)\mathrm{i}\left[G^{\mathrm{R}}_{CC}(\omega) - G^{\mathrm{A}}_{CC}(\omega)\right] \\ &\qquad - \mathrm{i}\left[(\Sigma_{\mathrm{em},\alpha})^{\mathrm{R}}_{CC}(\omega) - (\Sigma_{\mathrm{em},\alpha})^{\mathrm{A}}_{CC}(\omega)\right] G^<_{CC}(\omega)\Big\}, \end{aligned} \tag{2.48}$$

where we again used $\mathrm{Re}\, z = (z + z^*)/2$. In Eq. (2.48) we notice the definitions of the spectral function and the level-width function [see Eqs. (2.19) and (2.20)], and we may write the steady-state current as

$$I_\alpha = 2\mathrm{i}q \int \frac{\mathrm{d}\omega}{2\pi} \mathrm{Tr}_C \left[(\Sigma_{\mathrm{em},\alpha})^<_{CC}(\omega) A_{CC}(\omega) - (\Gamma_\alpha)_{CC}(\omega) G^<_{CC}(\omega) \right]. \tag{2.49}$$

Furthermore, we limit ourselves to a two-terminal setting and calculate the total current through the central region as $I = I_R - I_L$, and insert a fluctuation–dissipation type of relation for the embedding self-energy $(\Sigma_{\mathrm{em},\alpha})^<_{CC}(\omega) = \mathrm{i} f_\alpha(\omega)(\Gamma_\alpha)_{CC}(\omega)$ [73], where f_α is the Fermi function for the α-th lead; this is defined as $f_\alpha(\omega) = [\mathrm{e}^{\beta(\omega-\mu-V_\alpha)} + 1]^{-1}$ for the biased Fermi level. Then, we get *the Meir–Wingreen formula* [97, 117]

$$\begin{aligned} I &= 2\mathrm{i}q \int \frac{\mathrm{d}\omega}{2\pi} \mathrm{Tr}_C \Big\{ \left[f_L(\omega)(\Gamma_L)_{CC}(\omega) - f_R(\omega)(\Gamma_R)_{CC}(\omega) \right] \left[G^\mathrm{R}_{CC}(\omega) - G^\mathrm{A}_{CC}(\omega) \right] \\ &\quad + \left[(\Gamma_L)_{CC}(\omega) - (\Gamma_R)_{CC}(\omega) \right] G^<_{CC}(\omega) \Big\}. \end{aligned} \tag{2.50}$$

Since Eq. (2.50) follows as the long-time limit of Eq. (2.46), we may regard Eq. (2.46) as a time-dependent generalization of the Meir–Wingreen formula which also takes the initial correlations into account.

2.2.3 Landauer–Büttiker formula

Let us then consider another well-known steady-state result, and start from Eq. (2.49). In the absence of interactions we may write the lesser Green's function simply in terms of the embedding self-energy as (since the many-body self-energy is zero) [73]

$$G^<_{CC}(\omega) = G^\mathrm{R}_{CC}(\omega)(\Sigma_{\mathrm{em}})^<_{CC}(\omega) G^\mathrm{A}_{CC}(\omega), \tag{2.51}$$

where $(\Sigma_{\mathrm{em}})^<_{CC}(\omega) = \sum_\alpha (\Sigma_{\mathrm{em},\alpha})^<_{CC}(\omega)$. In this case, we may also insert the same fluctuation–dissipation relation for the lesser self-energy as above, and we obtain for the current through the interface between the central region and the α-th lead

$$\begin{aligned} I_\alpha &= 2\mathrm{i}q \int \frac{\mathrm{d}\omega}{2\pi} \sum_\beta \mathrm{Tr}_C \Big[\mathrm{i} f_\alpha(\omega)(\Gamma_\alpha)_{CC}(\omega) G^\mathrm{R}_{CC}(\omega)(\Gamma_\beta)_{CC}(\omega) G^\mathrm{A}_{CC}(\omega) \\ &\qquad - \mathrm{i} f_\beta(\omega)(\Gamma_\alpha)_{CC}(\omega) G^\mathrm{R}_{CC}(\omega)(\Gamma_\beta)_{CC}(\omega) G^\mathrm{A}_{CC}(\omega) \Big] \\ &= 2q \int \frac{\mathrm{d}\omega}{2\pi} \sum_\beta \left[f_\beta(\omega) - f_\alpha(\omega) \right] T_{\alpha\beta}(\omega), \end{aligned} \tag{2.52}$$

where we defined *the transmission function*

$$T_{\alpha\beta}(\omega) = \mathrm{Tr}_C \left[(\Gamma_\alpha)_{CC}(\omega) G^\mathrm{R}_{CC}(\omega)(\Gamma_\beta)_{CC}(\omega) G^\mathrm{A}_{CC}(\omega) \right]. \tag{2.53}$$

Limiting ourselves again to a two-terminal setting, we may evaluate the current through the noninteracting system as a difference $I = I_R - I_L$

$$I = 4q \int \frac{\mathrm{d}\omega}{2\pi} \left[f_L(\omega) - f_R(\omega) \right] \mathrm{Tr}_C \left[(\Gamma_L)_{CC}(\omega) G^{\mathrm{R}}_{CC}(\omega) (\Gamma_R)_{CC}(\omega) G^{\mathrm{A}}_{CC}(\omega) \right] \tag{2.54}$$

which is typically called *the Landauer–Büttiker formula* [73, 91, 92, 117]. If we know the transmission function $T(\omega) = T_{LR}(\omega)$, the conductance of the central region may be calculated from *the Landauer formula* [91, 117]

$$G = \frac{2e^2}{h} T(\omega) = \frac{2e^2}{h} \mathrm{Tr}_C \left[(\Gamma_L)_{CC}(\omega) G^{\mathrm{R}}_{CC}(\omega) (\Gamma_R)_{CC}(\omega) G^{\mathrm{A}}_{CC}(\omega) \right], \tag{2.55}$$

where e is the electron charge and h the Planck's constant. The factor $G_0 = 2e^2/h$ is often termed *the conductance quantum*.

2.2.4 Basic concepts and an example calculation

Let us illustrate the basic concepts in quantum transport and the use of the Landauer–Büttiker formalism discussed above by means of an example. Consider an ethylene molecule C_2H_4 and a single π-orbital structure around the two carbon atoms. We choose accordingly the basis as the states $|1\rangle$ and $|2\rangle$, where the π-electron is localized around either the 1st or the 2nd carbon atom. The Hamiltonian then takes the form

$$H_{CC} = \begin{pmatrix} \epsilon_0 & -t \\ -t & \epsilon_0 \end{pmatrix}, \tag{2.56}$$

where ϵ_0 is the on-site energy for a carbon atom and t is a probability amplitude for an electron to jump from one carbon atom to the other. The energies and the corresponding stationary states of the Hamiltonian are

$$\epsilon_\pm = \epsilon_0 \pm t, \qquad |\epsilon_\pm\rangle = \frac{1}{\sqrt{2}} \left(|1\rangle \mp |2\rangle \right). \tag{2.57}$$

We could then express the Hamiltonian also in the molecular orbital basis as

$$\widetilde{H}_{CC} = \begin{pmatrix} \epsilon_- & 0 \\ 0 & \epsilon_+ \end{pmatrix}. \tag{2.58}$$

Then, we want to couple the molecule to two leads, and the coupling is described by the embedding self-energy

$$(\Sigma_{\mathrm{em},\alpha})^{\mathrm{R}}_{CC}(\omega) = -\mathrm{i}\,\mathrm{diag}(\gamma_{-,\alpha}/2, \gamma_{+,\alpha}/2), \tag{2.59}$$

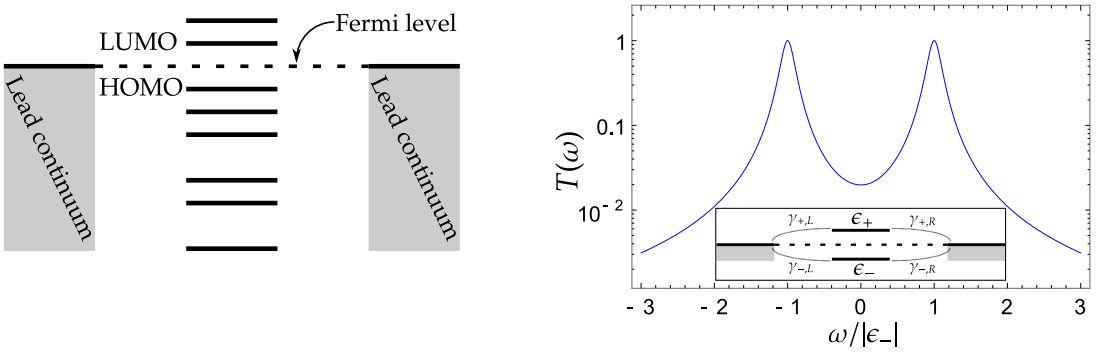

(a) Transport setup for a molecule (discrete spectrum) attached to two leads (continuum spectrum). The Fermi energy is in the HOMO–LUMO gap.

(b) Transmission of the two-level molecule as a function of energy. The inset shows the transport setup through the π orbitals and the parameters corresponding to Eq. (2.60).

Fig. 2.3: Basic concepts in a transport setup explained by an example calculation.

i.e., $(\Gamma_\alpha)_{CC}(\omega) = (\Gamma_\alpha)_{CC} = \mathrm{diag}(\gamma_{-,\alpha}, \gamma_{+,\alpha})$ with $\gamma_{\mp,\alpha}$ being positive (real) constants. As the level-width functions are frequency independent, this is also called *wide-band approximation* (WBA) since the frequency dependency of the lead states is considered constant when compared to the two discrete states of the central region. In this approximation, also the real parts of the embedding self-energy may be dropped due to Kramers–Kronig relations [73, 118] (if the imaginary part of the embedding self-energy is constant, then the real part becomes zero), or they may be absorbed into $\epsilon_\pm$. In addition to the simple π-orbital framework, there are also σ orbitals in the ethylene molecule to keep the structure together. However, the π orbitals give, in this case, the *highest occupied molecular orbital* (HOMO) and the *lowest unoccupied molecular orbital* (LUMO) which then are responsible for the electron transport through the structure. We will not describe these orbitals rigorously here but only state that the level structure of the central region is, in principle, more complicated than in Eq. (2.57). More generally, the transport setup is something like in Fig. 2.3a. Here the levels below the Fermi level are occupied whereas the states above the Fermi level are unoccupied. The leads' continuum of states and the discrete spectrum of the molecule may also be shifted in energy to model voltage profiles, i.e., biasing and gating.

Typically we are only interested in the channels responsible for the transport, in this case, the π orbitals, and we may evaluate the transmission function by inserting the matrix structures into Eqs. (2.17) and (2.53) and find

$$\begin{aligned} T(\omega) &= \mathrm{Tr}_C\left[(\Gamma_L)_{CC} G^{\mathrm{R}}_{CC}(\omega)(\Gamma_R)_{CC} G^{\mathrm{A}}_{CC}(\omega)\right] \\ &= \frac{\gamma_{-,L}\gamma_{-,R}}{(\omega-\epsilon_-)^2 + (\gamma_{-,L}+\gamma_{-,R})^2/4} + \frac{\gamma_{+,L}\gamma_{+,R}}{(\omega-\epsilon_+)^2 + (\gamma_{+,L}+\gamma_{+,R})^2/4}. \end{aligned} \tag{2.60}$$

We plot the transmission in Fig. 2.3b with parameters $\epsilon_+ = -\epsilon_-$ and $\gamma_{-,L} = \gamma_{+,L} = \gamma_{-,R} = \gamma_{+,R} = |\epsilon_-|/10$. We notice that the transmission approaches one when the energy is in resonance with the molecular orbitals and that it decays as ω^{-2} elsewhere. This means that when we expose the system to the amount of energy corresponding to the resonances, we get a functioning transmission channel. The transmission and further the conductance given by the Landauer formula in Eq. (2.55) work in this way as *response functions*: they describe the system's response to an external perturbation, in this case, given by the parameters leading to the resonant energy levels. The width of the resonance peaks is determined by the parameters $\gamma_{\mp,\alpha}$. This means that when the coupling of the molecule to the leads is stronger the resonances become wider and it is easier to get a nonzero transmission and conductance even if the external perturbation did not match the resonant level exactly.

2.2.5 Equations of motion for a noninteracting central molecule within the wide-band approximation

When deriving the equations of motion (2.38) in the previous section we defined the embedding self-energy, Σ_{em}, accounting for the coupling between the molecule and the lead environment. In addition to the isolated Green's function $G_{\alpha\alpha}$ this quantity, as well, is independent of the electronic interactions, and is completely specified by the Hamiltonian of the reservoirs

$$(\Sigma_{\text{em},\alpha})^{\text{R}}_{mn}(\omega) = \sum_k (h_{C\alpha})_{mk}[g^{\text{R}}_{\alpha\alpha}(\omega)]_{kk}(h_{\alpha C})_{kn} = \sum_k T_{mk\alpha}\frac{1}{(\omega + \text{i}\eta) - (\epsilon_{k\alpha} + V_\alpha)}T_{k\alpha n}\,, \tag{2.61}$$

where we wrote explicitly the diagonal elements of the lead Hamiltonian on the horizontal branch of the Keldysh contour. The imaginary part of the embedding self-energy is related to the level-width function

$$(\Gamma_\alpha)_{mn}(\omega) = 2\pi\sum_k T_{mk\alpha}\delta(\omega - \epsilon_{k\alpha} - V_\alpha)T_{k\alpha n}. \tag{2.62}$$

Also, as seen in the example calculation in the previous section, for these objects WBA is often assumed, i.e., that the eigenvalues of the Hamiltonian for the central molecule are well inside the continuum spectrum of the reservoirs $\epsilon_{k\alpha}$. In WBA the level-width function is assumed frequency independent and the retarded Keldysh component of the embedding self-energy becomes [see also Eq. (2.11)] for indices $m, n \in C$

$$(\Sigma_{\text{em},\alpha})^{\text{R}}_{mn}(\omega) \approx -\frac{\text{i}}{2}(\Gamma_\alpha)_{mn}. \tag{2.63}$$

This means that when the energy bands of the leads are 'wide' the embedding self-energy can be assumed to be a purely imaginary constant with respect to frequency ω.

Employing WBA for the embedding self-energy in time domain therefore gives

$$(\Sigma_{\mathrm{em},\alpha})^{\mathrm{R}}_{mn}(t,t') = \int_{-\infty}^{\infty} \frac{\mathrm{d}\omega}{2\pi} \mathrm{e}^{-\mathrm{i}\omega(t-t')} (\Sigma_{\mathrm{em},\alpha})^{\mathrm{R}}_{mn}(\omega) = -\frac{\mathrm{i}}{2}(\Gamma_\alpha)_{mn}\delta(t-t'). \tag{2.64}$$

Even though the form of this function is, at this stage, rather abstract, this is a key step when we start solving the equations of motion (2.38). When we drop the interactions, i.e., consider the limit of free electrons or ballistic transport, and set $\Sigma_{\mathrm{mb}} = 0$, we are left with the contribution only from the embedding self-energy on the right-hand side of Eq. (2.38). In addition to this, when we employ the WBA for the embedding self-energy as in Eq. (2.64) the equation of motion for G becomes a closed differential equation which can be solved analytically.

Now we apply the assumption of a noninteracting central molecule. Then the many-body self-energy for the central part Σ_{mb} in Eq. (2.38) vanishes and we are left with the embedding self-energy Σ_{em} only. The equations of motion simplify correspondingly (let us also lighten the notation by dropping the subscripts '*CC*' and 'em' as there should be no danger of misunderstanding any more)

$$\left[\mathrm{i}\frac{\mathrm{d}}{\mathrm{d}z} - h(z)\right] G(z,z') = \delta(z,z') + \int_\gamma \mathrm{d}\bar{z}\Sigma(z,\bar{z})G(\bar{z},z'), \tag{2.65}$$

$$G(z,z')\left[-\mathrm{i}\frac{\overleftarrow{\mathrm{d}}}{\mathrm{d}z'} - h(z')\right] = \delta(z,z') + \int_\gamma \mathrm{d}\bar{z}G(z,\bar{z})\Sigma(\bar{z},z'). \tag{2.66}$$

(Let us, from now on, also call the embedding self-energy simply as the self-energy since it is the only self-energy contribution left.) By using the Langreth rules [73, 116] in these equations of motion, (2.65) and (2.66), we are able to extract the lesser Green's function, $G^<$, from which many interesting physical quantities, such as electron densities and currents, can be obtained. We are mainly interested in the time-diagonal of the lesser Green's function $G^<(t,t)$ since this is directly related to the one-particle density matrix as $\rho(t) = -\mathrm{i}G^<(t,t)$, and this quantity can be obtained by subtracting Eq. (2.66) from Eq. (2.65), then setting $z = t_-$ and $z' = t'_+$, and then taking the time-local limit $t_+ \to t_-$. This procedure involves somewhat tedious bookkeeping for which the details can be found in Pub. [I] and we state here only the result

$$\mathrm{i}\frac{\mathrm{d}}{\mathrm{d}t}G^<(t,t) - [h(t), G^<(t,t)] = -\left[G^{\mathrm{R}} \cdot \Sigma^< + G^< \cdot \Sigma^{\mathrm{A}} + G^\rceil \star \Sigma^\lceil\right](t,t) + \mathrm{h.c.} \tag{2.67}$$

with the time-convolutions on the Keldysh contour being defined in Eq. (2.47). This is the final form for the equation of motion for the lesser Green's function in the equal-time limit we are trying to solve. The underlining assumption in deriving Eq. (2.67) is the neglecting of the electron–electron interactions. Although not yet explicitly present in Eq. (2.67), the WBA for the self-energy is another assumption

we do in order to have a closed equation for G. This seems a rather unreasonable price to pay but the reward is that Eq. (2.67) may be solved analytically. If we lift the assumptions, we are left with solving numerically the full Kadanoff–Baym equations (2.27) and (2.28) which itself is a very demanding task although the reward is the more complete description of the underlining physical processes in the quantum transport setup.

From Eq. (2.67) we may already extract some physical information about the transport setup. If we set the right-hand side to zero, we have a reduction to a Liouville-type equation for the one-particle density matrix $\rho = -\mathrm{i}G^<$ of the isolated central region. The self-energy, by construction, accounts for the openness of region C. The terms inside the square brackets also have a transparent physical interpretation. The first term is a convolution between the propagator in region C, G^R and the probability of finding an electron in the lead $\Sigma^<$. This can be interpreted as a source term describing the injection of electrons into region C. The second term has the opposite structure: a propagator in the leads, Σ^A, is convolved with $G^<$ which is proportional to the probability of finding an electron in region C. This term can therefore be interpreted as a drain term and is responsible for damping and equilibration effects. The last term accounts for the initial preparation of the system. In *the partitioned approach*, where the terminals are considered initially uncontacted and in equilibrium at different chemical potentials, this term would be zero since the hopping integrals $T_{k\alpha m} = 0$ in equilibrium [93, 94, 99]. However, in *the partition-free approach* [95, 96], where the system is initially contacted and in equilibrium at a unique chemical potential and then driven out of equilibrium by a potential between the terminals, this term is nonzero and accounts for the initial coupling of the central region to the leads.

2.3 Solving the equations of motion for the Green's function

As we have now obtained an integro–differential equation of motion (2.67) for the equal-time lesser Green's function, we would like to solve this equation in a closed form. For closing the equation for $G^<$, i.e., that the solution does not involve any iteration or time-propagation schemes, we would need the time-convolutions on right-hand side of Eq. (2.67). In particular, the time-convolution involving $G^<$ should be coupled with the terms on the left-hand side. For this, we employ the wide-band approximation discussed in the previous section.

First, we see how the different Keldysh components of the self-energies can be obtained from the WBA result for the retarded/advanced self-energy. Second, we

will evaluate the corresponding Green's function components to be inserted in the convolution integrals in Eq. (2.67). Once we have expressions for the time-convolutions, the remaining differential equation may be solved uniquely. Most of the details of the derivations will be deferred to appendix.

2.3.1 Effective Hamiltonian and the corresponding eigenbasis

Before solving Eq. (2.67) we need to find expressions for the time-convolutions inside the square brackets on the right-hand side. This procedure starts from the WBA for the self-energy; from the retarded and advanced Keldysh components we get an expression for the Matsubara component, and further from this we can derive expressions for the left/right and greater/lesser components. Similarly, when we know the Matsubara self-energy, we may express the Matsubara Green's function, and further use this to derive the left/right components of the Green's function. From the WBA we also readily get the retarded/advanced Green's functions. These derivations of the different Keldysh components are straightforward but a little technical so we shift the details to Appendix A.1.1, and state here only the necessary expressions in order to proceed. For further convenience, we introduce a non-hermitian *effective Hamiltonian* as

$$h_{\text{eff}} = h - \frac{\mathrm{i}}{2}\Gamma; \qquad h_{\text{eff}}^{\dagger} = h + \frac{\mathrm{i}}{2}\Gamma, \tag{2.68}$$

where $\Gamma = \sum_\alpha \Gamma_\alpha$ is a positive semi-definite matrix accounting for the total contribution from the coupling of the central molecule to leads α, see Eq. (2.63). Due to non-hermiticity this object has separate left and right eigenvectors forming a mutually *biorthogonal* set $\{|\Psi_j^{\text{L}}\rangle, |\Psi_j^{\text{R}}\rangle\}$ with

$$\begin{cases} \langle\Psi_j^{\text{L}}|h_{\text{eff}} = \epsilon_j\langle\Psi_j^{\text{L}}|, \\ h_{\text{eff}}|\Psi_j^{\text{R}}\rangle = \epsilon_j|\Psi_j^{\text{R}}\rangle, \end{cases} \tag{2.69}$$

where the eigenvalues ϵ are, in general, complex. By the biorthogonality we have $\langle\Psi_j^{\text{L}}|\Psi_k^{\text{R}}\rangle = \delta_{jk}\langle\Psi_j^{\text{L}}|\Psi_j^{\text{R}}\rangle$, where we can choose an appropriate normalization of the diagonal elements. The resolution of identity in terms of the left/right eigenbasis also works pairwise

$$\hat{\mathbb{1}} = \sum_j \frac{|\Psi_j^{\text{R}}\rangle\langle\Psi_j^{\text{L}}|}{\langle\Psi_j^{\text{L}}|\Psi_j^{\text{R}}\rangle} = \sum_j \frac{|\Psi_j^{\text{L}}\rangle\langle\Psi_j^{\text{R}}|}{\langle\Psi_j^{\text{R}}|\Psi_j^{\text{L}}\rangle}. \tag{2.70}$$

2.3.2 Terms in the equation of motion (2.67)

The Keldysh components of the self-energies and Green's functions in Eq. (2.67) in terms of the effective Hamiltonian read (see App. A.1.1)

$$\Sigma^<_{\alpha,mn}(t,t') = \mathrm{i}\Gamma_{\alpha,mn}\int\frac{\mathrm{d}\omega}{2\pi}f(\omega-\mu)\mathrm{e}^{-\mathrm{i}(\omega+V_\alpha)(t-t')}, \tag{2.71}$$

$$\Sigma^\lceil_{\alpha,mn}(\tau,t) = \Gamma_{\alpha,mn}\frac{1}{-\mathrm{i}\beta}\sum_q \mathrm{e}^{-\omega_q\tau}\int\frac{\mathrm{d}\omega}{2\pi}\frac{\mathrm{e}^{\mathrm{i}(\omega+V_\alpha)t}}{\omega_q-\omega+\mu}, \tag{2.72}$$

$$G^\mathrm{R}(t,t') = -\mathrm{i}\theta(t-t')\mathrm{e}^{-\mathrm{i}h_\mathrm{eff}(t-t')}, \tag{2.73}$$

$$G^\rceil(t,\tau) = \mathrm{e}^{-\mathrm{i}h_\mathrm{eff}t}\left[G^\mathrm{M}(0,\tau)-\int_0^t\mathrm{d}t'\mathrm{e}^{\mathrm{i}h_\mathrm{eff}t'}\int_0^\beta\mathrm{d}\bar\tau\Sigma^\rceil(t',\bar\tau)G^\mathrm{M}(\bar\tau,\tau)\right], \tag{2.74}$$

where the sum over q is a sum over Matsubara frequencies $\omega_q = \frac{(2q+1)\pi}{-\mathrm{i}\beta}$ and f is the Fermi function. The advanced self-energy can be found from Eq. (2.64) by conjugating. Inserting these expressions into the definitions of the time-convolutions in Eq. (2.67) leads to (see App. A.1.2)

$$\left[G^\mathrm{R}\cdot\Sigma^<\right](t,t) = \mathrm{i}\sum_\alpha\int\frac{\mathrm{d}\omega}{2\pi}f(\omega-\mu)\left[1-\mathrm{e}^{\mathrm{i}(\omega+V_\alpha-h_\mathrm{eff})t}\right]G^\mathrm{R}(\omega+V_\alpha)\Gamma_\alpha, \tag{2.75}$$

$$\left[G^<\cdot\Sigma^\mathrm{A}\right](t,t) = \frac{\mathrm{i}}{2}G^<(t,t)\Gamma, \tag{2.76}$$

$$\left[G^\rceil\star\Sigma^\lceil\right](t,t) = \mathrm{i}\int\frac{\mathrm{d}\omega}{2\pi}f(\omega-\mu)\sum_\alpha\mathrm{e}^{\mathrm{i}(\omega+V_\alpha-h_\mathrm{eff})t}G^\mathrm{R}(\omega)\Gamma_\alpha. \tag{2.77}$$

2.3.3 Time-dependent density matrix and its interpretation

Then the expressions in the above equations may be inserted into Eq. (2.67), and this way we find

$$\begin{aligned}
&\mathrm{i}\frac{\mathrm{d}}{\mathrm{d}t}G^<(t,t)-[h,G^<(t,t)]\\
=\;&-\left\{\mathrm{i}\sum_\alpha\int\frac{\mathrm{d}\omega}{2\pi}f(\omega-\mu)\left[1-\mathrm{e}^{\mathrm{i}(\omega+V_\alpha-h_\mathrm{eff})t}\right]G^\mathrm{R}(\omega+V_\alpha)\Gamma_\alpha+\frac{\mathrm{i}}{2}G^<(t,t)\Gamma\right.\\
+\;&\left.\mathrm{i}\int\frac{\mathrm{d}\omega}{2\pi}f(\omega-\mu)\sum_\alpha\mathrm{e}^{\mathrm{i}(\omega+V_\alpha-h_\mathrm{eff})t}G^\mathrm{R}(\omega)\Gamma_\alpha\right\}+\mathrm{h.c.}
\end{aligned} \tag{2.78}$$

which is a nonhomogeneous, linear, first-order differential equation for $G^<(t,t)$ and, therefore, it can be solved explicitly. The solution is worked out in A.1.3 and reads

$$\begin{aligned} -\mathrm{i}G^<(t,t) &= \int \frac{\mathrm{d}\omega}{2\pi} f(\omega-\mu) \sum_\alpha \Big\{ A_\alpha(\omega+V_\alpha) \\ &+ V_\alpha \left[\mathrm{e}^{\mathrm{i}(\omega+V_\alpha-h_{\mathrm{eff}})t} G^{\mathrm{R}}(\omega) A_\alpha(\omega+V_\alpha) + \mathrm{h.c.} \right] \\ &+ V_\alpha^2 \mathrm{e}^{-\mathrm{i}h_{\mathrm{eff}}t} G^{\mathrm{R}}(\omega) A_\alpha(\omega+V_\alpha) G^{\mathrm{A}}(\omega) \mathrm{e}^{\mathrm{i}h_{\mathrm{eff}}^\dagger t} \Big\} , \end{aligned} \tag{2.79}$$

where we introduced the partial spectral function as [cf. Eq. (2.21)]

$$A_\alpha(\omega) = G^{\mathrm{R}}(\omega) \Gamma_\alpha G^{\mathrm{A}}(\omega) . \tag{2.80}$$

The full nonequilibrium spectral function is $A(\omega) = \sum_\alpha A_\alpha(\omega)$.

In Eq. (2.79) we have an explicit closed formula for the equal-time $G^<$ or, equivalently, for the time-dependent reduced one-particle density matrix (TD1RDM). This is a generalization of the static density matrix derived in the framework of Landauer and Büttiker, in Sec. 2.1, see Eq. (2.22). We see that the first row of Eq. (2.79), i.e., the time-independent part exactly corresponds to the form in Eq. (2.22) (with the addition of a bias voltage). Now, we may investigate what is the role of time-dependence, since all the terms inside the frequency integral in Eq. (2.79) may be calculated separately, and no time-propagation nor self-consistency algorithms are needed. By analyzing the terms we extract the following properties:

1. With no external bias, $V_\alpha = 0$, only the first row contributes. This term correctly gives the equilibrium value of the equal-time $G^<$ since at zero bias $\sum_\alpha A_\alpha(\omega)$ is the equilibrium spectral function, see also Eq. (2.22).

2. Both the second and the third row vanish exponentially in the long-time limit, and the equal-time $G^<$ approaches a unique steady-state value.

3. The transient dynamics is given by the second and the third row. By inserting a complete set of eigenstates of the effective Hamiltonian h_{eff}, see Eq. (2.69), we notice that:

   (a) The second row gives rise to oscillations with frequency $\omega_j = |\mu + V_\alpha - \mathrm{Re}\,\epsilon_j|$. These oscillations correspond to transitions between the biased Fermi level of the leads and the resonant levels of the central molecule (at comparatively low enough temperature).

   (b) The third term accounts for intramolecular transitions and gives rise to oscillations with frequency $\omega_{jk} = |\mathrm{Re}\,\epsilon_j - \mathrm{Re}\,\epsilon_k|$. These oscillations are visible only if the effective Hamiltonian h_{eff} does *not* commute with Γ_α. In the case that $[h_{\mathrm{eff}}, \Gamma_\alpha] = 0$ the time dependence of the third term is of the form $\mathrm{e}^{-\mathrm{i}h_{\mathrm{eff}}t + \mathrm{i}h_{\mathrm{eff}}^\dagger t} = \mathrm{e}^{-\Gamma t}$.

2.3.4 Time-dependent Landauer–Büttiker formula

As discussed earlier in Sec. 2.2.2 the time-dependent current through the interface between the central region and the α-th lead is calculated simply by

$$I_\alpha(t) = 4q\,\mathrm{Re}\left\{\mathrm{Tr}\left[\Sigma_\alpha^< \cdot G^\mathrm{A} + \Sigma_\alpha^\mathrm{R} \cdot G^< + \Sigma_\alpha^\rceil \star G^\lceil\right](t,t)\right\}, \tag{2.81}$$

where we shall use $q = -1$ for the electron charge and $\mathrm{Re}\{\mathrm{Tr}[A]\} = \mathrm{Tr}\{A + A^\dagger\}/2$ for the trace. Each of the terms in Eq. (2.81) carries similar information as already discussed with Eq. (2.67). For the terms inside Eq. (2.81) we may use previously obtained results in Eqs. (2.75), (2.76) and (2.77) with minor modifications:

$$\left[\Sigma_\alpha^< \cdot G^\mathrm{A}\right](t,t) = \mathrm{i}\int \frac{\mathrm{d}\omega}{2\pi} f(\omega-\mu)\Gamma_\alpha G^\mathrm{A}(\omega+V_\alpha)\left[1 - \mathrm{e}^{-\mathrm{i}(\omega+V_\alpha-h_\mathrm{eff}^\dagger)t}\right], \tag{2.82}$$

$$\left[\Sigma_\alpha^\mathrm{R} \cdot G^<\right](t,t) = -\frac{\mathrm{i}}{2}\Gamma_\alpha G^<(t,t), \tag{2.83}$$

$$\left[\Sigma_\alpha^\rceil \star G^\lceil\right](t,t) = \mathrm{i}\int \frac{\mathrm{d}\omega}{2\pi} f(\omega-\mu)\Gamma_\alpha G^\mathrm{A}(\omega)\mathrm{e}^{-\mathrm{i}(\omega+V_\alpha-h_\mathrm{eff}^\dagger)t}, \tag{2.84}$$

and correspondingly for the complex conjugated ones. In addition, we may use the already obtained result for $G^<(t,t)$ in Eq. (2.79). After some algebra (see App. A.1.4) we arrive at

$$\begin{aligned} I_\alpha(t) = -2\int \frac{\mathrm{d}\omega}{2\pi} f(\omega-\mu) \sum_\beta \mathrm{Tr}\Big\{ & \\ & \Gamma_\alpha G^\mathrm{R}(\omega+V_\beta)\Gamma_\beta G^\mathrm{A}(\omega+V_\beta) - \Gamma_\alpha G^\mathrm{R}(\omega+V_\alpha)\Gamma_\beta G^\mathrm{A}(\omega+V_\alpha) \\ + \; & V_\beta\left[\Gamma_\alpha \mathrm{e}^{\mathrm{i}(\omega+V_\beta-h_\mathrm{eff})t} G^\mathrm{R}(\omega)\left(-\mathrm{i}\delta_{\alpha\beta}G^\mathrm{R}(\omega+V_\beta) + A_\beta(\omega+V_\beta)\right) + \mathrm{h.c.}\right] \\ + \; & V_\beta^2 \Gamma_\alpha \mathrm{e}^{-\mathrm{i}h_\mathrm{eff}t} G^\mathrm{R}(\omega) A_\beta(\omega+V_\beta) G^\mathrm{A}(\omega)\mathrm{e}^{\mathrm{i}h_\mathrm{eff}^\dagger t}\Big\}. \end{aligned} \tag{2.85}$$

The physical interpretation of the terms in Eq. (2.85) is similar to the one after Eq. (2.79). We have a steady-state part given by the first two rows, which can be identified as the Landauer–Büttiker formula in Eq. (2.54). The time-dependent part is given by the second and the third rows, and it vanishes exponentially in the long-time limit and the oscillations in the current have the same structure as in the reduced one-particle density matrix.

2.3.5 Evaluating the densities and currents in practice

Looking at the final formulae in Eqs. (2.79) and (2.85) we are left with numerical integration. These are one-dimensional integrals over the frequency ω but they

may be tedious to perform, at least for larger systems. The integrands (related to the spectral functions) for larger systems are, in fact, heavily oscillatory and spiked functions. Although we know the positions of the spectral peaks (as the real parts of the eigenvalues of h_{eff}), the dense frequency grids (even if adaptive) to model the spectral peaks accurately might be computationally rather expensive. There is, however, a way around this problem by looking at the matrix structures more carefully.

We may expand the results in Eq. (2.79) and (2.85) in terms of the eigenbasis of the non-hermitian effective Hamiltonian h_{eff}. As noticed earlier in Eq. (2.69), this object has separate left and right eigenvectors, hence, extra care must be taken. We notice that in Eq. (2.79), in every term there is h_{eff} on the left and $h_{\text{eff}}^\dagger$ on the right. This in mind, and looking at how the matrix operates in Eq. (2.69), we choose to expand in the "left–left" eigenbasis, i.e., we multiply the density matrix $\rho(t) = -\mathrm{i}G^<(t,t)$ in Eq. (2.79) from left by a row vector $\langle\Psi_j^{\text{L}}|$ and from the right by a column vector $|\Psi_k^{\text{L}}\rangle$. This gives

$$
\begin{aligned}
&\rho_{jk}(t) \coloneqq \langle\Psi_j^{\text{L}}|\rho(t)|\Psi_k^{\text{L}}\rangle \\
= &\sum_\alpha \int \frac{\mathrm{d}\omega}{2\pi} f(\omega-\mu)\left\{\langle\Psi_j^{\text{L}}|\frac{1}{\omega+V_\alpha-h_{\text{eff}}}\Gamma_\alpha\frac{1}{\omega+V_\alpha-h_{\text{eff}}^\dagger}|\Psi_k^{\text{L}}\rangle\right. \\
+ &V_\alpha\left[\langle\Psi_j^{\text{L}}|\mathrm{e}^{\mathrm{i}(\omega+V_\alpha-h_{\text{eff}})t}\frac{1}{\omega-h_{\text{eff}}}\frac{1}{\omega+V_\alpha-h_{\text{eff}}}\Gamma_\alpha\frac{1}{\omega+V_\alpha-h_{\text{eff}}^\dagger}|\Psi_k^{\text{L}}\rangle+\text{h.c.}\right] \\
+ &\left.V_\alpha^2\langle\Psi_j^{\text{L}}|\mathrm{e}^{-\mathrm{i}h_{\text{eff}}t}\frac{1}{\omega-h_{\text{eff}}}\frac{1}{\omega+V_\alpha-h_{\text{eff}}}\Gamma_\alpha\frac{1}{\omega+V_\alpha-h_{\text{eff}}^\dagger}\frac{1}{\omega-h_{\text{eff}}^\dagger}\mathrm{e}^{\mathrm{i}h_{\text{eff}}t}|\Psi_k^{\text{L}}\rangle\right\}. \qquad (2.86)
\end{aligned}
$$

From Eq. (2.69) we know how the effective Hamiltonian h_{eff} operates on its eigenvectors, and we obtain

$$
\begin{aligned}
&\rho_{jk}(t) \\
= &\sum_\alpha \int \frac{\mathrm{d}\omega}{2\pi} f(\omega-\mu)\left\{\frac{1}{\omega+V_\alpha-\epsilon_j}\langle\Psi_j^{\text{L}}|\Gamma_\alpha|\Psi_k^{\text{L}}\rangle\frac{1}{\omega+V_\alpha-\epsilon_k^*}\right. \\
+ &V_\alpha\left[\mathrm{e}^{\mathrm{i}(\omega+V_\alpha-\epsilon_j)t}\frac{1}{\omega-\epsilon_j}\frac{1}{\omega+V_\alpha-\epsilon_j}\langle\Psi_j^{\text{L}}|\Gamma_\alpha|\Psi_k^{\text{L}}\rangle\frac{1}{\omega+V_\alpha-\epsilon_k^*}+\text{h.c.}\right] \\
+ &\left.V_\alpha^2\mathrm{e}^{-\mathrm{i}\epsilon_j t}\frac{1}{\omega-\epsilon_j}\frac{1}{\omega+V_\alpha-\epsilon_j}\langle\Psi_j^{\text{L}}|\Gamma_\alpha|\Psi_k^{\text{L}}\rangle\frac{1}{\omega+V_\alpha-\epsilon_k^*}\frac{1}{\omega-\epsilon_k^*}\mathrm{e}^{\mathrm{i}\epsilon_k^* t}\right\}. \qquad (2.87)
\end{aligned}
$$

This can be written in a very compact form by introducing

$$
\begin{aligned}
\Gamma_{\alpha,jk} &= \langle\Psi_j^{\text{L}}|\Gamma_\alpha|\Psi_k^{\text{L}}\rangle, &(2.88)\\
\Lambda_{\alpha,jk} &= \int\frac{\mathrm{d}\omega}{2\pi}\frac{f(\omega-\mu)}{(\omega+V_\alpha-\epsilon_j)(\omega+V_\alpha-\epsilon_k^*)}, &(2.89)
\end{aligned}
$$

$$\Pi_{\alpha,jk}(t) = \int \frac{\mathrm{d}\omega}{2\pi} \frac{f(\omega-\mu)\mathrm{e}^{\mathrm{i}(\omega+V_\alpha-\epsilon_j)t}}{(\omega-\epsilon_j)(\omega+V_\alpha-\epsilon_j)(\omega+V_\alpha-\epsilon_k^*)}, \tag{2.90}$$

$$\Omega_{\alpha,jk} = \int \frac{\mathrm{d}\omega}{2\pi} \frac{f(\omega-\mu)}{(\omega-\epsilon_j)(\omega+V_\alpha-\epsilon_j)(\omega+V_\alpha-\epsilon_k^*)(\omega-\epsilon_k^*)}. \tag{2.91}$$

Then, the density matrix elements in the left–left eigenbasis become

$$\rho_{jk}(t) = \sum_\alpha \left\{ \Gamma_{\alpha,jk}\Lambda_{\alpha,jk} + V_\alpha \Gamma_{\alpha,jk}\left[\Pi_{\alpha,jk}(t) + \Pi^*_{\alpha,kj}(t)\right] + V_\alpha^2 \Gamma_{\alpha,jk}\mathrm{e}^{-\mathrm{i}(\epsilon_j-\epsilon_k^*)t}\Omega_{\alpha,jk}\right\}. \tag{2.92}$$

It is important to notice that we only expressed the earlier result in a particular basis but the original complexity in the frequency integrals is still present in evaluating Eqs. (2.89), (2.90) and (2.91).

In Pub. [II] we evaluated the integrals in Eqs. (2.89), (2.90) and (2.91) analytically in the zero-temperature limit. The Fermi function in the zero-temperature limit reduces to the Heaviside function, and adjusting accordingly the integrals' limits, we get the following explicit expressions (the superscript '0' denotes zero temperature)

$$\begin{aligned} &\Lambda^0_{\alpha,jk} \\ &= \frac{\mathrm{Log}(\epsilon_k^*-\mu_\alpha) - \mathrm{Log}(\epsilon_j-\mu_\alpha)}{2\pi(\epsilon_k^*-\epsilon_j)}, \end{aligned} \tag{2.93}$$

$$\begin{aligned} &\Pi^0_{\alpha,jk}(t) \\ &= \frac{\mathrm{e}^{-\mathrm{i}(\epsilon_j-\mu_\alpha)t}\left\{F[\mathrm{i}(\epsilon_k^*-\mu_\alpha)t] + \frac{\epsilon_k^*-\epsilon_j-V_\alpha}{V_\alpha}F[\mathrm{i}(\epsilon_j-\mu_\alpha)t] - \frac{\epsilon_k^*-\epsilon_j}{V_\alpha}F[\mathrm{i}(\epsilon_j-\mu)t]\right\}}{2\pi(\epsilon_k^*-\epsilon_j)(\epsilon_k^*-\epsilon_j-V_\alpha)}, \end{aligned} \tag{2.94}$$

$$\begin{aligned} &\Omega^0_{\alpha,jk} \\ &= \frac{1}{2\pi\left[(\epsilon_k^*-\epsilon_j)V_\alpha^3 - (\epsilon_k^*-\epsilon_j)^3 V_\alpha\right]}\left\{(\epsilon_k^*-\epsilon_j+V_\alpha)\left[\mathrm{Log}(\epsilon_k^*-\mu_\alpha) - \mathrm{Log}(\epsilon_j-\mu)\right]\right. \\ &\quad \left. + (\epsilon_k^*-\epsilon_j-V_\alpha)\left[\mathrm{Log}(\epsilon_j-\mu_\alpha) - \mathrm{Log}(\epsilon_k^*-\mu)\right]\right\}, \end{aligned} \tag{2.95}$$

where we defined $\mu_\alpha = \mu + V_\alpha$ and

$$F(z) = \begin{cases} \mathrm{e}^z\left[2\pi\mathrm{i} - \mathrm{E}_1(z)\right], & \text{if } \mathrm{Arg}(z) \in]-\pi, -\pi/2] \\ -\mathrm{e}^z\mathrm{E}_1(z), & \text{otherwise.} \end{cases} \tag{2.96}$$

Log is the principal branch complex logarithm function, Arg the principal argument and E_1 the exponential integral function:

$$\mathrm{E}_1(z) = \int_1^\infty \frac{\mathrm{e}^{-zt}}{t}\,\mathrm{d}t. \tag{2.97}$$

The piecewise definition of the function F is due to branch cuts in the z-plane. Now, the complexity of the numerical integration is overcome as we have analytic expressions where we can simply insert our system parameters. (However, this finding does not necessarily mean the final expressions would not be complicated.) It is still to be noted, that the expressions include a special function (the exponential integral) which again, in principle, needs a numerical integration. However, the algorithms presented in Ref. [119] offer a very fast and accurate treatment.

As can be seen from expressions in Eqs. (2.93), (2.94) and (2.95) the case of degenerate eigenvalues ϵ_j (when the imaginary part is zero) leads to unphysical results because of denominators going to zero. It is, regardless of that, possible that the structure of the single-particle Hamiltonian h would together with the coupling matrices Γ_α produce such an effective Hamiltonian h_{eff} with $\epsilon_j = \epsilon_k^*$. In this case, consider the left/right eigenbasis of the effective Hamiltonian h_{eff}. Since $h_{\text{eff}} = h - \frac{\mathrm{i}}{2}\Gamma$, where h and Γ are hermitian matrices, then

$$\epsilon_j \langle \Psi_j^{\mathrm{L}} | \Psi_j^{\mathrm{L}} \rangle = \langle \Psi_j^{\mathrm{L}} | h_{\text{eff}} | \Psi_j^{\mathrm{L}} \rangle = \langle \Psi_j^{\mathrm{L}} | h | \Psi_j^{\mathrm{L}} \rangle - \frac{\mathrm{i}}{2} \langle \Psi_j^{\mathrm{L}} | \Gamma | \Psi_j^{\mathrm{L}} \rangle, \tag{2.98}$$

and we may solve for the eigenvalue

$$\epsilon_j = \frac{\langle \Psi_j^{\mathrm{L}} | h | \Psi_j^{\mathrm{L}} \rangle}{\langle \Psi_j^{\mathrm{L}} | \Psi_j^{\mathrm{L}} \rangle} - \frac{\frac{\mathrm{i}}{2} \langle \Psi_j^{\mathrm{L}} | \Gamma | \Psi_j^{\mathrm{L}} \rangle}{\langle \Psi_j^{\mathrm{L}} | \Psi_j^{\mathrm{L}} \rangle}. \tag{2.99}$$

Since the expectation values are real and the norms positive, we get

$$\operatorname{Im} \epsilon_j = -\frac{1}{2} \frac{\langle \Psi_j^{\mathrm{L}} | \Gamma | \Psi_j^{\mathrm{L}} \rangle}{\langle \Psi_j^{\mathrm{L}} | \Psi_j^{\mathrm{L}} \rangle} < 0 \tag{2.100}$$

meaning that the eigenvalues of h_{eff} lie in the lower-half plane (and correspondingly the ones of $h_{\text{eff}}^\dagger$ in the upper-half plane). Then, suppose that $\operatorname{Im} \epsilon_j = 0$. This gives $\langle \Psi_j^{\mathrm{L}} | \Gamma | \Psi_j^{\mathrm{L}} \rangle = 0$, and since the level-width matrices are calculated from the tunneling matrices by $\Gamma \sim T^\dagger T$, we get

$$\langle \Psi_j^{\mathrm{L}} | T^\dagger T | \Psi_j^{\mathrm{L}} \rangle = 0 \;\Rightarrow\; \langle \Phi_j^{\mathrm{L}} | \Phi_j^{\mathrm{L}} \rangle = 0, \tag{2.101}$$

where $|\Phi_j^{\mathrm{L}}\rangle = T|\Psi_j^{\mathrm{L}}\rangle$. Having then a zero-norm vector $|\Phi_j^{\mathrm{L}}\rangle$ it means that vector itself must be zero: $0 = |\Phi_j^{\mathrm{L}}\rangle = T|\Psi_j^{\mathrm{L}}\rangle$ for all j. This means that $|\Psi_j^{\mathrm{L}}\rangle$ is an eigenvector of T with zero eigenvalue. In particular, $\Gamma|\Psi_j^{\mathrm{L}}\rangle = T^\dagger T|\Psi_j^{\mathrm{L}}\rangle = 0$, and hence

$$\Gamma_{jk} = \langle \Psi_j^{\mathrm{L}} | \Gamma | \Psi_k^{\mathrm{L}} \rangle = 0, \;\forall j,k. \tag{2.102}$$

Therefore, we do not have to calculate anything when $\operatorname{Im} \epsilon_j = 0$ because then the $\Gamma_{\alpha,jk}$ terms in the final formula [Eq. (2.92)] give zero contribution.

Recently, in Pub. [IV] the integrals in Eqs. (2.89), (2.90) and (2.91) were also performed analytically for arbitrary nonzero temperatures in the Fermi functions.[1] As this is a somewhat technical extension to the above formalism (evaluating complex integrals with Matsubara poles), only the final expressions are given here (the details can be found in Pub. [IV] and Ref. [120])

$$\Lambda_{\alpha,jk} = \frac{\mathrm{i}}{\epsilon_k^* - \epsilon_j}\left\{\frac{1}{\mathrm{e}^{\beta(\epsilon_k^*-\mu_\alpha)}+1} + \frac{1}{2\pi\mathrm{i}}\left[\psi\left(\frac{1}{2} - \frac{\beta(\epsilon_k^*-\mu_\alpha)}{2\pi\mathrm{i}}\right) - \psi\left(\frac{1}{2} - \frac{\beta(\epsilon_j-\mu_\alpha)}{2\pi\mathrm{i}}\right)\right]\right\}, \tag{2.103}$$

$$\begin{aligned}\Pi_{\alpha,jk}(t) = {} & \frac{\mathrm{i}}{(\epsilon_k^*-\epsilon_j)(\epsilon_k^*-\epsilon_j-V_\alpha)}\left\{\frac{\mathrm{e}^{-\mathrm{i}(\epsilon_j-\epsilon_k^*)t}}{\mathrm{e}^{\beta(\epsilon_k^*-\mu_\alpha)}+1} + \mathrm{i}\mathrm{e}^{-\pi t/\beta}\mathrm{e}^{-\mathrm{i}(\epsilon_j-\mu_\alpha)t}\times\right. \\ & \left.\left[\bar{F}(\epsilon_k^*-\mu_\alpha,t,\beta) + \frac{\epsilon_k^*-\epsilon_j-V_\alpha}{V_\alpha}\bar{F}(\epsilon_j-\mu_\alpha,t,\beta) - \frac{\epsilon_k^*-\epsilon_j}{V_\alpha}\bar{F}(\epsilon_j-\mu,t,\beta)\right]\right\},\end{aligned} \tag{2.104}$$

$$\begin{aligned}\Omega_{\alpha,jk} = {} & \frac{\frac{\mathrm{i}}{\mathrm{e}^{\beta(\epsilon_k^*-\mu)}+1} - \frac{1}{2\pi}\left[\psi\left(\frac{1}{2} - \frac{\beta(\epsilon_j-\mu_\alpha)}{2\pi\mathrm{i}}\right) - \psi\left(\frac{1}{2} - \frac{\beta(\epsilon_k^*-\mu)}{2\pi\mathrm{i}}\right)\right]}{(\epsilon_k^*-\epsilon_j)(\epsilon_k^*-\epsilon_j+V_\alpha)V_\alpha} \\ & - \frac{\frac{\mathrm{i}}{\mathrm{e}^{\beta(\epsilon_k^*-\mu_\alpha)}+1} - \frac{1}{2\pi}\left[\psi\left(\frac{1}{2} - \frac{\beta(\epsilon_j-\mu)}{2\pi\mathrm{i}}\right) - \psi\left(\frac{1}{2} - \frac{\beta(\epsilon_k^*-\mu_\alpha)}{2\pi\mathrm{i}}\right)\right]}{(\epsilon_k^*-\epsilon_j)(\epsilon_k^*-\epsilon_j-V_\alpha)V_\alpha},\end{aligned} \tag{2.105}$$

where ψ is the digamma function [121] and we defined another special function by

$$\bar{F}(z,t,\beta) = \frac{1}{\mathrm{i}\beta z + \pi}\,{}_2F_1\left(1, \frac{1}{2} + \frac{\mathrm{i}\beta z}{2\pi}, \frac{3}{2} + \frac{\mathrm{i}\beta z}{2\pi}, \mathrm{e}^{-2\pi t/\beta}\right) \tag{2.106}$$

with ${}_2F_1$ being the hypergeometric function [122]. Inserting Eqs. (2.103), (2.104) and (2.105) into Eq. (2.92) gives then the TD1RDM at arbitrary temperature. When the asymptotic behaviour of the digamma and hypergeometric function is studied, the results in Eqs. (2.103), (2.104) and (2.105) can be shown to reduce to those in the zero-temperature limit [Eqs. (2.93), (2.94) and (2.95)], i.e., when $\beta \to \infty$.

Having now the full one-particle density matrix expressed in a general basis of the central region, we typically want to work specifically in a localized *site* basis of the central region. Evaluating the TD1RDM in the site basis (or in any physically relevant basis), $\{|m\rangle, |n\rangle\}$, is then readily done as a basis transformation from the 'left–left' eigenbasis to the desired one

$$\langle m|\rho(t)|n\rangle = \sum_{jk}\frac{\langle m|\Psi_j^{\mathrm{R}}\rangle}{\langle\Psi_j^{\mathrm{L}}|\Psi_j^{\mathrm{R}}\rangle}\frac{\langle\Psi_k^{\mathrm{R}}|n\rangle}{\langle\Psi_k^{\mathrm{R}}|\Psi_k^{\mathrm{L}}\rangle}\langle\Psi_j^{\mathrm{L}}|\rho(t)|\Psi_k^{\mathrm{L}}\rangle, \tag{2.107}$$

[1] To be supplemented in Ref. [120]

where $\{|\Psi^{\mathrm{R}}\rangle\}$ are the right eigenvectors of h_{eff}; this form in Eq. (2.107) follows from the biorthogonality of the left/right eigenvectors of a non-hermitian matrix. In the case of site basis, the diagonal elements of the density matrix give the charge densities corresponding to each atomic site of the central region whereas the off-diagonal elements give rise to transitions between sites, i.e., bond currents. Since the Green's function in Eq. (2.25) is of the form $G_{nm} = -\mathrm{i}\langle\mathcal{T}(\hat{d}_n\hat{d}_m^\dagger)\rangle$, and the density matrix is calculated from the lesser component as $\rho_{nm} = -\mathrm{i}G^<_{nm} = \langle\hat{d}_m^\dagger\hat{d}_n\rangle$, the bond-current operator may be defined, corresponding to current from site n to m,

$$\hat{J}_{mn} = -\mathrm{i}\left(T_{mn}\hat{d}_m^\dagger\hat{d}_n - \mathrm{h.c.}\right), \tag{2.108}$$

where $T_{mn} = T^*_{nm}$ are the hopping matrix elements in the central region. The expectation value of Eq. (2.108) then gives the bond currents

$$\langle\hat{J}_{mn}\rangle = J_{mn} = 2T_{mn}\,\mathrm{Im}\left[\rho_{nm}\right]. \tag{2.109}$$

Between the charge densities and bond currents there is an obvious continuity property

$$\partial_t n_m = \sum_n J_{mn} \tag{2.110}$$

meaning that the currents flowing in and out of site m must add up to the temporal change of density in that site.

2.4 Perturbations, superconductivity and time-dependent fields

In the previous sections we have introduced a time-dependent quantum transport model for which we could find an analytic solution reducing to earlier known results by Meir and Wingreen and Landauer and Büttiker. We also performed the frequency integrals analytically so that the final expressions could be implemented in terms of special functions such as the exponential integrals, digamma and hypergeometric functions.

In this section we further extend the transport model to include local perturbations in the central region. In practice, this amounts to adding separate Hamiltonians for the central region for the vertical and horizontal branches of the Keldysh contour; in equilibrium (Matsubara) the Hamiltonian takes the same form as in the previous section where as out of equilibrium we will consider another Hamiltonian including, e.g., on-site potential terms or complex phases for the hopping terms. It turns out, that this inclusion does not complicate the equations of motion considerably, and similar solution as in the previous section may be obtained.

2.4.1 Gate voltages, general potential profiles or magnetic fields within the central region

When studying transport in systems that are larger than, say few atoms, the step potential for the lead bias window may be questionable. In order to model a more realistic voltage profile, we could take a linear gate voltage within the central region, ranging from the left-lead biased energy levels to the right-lead biased energy levels. The gate profile in the central region could, for instance, take the following form

$$u(x) = -\frac{2V}{L}x + V, \tag{2.111}$$

where $\pm V$ is the bias window in the leads, L is the length of the central region and x is the coordinate in the central region, measured from the left lead's interface. A gate voltage of this form would then be included as on-site terms to the Hamiltonian of the central region

$$\widetilde{h} = h + \sum_{n,\sigma} u_n \hat{d}^\dagger_{n,\sigma}\hat{d}_{n,\sigma}. \tag{2.112}$$

Let us, however, keep the perturbation as general as possible, and simply state that the perturbed Hamiltonian of the central region is

$$\widetilde{h}_{mn} = T_{mn} + u_{mn}\ , \tag{2.113}$$

where $h = T$ is the non-perturbed Hamiltonian for the central region (ground state, Matsubara) and u is the perturbation in the central region which can take arbitrary forms. This means that we are not restricted to only additional on-site terms since $[\widetilde{h}, h] \neq 0$, in general.

Let us also briefly discuss the inclusion of a magnetic field; this contribution for the central region may be added by the Peierls substitution [123–125]. Instead of adding a perturbation u as in Eq. (2.113) we now transform the central region's Hamiltonian in terms of the phase factors α_{mn} which appear in the hopping matrix elements as

$$\widetilde{h}_{mn} = T_{mn}\mathrm{e}^{\mathrm{i}\alpha_{mn}} \tag{2.114}$$

with $\alpha_{mn} = -\alpha_{nm}$. Along a closed loop these factors yield the magnetic flux (normalized to the flux quantum $\Phi_0 = h/2e$). Let us look at the phase factors more thoroughly. Consider a lattice shown in Fig. 2.4 where we have an external magnetic field pointing in the negative z direction whereas the lattice itself is located in the xy-plane. The magnetic field therefore has the form $\vec{B} = -B\hat{e}_z$ for which we may choose the corresponding vector potential (in a convenient gauge) as $\vec{A} = \frac{B}{2}(y, -x, 0)^{\mathrm{T}}$. It is easily verified that $\vec{\nabla} \times \vec{A} = \vec{B}$. The magnetic flux is defined as a surface integral

$$\Phi = \iint_S \vec{B} \cdot \mathrm{d}\vec{S} = \oint_\gamma \vec{A} \cdot \mathrm{d}\vec{r}, \tag{2.115}$$

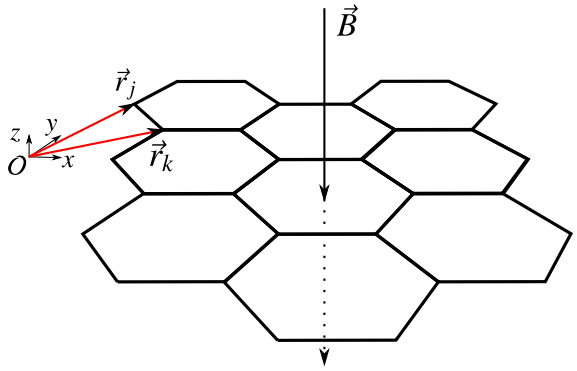

Fig. 2.4: Lattice in an external magnetic field.

where S is, in this case, a surface within the xy-plane in Fig. 2.4. By writing the magnetic field $\vec{B}$ in terms of the vector potential and using Stokes' theorem we may also write the second identity in Eq. (2.115) where γ is a path encircling the surface S counter-clockwise. By looking at Fig. 2.4 we see that the closed loops for the path integral are composed of paths between lattice points j and k: $\vec{r}_{jk} = \vec{r}_k - \vec{r}_j$. Between the lattice points j and k we may therefore parametrize the path as

$$\vec{\gamma}_{jk}(t) = (1-t)\vec{r}_j + t\vec{r}_k \quad \text{with} \quad t \in [0,1] \quad \text{and} \quad \frac{\mathrm{d}}{\mathrm{d}t}\vec{\gamma}_{jk}(t) = -\vec{r}_j + \vec{r}_k. \tag{2.116}$$

Then, the phase corresponding to the flux between lattice points j and k can be calculated as

$$\begin{aligned} \Phi_{jk} &= \int_{\gamma_{jk}} \vec{A}\cdot \mathrm{d}\vec{\gamma}_{jk} = \int_0^1 \vec{A}(\vec{\gamma}_{jk}(t))\cdot \frac{\mathrm{d}}{\mathrm{d}t}\vec{\gamma}_{jk}(t)\mathrm{d}t \\ &= \int_0^1 \frac{B}{2}\Big((1-t)y_j + ty_k, -(1-t)x_j - tx_k, 0\Big)\cdot\Big(-x_j + x_k, -y_j + y_k, -z_j + z_k\Big)\,\mathrm{d}t \\ &= \frac{B}{2}(x_k y_j - x_j y_k). \end{aligned} \tag{2.117}$$

The Peierls phase factors are indeed related to the magnetic flux by $\alpha_{mn} = \frac{e}{\hbar}\int_{\vec{r}_m}^{\vec{r}_n}\vec{A}\cdot\mathrm{d}\vec{r}$, where the line integral of the vector potential $\vec{A}$ goes from site m to site n [123, 125–127]. The prefactor $e/\hbar$ will therefore render the exponent in Eq. (2.114) dimensionless. (In Gaussian units an extra factor of the speed of light, c, appears.) Inclusion of the magnetic flux density B in the hopping matrix is therefore done by

$$T_{mn} \to T_{mn}\mathrm{e}^{\mathrm{i}\frac{e}{\hbar}\frac{B}{2}(x_n y_m - x_m y_n)} = T_{mn}\mathrm{e}^{2\pi\mathrm{i}B(x_n y_m - x_m y_n)/\Phi_0}, \tag{2.118}$$

where we inserted the flux quantum Φ_0. We see, that the transformation along a closed loop (2π) normalizes exactly to the flux quantum, the magnetic flux originating from $\sim Bx^2$. For these considerations, it is also sometimes advantageous

to introduce a quantity called *magnetic length*, $l_B = \sqrt{\hbar/eB}$, for which the physical meaning is the length of electron trajectory along which this electron gains a phase factor comparable with 2π from the magnetic field. Normally, the magnetic length is a rather large distance but when it is comparable to the lattice constant, it means that the magnetic field strength is comparable with electric field strength in the atom (which is a rare situation).

In the case of perturbed central region, we also need to adjust the bond current in Eq. (2.109) to include the corresponding hopping matrix elements as

$$J_{mn} = 2\,\mathrm{Im}[T_{mn}\mathrm{e}^{\mathrm{i}\alpha_{mn}}\rho_{nm}]. \tag{2.119}$$

Now that we have two different Hamiltonians for the central region, one for the unperturbed and one for the perturbed system, we have to adjust the derivation for the TD1RDM worked out earlier. By carefully studying the steps we notice that nothing changes in the equations of motion or in the self-energy calculations. It is only the Green's functions' components in Eqs. (2.73) and (2.74) that need to be adjusted according to either unperturbed or perturbed Hamiltonians. We see that the Matsubara Green's function should include only the ground-state Hamiltonian h. On the other hand, for Green's functions having components on the horizontal branch of the Keldysh contour, also the perturbation is present, hence, there we use the Hamiltonian $\widetilde{h}$.

In Eq. (A.11) we have to deal with both h and $\widetilde{h}$ and we get

$$G^{\rceil}(t,\tau) = \mathrm{e}^{-\mathrm{i}\widetilde{h}_{\mathrm{eff}}t}\left[G^{\mathrm{M}}(0,\tau) - \int_0^t \mathrm{d}t'\mathrm{e}^{\mathrm{i}\widetilde{h}_{\mathrm{eff}}t'}\int_0^\beta \mathrm{d}\bar{\tau}\Sigma^{\rceil}(t',\bar{\tau})G^{\mathrm{M}}(\bar{\tau},\tau)\right]. \tag{2.120}$$

Similarly for the retarded Green's function in Eq. (A.17)

$$G^{\mathrm{R}}(t-t') = -\mathrm{i}\theta(t-t')\mathrm{e}^{-\widetilde{h}_{\mathrm{eff}}(t-t')}. \tag{2.121}$$

Then, in the derivation, we should change all the rest accordingly. First, introduce a notation for the Green's functions: If the function is to be evaluated with the perturbed Hamiltonian, we put a *tilde* above, otherwise it is evaluated with the unperturbed Hamiltonian (i.e., as before)

$$\widetilde{G}^{\mathrm{R}}(\omega) = \frac{1}{\omega - \widetilde{h}_{\mathrm{eff}}}, \quad G^{\mathrm{A}}(\omega) = \frac{1}{\omega - h^{\dagger}_{\mathrm{eff}}}, \quad \text{and so on.} \tag{2.122}$$

Because of these changes, also some terms in the equation of motion change:

$$\left[G^{\mathrm{R}}\cdot\Sigma^{<}\right](t,t) = \mathrm{i}\sum_\alpha \int \frac{\mathrm{d}\omega}{2\pi} f(\omega-\mu)\left[1-\mathrm{e}^{-\mathrm{i}(\omega+V_\alpha-\widetilde{h}_{\mathrm{eff}})t}\right]\widetilde{G}^{\mathrm{R}}(\omega+V_\alpha)\Gamma_\alpha \tag{2.123}$$

and

$$\left[G^{\rceil} \star \Sigma^{\lceil}\right](t,t) = \mathrm{i}\int \frac{\mathrm{d}\omega}{2\pi} f(\omega-\mu)\sum_{\alpha} \mathrm{e}^{\mathrm{i}(\omega+V_\alpha-\widetilde{h}_{\mathrm{eff}})t} G^{\mathrm{R}}(\omega)\Gamma_\alpha. \tag{2.124}$$

Equation (2.124) here requires some thinking (going through the derivation in App. A.1.2 and checking what changes). In Eq. (2.124) the retarded Green's function (without a tilde) follows from the analytic continuation of the Matsubara Green's function, and therefore it is calculated from the unperturbed Hamiltonian.

The equation of motion, to be solved for $G^{<}(t,t)$, is then

$$\begin{aligned} & \mathrm{i}\frac{\mathrm{d}}{\mathrm{d}t}G^{<}(t,t) - \left[\widetilde{h}(t), G^{<}(t,t)\right] \\ = & -\Bigg\{\mathrm{i}\sum_{\alpha}\int \frac{\mathrm{d}\omega}{2\pi} f(\omega-\mu)\left[1-\mathrm{e}^{\mathrm{i}(\omega+V_\alpha-\widetilde{h}_{\mathrm{eff}})t}\right]\widetilde{G}^{\mathrm{R}}(\omega+V_\alpha)\Gamma_\alpha + \frac{\mathrm{i}}{2}\Gamma G^{<}(t,t) \\ & +\mathrm{i}\int \frac{\mathrm{d}\omega}{2\pi} f(\omega-\mu)\sum_{a} \mathrm{e}^{\mathrm{i}(\omega+V_\alpha-\widetilde{h}_{\mathrm{eff}})t} G^{\mathrm{R}}(\omega)\Gamma_\alpha\Bigg\} + \mathrm{h.c.}. \end{aligned} \tag{2.125}$$

This may be solved in a similar fashion as earlier, see App. A.1.5. The solution is

$$\begin{aligned} -\mathrm{i}G^{<}(t,t) = & \int \frac{\mathrm{d}\omega}{2\pi} f(\omega-\mu)\sum_{\alpha}\Big\{\widetilde{G}^{\mathrm{R}}(\omega+V_\alpha)\Gamma_\alpha\widetilde{G}^{\mathrm{A}}(\omega+V_\alpha) \\ & +\left[\mathrm{e}^{\mathrm{i}(\omega+V_\alpha-\widetilde{h}_{\mathrm{eff}})t} G^{\mathrm{R}}(\omega)\widetilde{V}_\alpha\widetilde{G}^{\mathrm{R}}(\omega+V_\alpha)\Gamma_\alpha\widetilde{G}^{\mathrm{A}}(\omega+V_\alpha) + \mathrm{h.c.}\right] \\ & +\mathrm{e}^{-\mathrm{i}\widetilde{h}_{\mathrm{eff}}t} G^{\mathrm{R}}(\omega)\widetilde{V}_\alpha\widetilde{G}^{\mathrm{R}}(\omega+V_\alpha)\Gamma_\alpha\widetilde{G}^{\mathrm{A}}(\omega+V_\alpha)\widetilde{V}_\alpha^{\dagger} G^{\mathrm{A}}(\omega)\mathrm{e}^{\mathrm{i}\widetilde{h}_{\mathrm{eff}}^{\dagger}t}\Big\}, \end{aligned} \tag{2.126}$$

where $\widetilde{V}_\alpha = V_\alpha\mathbb{1} - u$. Equation (2.126) is the final result for the TD1RDM in the case of perturbed central regions. This can easily be checked to reduce to the earlier result in Eq. (2.79) when $u = 0$ and $\widetilde{h} = h$. The interpretation of the different terms is naturally the same as earlier in Eq. (2.79) as Eq. (2.126) includes a mere extension to the Hamiltonian for the central region.

Similarly as earlier in Sec. 2.3.5, we are now, in Eq. (2.126), left with a same type of frequency integral. This integral may be evaluated analytically by expanding in bases $\{|\Psi^{\mathrm{L}}\rangle, |\Psi^{\mathrm{R}}\rangle\}$ (for h_{eff}) and $\{|\widetilde{\Psi}^{\mathrm{L}}\rangle, |\widetilde{\Psi}^{\mathrm{R}}\rangle\}$ (for $\widetilde{h}_{\mathrm{eff}}$). Because h and $\widetilde{h}$ do not necessarily commute (in the case of non-diagonal perturbations, etc.), not only do the eigenvalue spectra differ (more than for a constant shift) but also the left/right eigenstates are non-trivially separate. In the second row of Eq. (2.126), for instance, we need to insert a complete set of left/right eigenstates of h_{eff}, as a resolution of identity, in between the first exponential and G^{R}, and so on. Then, we end up having sums and overlaps between the unperturbed and perturbed bases. When the perturbation vanishes ($u \to 0$) these overlaps should reduce to the unperturbed result.

The density matrix expanded in the 'left–left' eigenbasis of the perturbed effective Hamiltonian $\widetilde{h}_{\mathrm{eff}}$ reads (see App. A.1.5)

$$\rho_{jk}(t) = \sum_{\alpha} \left[\widetilde{\Gamma}_{\alpha,jk} \widetilde{\Lambda}_{\alpha,jk} + \widetilde{\Pi}_{\alpha,jk}(t) + \widetilde{\Pi}^{*}_{\alpha,kj}(t) + \widetilde{\Omega}_{\alpha,jk}(t) \right] \tag{2.127}$$

with

$$\widetilde{\Gamma}_{\alpha,jk} = \langle \widetilde{\Psi}^{\mathrm{L}}_{j} | \Gamma_{\alpha} | \widetilde{\Psi}^{\mathrm{L}}_{k} \rangle, \tag{2.128}$$

$$\widetilde{\Lambda}_{\alpha,jk} = \int \frac{\mathrm{d}\omega}{2\pi} \frac{f(\omega-\mu)}{(\omega + V_\alpha - \widetilde{\epsilon}_j)(\omega + V_\alpha - \widetilde{\epsilon}^{*}_{k})}, \tag{2.129}$$

$$\widetilde{\Pi}_{\alpha,jk}(t) = \sum_{mn} \frac{\langle \widetilde{\Psi}^{\mathrm{L}}_{j} | \Psi^{\mathrm{R}}_{m} \rangle \langle \Psi^{\mathrm{L}}_{m} | \widetilde{V}_\alpha | \widetilde{\Psi}^{\mathrm{R}}_{n} \rangle \widetilde{\Gamma}_{\alpha,nk}}{\langle \Psi^{\mathrm{L}}_{m} | \Psi^{\mathrm{R}}_{m} \rangle \langle \widetilde{\Psi}^{\mathrm{L}}_{n} | \widetilde{\Psi}^{\mathrm{R}}_{n} \rangle} \int \frac{\mathrm{d}\omega}{2\pi} \frac{f(\omega-\mu) \mathrm{e}^{\mathrm{i}(\omega + V_\alpha - \widetilde{\epsilon}_j)t}}{(\omega - \epsilon_m)(\omega + V_\alpha - \widetilde{\epsilon}_n)(\omega + V_\alpha - \widetilde{\epsilon}^{*}_{k})}, \tag{2.130}$$

$$\begin{aligned} \widetilde{\Omega}_{\alpha,jk}(t) = & \sum_{mnpq} \frac{\langle \widetilde{\Psi}^{\mathrm{L}}_{j} | \Psi^{\mathrm{R}}_{m} \rangle \langle \Psi^{\mathrm{L}}_{m} | \widetilde{V}_\alpha | \widetilde{\Psi}^{\mathrm{R}}_{n} \rangle \widetilde{\Gamma}_{\alpha,np} \langle \widetilde{\Psi}^{\mathrm{R}}_{p} | \widetilde{V}^{\dagger}_{\alpha} | \Psi^{\mathrm{L}}_{q} \rangle \langle \Psi^{\mathrm{R}}_{q} | \widetilde{\Psi}^{\mathrm{L}}_{k} \rangle}{\langle \Psi^{\mathrm{L}}_{m} | \Psi^{\mathrm{R}}_{m} \rangle \langle \widetilde{\Psi}^{\mathrm{L}}_{n} | \widetilde{\Psi}^{\mathrm{R}}_{n} \rangle \langle \widetilde{\Psi}^{\mathrm{R}}_{p} | \widetilde{\Psi}^{\mathrm{L}}_{p} \rangle \langle \Psi^{\mathrm{R}}_{q} | \Psi^{\mathrm{L}}_{q} \rangle} \\ & \times \mathrm{e}^{-\mathrm{i}(\widetilde{\epsilon}_j - \widetilde{\epsilon}^{*}_{k})t} \int \frac{\mathrm{d}\omega}{2\pi} \frac{f(\omega-\mu)}{(\omega - \epsilon_m)(\omega + V_\alpha - \widetilde{\epsilon}_n)(\omega + V_\alpha - \widetilde{\epsilon}^{*}_{p})(\omega - \epsilon^{*}_{q})}, \end{aligned} \tag{2.131}$$

where the eigenvalues ϵ and $\widetilde{\epsilon}$ refer to the complex eigenvalues of h_{eff} and $\widetilde{h}_{\mathrm{eff}}$, respectively. In the limit $\widetilde{h}_{\mathrm{eff}} \to h_{\mathrm{eff}}$ this result can be checked to reduce to the earlier result in Eq. (2.92). In Pub. [II] we also evaluated these integrals in the zero-temperature limit (the superscript '0' refers to zero temperature)

$$\widetilde{\Gamma}^{0}_{\alpha,jk} = \langle \widetilde{\Psi}^{\mathrm{L}}_{j} | \Gamma_{\alpha} | \widetilde{\Psi}^{\mathrm{L}}_{k} \rangle, \tag{2.132}$$

$$\widetilde{\Lambda}^{0}_{\alpha,jk} = \frac{\mathrm{Log}(\widetilde{\epsilon}^{*}_{k} - \mu_\alpha) - \mathrm{Log}(\widetilde{\epsilon}_j - \mu_\alpha)}{2\pi(\widetilde{\epsilon}^{*}_{k} - \widetilde{\epsilon}_j)}, \tag{2.133}$$

$$\begin{aligned} & \widetilde{\Pi}^{0}_{\alpha,jk}(t) \\ = & \sum_{m,n} \frac{\langle \widetilde{\Psi}^{\mathrm{L}}_{j} | \Psi^{\mathrm{R}}_{m} \rangle \langle \Psi^{\mathrm{L}}_{m} | \widetilde{V}_\alpha | \widetilde{\Psi}^{\mathrm{R}}_{n} \rangle \widetilde{\Gamma}_{\alpha,nk}}{\langle \Psi^{\mathrm{L}}_{m} | \Psi^{\mathrm{R}}_{m} \rangle \langle \widetilde{\Psi}^{\mathrm{L}}_{n} | \widetilde{\Psi}^{\mathrm{R}}_{n} \rangle} \frac{\mathrm{e}^{-\mathrm{i}(\widetilde{\epsilon}_j - \mu_\alpha)t}}{2\pi(\widetilde{\epsilon}^{*}_{k} - \widetilde{\epsilon}_n)(\widetilde{\epsilon}^{*}_{k} - \epsilon_m - V_\alpha)} \\ & \times \left\{ F[\mathrm{i}(\widetilde{\epsilon}^{*}_{k} - \mu_\alpha)t] - \frac{\widetilde{\epsilon}^{*}_{k} - \epsilon_m - V_\alpha}{\widetilde{\epsilon}_n - \epsilon_m - V_\alpha} F[\mathrm{i}(\widetilde{\epsilon}_n - \mu_\alpha)t] + \frac{\widetilde{\epsilon}^{*}_{k} - \widetilde{\epsilon}_n}{\widetilde{\epsilon}_n - \epsilon_m - V_\alpha} F[\mathrm{i}(\epsilon_m - \mu)t] \right\}, \end{aligned} \tag{2.134}$$

$$
\begin{aligned}
&\widetilde{\Omega}^0_{\alpha,jk}(t) \\
&= \sum_{mnpq} \frac{\langle\widetilde{\Psi}^{\mathrm{L}}_j|\Psi^{\mathrm{R}}_m\rangle\langle\Psi^{\mathrm{L}}_m|\widetilde{V}_\alpha|\widetilde{\Psi}^{\mathrm{R}}_n\rangle\widetilde{\Gamma}_{\alpha,np}\langle\widetilde{\Psi}^{\mathrm{R}}_p|\widetilde{V}^\dagger_\alpha|\Psi^{\mathrm{L}}_q\rangle\langle\Psi^{\mathrm{R}}_q|\widetilde{\Psi}^{\mathrm{L}}_k\rangle}{\langle\Psi^{\mathrm{L}}_m|\Psi^{\mathrm{R}}_m\rangle\langle\widetilde{\Psi}^{\mathrm{L}}_n|\widetilde{\Psi}^{\mathrm{R}}_n\rangle\langle\widetilde{\Psi}^{\mathrm{R}}_p|\widetilde{\Psi}^{\mathrm{L}}_p\rangle\langle\Psi^{\mathrm{R}}_q|\Psi^{\mathrm{L}}_q\rangle} \frac{\mathrm{e}^{-\mathrm{i}(\widetilde{\epsilon}_j-\widetilde{\epsilon}^*_k)t}}{2\pi} \\
&\times\left[\frac{\mathrm{Log}(\epsilon_m-\mu)}{(\epsilon_m-\widetilde{\epsilon}_n+V_\alpha)(\epsilon_m-\widetilde{\epsilon}^*_p+V_\alpha)(\epsilon_m-\epsilon^*_q)}+\frac{\mathrm{Log}(\widetilde{\epsilon}_n-\mu_\alpha)}{(\widetilde{\epsilon}_n-\epsilon_m-V_\alpha)(\widetilde{\epsilon}_n-\widetilde{\epsilon}^*_p)(\widetilde{\epsilon}_n-\epsilon^*_q-V_\alpha)}\right. \\
&\left.+\frac{\mathrm{Log}(\epsilon^*_q-\mu)}{(\epsilon^*_q-\epsilon_m)(\epsilon^*_q-\widetilde{\epsilon}_n+V_\alpha)(\epsilon^*_q-\widetilde{\epsilon}^*_p+V_\alpha)}+\frac{\mathrm{Log}(\widetilde{\epsilon}^*_p-\mu_\alpha)}{(\widetilde{\epsilon}^*_p-\epsilon_m-V_\alpha)(\widetilde{\epsilon}^*_p-\widetilde{\epsilon}_n)(\widetilde{\epsilon}^*_p-\epsilon^*_q-V_\alpha)}\right],
\end{aligned}
\tag{2.135}
$$

where the electro-chemical potential is as earlier $\mu_\alpha = \mu + V_\alpha$ and the function F is as in Eq. (2.96). Also these results can be checked to reduce to the earlier results when $\widetilde{\epsilon} \to \epsilon$. Inserting Eqs. (2.133), (2.134) and (2.135) into Eq. (2.127) gives then the TD1RDM for perturbed central regions at the zero-temperature limit.

Yet another extension is to be presented in Ref. [120] where also the corresponding results for Eq. (2.127) at nonzero temperatures are written in terms of the digamma and hypergeometric functions [see the discussion after Eqs. (2.103), (2.104) and (2.105)]. We list the final expressions here for completeness

$$
\begin{aligned}
&\widetilde{\Lambda}_{\alpha,jk} \\
&= \frac{\mathrm{i}}{\widetilde{\epsilon}^*_k-\widetilde{\epsilon}_j}\left\{\frac{1}{\mathrm{e}^{\beta(\widetilde{\epsilon}^*_k-\mu_\alpha)}+1}+\frac{1}{2\pi\mathrm{i}}\left[\psi\left(\frac{1}{2}-\frac{\beta(\widetilde{\epsilon}^*_k-\mu_\alpha)}{2\pi\mathrm{i}}\right)-\psi\left(\frac{1}{2}-\frac{\beta(\widetilde{\epsilon}_j-\mu_\alpha)}{2\pi\mathrm{i}}\right)\right]\right\},
\end{aligned}
\tag{2.136}
$$

$$
\begin{aligned}
&\widetilde{\Pi}_{\alpha,jk}(t) \\
&= \sum_{mn} \frac{\langle\widetilde{\Psi}^{\mathrm{L}}_j|\Psi^{\mathrm{R}}_m\rangle\langle\Psi^{\mathrm{L}}_m|\widetilde{V}_\alpha|\widetilde{\Psi}^{\mathrm{R}}_n\rangle\widetilde{\Gamma}_{\alpha,nk}}{\langle\Psi^{\mathrm{L}}_m|\Psi^{\mathrm{R}}_m\rangle\langle\widetilde{\Psi}^{\mathrm{L}}_n|\widetilde{\Psi}^{\mathrm{R}}_n\rangle}\times \\
&\frac{\mathrm{i}}{(\widetilde{\epsilon}^*_k-\widetilde{\epsilon}_n)(\widetilde{\epsilon}^*_k-\epsilon_m-V_\alpha)}\left\{\frac{\mathrm{e}^{-\mathrm{i}(\widetilde{\epsilon}_j-\widetilde{\epsilon}^*_k)t}}{\mathrm{e}^{\beta(\widetilde{\epsilon}^*_k-\mu_\alpha)}+1}+\mathrm{i}\mathrm{e}^{-\pi t/\beta}\mathrm{e}^{-\mathrm{i}(\widetilde{\epsilon}_j-\mu_\alpha)t}\times\right. \\
&\left.\left[\bar{F}(\widetilde{\epsilon}^*_k-\mu_\alpha,t,\beta)-\frac{\widetilde{\epsilon}^*_k-\epsilon_m-V_\alpha}{\widetilde{\epsilon}_n-\epsilon_m-V_\alpha}\bar{F}(\widetilde{\epsilon}_n-\mu_\alpha,t,\beta)+\frac{\widetilde{\epsilon}^*_k-\widetilde{\epsilon}_n}{\widetilde{\epsilon}_n-\epsilon_m-V_\alpha}\bar{F}(\epsilon_m-\mu,t,\beta)\right]\right\},
\end{aligned}
\tag{2.137}
$$

$$
\begin{aligned}
&\widetilde{\Omega}_{\alpha,jk} \\
&= \sum_{mnpq} \frac{\langle\widetilde{\Psi}_j^{\mathrm{L}}|\Psi_m^{\mathrm{R}}\rangle\langle\Psi_m^{\mathrm{L}}|\widetilde{V}_\alpha|\widetilde{\Psi}_n^{\mathrm{R}}\rangle\widetilde{\Gamma}_{\alpha,np}\langle\widetilde{\Psi}_p^{\mathrm{R}}|\widetilde{V}_\alpha^\dagger|\Psi_q^{\mathrm{L}}\rangle\langle\Psi_q^{\mathrm{R}}|\widetilde{\Psi}_k^{\mathrm{L}}\rangle}{\langle\Psi_m^{\mathrm{L}}|\Psi_m^{\mathrm{R}}\rangle\langle\widetilde{\Psi}_n^{\mathrm{L}}|\widetilde{\Psi}_n^{\mathrm{R}}\rangle\langle\widetilde{\Psi}_p^{\mathrm{R}}|\widetilde{\Psi}_p^{\mathrm{L}}\rangle\langle\Psi_q^{\mathrm{R}}|\Psi_q^{\mathrm{L}}\rangle} \mathrm{e}^{-\mathrm{i}(\widetilde{\epsilon}_j-\widetilde{\epsilon}_k^*)t} \times \\
&\quad \left\{ \frac{1}{(\epsilon_m-\widetilde{\epsilon}_n+V_\alpha)(\epsilon_m-\widetilde{\epsilon}_p^*+V_\alpha)(\epsilon_m-\epsilon_q^*)} \frac{1}{2\pi}\psi\left(\frac{1}{2}-\frac{\beta(\epsilon_m-\mu)}{2\pi\mathrm{i}}\right)\right. \\
&+ \frac{1}{(\widetilde{\epsilon}_n-\epsilon_m-V_\alpha)(\widetilde{\epsilon}_n-\widetilde{\epsilon}_p^*)(\widetilde{\epsilon}_n-\epsilon_q^*-V_\alpha)} \frac{1}{2\pi}\psi\left(\frac{1}{2}-\frac{\beta(\widetilde{\epsilon}_n-\mu_\alpha)}{2\pi\mathrm{i}}\right) \\
&+ \frac{1}{(\epsilon_q^*-\epsilon_m)(\epsilon_q^*-\widetilde{\epsilon}_n+V_\alpha)(\epsilon_q^*-\widetilde{\epsilon}_p^*+V_\alpha)} \left[\frac{\mathrm{i}}{\mathrm{e}^{\beta(\epsilon_q^*-\mu)}+1}+\frac{1}{2\pi}\psi\left(\frac{1}{2}-\frac{\beta(\epsilon_q^*-\mu)}{2\pi\mathrm{i}}\right)\right] \\
&+ \left.\frac{1}{(\widetilde{\epsilon}_p^*-\epsilon_m-V_\alpha)(\widetilde{\epsilon}_p^*-\widetilde{\epsilon}_n)(\widetilde{\epsilon}_p^*-\epsilon_q^*-V_\alpha)} \left[\frac{\mathrm{i}}{\mathrm{e}^{\beta(\widetilde{\epsilon}_p^*-\mu_\alpha)}+1}+\frac{1}{2\pi}\psi\left(\frac{1}{2}-\frac{\beta(\widetilde{\epsilon}_p^*-\mu_\alpha)}{2\pi\mathrm{i}}\right)\right]\right\},
\end{aligned}
\tag{2.138}
$$

where $\bar{F}$ is given by Eq. (2.106). Inserting Eqs. (2.136), (2.137) and (2.138) into Eq. (2.127) gives then the TD1RDM for perturbed central regions at arbitrary temperatures.

2.4.2 Extension to normal metal – superconducting – normal metal (NSN) junctions

In Pub. [IV] (and in Ref. [120]) we also consider an extension to the central regions being superconducting. The transport setup is otherwise similar to Sec. 2.2 but we will discuss the extension via Nambu matrices [128–131].

In order to model a superconducting island, we add a pairing field operator $\hat{\Delta}$ to the Hamiltonian of the central region by

$$
\hat{H}_{CC} = \sum_{mn\sigma} T_{mn}\hat{d}_{m\sigma}^\dagger\hat{d}_{n\sigma} + \sum_{mn,\sigma\sigma'}\left(\Delta_{mn,\sigma\sigma'}\hat{d}_{m\sigma}^\dagger\hat{d}_{n\sigma'}^\dagger + \Delta_{mn,\sigma\sigma'}^*\hat{d}_{m\sigma'}\hat{d}_{n\sigma}\right). \tag{2.139}
$$

This may be rewritten in a compact form by introducing the 4-component Nambu spinors [128, 132, 133]

$$
\underline{\hat{\Phi}}_m = \begin{pmatrix}\hat{\Phi}_m^1\\ \hat{\Phi}_m^2\\ \hat{\Phi}_m^3\\ \hat{\Phi}_m^4\end{pmatrix} = \begin{pmatrix}\hat{d}_{m\uparrow}\\ \hat{d}_{m\downarrow}\\ \hat{d}_{m\uparrow}^\dagger\\ \hat{d}_{m\downarrow}^\dagger\end{pmatrix}; \quad \left\{\hat{\Phi}_m^\mu, (\hat{\Phi}_n^\nu)^\dagger\right\} = \delta_{mn}\delta^{\mu\nu}, \tag{2.140}
$$

where the anticommutation relation is to be understood component-wise ($\{\mu,\nu\} \in \{1,2,3,4\}$). Quantities in the 4-by-4 Nambu space will be denoted by an underline. The Hamiltonian for the central region now reads

$$\underline{\hat{H}}_{CC} = \sum_{mn} (\underline{\hat{\Phi}}_m)^\dagger \underline{\xi}_{mn} \underline{\hat{\Phi}}_n \,, \tag{2.141}$$

with

$$\underline{\xi}_{mn} = \begin{pmatrix} T_{mn}/2 & 0 & \Delta_{mn,\uparrow\uparrow} & \Delta_{mn,\uparrow\downarrow} \\ 0 & T_{mn}/2 & \Delta_{mn,\downarrow\uparrow} & \Delta_{mn,\downarrow\downarrow} \\ \Delta^*_{mn,\uparrow\uparrow} & \Delta^*_{mn,\downarrow\uparrow} & -T_{mn}/2 & 0 \\ \Delta^*_{mn,\uparrow\downarrow} & \Delta^*_{mn,\downarrow\downarrow} & 0 & -T_{mn}/2 \end{pmatrix} \tag{2.142}$$

similar to the form of Bogoliubov–de Gennes [134, 135]. Expanding Eq. (2.141) gives Eq. (2.139) (under the assumption of a symmetric hopping matrix which typically is the case) modulo a constant $\sum_m T_{mm}$ which can be regarded as a reference point to the total energy. The constant follows from the anticommutation relations of the creation and annihilation operators. For the lead and coupling parts of the Hamiltonian similar interpretation is done although we will keep the leads as normal metal. We have the lead Hamiltonian of the form (2.142) but without the off-diagonal terms

$$\underline{\hat{H}}_{\alpha\alpha} = \sum_{k\alpha} (\underline{\hat{\Phi}}_{k\alpha})^\dagger \underline{\epsilon}_{k\alpha} (\underline{\hat{\Phi}}_{k\alpha}) \tag{2.143}$$

with $\underline{\epsilon}_{k\alpha} = [\epsilon_{k\alpha} + \theta(t)V_\alpha]\mathrm{diag}(1,1,-1,-1)/2$. Also here, by expanding Eq. (2.143), the lead part of the Hamiltonian in Eq. (2.23) (with the bias voltage V_α added to the energy spectrum) is recovered modulo a constant $\sum_{k\alpha} \epsilon_{k\alpha}$ which can be regarded as a reference to the total energy. The central region's m-th site will be coupled to the k-th basis function of the α-th lead via $T_{mk\alpha}$, and there will be no pairing potential in the coupling Hamiltonian either [133]

$$\underline{\hat{H}}_{C\alpha} = \sum_{mk\alpha} (\underline{\hat{\Phi}}_m)^\dagger \underline{\chi}_{mk\alpha} \underline{\hat{\Phi}}_{k\alpha}; \quad \underline{\hat{H}}_{\alpha C} = (\underline{\hat{H}}_{C\alpha})^\dagger \tag{2.144}$$

with $\underline{\chi}_{mk\alpha} = T_{mk\alpha}\mathrm{diag}(1,1,-1,-1)$. Also in this case the coupling part of the Hamiltonian in Eq. (2.23) follows by expanding Eq. (2.144) assuming the hopping matrix to be symmetric. This time, however, no extra constants arise since the creation and annihilation operators in different regions (α, C) anticommute. The one-electron Green's function in the above setup is defined as a time-ordered tensor product of the spinor field operators [132]

$$\underline{G}_{xy}(z,z') = -\mathrm{i}\langle \mathcal{T}_\gamma [\underline{\hat{\Phi}}_x(z) \otimes \underline{\hat{\Phi}}^\dagger_y(z')] \rangle, \tag{2.145}$$

where the time-ordering operator $\mathcal{T}_\gamma$ is taken for the variables z, z' on the Keldysh contour γ. The form in Eq. (2.145) automatically handles both normal and anomalous components of the Green's function [136]. The matrix elements in the Green's

function in Eq. (2.145) (indices x, y belonging either to the leads or to the central region) label the transport setup in the following block form

$$\underline{\boldsymbol{h}} = \begin{pmatrix} \underline{h}_{11} & 0 & \cdots & \underline{h}_{1C} \\ 0 & \underline{h}_{22} & \cdots & \underline{h}_{2C} \\ \vdots & \vdots & \ddots & \vdots \\ \underline{h}_{C1} & \underline{h}_{C2} & \cdots & \underline{h}_{CC} \end{pmatrix}; \qquad \underline{\boldsymbol{G}} = \begin{pmatrix} \underline{G}_{11} & \underline{G}_{12} & \cdots & \underline{G}_{1C} \\ \underline{G}_{21} & \underline{G}_{22} & \cdots & \underline{G}_{2C} \\ \vdots & \vdots & \ddots & \vdots \\ \underline{G}_{C1} & \underline{G}_{C2} & \cdots & \underline{G}_{CC} \end{pmatrix} \tag{2.146}$$

with $(\underline{h}_{\alpha\alpha'})_{kk'} = (\underline{h}_{\alpha\alpha'})_{kk'}(t) = \underline{\epsilon}_{k\alpha}\delta_{\alpha\alpha'}\delta_{kk'}$ for the leads, $(\underline{h}_{CC})_{mn} = \underline{\xi}_{mn}$ for the central region, and $(\underline{h}_{C\alpha})_{mk\alpha} = \underline{\chi}_{mk\alpha}$ for the couplings. We denote the matrices for the full transport setup as boldface symbols. As earlier, we notice how the lead blocks, $h_{\alpha\alpha} = h_{\alpha\alpha}(z)$, are different for the vertical and horizontal branches of the Keldysh contour due to the shift in energy levels at $t > 0$. Also, notice that the block structure in Eq. (2.146) does not refer to the Nambu space but it is of dimension $(N_{\text{lead}} + 1) \times (N_{\text{lead}} + 1)$ where N_{lead} is the number of leads. Each block then accounts for the individual dimension of the corresponding partition. We may derive the equation of motion for the Green's function by

$$\mathrm{i}\partial_z \underline{G}_{xy}(z, z') = \partial_z \left[\theta(z, z') \langle \underline{\hat{\Phi}}_x(z) \otimes \underline{\hat{\Phi}}_y^\dagger(z') \rangle - \theta(z', z) \langle \underline{\hat{\Phi}}_y^\dagger(z') \otimes \underline{\hat{\Phi}}_x(z) \rangle \right], \tag{2.147}$$

where the step function is defined, as earlier, on the Keldysh contour γ according to the time-ordering operator $\mathcal{T}_\gamma$ [73]. Evaluating the derivative gives

$$\mathrm{i}\partial_z \underline{G}_{xy}(z, z') = \delta(z, z') \left\langle \left\{ \underline{\hat{\Phi}}_x(z), \underline{\hat{\Phi}}_y^\dagger(z') \right\} \right\rangle - \mathrm{i} \langle \mathcal{T}_\gamma [\mathrm{i}\partial_z \underline{\hat{\Phi}}_x(z)] \otimes \underline{\hat{\Phi}}_y^\dagger(z') \rangle, \tag{2.148}$$

where the anticommutator gives simply $\delta_{xy}\underline{\mathbb{1}}$ (here $\underline{\mathbb{1}}$ refers to a unit matrix in Nambu basis), and the evolution of the spinor operator can further be derived from its equation of motion

$$\mathrm{i}\partial_z \underline{\hat{\Phi}}_x(z) = [\underline{\hat{\Phi}}_x(z), \underline{\hat{H}}] = [\underline{\hat{\Phi}}_x(z), \underline{\hat{H}}_{\alpha\alpha}] + [\underline{\hat{\Phi}}_x(z), \underline{\hat{H}}_{CC}] + [\underline{\hat{\Phi}}_x(z), \underline{\hat{H}}_{C\alpha}] + [\underline{\hat{\Phi}}_x(z), \underline{\hat{H}}_{\alpha C}]. \tag{2.149}$$

The above commutators with Eqs. (2.141), (2.143), and (2.144) may be evaluated using $[A, BC] = \{A, B\}C - B\{A, C\}$ and the anticommutation relations in Eq. (2.140). It is important to notice here that the index x may belong to any region in the transport setup. For example, if $x \in C$, then only the corresponding commutators are nonzero

$$\mathrm{i}\partial_z \hat{\Phi}_x^\mu(z) = \sum_{n\zeta} \xi_{xn}^{\mu\zeta} \hat{\Phi}_n^\zeta + \sum_{k\alpha\zeta} \chi_{xk\alpha}^{\mu\zeta} \hat{\Phi}_{k\alpha}^\zeta. \tag{2.150}$$

Inserting this into Eq. (2.148) and using the definition of the Green's function in Eq. (2.145) gives

$$\mathrm{i}\partial_z \underline{G}_{xy}(z, z') = \delta(z, z')\delta_{xy}\underline{\mathbb{1}} + \sum_l (\underline{\xi}_{xl} + \underline{\chi}_{xl}) \underline{G}_{ly}(z, z') \tag{2.151}$$

with l being a general index either in the central region or in the lead sector. The adjoint equation can be derived similarly, and we may generalize to the full equations of motion for the whole transport setup as (here $\underline{\mathbf{1}}$ refers to a unit matrix in the combined transport and Nambu basis)

$$\left[\mathrm{i}\frac{\mathrm{d}}{\mathrm{d}z}\underline{\mathbf{1}} - \underline{\boldsymbol{h}}(z)\right]\underline{\boldsymbol{G}}(z,z') = \delta(z,z')\underline{\mathbf{1}}, \tag{2.152}$$

$$\underline{\boldsymbol{G}}(z,z')\left[-\mathrm{i}\frac{\overleftarrow{\mathrm{d}}}{\mathrm{d}z'}\underline{\mathbf{1}} - \underline{\boldsymbol{h}}(z')\right] = \delta(z,z')\underline{\mathbf{1}}, \tag{2.153}$$

which the Green's function satisfies being antiperiodic along the contour (Kubo–Martin–Schwinger boundary condition). As the equations of motion are exactly the same as those in Eqs. (2.65) and (2.66), we may in similar fashion using the Langreth rules [73, 116] derive the following equation for the lesser Green's function with indices on the central molecule $\underline{G}^<_{CC}$ (for which we will right away drop the subscript 'CC' as we are only interested in the quantities within the central region)

$$\mathrm{i}\frac{\mathrm{d}}{\mathrm{d}t}\underline{G}^<(t,t) - [\underline{h}_{CC}(t), \underline{G}^<(t,t)] = -\left[\underline{G}^{\mathrm{R}}\cdot\underline{\Sigma}^< + \underline{G}^<\cdot\underline{\Sigma}^{\mathrm{A}} + \underline{G}^{\rceil}\star\underline{\Sigma}^{\lceil}\right](t,t) + \mathrm{h.c.}, \tag{2.154}$$

where the time-convolutions on the horizontal and vertical branches of the Keldysh contour are defined as before. Also here, we describe the leads within the WBA, where the electronic levels of the central region are in a narrow range compared to the lead bandwidth, and the retarded Keldysh component of the self-energy becomes

$$\underline{\Sigma}^{\mathrm{R}}_{\alpha,mn}(\omega) = \sum_k \underline{\chi}_{mk\alpha}\frac{1}{\omega - \underline{\epsilon}_{k\alpha} + \mathrm{i}\eta}\underline{\chi}_{k\alpha n} \approx -\mathrm{i}\underline{\Gamma}_{\alpha,mn}/2. \tag{2.155}$$

Looking at Eq. (2.154) and the earlier equation of motion (2.67) we may use the fact that the same equations have the same solutions, i.e., including the pairing field in the Hamiltonian of the central region adds no extra complication to the evolution of the Green's function. The only difference is in the interpretation of the matrices in Nambu space. In particular, the lesser Green's function in the equal-time limit, $\underline{\rho}(t) = -\mathrm{i}\underline{G}^<(t,t)$, can be solved analytically as we have done earlier, and this gives the time-dependent reduced one-particle density matrix. The lesser Green's function is commonly expressed in terms of the normal ($G^<_{\sigma\sigma'}$) and anomalous ($F^<_{\sigma\sigma'}$)

components [131]:

$$
\begin{aligned}
-\mathrm{i}(\underline{G}^{<})_{mn}(t,t) &= -\mathrm{i}\begin{pmatrix}
(G^{<}_{\uparrow\uparrow})_{mn}(t,t) & (G^{<}_{\downarrow\uparrow})_{mn}(t,t) & (-F^{>}_{\uparrow\uparrow})_{nm}(t,t) & (-F^{>}_{\downarrow\uparrow})_{nm}(t,t) \\
(G^{<}_{\uparrow\downarrow})_{mn}(t,t) & (G^{<}_{\downarrow\downarrow})_{mn}(t,t) & (-F^{>}_{\uparrow\downarrow})_{nm}(t,t) & (-F^{>}_{\downarrow\downarrow})_{nm}(t,t) \\
(\bar{F}^{<}_{\uparrow\uparrow})_{mn}(t,t) & (\bar{F}^{<}_{\downarrow\uparrow})_{mn}(t,t) & (-G^{>}_{\uparrow\uparrow})_{nm}(t,t) & (-G^{>}_{\downarrow\uparrow})_{nm}(t,t) \\
(\bar{F}^{<}_{\uparrow\downarrow})_{mn}(t,t) & (\bar{F}^{<}_{\downarrow\downarrow})_{mn}(t,t) & (-G^{>}_{\uparrow\downarrow})_{nm}(t,t) & (-G^{>}_{\downarrow\downarrow})_{nm}(t,t)
\end{pmatrix} \\
&= \begin{pmatrix}
\langle \hat{d}^{\dagger}_{n\uparrow}(t)\hat{d}_{m\uparrow}(t)\rangle & \langle \hat{d}^{\dagger}_{n\downarrow}(t)\hat{d}_{m\uparrow}(t)\rangle & \langle \hat{d}_{n\uparrow}(t)\hat{d}_{m\uparrow}(t)\rangle & \langle \hat{d}_{n\downarrow}(t)\hat{d}_{m\uparrow}(t)\rangle \\
\langle \hat{d}^{\dagger}_{n\uparrow}(t)\hat{d}_{m\downarrow}(t)\rangle & \langle \hat{d}^{\dagger}_{n\downarrow}(t)\hat{d}_{m\downarrow}(t)\rangle & \langle \hat{d}_{n\uparrow}(t)\hat{d}_{m\downarrow}(t)\rangle & \langle \hat{d}_{n\downarrow}(t)\hat{d}_{m\downarrow}(t)\rangle \\
\langle \hat{d}^{\dagger}_{n\uparrow}(t)\hat{d}^{\dagger}_{m\uparrow}(t)\rangle & \langle \hat{d}^{\dagger}_{n\downarrow}(t)\hat{d}^{\dagger}_{m\uparrow}(t)\rangle & \langle \hat{d}_{n\uparrow}(t)\hat{d}^{\dagger}_{m\uparrow}(t)\rangle & \langle \hat{d}_{n\downarrow}(t)\hat{d}^{\dagger}_{m\uparrow}(t)\rangle \\
\langle \hat{d}^{\dagger}_{n\uparrow}(t)\hat{d}^{\dagger}_{m\downarrow}(t)\rangle & \langle \hat{d}^{\dagger}_{n\downarrow}(t)\hat{d}^{\dagger}_{m\downarrow}(t)\rangle & \langle \hat{d}_{n\uparrow}(t)\hat{d}^{\dagger}_{m\downarrow}(t)\rangle & \langle \hat{d}_{n\downarrow}(t)\hat{d}^{\dagger}_{m\downarrow}(t)\rangle
\end{pmatrix}
\end{aligned}
\tag{2.156}
$$

which is obtained by expanding the product in Eq. (2.145). Here we will not write the full expressions for the TD1RDM anymore because the same results from earlier, Eqs. (2.92) and (2.127), apply by only interpreting the indices in Nambu space, see also Pub. [IV].

Let us motivate the discussion for the NSN setup by means of a simple example. We simplify the pairing field to be spatially local and only couple opposite spins (as in Cooper pairs)

$$
\hat{\Delta} = \sum_{m} \Delta_m \hat{d}^{\dagger}_{m\uparrow}\hat{d}^{\dagger}_{m\downarrow}. \tag{2.157}
$$

Consider a single dot connected to two leads for which the Hamiltonian can be written as $\hat{H} = \hat{H}_{\mathrm{lead}} + \hat{H}_{\mathrm{tun}} + \hat{H}_{\mathrm{dot}}$ with

$$
\hat{H}_{\mathrm{lead}} = \sum_{k\alpha\sigma} \epsilon_{k\alpha}\hat{d}^{\dagger}_{k\alpha\sigma}\hat{d}_{k\alpha\sigma}\,, \tag{2.158}
$$

$$
\hat{H}_{\mathrm{tun}} = \sum_{k\alpha\sigma} t_{k\alpha 0}\hat{d}^{\dagger}_{k\alpha\sigma}\hat{d}_{0\sigma} + \sum_{k\alpha\sigma} t^{*}_{k\alpha 0}\hat{d}^{\dagger}_{0\sigma}\hat{d}_{k\alpha\sigma}\,, \tag{2.159}
$$

$$
\hat{H}_{\mathrm{dot}} = \epsilon_0 \sum_{\sigma} \hat{d}^{\dagger}_{0\sigma}\hat{d}_{0\sigma} + \Delta_0 \hat{d}^{\dagger}_{0\uparrow}\hat{d}^{\dagger}_{0\downarrow} + \Delta^{*}_0 \hat{d}_{0\downarrow}\hat{d}_{0\uparrow} \tag{2.160}
$$

with $\epsilon_{k\alpha}$ giving the level structure of the leads $\alpha \in \{L, R\}$, $t_{k\alpha 0}$ corresponding to the tunneling strength between the leads and the dot, and ϵ_0, Δ_0 being the energy and the pairing strength in the dot, respectively. The creation and annihilation operators $\hat{d}^{\dagger}, \hat{d}$ obey the usual fermionic operator algebra: $\{\hat{d}_{x\sigma}, \hat{d}^{\dagger}_{y\sigma'}\} = \delta_{xy}\delta_{\sigma\sigma'}$ for $\{x, y\} \in \{k\alpha, 0\}$ and $\{\sigma, \sigma'\} \in \{\uparrow, \downarrow\}$. Let us introduce a new set of *anti*-operators $\hat{\bar{d}}_{x\sigma} = \hat{d}^{\dagger}_{x\sigma}$ which naturally obey the same commutation relation $\{\hat{\bar{d}}_{x\sigma}, \hat{\bar{d}}^{\dagger}_{y\sigma'}\} = \delta_{xy}\delta_{\sigma\sigma'}$. The Hamiltonian

can now be rewritten in terms of the new and old operators as

$$\begin{aligned}\hat{H} &= \sum_{k\alpha} \epsilon_{k\alpha} \hat{d}^\dagger_{k\alpha\uparrow} \hat{d}_{k\alpha\uparrow} + \sum_{k\alpha} (-\epsilon_{k\alpha}) \hat{\bar{d}}^\dagger_{k\alpha\downarrow} \hat{\bar{d}}_{k\alpha\downarrow} + \sum_{k\alpha} \epsilon_{k\alpha} \\ &+ \sum_{k\alpha} \left(t_{k\alpha 0} \hat{d}^\dagger_{k\alpha\uparrow} \hat{d}_{0\uparrow} + t^*_{k\alpha 0} \hat{d}^\dagger_{0\uparrow} \hat{d}_{k\alpha\uparrow} \right) + \sum_{k\alpha} \left[(-t_{k\alpha 0}) \hat{\bar{d}}^\dagger_{0\downarrow} \hat{\bar{d}}_{k\alpha\downarrow} + (-t^*_{k\alpha 0}) \hat{\bar{d}}^\dagger_{k\alpha\downarrow} \hat{\bar{d}}_{0\downarrow} \right] \\ &+ \epsilon_0 \hat{d}^\dagger_{0\uparrow} \hat{d}_{0\uparrow} + (-\epsilon_0) \hat{\bar{d}}^\dagger_{0\downarrow} \hat{\bar{d}}_{0\downarrow} + \epsilon_0 + \Delta_0 \hat{d}^\dagger_{0\uparrow} \hat{\bar{d}}_{0\downarrow} + \Delta^*_0 \hat{\bar{d}}^\dagger_{0\downarrow} \hat{d}_{0\uparrow} \,, \end{aligned} \tag{2.161}$$

where the constant shift, $\epsilon_0 + \sum_{k\alpha} \epsilon_{k\alpha}$, occurs due to the anticommutation relations. The constant does not modify the overall structure but sets a reference point to the total energy. We could even choose the dot energy to be $\epsilon_0 = -\sum_{k\alpha} \epsilon_{k\alpha}$ for convenience, or we could assume the leads to be in half-filling with $\sum_{k\alpha} \epsilon_{k\alpha} = 0$, etc. The important thing is that the other terms in the Hamiltonian have a similar structure, and we may model the dot part as in the following figure

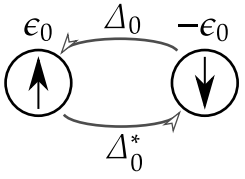

$$\begin{pmatrix} \epsilon_0 & \Delta_0 \\ \Delta_0^* & -\epsilon_0 \end{pmatrix}$$

where the matrix is of the form of Eq. (2.142) and the corresponding eigenvalues are $\epsilon_\pm = \pm\sqrt{\epsilon_0^2 + |\Delta_0|^2}$. The transport setup corresponding to Eq. (2.161) can then be viewed through the following energy diagram

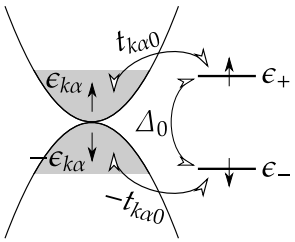

The coupling terms $t_{k\alpha 0}$ connect separately the spin-up and spin-down particles between the leads and the dot, and the pair strength term Δ_0 acts as a hopping term flipping the spins within the dot. This setup can also be made more general by a non-local Δ as in Eq. (2.142).

According to this picture for the NSN setup and the Nambu structure in Eq. (2.156) we will adjust the expressions for the local bond currents in Eq. (2.119) as

$$J_{mn}(t) = -\sum_\sigma \left[T_{mn} (G^<_{\sigma\sigma})_{nm}(t,t) + \text{h.c.} \right], \tag{2.162}$$

where the spin is explicitly taken into account. The Cooper pair density may be evaluated by

$$P_m(t) = \mathrm{i}(F^{>}_{\downarrow\uparrow})_{mm}(t,t)\mathrm{e}^{2\mathrm{i}T_{mm}t}. \tag{2.163}$$

Together these expressions satisfy the continuity equation [131]

$$\frac{\mathrm{d}}{\mathrm{d}t}n_m(t) = \sum_n J_{mn}(t) - 4\,\mathrm{Im}[\Delta^*_m P_m(t)\mathrm{e}^{-2\mathrm{i}T_{mm}t}], \tag{2.164}$$

where the site density is the expectation value $n_m = \langle \hat{n}_m \rangle$ of $\hat{n}_m = \sum_\sigma \hat{d}^\dagger_{m\sigma}\hat{d}_{m\sigma}$. In the Nambu representation of the lesser Green's function the diagonal blocks therefore give rise to the bond current, whereas the off-diagonal blocks correspond to the Cooper pair density. In the continuity equation (2.164) the two different terms on the right-hand side can also be identified as the normal current and the supercurrent.

2.4.3 Arbitrary time-dependence in the bias profile

In 2015, Ridley et al. derived an extension to the formalism presented in this thesis [101]. This is an obvious and very useful extension of the present work, and it deserves a short discussion. In their work, they consider an arbitrary time-dependence for the bias voltage $V_\alpha(t)$ in the α-th lead. The key finding in their work is that this time-dependent part of the Hamiltonian

$$\hat{V}(t) = \sum_{k\alpha,\sigma} V_\alpha(t)\hat{d}^\dagger_{k\alpha,\sigma}\hat{d}_{k\alpha,\sigma} \tag{2.165}$$

commutes with the rest of the Hamiltonian for each α separately. Hence, the contour ordering can be omitted when calculating the corresponding evolution operator. In other words, these terms can be removed from the contour-ordered product of Hamiltonians in the time evolution. This leads to the fact that the expressions for the creation and annihilation operators in the Heisenberg representation can be written as

$$\hat{d}_{k\alpha,\sigma}(t) = \hat{d}_{k\alpha,\sigma}\mathrm{e}^{-\mathrm{i}\phi_{k\alpha}(t,t_0)} = [\hat{d}^\dagger_{k\alpha}(t)]^\dagger \tag{2.166}$$

with t_0 being the time when the voltage is switched on, and

$$\phi_{k\alpha}(t,t_0) = (t-t_0)\epsilon_{k\alpha} + \int_{t_0}^{t} \mathrm{d}\tau V_\alpha(\tau) = (t-t_0)\epsilon_{k\alpha} + \psi_{k\alpha}(t,t_0). \tag{2.167}$$

Then, similar derivations for the different Keldysh components for the self-energies and Green's functions as presented in this thesis may be carried out. In addition, in Ref. [101] the whole two-time plane for the Kadanoff–Baym equations is considered,

and they arrive at the following expression for the lesser and greater two-time Green's functions

$$G^{\gtrless}(t_1,t_2) = \mp \mathrm{i}\int \frac{\mathrm{d}\omega}{2\pi} f(\mp(\omega-\mu)) \sum_\alpha S_\alpha(t_1,t_0,\omega)\Gamma_\alpha S_\alpha^\dagger(t_2,t_0,\omega), \quad (2.168)$$

$$S_\alpha(t,t_0,\omega) = \mathrm{e}^{-\mathrm{i}h_{\mathrm{eff}}(t-t_0)}\left[G^{\mathrm{R}}(\omega) - \mathrm{i}K_\alpha(t,t_0,\omega)\right], \quad (2.169)$$

$$K_\alpha(t,t_0,\omega) = \int_{t_0}^{t} \mathrm{d}t' \mathrm{e}^{-\mathrm{i}(\omega-h_{\mathrm{eff}})(t'-t_0)} \mathrm{e}^{-\mathrm{i}\psi_\alpha(t',t_0)}, \quad (2.170)$$

$$\psi_\alpha(t,t_0) = \int_{t_0}^{t} \mathrm{d}\tau V_\alpha(\tau). \quad (2.171)$$

This can be checked to reduce to the equal-time lesser Green's function in Eq. (2.79) when the bias voltage is constant: $V_\alpha(\tau) = V_\alpha$. It is important to notice that in the present thesis (and in Pubs. [I, II] herein) only the equal time lesser Green's function is derived as this is sufficient to calculate the densities and currents in the studied structures. However, the two-time Green's functions in Eq. (2.168) are required for the calculation of other physical quantities such as noise spectra [137–139].

2.5 Phononic heat transport in the transient regime

So far, the presented theoretical models have only considered electronic transport. We have based the description of our system of interest into the nonequilibrium Green's function whose time-evolution has provided us with the transient information of the transport mechanisms. By introducing two rather strong assumptions – noninteracting particles and wide-band approximation for the lead environment, we have managed to solve analytically the time-evolution governing equations of motion for the Green's function. In this section, we discuss similar methodology applied to a *harmonic lattice* describing the transport of phonons, i.e., it is a model for heat transport. The discussion follows the structure for the theoretical development in Pub. [V].

It is worth pointing out that in the electronic case we were consistently employing the partition-free approach with the systems being initially contacted in a global thermal equilibrium. Then, the bias was switched on instantaneously and all the nonequilibrium behaviour followed from that perturbation. Here, in the case of the phonon transport, instantaneous switch of a temperature difference is problematic and we consider a partitioned approach with the subsystems being initially uncontacted at separate temperatures. Admittedly, this is a somewhat artificial initial configuration of the entire system, which might not be easy to reproduce experimentally, and the transient behaviour is partly induced by the contacting and not

only by the temperature difference. In steady state, however, this information about the initial condition is washed away.

2.5.1 Transport setup and assumptions

We model heat transport in a nanomechanical device composed of harmonic lattices of different temperatures connected as coupled quantum oscillators. The description is for noninteracting phonons only. The Hamiltonian for this sort of a setup can be written in terms of momentum and displacement field operators ($\hbar = 1$) [56, 140] (which obey the canonical commutation relation)

$$\hat{H} = \sum_j \frac{\hat{p}_j^2}{2m_j} + \sum_{j,k} \frac{1}{2} \hat{u}_j K_{jk} \hat{u}_k \tag{2.172}$$

with indices $\{j,k\} \in N$ running over the basis of the studied system, m_j being the mass of the j-th atom, and K_{jk} being the elements of the positive definite force constant matrix. We will define new field operators as mass-normalized ones $\hat{u}'_j = \sqrt{m_j}\hat{u}_j$ and $\hat{p}'_j = \hat{p}_j/\sqrt{m_j}$ obeying the same commutation relations, and write further

$$\hat{H} = \sum_j \frac{1}{2}(\hat{p}'_j)^2 + \sum_{jk} \frac{1}{2} \hat{u}'_j K'_{jk} \hat{u}'_k = \frac{1}{2} \sum_{jk,\mu\nu} \hat{\phi}_j^\mu \Omega_{jk}^{\mu\nu} \hat{\phi}_k^\nu \,, \tag{2.173}$$

where also the spring constant matrix was transformed as $K'_{jk} = K_{jk}/\sqrt{m_j m_k}$, and we composed new field operators as

$$\hat{\boldsymbol{\phi}}_j = \begin{pmatrix} \hat{\phi}_j^1 \\ \hat{\phi}_j^2 \end{pmatrix} = \begin{pmatrix} \hat{u}'_j \\ \hat{p}'_j \end{pmatrix}. \tag{2.174}$$

The matrix elements of the block matrix Ω_{jk} are then given by

$$\boldsymbol{\Omega}_{jk} = \begin{pmatrix} \Omega_{jk}^{11} & \Omega_{jk}^{12} \\ \Omega_{jk}^{21} & \Omega_{jk}^{22} \end{pmatrix} = \begin{pmatrix} K'_{jk} & 0 \\ 0 & \delta_{jk} \end{pmatrix}. \tag{2.175}$$

Matrices in the 2×2 *up*-basis are from now on denoted with boldface symbols. The motivation behind the "spinor"-like $\hat{\boldsymbol{\phi}}$-operator representation is that when we study the time evolution we will get first order (differential) equations instead of second order equations in time [56, 141–143]. (Compare also the *up*-spinor representation to the Nambu spinor representation in the previous section.) The canonical commutation relations are encoded in the field operators $\hat{\boldsymbol{\phi}}$ as

$$\left[\hat{\phi}_j^\mu, \hat{\phi}_k^\nu\right] = \delta_{jk} \alpha^{\mu\nu} \quad \text{with} \quad \alpha = \begin{pmatrix} 0 & \mathrm{i} \\ -\mathrm{i} & 0 \end{pmatrix}. \tag{2.176}$$

The matrix α therefore encodes the commutation relations, and it also holds $\alpha^2 = \mathbb{1}$. We will accordingly define the phononic Green's function for time arguments on the Keldysh contour ($\{z, z'\} \in \gamma$) as

$$D^{\mu\nu}_{jk}(z, z') = -\mathrm{i}\langle \mathcal{T}_\gamma [\hat{\phi}^\mu_j(z) \hat{\phi}^\nu_k(z')] \rangle, \tag{2.177}$$

where $\mathcal{T}_\gamma$ is the contour-time ordering operator and $\langle \cdot \rangle$ is an ensemble average [141, 142]. The equations of motion for the Green's function can be expressed through the time evolution of the field operators $\hat{\boldsymbol{\phi}}$, and they read as (see App. A.2.1)

$$\mathrm{i}\partial_z \boldsymbol{D}_{jk}(z, z') = \alpha \delta_{jk} \delta(z, z') + \sum_q \alpha \boldsymbol{\Omega}_{jq} \boldsymbol{D}_{qk}(z, z'), \tag{2.178}$$

$$-\mathrm{i}\partial_{z'} \boldsymbol{D}_{jk}(z, z') = \alpha \delta_{jk} \delta(z, z') + \sum_q \boldsymbol{D}_{jq}(z, z') \boldsymbol{\Omega}_{qk} \alpha. \tag{2.179}$$

It is also worth noticing that, as we dropped the indices μ, ν, Eqs. (2.178) and (2.179) are matrix equations in the 2×2 *up* representation (boldface symbols).

Let us look more specifically at a transport setup shown in Fig. 2.5. Similarly as in the electronic case, the full Hamiltonian can be expressed as a composition of three parts: the left reservoir (L), the central system (C), and the right reservoir (R)

$$\boldsymbol{\Omega} = \begin{pmatrix} \boldsymbol{\Omega}_{LL} & \boldsymbol{\Omega}_{LC} & 0 \\ \boldsymbol{\Omega}_{CL} & \boldsymbol{\Omega}_{CC} & \boldsymbol{\Omega}_{CR} \\ 0 & \boldsymbol{\Omega}_{RC} & \boldsymbol{\Omega}_{RR} \end{pmatrix}, \tag{2.180}$$

i.e., the different subsystems are coupled apart from a direct coupling between the reservoirs. In Eq. (2.180) each diagonal block is a $2N_C$-by-$2N_C$ or $2N_\lambda$-by-$2N_\lambda$ matrix for $\lambda \in \{L, R\}$. (In the electronic case, we denoted the leads by an index α but this symbol is now reserved for the *up*-commutator matrix in Eq. (2.176); we denote the reservoirs in the phononic case with an index λ.) The block structures for the diagonal elements are simply those discussed earlier

$$(\boldsymbol{\Omega}_{CC})_{j_C k_C} = \begin{pmatrix} K'_{j_C k_C} & 0 \\ 0 & \delta_{j_C k_C} \end{pmatrix}; \quad (\boldsymbol{\Omega}_{\lambda\lambda})_{j_\lambda k_\lambda} = \begin{pmatrix} K'_{j_\lambda k_\lambda} & 0 \\ 0 & \delta_{j_\lambda k_\lambda} \end{pmatrix}. \tag{2.181}$$

The different regions, however, couple only through the displacement term, so the block structures for the off-diagonal elements are given by

$$(\boldsymbol{\Omega}_{C\lambda})_{j_C k_\lambda} = \begin{pmatrix} K'_{j_C k_\lambda} & 0 \\ 0 & 0 \end{pmatrix}; \quad (\boldsymbol{\Omega}_{\lambda C})_{j_\lambda k_C} = \begin{pmatrix} K'_{j_\lambda k_C} & 0 \\ 0 & 0 \end{pmatrix} \tag{2.182}$$

for $\lambda \in \{L, R\}$.

We are mainly interested in the transport properties of the central system, so we extract the component corresponding to the central region, CC, from the equations

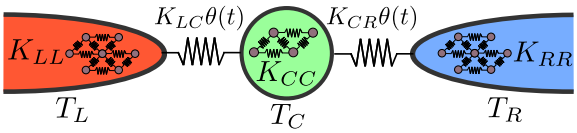

Fig. 2.5: Heat transport setup where a central system of interest is connected to two reservoirs of different temperatures. The internal structures and couplings (drawn only as a visualization) are defined by the force constant matrices K. The coupling refers to partitioned approach where the different systems are uncoupled at times $t < 0$ and coupled at times $t \geq 0$ when the system is driven out of equilibrium.

of motion (2.178) and (2.179). We lighten the notation here a little by letting C label the elements in the central region and λ the elements in the reservoirs. This procedure leads to the following set of equations (see App. A.2.1)

$$(\mathrm{i}\mathbf{1}_{CC}\partial_z - \boldsymbol{\alpha}_{CC}\boldsymbol{\Omega}_{CC})\boldsymbol{D}_{CC}(z,z') = \boldsymbol{\alpha}_{CC}\delta(z,z') + \boldsymbol{\alpha}_{CC}\boldsymbol{I}_{CC,1}(z,z'), \tag{2.183}$$

$$\boldsymbol{D}_{CC}(z,z')(-\mathrm{i}\mathbf{1}_{CC}\overleftarrow{\partial}_{z'} - \boldsymbol{\Omega}_{CC}\boldsymbol{\alpha}_{CC}) = \boldsymbol{\alpha}_{CC}\delta(z,z') + \boldsymbol{I}_{CC,2}(z,z')\boldsymbol{\alpha}_{CC}, \tag{2.184}$$

$$\boldsymbol{I}_{CC,1}(z,z') = \int_\gamma \mathrm{d}\bar{z}\boldsymbol{\Pi}_{CC}(z,\bar{z})\boldsymbol{D}_{CC}(\bar{z},z'), \tag{2.185}$$

$$\boldsymbol{I}_{CC,2}(z,z') = \int_\gamma \mathrm{d}\bar{z}\boldsymbol{D}_{CC}(z,\bar{z})\boldsymbol{\Pi}_{CC}(\bar{z},z'), \tag{2.186}$$

$$\boldsymbol{\Pi}_{CC}(z,z') = \sum_\lambda \boldsymbol{\Omega}_{C\lambda}\boldsymbol{d}_{\lambda\lambda}(z,z')\boldsymbol{\Omega}_{\lambda C}, \tag{2.187}$$

$$(\mathrm{i}\mathbf{1}_{\lambda\lambda}\partial_z - \boldsymbol{\alpha}_{\lambda\lambda}\boldsymbol{\Omega}_{\lambda\lambda})\boldsymbol{d}_{\lambda\lambda}(z,z') = \boldsymbol{\alpha}_{\lambda\lambda}\delta(z,z'). \tag{2.188}$$

In the derivation, we introduced $\boldsymbol{d}_{\lambda\lambda}$ as the isolated phonon Green's function in the reservoir λ satisfying the equation of motion (2.188) with the reservoir Hamiltonian $\boldsymbol{\Omega}_{\lambda\lambda}$. We also wrote $\boldsymbol{\alpha}_{CC} \coloneqq \alpha \otimes \mathbf{1}_{CC}$ and $\boldsymbol{\alpha}_{\lambda\lambda} \coloneqq \alpha \times \mathbf{1}_{\lambda\lambda}$ as $2N_C \times 2N_C$ and $2N_\lambda \times 2N_\lambda$ matrices, respectively. Also, as we consider only noninteracting phonons (no electron–phonon or phonon–phonon interactions), the self-energy term $\boldsymbol{\Pi}_{CC}$ in the collision integrals (2.185) and (2.186) is given solely as *the embedding self-energy* defined in terms of the coupling Hamiltonians $\boldsymbol{\Omega}_{C\lambda}$ in Eq. (2.187). From Eq. (2.183) and its adjoint equation (2.184) we can derive an equation of motion for the lesser Green's function $\boldsymbol{D}^<_{CC}$ by using the Langreth rules [73, 116] for the collision integrals. Particularly, we are interested in the time-dependent phonon density matrix given by the equal-time lesser Green's function $\boldsymbol{\rho}(t) = \mathrm{i}\boldsymbol{D}^<_{CC}(t,t)$, and for this we simply consider only the time-diagonal elements. The procedure involves subtracting Eq. (2.184) from Eq. (2.183) which, in the equal-time limit, leads to the partial derivatives adding up to the total derivative, and in total we get

$$\mathrm{i}\frac{\mathrm{d}}{\mathrm{d}t}\boldsymbol{D}^<(t,t) - [\boldsymbol{\alpha}\boldsymbol{\Omega}\boldsymbol{D}^<(t,t) - \boldsymbol{D}^<(t,t)\boldsymbol{\Omega}\boldsymbol{\alpha}] = -\{[\boldsymbol{D}^\mathrm{R}\cdot\boldsymbol{\Pi}^<] + [\boldsymbol{D}^<\cdot\boldsymbol{\Pi}^\mathrm{A}] + [\boldsymbol{D}^\rceil \star \boldsymbol{\Pi}^\lceil]\}(t,t)\boldsymbol{\alpha} + \mathrm{h.c.}, \tag{2.189}$$

where we defined, similarly as in the electronic case, the time-convolutions on the contour γ as $[a \cdot b](t,t) = \int_0^\infty \mathrm{d}\bar{t} a(t,\bar{t})b(\bar{t},t)$ and $[a \star b](t,t) = -\mathrm{i}\int_0^\beta \mathrm{d}\bar{\tau} a(t,\bar{\tau})b(\bar{\tau},t)$ for Keldysh functions a and b, and we also dropped the subscripts CC as there should be no room for misunderstanding. Strictly speaking the derivation of Eq. (2.189) requires a single inverse temperature $\beta = 1/T$ for the whole system because of the convolution along the imaginary axis. As we will consider partitioned systems, imaginary-time convolutions vanish and we can assign different temperatures to different subsystems. The interpretation for Eq. (2.189) is exactly the same as in the electronic case, see Eq. (2.67): If we did not have the central system embedded into the environment, the self-energy terms would simply be zero, and we would be left with a Liouville-type equation for the time-evolution of the one-phonon reduced density matrix for an isolated central region. The self-energy terms, therefore, account for the open transport setup where a finite central region is embedded into the environment.

So far, the discussion has been rather general, and Eq. (2.189) also applies to many different setups beyond the present study. Similarly as in the electronic case, our aim is to solve (analytically) this integro-differential equation for $\boldsymbol{D}^<$ and then extract dynamical quantities such as heat currents from the time-dependent phonon density matrix. As the equations to solve are almost equivalent to the electronic transport (the difference being in the matrix $\boldsymbol{\alpha}$ and furthermore the composed *up*-representation of the Green's function components), it is easy to follow a very similar path in deriving the analytic result for the phonon density matrix.

For solving the equation (2.189) we need to make some approximations, first one being *the partitioned* approach, i.e., all regions in the transport setup are initially ($t < 0$) uncoupled and in separate thermodynamical equilibrium. At $t = 0$ we couple the different regions and drive the systems out of equilibrium via a temperature difference, see Fig. 2.5. In contrast to the electronic case, this procedure disregards the initial couplings: $\boldsymbol{\Omega}_{\lambda C} = 0$ in equilibrium, so the integrations along the vertical track of the Keldysh contour in Eq. (2.189) are simply left out. The remaining two terms can be interpreted as a source/drain and a damping/equilibration term. The drain (source) term is a convolution between the propagator in the central region, $\boldsymbol{D}^\mathrm{A}$ (h.c.), and the lesser embedding self-energy $\boldsymbol{\Pi}^<$ which is proportional to the probability of finding a phonon in the reservoirs, i.e., it describes the extraction (insertion) of phonons out of (into) the central region. The second term is a convolution between the propagator in the reservoirs, $\boldsymbol{\Pi}^\mathrm{R}$ (h.c.) and the lesser Green's function in the central region $\boldsymbol{D}^<$ which is proportional to the probability of finding a phonon in the central region, i.e., it is responsible for damping (equilibration) effects.

Next, we need an approximation for the embedding self-energy, $\boldsymbol{\Pi}^\mathrm{R}$, typically expressed as a wide-band approximation where the energy scale of the central region

is much more narrow than the energy scale of the reservoirs. This makes the self-energies in time domain to be proportional to delta functions (and derivatives of delta functions) which, in turn, closes the equation for $\boldsymbol{D}^<$. Given an approximation for $\boldsymbol{\Pi}^\mathrm{R}$, we may derive $\boldsymbol{\Pi}^<$ from a fluctuation–dissipation relation and $\boldsymbol{D}^\mathrm{R}$ from a Dyson-type of equation.

2.5.2 Embedding self-energy and frequency cut-off

Let us start by considering the coupling of the central region to the reservoirs and the embedding self-energy. For Eq. (2.187) we need the coupling Hamiltonians and the reservoir Green's function. And, as we are considering the retarded component of the embedding self-energy, we need to find an expression for $\boldsymbol{d}^\mathrm{R}$. For the isolated phonon Green's function in the reservoir λ we have the following expression

$$\begin{aligned} \boldsymbol{d}_{\lambda\lambda}(z,z') &= -\mathrm{i}\boldsymbol{\alpha}_{\lambda\lambda}\theta(z,z')\bar{f}_\lambda(\boldsymbol{\Omega}_{\lambda\lambda}\boldsymbol{\alpha}_{\lambda\lambda})\mathrm{e}^{-\mathrm{i}\boldsymbol{\Omega}_{\lambda\lambda}\boldsymbol{\alpha}_{\lambda\lambda}(z-z')} \\ &\quad -\mathrm{i}\boldsymbol{\alpha}_{\lambda\lambda}\theta(z',z)f_\lambda(\boldsymbol{\Omega}_{\lambda\lambda}\boldsymbol{\alpha}_{\lambda\lambda})\mathrm{e}^{-\mathrm{i}\boldsymbol{\Omega}_{\lambda\lambda}\boldsymbol{\alpha}_{\lambda\lambda}(z-z')} \end{aligned} \tag{2.190}$$

which can be checked to satisfy Eq. (2.188) by direct differentiation. In the above expression $\bar{f}_\lambda = 1 + f_\lambda$ and $f_\lambda(\omega) = (\mathrm{e}^{\beta_\lambda\omega} - 1)^{-1}$ is the Bose–Einstein distribution (for reservoir λ). This will also give the density matrix for an isolated system when $z' \to z^+$. By using the above expression for the uncoupled Green's function we may derive different Keldysh components and calculate the retarded embedding self-energy from Eq. (2.187), see App. A.2.2. We find that the real and imaginary parts of the retarded embedding self-energy

$$\boldsymbol{\Pi}^\mathrm{R}_\lambda(\omega) = \begin{pmatrix} \Pi^\mathrm{R}_\lambda(\omega) & 0 \\ 0 & 0 \end{pmatrix} =: \boldsymbol{\Lambda}_\lambda(\omega) - \frac{\mathrm{i}}{2}\boldsymbol{\Gamma}'_\lambda(\omega) \tag{2.191}$$

are, respectively, even and odd functions in frequency ω. We will accordingly make approximations so that

$$\boldsymbol{\Lambda}_\lambda(\omega) \approx \boldsymbol{\Lambda}_\lambda(\omega = 0) = \boldsymbol{\Lambda}_{0,\lambda}\ , \tag{2.192}$$

$$\boldsymbol{\Gamma}_\lambda(\omega) \approx \omega\left.\frac{\partial\boldsymbol{\Gamma}_\lambda}{\partial\omega}\right|_{\omega=0} = \omega\boldsymbol{\Gamma}'_{0,\lambda}. \tag{2.193}$$

In contrast to the conventional wide-band approximation in electronic transport, now the retarded embedding self-energy is not a purely imaginary constant. Instead, the imaginary part will be frequency dependent (linearized approximation) whereas the real part will be constant. Also, as the matrices K are by construction positive definite, then from Eq. (2.192) we get that $\boldsymbol{\Lambda}_{0,\lambda}$ is negative definite [also see Eq. (A.96)] and from Eqs. (2.191) and (2.193) that $\boldsymbol{\Gamma}'_{0,\lambda}$ is positive definite. This approximation for the real and imaginary parts of the embedding self-energy

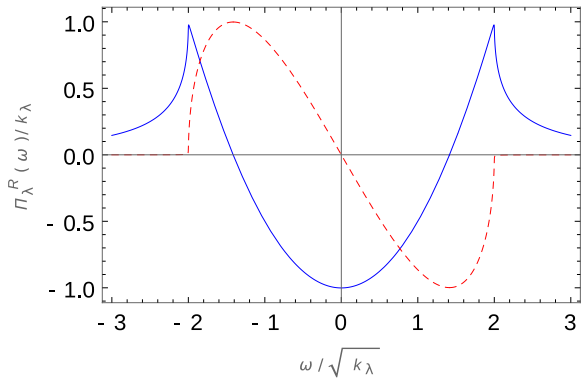

Fig. 2.6: Frequency dependency of the retarded embedding self-energy for the infinite coupled spring model: Solid blue line is the real part and dashed red line is the imaginary part. The axes are scaled with the inter atom spring constant k_λ.

function does not satisfy the Kramers–Kronig relations [73, 118], and for this reason we momentarily consider a frequency cut-off regulating divergent behaviour. Compared to Eqs. (2.192) and (2.193) similar wide-band-like approximations for the self-energy have been proposed in Refs. [144, 145] where the embedding self-energy is approximated as a purely imaginary sign function. However, due to the structure of the sign function, this approximation also violates the Kramers–Kronig relations.

This approximation also corresponds to the form calculated explicitly for a uniform one-dimensional system of N coupled springs [146]. We will take this model for our reservoirs (N_λ sites coupled with equal springs) and construct the embedding self-energy accordingly. In this model, the force constant matrix $K_{\lambda\lambda}$ has diagonal elements $2k_\lambda + k_{\lambda,0}$ and the first off-diagonal elements $-k_\lambda$. For simplicity, we let the on-site term be zero $k_{\lambda,0} = 0$ as it only corresponds to a shift in the phonon band. In the limit $N_\lambda \to \infty$ the retarded embedding self-energy is given by $\Pi_\lambda^{\mathrm{R}}(\omega) = -k_\lambda z$ where z is the solution to the quadratic equation (see Sec. 7 in Ref. [146])

$$k_\lambda z^{-1} + (\omega + \mathrm{i}\eta)^2 - 2k_\lambda + k_\lambda z = 0. \tag{2.194}$$

The solutions are plotted in Fig. 2.6 ($\eta \to 0$) against ω. The imaginary part of the self-energy will be nonzero for $|\omega| < 2\sqrt{k_\lambda}$ introducing the phonon bandwidth. The behaviour of the approximations in Eqs. (2.192) and (2.193) around $\omega = 0$ is also visible in Fig. 2.6.

In contrast to Ref. [146] small adjustments are still in order for the values in Eqs. (2.192) and (2.193): In our setup the coupling strength between the reservoirs and the central region is not the same as the spring constants inside the reservoirs or inside the central region. In this case, the retarded embedding self-energy is written

as

$$\Pi^{\mathrm{R}}(\omega) = -\frac{k_{\lambda C}^2}{k_\lambda} z(\omega), \tag{2.195}$$

$$z(\omega) = \frac{1}{2k_\lambda}\left[2k_\lambda - \omega^2 + \zeta_\lambda(\omega)\omega\sqrt{(\omega - 2\sqrt{k_\lambda})(\omega + 2\sqrt{k_\lambda})}\right] \tag{2.196}$$

with $\zeta_\lambda(\omega) = \mathrm{sgn}(\omega + 2\sqrt{k_\lambda})$ and where z still satisfies Eq. (2.194). The phonon bandwidth in this setup, $|\omega| < 2\sqrt{k_\lambda}$, is similar to the electron bandwidth in one-dimensional tight-binding lattice $|\epsilon| < 2t_{\mathrm{hop}}$ [73], where t_{hop} is the hopping integral between the tight-binding lattice sites, since $\sqrt{k_\lambda}$ can here be understood as a harmonic oscillator's characteristic mode $\omega = \sqrt{k/m}$. Within our approximation in Eqs. (2.192) and (2.193) we get $\Lambda_{0,\lambda} = \mathrm{Re}\,\Pi^{\mathrm{R}}(\omega = 0) = -k_{\lambda C}^2/k_\lambda$. Approximating the imaginary part (when $|\omega| < 2\sqrt{k_\lambda}$) is evaluated as the first order expansion at $\omega = 0$ as in Eq. (2.193): $\mathrm{Im}\,\Pi^{\mathrm{R}}(\omega) = \partial_\omega\,\mathrm{Im}\,\Pi^{\mathrm{R}}(\omega)\big|_{\omega=0}\,\omega = k_{\lambda C}^2/k_\lambda^{3/2}\omega$ giving $\Gamma'_{0,\lambda} = 2k_{\lambda C}^2/k_\lambda^{3/2}$.

It would also be possible to include the terminal site of the reservoirs into the description of the central region; we have an arbitrary matrix structure for the central region in $\boldsymbol{\Omega}_{CC}$, so this would not add any complications. In this way, also the coupling of the central region to the reservoirs is included in the central region's description and the parameter for the coupling strength can be chosen equal to the coupling parameter within the reservoirs. However, we continue with the form in Eq. (2.195).

Since the embedding self-energy only has nonzero components in the '*uu*' block, we express it now in the following form

$$\boldsymbol{\Pi}_\lambda^{\mathrm{R}}(\omega) = \begin{pmatrix} \Lambda_{0,\lambda} - \frac{\mathrm{i}\omega}{2}\Gamma'_{0,\lambda} & 0 \\ 0 & 0 \end{pmatrix} = \boldsymbol{\Lambda}_{0,\lambda} - \frac{\mathrm{i}\omega}{2}\boldsymbol{\Gamma}'_{0,\lambda}\,, \tag{2.197}$$

where each element of the 2×2 matrix is an $N_C \times N_C$ matrix. Also, summing over the different reservoirs λ gives the total embedding self-energy: $\boldsymbol{\Pi}^{\mathrm{R}} = \sum_{\lambda=L,R} \boldsymbol{\Pi}_\lambda^{\mathrm{R}}$, and this also applies to the real and imaginary parts $\boldsymbol{\Lambda}_0$ and $\boldsymbol{\Gamma}'_0$.

Compared to the conventional wide-band approximation here we might run into problems with our approximation for the embedding self-energy because of the unboundedness of the imaginary part $\omega\boldsymbol{\Gamma}'_0/2$ when $|\omega| \to \infty$. For this reason, we introduce a cut-off frequency ω_c above which the approximation for the embedding self-energy would simply be zero

$$\boldsymbol{\Pi}_\lambda^{\mathrm{R}}(\omega) = \theta(\omega_c - |\omega|)(\boldsymbol{\Lambda}_{0,\lambda} - \frac{\mathrm{i}\omega}{2}\boldsymbol{\Gamma}'_{0,\lambda}). \tag{2.198}$$

A natural choice for the cut-off frequency would be the phonon bandwidth; we could tune the considered frequency range by varying the reservoir parameters,

see Fig. 2.6. The lesser component of the embedding self-energy is then simply given by the fluctuation–dissipation relation [73]

$$\boldsymbol{\Pi}^{<}_{\lambda}(\omega) = \theta(\omega_c - |\omega|)[-\mathrm{i} f_\lambda(\omega)\omega \boldsymbol{\Gamma}'_{0,\lambda}]. \tag{2.199}$$

The cut-off frequency ω_c, on the other hand, also gives an energy scale above which the central system does not feel the embedding. In our partitioned approach, this relates to a time scale, after the contact, when the system is embedded. Since in the equation of motion our Green's functions $\boldsymbol{D}^{\mathrm{R,A}}$ appear together with the embedding self-energy, we will regard them as *embedded* ones, meaning they are calculated for the coupled system. In principle, there is a contribution from isolated Green's functions, $\boldsymbol{d}^{\mathrm{R,A}}$, but our approximation for the embedding self-energy together with the cut-off frequency neglects this. There is a more thorough discussion about the motivation for the cut-off frequency in App. A.2.3.

2.5.3 Solving the equations of motion

Based on our approximations discussed in the previous section we may now derive expression for the time convolutions in Eq. (2.189). More detailed calculations are presented in App. A.2.3 and we state here only the results.

For the convolution between the retarded (advanced) Green's function and lesser embedding self-energy the cut-off frequency is explicitly present as a step function, as in Eq. (2.199)

$$\left[\boldsymbol{D}^{\mathrm{R}} \cdot \boldsymbol{\Pi}^{<}\right](t,t) = -\mathrm{i} \sum_{\lambda=L,R} \int_{-\infty}^{\infty} \frac{\mathrm{d}\omega}{2\pi} \left[\mathbf{1} - \mathrm{e}^{\mathrm{i}(\omega - \boldsymbol{\Omega}_{\mathrm{eff}})t}\right] \boldsymbol{D}^{\mathrm{R}}(\omega)\theta(\omega_c - |\omega|)\omega f_\lambda(\omega)\boldsymbol{\Gamma}'_{0,\lambda}. \tag{2.200}$$

As the frequency integral is cut off, we evaluate $\boldsymbol{D}^{\mathrm{R}}$ in the limit $\omega_{c,\lambda} \to \infty$ [see Eq. (A.101)]:

$$\boldsymbol{D}^{\mathrm{R}}(\omega) = \frac{1}{\omega - \boldsymbol{\Omega}_{\mathrm{eff}}} \frac{1}{\boldsymbol{\alpha} + \frac{\mathrm{i}}{2}\boldsymbol{\Gamma}'_0}. \tag{2.201}$$

By conjugating Eq. (2.200), we also get

$$\left[\boldsymbol{\Pi}^{<} \cdot \boldsymbol{D}^{\mathrm{A}}\right](t,t) = -\mathrm{i} \sum_{\lambda=L,R} \int_{-\infty}^{\infty} \frac{\mathrm{d}\omega}{2\pi} \theta(\omega_c - |\omega|)\omega f_\lambda(\omega)\boldsymbol{\Gamma}'_{0,\lambda}\boldsymbol{D}^{\mathrm{A}}(\omega) \left[\mathbf{1} - \mathrm{e}^{-\mathrm{i}(\omega - \boldsymbol{\Omega}^{\dagger}_{\mathrm{eff}})t}\right], \tag{2.202}$$

where $\boldsymbol{D}^{\mathrm{A}}$ is found by conjugating Eq. (2.201). Here we defined the effective (non-hermitian) Hamiltonian as

$$\boldsymbol{\Omega}_{\mathrm{eff}} = \frac{1}{\boldsymbol{\alpha} + \frac{\mathrm{i}}{2}\boldsymbol{\Gamma}'_0}(\boldsymbol{\Omega} + \boldsymbol{\Lambda}_0). \tag{2.203}$$

It is worth noticing that in Eqs. (2.200) and (2.202) the integrands are proportional to $\omega f(\omega)$ which is unbounded when $\omega \to -\infty$. This diverging nature of the frequency integrals is then regulated by the cut-off frequency.

For the convolution between the lesser Green's function and the retarded/advanced embedding self-energy the cut-off frequency is more implicitly taken into account. As the lesser Green's function gives rise to oscillation frequencies corresponding to the physical setup, we may compare these frequencies to the ones encoded in the retarded/advanced embedding self-energy whose oscillation frequencies depend on the choice for the cut-off frequency. If we choose the cut-off frequency considerably higher than typical energy scales of the studied system we may regard the retarded/advanced embedding self-energies as in the limit $\omega_c \to \infty$, see details in App. A.2.3. The second convolution is then evaluated as

$$\left[\boldsymbol{D}^< \cdot \boldsymbol{\Pi}^{\mathrm{A}}\right](t,t) = \boldsymbol{D}^<(t,t)\boldsymbol{\Lambda}_0 + \left.\frac{\partial \boldsymbol{D}^<(t,t')}{\partial t'}\right|_{t'=t} \frac{\boldsymbol{\Gamma}_0'}{2}, \tag{2.204}$$

and by conjugating we also get

$$\left[\boldsymbol{\Pi}^{\mathrm{R}} \cdot \boldsymbol{D}^<\right](t,t) = \boldsymbol{\Lambda}_0\boldsymbol{D}^<(t,t) + \frac{\boldsymbol{\Gamma}_0'}{2} \left.\frac{\partial \boldsymbol{D}^<(t,t')}{\partial t}\right|_{t=t'}. \tag{2.205}$$

If we, on the other hand, fix the cut-off frequency at the phonon bandwidth, and want this description to be a good approximation, we should tune our system parameters such that the characteristic frequencies fall well into the cut-off regime, i.e., the spectrum of the studied system is narrow compared to the bandwidth of the reservoirs.

An important thing to notice is that the convolutions in Eqs. (2.204) and (2.205) depend not only directly on $\boldsymbol{D}^<$ but also on the time-derivative of $\boldsymbol{D}^<$ at equal-time limit. This means that inserting these expressions back into the equation of motion does not immediately close the equation for $\boldsymbol{D}^<$. However, we may insert the explicit time-evolution from Eqs. (2.183) and (2.184) for the derivative terms and then couple the terms accordingly. As Eqs. (2.183) and (2.184) include the same convolutions, we will gain similar terms by this procedure. But, as it turns out, this procedure still closes the equation for $\boldsymbol{D}^<$.

Now we are ready to insert Eqs. (2.200), (2.202), (2.204), and (2.205) into Eq. (2.189):

$$\begin{aligned}
&\mathrm{i}\frac{\mathrm{d}}{\mathrm{d}t}\boldsymbol{D}^{<}(t,t) - \left[\boldsymbol{\alpha}\boldsymbol{\Omega}\boldsymbol{D}^{<}(t,t) - \boldsymbol{D}^{<}(t,t)\boldsymbol{\Omega}\boldsymbol{\alpha}\right] \\
= \;& \boldsymbol{\alpha}\Bigg[-\mathrm{i}\sum_{\lambda=L,R}\int\frac{\mathrm{d}\omega}{2\pi}\theta(\omega_c-|\omega|)\omega f_\lambda(\omega)\boldsymbol{\Gamma}'_{0,\lambda}\boldsymbol{D}^{\mathrm{A}}(\omega)\left[\mathbf{1}-\mathrm{e}^{-\mathrm{i}(\omega-\boldsymbol{\Omega}^{\dagger}_{\mathrm{eff}})t}\right] \\
& +\boldsymbol{\Lambda}_0\boldsymbol{D}^{<}(t,t) + \frac{\boldsymbol{\Gamma}'_0}{2}\left.\frac{\partial\boldsymbol{D}^{<}(t,t')}{\partial t}\right|_{t=t'}\Bigg] \\
- \;& \Bigg[\boldsymbol{D}^{<}(t,t)\boldsymbol{\Lambda}_0 + \left.\frac{\partial\boldsymbol{D}^{<}(t,t')}{\partial t'}\right|_{t'=t}\frac{\boldsymbol{\Gamma}'_0}{2} \\
& -\mathrm{i}\sum_{\lambda=L,R}\int\frac{\mathrm{d}\omega}{2\pi}\theta(\omega_c-|\omega|)\omega f_\lambda(\omega)\left[\mathbf{1}-\mathrm{e}^{\mathrm{i}(\omega-\boldsymbol{\Omega}_{\mathrm{eff}})t}\right]\boldsymbol{D}^{\mathrm{R}}(\omega)\boldsymbol{\Gamma}'_{0,\lambda}\Bigg]\boldsymbol{\alpha}. \qquad (2.206)
\end{aligned}$$

Then, we will insert $\partial\boldsymbol{D}(t,t')/\partial t$ and $\partial\boldsymbol{D}(t,t')/\partial t'$ from Eqs. (2.183) and (2.184), and accordingly insert the consequent convolutions from Eqs. (2.200), (2.202), (2.204), and (2.205). By combining terms and simplifying we end up with (see App. A.2.4)

$$\begin{aligned}
&\mathrm{i}\frac{\mathrm{d}\boldsymbol{D}^{<}(t,t)}{\mathrm{d}t} - \boldsymbol{\Omega}_{\mathrm{eff}}\boldsymbol{D}^{<}(t,t) + \boldsymbol{D}^{<}(t,t)\boldsymbol{\Omega}^{\dagger}_{\mathrm{eff}} \\
= \;& -\mathrm{i}\sum_{\lambda=L,R}\int\frac{\mathrm{d}\omega}{2\pi}\theta(\omega_c-|\omega|)\omega f_\lambda(\omega)\Big\{\boldsymbol{\alpha}\boldsymbol{\Gamma}'_{0,\lambda}\boldsymbol{D}^{\mathrm{A}}(\omega)\left[\mathbf{1}-\mathrm{e}^{-\mathrm{i}(\omega-\boldsymbol{\Omega}^{\dagger}_{\mathrm{eff}})t}\right] \\
& -\left[\mathbf{1}-\mathrm{e}^{\mathrm{i}(\omega-\boldsymbol{\Omega}_{\mathrm{eff}})t}\right]\boldsymbol{D}^{\mathrm{R}}(\omega)\boldsymbol{\Gamma}'_{0,\lambda}\boldsymbol{\alpha}\Big\}. \qquad (2.207)
\end{aligned}$$

In the above expression, all the terms involving derivatives of the lesser Green's function [inserted $\partial\boldsymbol{D}(t,t')/\partial t$ and $\partial\boldsymbol{D}(t,t')/\partial t'$ from Eqs. (2.183) and (2.184)] vanished as we noticed, by evaluating simple matrix products, that

$$\boldsymbol{\Gamma}'_{0,(\lambda)}\boldsymbol{\alpha}\boldsymbol{\Lambda}_0 = \boldsymbol{\Lambda}_0\boldsymbol{\alpha}\boldsymbol{\Gamma}'_{0,(\lambda)} = \boldsymbol{\Gamma}'_{0,(\lambda)}\boldsymbol{\alpha}\boldsymbol{\Gamma}'_{0,(\lambda)} = 0. \qquad (2.208)$$

All the higher order derivatives are also truncated based on these matrix structures. In Eq. (2.207) we now have a linear, first order, nonhomogeneous differential equation for $\boldsymbol{D}^{<}$ which can be solved uniquely with an initial condition. Solving the differential equation is done almost identically to the electronic case but the procedure is still outlined in App. A.2.4; the solution is

$$\mathrm{i}\boldsymbol{D}^{<}(t,t) = \mathrm{i}\boldsymbol{D}^{<}_0(t,t) + \sum_{\lambda=L,R}\int_{-\omega_c}^{\omega_c}\frac{\mathrm{d}\omega}{2\pi}f_\lambda(\omega)\left[\mathbf{1}-\mathrm{e}^{\mathrm{i}(\omega-\boldsymbol{\Omega}_{\mathrm{eff}})t}\right]\boldsymbol{B}_\lambda(\omega)\left[\mathbf{1}-\mathrm{e}^{-\mathrm{i}(\omega-\boldsymbol{\Omega}^{\dagger}_{\mathrm{eff}})t}\right] \qquad (2.209)$$

with the initial condition

$$\mathrm{i}\boldsymbol{D}^{<}_0(t,t) = \mathrm{e}^{-\mathrm{i}\boldsymbol{\Omega}_{\mathrm{eff}}t}\boldsymbol{\alpha}f_C(\boldsymbol{\Omega}\boldsymbol{\alpha})\mathrm{e}^{\mathrm{i}\boldsymbol{\Omega}^{\dagger}_{\mathrm{eff}}t} \qquad (2.210)$$

stemming from the uncoupled lesser Green's function in the central region as in Eq. (A.87) where the Bose–Einstein distribution function f_C is then defined via an equilibrium temperature for the central region before coupling. The spectral function $\boldsymbol{B}_\lambda(\omega) = \boldsymbol{D}^{\mathrm{R}}(\omega)\omega\boldsymbol{\Gamma}'_{0,\lambda}\boldsymbol{D}^{\mathrm{A}}(\omega)$ can be evaluated as

$$\boldsymbol{B}_\lambda(\omega) = \frac{1}{\omega(\boldsymbol{\alpha} + \frac{\mathrm{i}}{2}\boldsymbol{\Gamma}'_0) - \boldsymbol{\Omega} - \boldsymbol{\Lambda}_0}\omega\boldsymbol{\Gamma}'_{0,\lambda}\frac{1}{\omega(\boldsymbol{\alpha} - \frac{\mathrm{i}}{2}\boldsymbol{\Gamma}'_0) - \boldsymbol{\Omega} - \boldsymbol{\Lambda}_0}. \tag{2.211}$$

Equation (2.209) is our final result for the time-dependent one-particle phonon density matrix. Remarkably, it is a closed expression, i.e., no time propagation is needed for evaluating the time-dependent density matrix, as was the case in the electronic transport as well. The form of the solution in Eq. (2.209) also follows the general structure of a Landauer–Büttiker type: a frequency integral over spectral ("transmission") functions [143, 147]. The transient behaviour is encoded in the exponentials: we have oscillations with frequencies $\omega_{jk} = |\mathrm{Re}\,\omega_{j,\mathrm{eff}} - \mathrm{Re}\,\omega_{k,\mathrm{eff}}|$ as transitions between the vibrational frequencies of the central region. Here ω_{eff} are the complex eigenvalues of the effective Hamiltonian $\boldsymbol{\Omega}_{\mathrm{eff}}$. Finally, $\omega f_\lambda(\omega)$ is well-behaving at $\omega = 0$ (although $f_\lambda(\omega)$ diverges at zero), and the cut-off frequency ω_c regulates the unbounded behaviour at $\omega \to -\infty$.

It is instructive to investigate few limiting cases for Eq. (2.209). At $t = 0$ the square brackets will simply vanish due to the exponentials being unit matrices, and therefore we are left with the uncoupled result, as should be the case due to the initial condition. This also happens if the systems remain uncoupled, i.e., $\boldsymbol{\Lambda}_0 = 0 = \boldsymbol{\Gamma}'_0$; then we are left with the free evolution of the initial state as $\boldsymbol{\Omega}_{\mathrm{eff}} \to \boldsymbol{\alpha}\boldsymbol{\Omega}$ and $\boldsymbol{B}_\lambda(\omega) \to 0$. The steady-state result comes from the limit $t \to \infty$ when the exponentials vanish due to the non-hermitian structure of $\boldsymbol{\Omega}_{\mathrm{eff}}$:

$$\boldsymbol{\rho}_{\mathrm{SS}} = \sum_{\lambda=L,R}\int_{-\omega_c}^{\omega_c}\frac{\mathrm{d}\omega}{2\pi}f_\lambda(\omega)\frac{1}{\boldsymbol{\alpha}\omega - \boldsymbol{\Omega} - (\boldsymbol{\Lambda}_0 - \frac{\mathrm{i}\omega}{2}\boldsymbol{\Gamma}'_0)}\omega\boldsymbol{\Gamma}'_{0,\lambda}\frac{1}{\boldsymbol{\alpha}\omega - \boldsymbol{\Omega} - (\boldsymbol{\Lambda}_0 + \frac{\mathrm{i}\omega}{2}\boldsymbol{\Gamma}'_0)}. \tag{2.212}$$

Within our self-energy approximation, $\boldsymbol{\Pi}^{\mathrm{R/A}}(\omega) = \theta(\omega_c - |\omega|)(\boldsymbol{\Lambda}_{0,\lambda} \mp \frac{\mathrm{i}\omega}{2}\boldsymbol{\Gamma}'_{0,\lambda})$, we may write Eq. (2.212) as

$$\boldsymbol{\rho}_{\mathrm{SS}} = \sum_{\lambda=L,R}\int_{-\infty}^{\infty}\frac{\mathrm{d}\omega}{2\pi}f_\lambda(\omega)\boldsymbol{D}^{\mathrm{R}}(\omega)\boldsymbol{\Gamma}_\lambda(\omega)\boldsymbol{D}^{\mathrm{A}}(\omega), \tag{2.213}$$

i.e., our time-dependent result reduces in the steady-state limit to the one derived in Ref. [148].

In addition, we notice that also in this case of phonon transport the integrals in Eq. (2.209) are possible to carry out analytically in a similar way as in Pub. [II]. This result for the time-dependent one-phonon density matrix can be expanded in the eigenbasis of the non-hermitian matrix $\boldsymbol{\Omega}_{\mathrm{eff}}$. Further, when the Bose function

is expressed as a Padé series [149, 150], the resulting frequency integrals may be written in terms of complex logarithms and exponential integral functions.

As the derived result provides information about the one-particle density matrix in the central region, we are interested in local quantities in this region. The local energy in the central region may be calculated as a sum over the 'uu' and 'pp' blocks of the product of the Hamiltonian and the density matrix [56, 143]

$$E(t) = \frac{\mathrm{i}}{2}\mathrm{Tr}\left[\boldsymbol{\Omega}\boldsymbol{D}^{<}(t,t)\right]. \tag{2.214}$$

The local heat current between the sites of the central region may be derived by considering the temporal change in local energy in a given site; this should amount to the sum of heat currents flowing in and out of that site [151–153]. The local energy for site j can be written as an expectation value $\epsilon_j = \langle \hat{H}_j \rangle$ of the local Hamiltonian $\hat{H}_j = [(\hat{p}'_j)^2 + \sum_k \hat{u}'_j K'_{jk} \hat{u}'_k]/2$. (This is chosen so that $\hat{H} = \sum_j \hat{H}_j$.) Then, for $\hat{H}$ being the total Hamiltonian for the central region [see Eq. (2.173)], we get from the Heisenberg equation

$$\frac{\mathrm{d}\epsilon_j}{\mathrm{d}t} = -\mathrm{i}\langle[\hat{H}_j, \hat{H}]\rangle = \sum_k \frac{1}{2} K'_{jk} \left(\langle \hat{u}'_j \hat{p}'_k \rangle - \langle \hat{u}'_k \hat{p}'_j \rangle \right), \tag{2.215}$$

where we used the commutation algebra of the momentum and displacement operators. This motivates to define the local (net) heat current between sites j and k as the up component of the density matrix

$$J^{Q}_{jk}(t) = \frac{1}{2} K'_{jk} \left(\langle \hat{u}'_j \hat{p}'_k \rangle - \langle \hat{u}'_k \hat{p}'_j \rangle \right)(t), \tag{2.216}$$

where the two terms can be regarded as "in-coming" (from k to j) and "out-going" (from j to k) heat current. This definition in Eq. (2.216) deviates a little from the conventional definitions for the heat current between a reservoir and the central region [56, 143] (see also the next subsection) since in our case there may be multiple (arbitrary) contacts between the sites in the central region contributing to the heat current through a given site.

2.5.4 Meir–Wingreen and Landauer like formulae

Although we can already evaluate local heat currents in transient regime within the central region by applying the result for the time-dependent density matrix in Eq. (2.209) and Eq. (2.216), we could also wonder about the thermal currents through the interface between the central region and the reservoirs. The following discussion is very similar to the one in Sec. 2.2.2 for electronic transport.

Energy or heat current from the λ-th reservoir to the central region can be defined through the rate of change in energy, or in the expectation value of the Hamiltonian, in reservoir λ

$$J_\lambda^Q(t) = -\left\langle \frac{\mathrm{d}\hat{H}_\lambda}{\mathrm{d}t} \right\rangle = -\mathrm{i}\left\langle \left[\hat{H}_\lambda, \hat{H}_{\mathrm{tot}}\right] \right\rangle, \tag{2.217}$$

where the second identity is due to the Heisenberg equation of motion;

$$\hat{H}_\lambda = \frac{1}{2}\sum_{\substack{j\in\lambda \\ k\in\lambda}} \left(\hat{p}_j^\lambda \hat{p}_k^\lambda \delta_{jk} + \hat{u}_j^\lambda K_{jk}^{\lambda\lambda} \hat{u}_k^\lambda\right) \tag{2.218}$$

is the Hamiltonian for reservoir λ and

$$\hat{H}_{\mathrm{tot}} = \frac{1}{2}\sum_{jk} \left(\hat{p}_j \hat{p}_k \delta_{jk} + \hat{u}_j K_{jk} \hat{u}_k\right) \tag{2.219}$$

is the full Hamiltonian (the indices j,k belonging to any sub-block L,C,R). The reservoir Hamiltonian commutes with itself and with the Hamiltonian of the central region (indices $j,k \in C$). The only nonzero contribution to the commutator therefore comes from the coupling part (with mixed components):

$$\begin{aligned} \left[\hat{H}_\lambda, \hat{H}_{\mathrm{tot}}\right] &= \left[\frac{1}{2}\sum_{jk}\left(\hat{p}_j^\lambda \hat{p}_k^\lambda \delta_{jk} + \hat{u}_j^\lambda K_{jk}^{\lambda\lambda}\hat{u}_k^\lambda\right),\ \frac{1}{2}\sum_{jk}\left(\hat{u}_j^\lambda K_{jk}^{\lambda C}\hat{u}_k^C + \hat{u}_j^C K_{jk}^{C\lambda}\hat{u}_k^\lambda\right)\right] \\ &= -\frac{\mathrm{i}}{2}\sum_{\substack{j\in\lambda \\ k\in C}}\left[K_{jk}^{\lambda C}\hat{p}_j^\lambda(t)\hat{u}_k^C(t) + K_{kj}^{C\lambda}\hat{u}_k^C(t)\hat{p}_j^\lambda(t)\right], \end{aligned} \tag{2.220}$$

where we used $[AB,C] = A[B,C] + [A,C]B$ for the commutator and the canonical commutation relations $[\hat{p}_j, \hat{u}_j] = -\mathrm{i}\delta_{jk}$, $[\hat{u}_j, \hat{u}_k] = 0 = [\hat{p}_j, \hat{p}_k]$, and expressed the displacement and momentum operators in the Heisenberg picture. As we are dealing with mass-normalized operators we may use $\dot{u} = p$ and further rewrite this as

$$\left[\hat{H}_\lambda, \hat{H}_{\mathrm{tot}}\right] = -\frac{\mathrm{i}}{2}\sum_{\substack{j\in\lambda \\ k\in C}}\left[K_{jk}^{\lambda C}\frac{\partial}{\partial t'}\hat{u}_j^\lambda(t')\hat{u}_k^C(t) + K_{kj}^{C\lambda}\hat{u}_k^C(t)\frac{\partial}{\partial t'}\hat{u}_j^\lambda(t')\right]_{t'=t}. \tag{2.221}$$

Then, by inserting into Eq. (2.217), the thermal current becomes

$$J_\lambda^Q(t) = -\mathrm{i}\mathrm{Tr}\left[\boldsymbol{\Omega}_{C\lambda}\frac{\partial}{\partial t'}\boldsymbol{D}_{\lambda C}^<(t',t)\right]_{t'=t}, \tag{2.222}$$

where we identified the definition of the Green's function, and replaced the sum over the block indices by a matrix product and a trace over the states in the central region. In App. A.2.1 we derived an expression for the Green's function $\boldsymbol{D}_{\lambda C}$ in

Eq. (A.82). Similar to the derivation of the Meir–Wingreen formula in the electronic case in Sec. 2.2.2 we may use the Langreth rules [73, 116] for this Green's function to be inserted in Eq. (2.222). This procedure leads to the following expression in the transient regime

$$J^Q_\lambda(t) = -\mathrm{i}\mathrm{Tr}\int_{t_0}^{\infty} \mathrm{d}\bar{t}\left[\frac{\partial}{\partial t'}\boldsymbol{\Pi}^<_{CC}(t',\bar{t})\boldsymbol{D}^\mathrm{A}_{CC}(\bar{t},t) + \frac{\partial}{\partial t'}\boldsymbol{\Pi}^\mathrm{R}_{CC}(t',\bar{t})\boldsymbol{D}^<_{CC}(\bar{t},t)\right]_{t'=t}, \tag{2.223}$$

where we identified the embedding self-energy $\boldsymbol{\Pi}$ from Eq. (2.187). Similar to Eq. (2.46), this result is very general as it is valid for any time t. In addition, if the Green's functions satisfied the full equations of motion, also the interactions would be taken into account. This derivation, however, was done based on the partitioned approach, and especially for small t the transient is affected by the contacting. In any case, at $t \to \infty$ the information about the initial configuration is washed away. More specifically, the only difference, compared to the electronic case, is in the contour and the corresponding Keldysh components coming from the Langreth rules; here the contour does not have a vertical complex part since the reservoirs are uncorrelated before the switch is turned on at t_0. The vertical contour would also be problematic to define for a system with two different temperatures.

In the steady-state limit we can extend $t_0 \to -\infty$, and the functions of two time variables become functions of the time difference only, and we may use the relation between the time-convolutions and Fourier transforms. The time-derivative will return a factor of $-\mathrm{i}\omega$ from the exponential in the Fourier transform:

$$J^Q_{\lambda,\mathrm{SS}} = -\int_{-\infty}^{\infty}\frac{\mathrm{d}\omega}{2\pi}\omega\mathrm{Tr}\left[\boldsymbol{\Pi}^<_{CC}(\omega)\boldsymbol{D}^\mathrm{A}_{CC}(\omega) + \boldsymbol{\Pi}^\mathrm{R}_{CC}(\omega)\boldsymbol{D}^<_{CC}(\omega)\right]. \tag{2.224}$$

The heat current must be real, so we may symmetrize this result by

$$J^Q_{\lambda,\mathrm{SS}} = \frac{1}{2}\left[J^Q_{\lambda,\mathrm{SS}} + (J^Q_{\lambda,\mathrm{SS}})^*\right] = -\int_{-\infty}^{\infty}\frac{\mathrm{d}\omega}{4\pi}\omega\mathrm{Tr}\left[\boldsymbol{D}^<_{CC}(\omega)\boldsymbol{\Pi}^>_{CC}(\omega) - \boldsymbol{D}^>_{CC}(\omega)\boldsymbol{\Pi}^<_{CC}(\omega)\right], \tag{2.225}$$

where we used $(\boldsymbol{\Pi}^<)^\dagger = -\boldsymbol{\Pi}^<$, $(\boldsymbol{D}^<)^\dagger = -\boldsymbol{D}^<$, $\mathrm{i}(\boldsymbol{D}^\mathrm{R} - \boldsymbol{D}^\mathrm{A}) = \mathrm{i}(\boldsymbol{D}^> - \boldsymbol{D}^<)$ and $\mathrm{i}(\boldsymbol{\Pi}^\mathrm{R} - \boldsymbol{\Pi}^\mathrm{A}) = \mathrm{i}(\boldsymbol{\Pi}^> - \boldsymbol{\Pi}^<)$ [73]. Here, it is also possible to separate the integration from $-\infty$ to 0 and from 0 to ∞ and using similar symmetry relations as above [73] we may write the heat current as

$$J^Q_{\lambda,\mathrm{SS}} = \int_{0}^{\infty}\frac{\mathrm{d}\omega}{2\pi}\omega\mathrm{Tr}\left[\boldsymbol{D}^<_{CC}(\omega)\boldsymbol{\Pi}^>_{CC}(\omega) - \boldsymbol{D}^>_{CC}(\omega)\boldsymbol{\Pi}^<_{CC}(\omega)\right], \tag{2.226}$$

cf. Refs. [146, 154]. The above expressions for the steady-state heat current are equivalent representations of *the Meir–Wingreen formula* for phonon transport. Yet another, commonly presented expression is in a two-terminal setting for the dif-

ference $J^Q_{\mathrm{SS}} = J^Q_{R,\mathrm{SS}} - J^Q_{L,\mathrm{SS}}$ in terms of the spectral functions and using a fluctuation–dissipation relation for the lesser self-energy $\boldsymbol{\Pi}^<(\omega) = -\mathrm{i} f(\omega)\boldsymbol{\Gamma}(\omega)$

$$\begin{aligned} J^Q_{\mathrm{SS}} &= \mathrm{i}\int_{-\infty}^{\infty}\frac{\mathrm{d}\omega}{4\pi}\omega\mathrm{Tr}\Big\{\left[f_L(\omega)\boldsymbol{\Gamma}_L(\omega) - f_R(\omega)\boldsymbol{\Gamma}_R(\omega)\right]\left[\boldsymbol{D}^{\mathrm{R}}_{CC}(\omega) - \boldsymbol{D}^{\mathrm{A}}_{CC}(\omega)\right] \\ &\qquad + \left[\boldsymbol{\Gamma}_L(\omega) - \boldsymbol{\Gamma}_R(\omega)\right]\boldsymbol{D}^<_{CC}(\omega)\Big\}, \end{aligned} \tag{2.227}$$

cf. Eq. (2.50). If we further explicitly assume noninteracting central region, we may write the lesser Green's function as $\boldsymbol{D}^<_{CC} = \boldsymbol{D}^{\mathrm{R}}_{CC}\boldsymbol{\Pi}^<_{CC}\boldsymbol{D}^{\mathrm{A}}_{CC}$. Using the same fluctuation relation for the lesser self-energy we get

$$J^Q_{\lambda,\mathrm{SS}} = \int_{-\infty}^{\infty}\frac{\mathrm{d}\omega}{4\pi}\sum_{\beta}\omega\left[f_\beta(\omega) - f_\lambda(\omega)\right]\mathrm{Tr}\left[\boldsymbol{\Gamma}_\lambda(\omega)\boldsymbol{D}^{\mathrm{R}}_{CC}\boldsymbol{\Gamma}_\beta(\omega)\boldsymbol{D}^{\mathrm{A}}_{CC}(\omega)\right]. \tag{2.228}$$

Limiting ourselves to a two-terminal setting and evaluating the difference $J^Q_{\mathrm{SS}} = J^Q_{R,\mathrm{SS}} - J^Q_{L,\mathrm{SS}}$ gives *the Landauer–Büttiker formula* for phonon transport

$$J^Q_{\mathrm{SS}} = \int_0^{\infty}\frac{\mathrm{d}\omega}{2\pi}\omega\left[f_L(\omega) - f_R(\omega)\right]\mathrm{Tr}\left[\boldsymbol{\Gamma}_R(\omega)\boldsymbol{D}^{\mathrm{R}}_{CC}\boldsymbol{\Gamma}_L(\omega)\boldsymbol{D}^{\mathrm{A}}_{CC}(\omega)\right], \tag{2.229}$$

cf. Ref. [146]. The thermal conductance could further be defined via $\lim_{\Delta T\to 0} J^Q_{\mathrm{SS}}/\Delta T$ where ΔT is the difference in the temperatures in the reservoirs. This would lead to otherwise similar formula as Eq. (2.229) but with a derivative of the Bose functions with respect to temperature.

3 Results

In this chapter, a selection the results in Pubs. [I–V] is summarized (Secs. 3.2–3.7). Before that we have a brief introduction (Sec. 3.1) to the transport simulations in specific model systems. In this introductory part we assess the validity, accuracy, and computational cost of the methodology discussed in the previous chapter when compared to different numerical methods. For the purpose of a self-contained presentation, figures from the publications will be replicated when necessary.

3.1 Transport simulation comparisons between different methods

3.1.1 Transport setup and the comparative methods

We will first look at few numerical examples of transport studies based on the formalism discussed in Chap. 2. As the developed method of solving the equations of motion for noninteracting systems in WBA is new, we would like to see how it compares with other methods. To this end, we will study transport through simple systems, e.g., molecules consisting of one or two energy levels, simple one-dimensional atomic chains of moderate lengths (in the order of tens of atoms) and also a bit larger graphene based nanostructures. The transport setup is generally of the form in Fig. 3.1 where t_C, t_α and $t_{\alpha C}$ are the hopping parameters in the central region, in the leads, and between one and another, respectively (although not restricted to only one parameter per region). The resonance widths Γ_α depend on the hopping parameters. The possible parameters for the central region also include arbitrary potential profile u and superconducting gap Δ. Environmental conditions are handled by the parameters for the bias voltage V_α (with respect to the chemical potential μ) and inverse temperature β.

We will use the developed time-dependent extension to the Landauer–Büttiker formalism, here referred to as 'LB'. As a comparison we will solve the equations of motion for the Green's function numerically using an embedding scheme [112]. This involves a time-stepping algorithm in propagating the Kadanoff–Baym equations [73, 113], here referred to as 'KB'. More specifically, in the KB solver Eq. (2.38) is

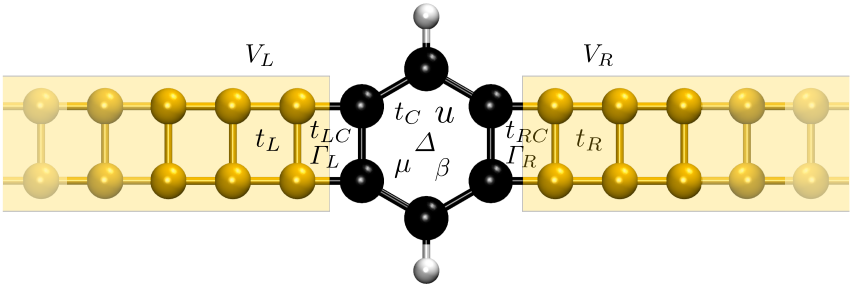

Fig. 3.1: General transport setup for the comparison simulations to be presented in this section.

decomposed into real-time equations for each Keldysh component and then propagated in the two-time plane. For the single-particle Hamiltonian we may choose exactly the same description as in LB. As we are benchmarking a noninteracting model in LB, we put the many-body self-energy to zero in KB and only include the embedding part. For the embedding self-energy in KB we are, however, not limited by the WBA but we may include the exact energy band structure for the leads.

We will also, as a comparison, perform a simple calculation of propagating single-particle Hartree–Fock orbitals of a finite system [155, 156] using the implicit midpoint rule, i.e., the Crank–Nicholson method [157] (referred to as 'HF'); the finite system is composed of two leads and a central system of interest, and the leads are chosen long enough to avoid reflections and other finite-size effects. More specifically, in the HF solver a finite system for the leads and the central region is composed as a single-particle tight-binding Hamiltonian $\hat{H}$. The Hamiltonian may vary in time, so we may include the bias voltage for the lead parts as on-site terms. As we are comparing with a noninteracting model in LB we do not consider interactions even though they could be included here in the Hartree–Fock level. The time-evolution of the single-particle orbitals $\varphi(t)$ is obtained as a numerical solution to a linear system [157], $\hat{A}\varphi(t+\Delta t) = b$, where $\hat{A} = \hat{\mathbb{1}} + \mathrm{i}\Delta t\hat{H}(t+\Delta t/2)/2$ and $b = [\hat{\mathbb{1}} - \mathrm{i}\Delta t\hat{H}(t+\Delta t/2)/2]\varphi(t)$. In addition, in HF we are not limited by the embedding scheme (or the WBA either) since the full finite system is solved explicitly.

As the LB method presented in Chap. 2 provides computational simplification when quantities of interest can be expressed in closed form, we would like to compare the computational cost with KB and HF. The numerical implementation of Eqs. (2.79), (2.85) and (2.126) is straightforward:

1. The Hamiltonian matrix for the central region and the coupling matrices between the central region and the leads are constructed.

2. The effective Hamiltonian, Green's functions and spectral functions are constructed. Diagonalization of h_{eff} is needed for eigendecomposition.

3. Numerical integration over the frequency ω is performed, preferably in an adaptive grid due to the spiky behaviour of the spectral functions.

(4. As each time step can be evaluated separately, the computation is considerably sped up by parallelization.)

When the frequency integrals are evaluated analytically, we end up with the implementation of Eqs. (2.92) and (2.127) which is computationally less demanding but implementation-wise perhaps more tedious due to the collection of complex special functions. For the phonon density matrix in Eq. (2.209) the procedure is the same as above. A computationally inclined reader might be interested in the repositories in Refs. [158, 159] although these codes are to be taken with a grain of salt.

The difference between numerical time propagation of the Kadanoff–Baym equations and using the extended Landauer-Büttiker formalism is something to be considered, at least when the studied systems become larger. We performed the comparisons using a regular desktop computer with Intel Core i5-2400 CPU @ 3.10 GHz × 4, 4 GB RAM and GCC version 4.7.2. These calculations were done using only a single core to better benchmark the computational cost between different methods. In the end of this section, when we benchmark the LB method further, we also discuss the parallelization for multi-core clusters.

3.1.2 Time-dependent current between the interface of a one-level system and a lead

The first example is simply a one-level system sandwiched between two leads at zero temperature. This model was studied in Ref. [96], so the comparison results between different methods presented here should be compared with the cited paper. We let, for simplicity the on-site energy of the central level be zero and set the chemical potential also to this value. We fix the tunneling rate between the central level and the leads to be $\Gamma_{\text{L}} = \Gamma_{\text{R}} = \Gamma$ and relate the other parameters to this energy scale. This means the hopping strength $t_{\alpha C}$ between the leads and the central level, and the hopping strength in the leads t_α are related by $\Gamma_\alpha = 2t_{\alpha C}^2/|t_\alpha|$ in WBA. We bias the left lead to $V_{\text{L}} = 5\Gamma$ (with respect to the chemical potential $\mu = 0$) and let the right lead remain unbiased $V_{\text{R}} = 0$. In Fig. 3.2a we show the time-dependent current through the right interface, i.e., between the central level and the right lead. The calculations involved 500 time steps of length $\Delta t = 0.006\,\Gamma^{-1}$. In the HF calculation the finite leads were of length 60 atoms in a chain. A value of $\Gamma = 0.2$ was assigned for the tunneling rate.

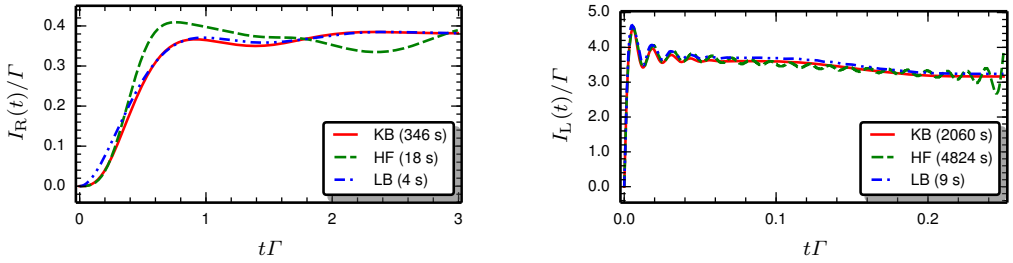

(a) Current through the right interface of a one-level system between two leads.

(b) Current through the left interface of a two-level system between two leads.

Fig. 3.2: Comparison of the time-dependent current using three different methods. Computation wall-times are marked in the legend.

We see how all the methods give qualitatively similar results with varying computational cost. The model is very simple, and the observed oscillation of the current is simply due to one relevant energy scale in the setup: the difference between the biased left lead and the zero energy of the central system. The chosen tunneling energy scale $\Gamma = 0.2$ is of moderate strength (compared to other parameters), and we expect LB to compare moderately with the full embedding in KB. In fact, using the WBA in LB overestimates the beginning of the transient since the tunneling rate is assumed too large for the channels close to the band edge. This, however, is correctly taken into account in KB and HF where the energy dependency of the tunneling for different channels is handled accordingly. At later times this does not give considerable differences and LB and KB are essentially on top of each other. HF, however, starts to behave differently at later times as the finite-size effects start to play a role; a virtual oscillation around the steady-state current is due to reflections from the system boundaries.

3.1.3 Time-dependent current through the interface of a molecule of two energy levels and a lead

The second example is a two-level molecule (say, HOMO and LUMO) attached to two leads at zero temperature. We let the molecular energy levels be $\{\epsilon_0 - \delta, \epsilon_0 + \delta\}$ and couple both levels to the leads with equal strength Γ. This model is a textbook example in [73] where a similar calculation was performed. Also here, the hopping strength $t_{\alpha C}$ between the leads and the central levels, and the hopping strength in the leads t_α are related by $\Gamma_\alpha = 2t_{\alpha C}^2/|t_\alpha|$ in WBA. We bias the left lead to $V_L = 2\epsilon_0$ (with respect to the chemical potential $\mu = 0$) and let the right lead remain without a level shift $V_R = 0$. In contrast to the previous example, we now look at weak coupling,

in which we expect WBA to be rather similar to the embedded KB propagation. We let $\epsilon_0 = 500\Gamma$, $\delta = 20\Gamma$ and $\Gamma = 0.001$.

In Fig. 3.2b we show the time-dependent current through the left interface, i.e., between the central levels and the left lead. Because of the weak coupling, the calculations involved a bit longer simulation: 1000 time steps of length $\Delta t = 0.00025\,\Gamma^{-1}$. In the Hartree–Fock calculation the finite leads were chosen to be of length 250 atoms in a chain, which was tested to be appropriate for the studied time scales. In this case also, we see how all the methods give roughly similar results. Now the beginning of the transient is described correctly also by LB as WBA is a fairly good approximation. The slight discrepancies between LB and KB for later times is due to numerical integration: weak coupling causes very narrow and intense peaks in the spectral functions to be integrated in LB. We can, however, go around this problem by performing more accurate numerical integration which naturally increases the computational cost (although relatively low) in LB. Also here HF, for later times, starts to show finite-size effects due to reflections. It is also important to notice that as we go towards the parameter range of WBA the propagation times and system sizes in KB and HF increase. This means a nice 'bonus': Using LB for this parameter range gives reliable results in just a fraction of computation time.

3.1.4 Time-dependent bond current through an atomic chain

Next, let us look at a larger system, yet something that can be computed using the full KB propagation. For larger calculations we are limited by the RAM of the benchmark computer because storing the Green's function elements for larger systems and longer time propagations needs a rapidly increasing amount of memory [114]. Also in HF propagation, as the size of the central region grows and the transient saturation takes a longer time, we need to allocate longer leads to avoid finite-size effects. We take a 10-site tight-binding chain as the central region in between two metallic, semi-infinite leads; this setup could model transport through a long alkane molecule, for instance. We fix the hopping in the central region as $t_C = -1.0$, and relate the other parameters to this energy scale. We choose weak coupling regime for WBA to work, and choose accordingly the coupling and lead parameters as $t_{\alpha C} = t_C/5$ and $t_\alpha = 8t_C$ so that the resonances are narrow: $\Gamma_\alpha = 2t_{\alpha C}^2/t_\alpha = |t_C|/100$. We bias the leads symmetrically to $V_L = V = -V_R = 2|t_C|$ and keep the system at finite temperature $\beta = 10/|t_C|$. Although this is a nonzero temperature ($k_\mathrm{B}T = |t_C|/10$), it is still in a very low (sub-Kelvin) range for the thermal excitations compared to the other energy scales in the setup.

We evaluate the current through the central region as the bond current in the middle (between the fifth and the sixth site) by using the full KB propagation, finite-size HF

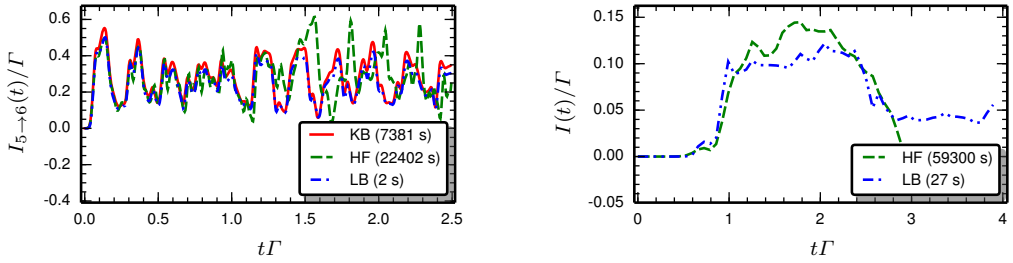

(a) Current in the middle of a 10-site chain between two leads.

(b) Current in the middle of a graphene ribbon between 2D leads.

Fig. 3.3: Comparison of the time-dependent current using three (panel a) and two (panel b) different methods. Computation wall-times are marked in the legend.

with one-dimensional leads of length 500 sites, and LB with analytical expressions in terms of digamma and hypergeometric functions in Eqs. (2.103), (2.104) and (2.105). Total of 500 time steps of length $0.005\Gamma^{-1}$ were computed and the results can be seen in Fig. 3.3a. For larger systems the difference in the computational cost between the propagation methods (KB and HF) and the closed solution (LB) becomes immense. Still, the results are very congruent; HF only starts to deviate from the rest when the finite-size effects start to have an influence (around $t\Gamma = 1.3$). The small discrepancies between KB and LB are mainly numerical errors as the step length might affect the KB results rather strongly [113, 114].

3.1.5 Time-dependent bond current through a graphene ribbon

The advantages in LB method indeed lie in studying large systems, and therefore we present yet another comparison which, however, is too large for a full KB calculation, so we only compare HF and LB. We have an armchair graphene nanoribbon of 120 sites (more specifically, a 6-aGNR of length $\sim$ 4 nm [160]) as the central region and two-dimensional rectangular tight-binding leads of $3 \times 400 = 1200$ sites (rows $\times$ columns) for the HF propagation. The graphene nanoribbon is parametrized in a single π-orbital framework with nearest-neighbour hopping -2.7 eV [89], and the coupling between the central region and the leads is constructed so that the tunneling rate becomes $\Gamma_\alpha = 0.1$ eV for each lead. The system is in zero temperature and is driven out of equilibrium by a one-sided bias voltage on the left lead: $V_L = 2.5$ eV, $V_R = 0$.

For the LB calculation we use the analytic expression in Eqs. (2.93), (2.94) and (2.95) in terms of logarithms and exponential integral functions. Due to a rather large

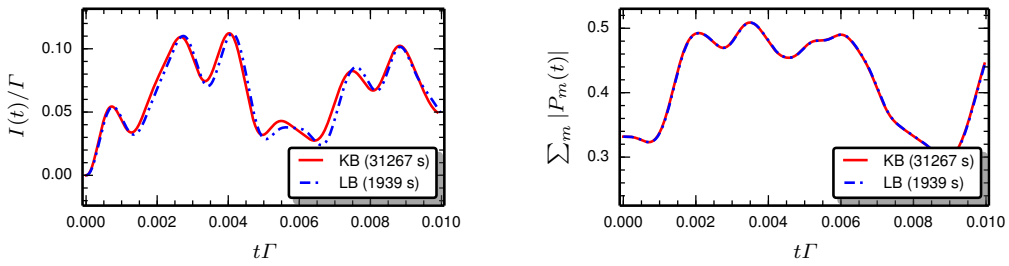

(a) Time-dependent current through the superconducting benzene-like molecule.

(b) Time-dependent Cooper pair density in the benzene-like molecule.

Fig. 3.4: Comparison of two different methods. Computation wall-times are marked in the legend.

system, we perform a calculation of only 60 time steps of length $\Delta t = 0.07\Gamma^{-1}$ (even the HF propagation is rather tedious), and in Fig. 3.3b we show the total current through the nanoribbon as a sum over individual bond currents through an interface in the middle of the ribbon. Also in this case, the LB captures, at least qualitatively, the essential features of the transient oscillation in a fraction of computational cost compared to the HF. It is worth mentioning, however, that these data points only represent the very beginning of a considerably longer transient, and already for this large leads in the HF propagation, the finite-size effects come out during the first transient oscillation.

3.1.6 Time-dependent current and Cooper pair density in an NSN junction

As a last benchmark for this section we consider a superconducting central region together with a potential profile. We have a benzene-like molecule, 6 carbon atoms on a ring with 2 hydrogen atoms on the edge, as the central region connected to two-dimensional leads. (This is exactly the setup depicted in Fig. 3.1.) The molecule is described like a hydrogen-passivated graphene ribbon, a single π-orbital lattice with nearest-neighbour hopping $|t_C| = 2.7$ eV and modified tight-binding parameters $\epsilon' = 0.66t_C$, $t'_C = 2.2t_C$ for hydrogen on-site energies and hydrogen–carbon hopping, respectively [90]. In this "toy model" for superconductivity we introduce a pairing field (i.e., the superconducting gap) for the molecule as $\Delta = |t_C|/10$. The molecule in its normal state is already semiconducting, so the full energy gap depends on both the tight-binding parameters and the pairing strength parameter Δ. We bias the molecule symmetrically $V = V_L = -V_R = |t_C|$ and put an on-site gating potential $u \in \{|t_C|/2, 0, -|t_C|/2\}$ so that the potential decreases linearly from

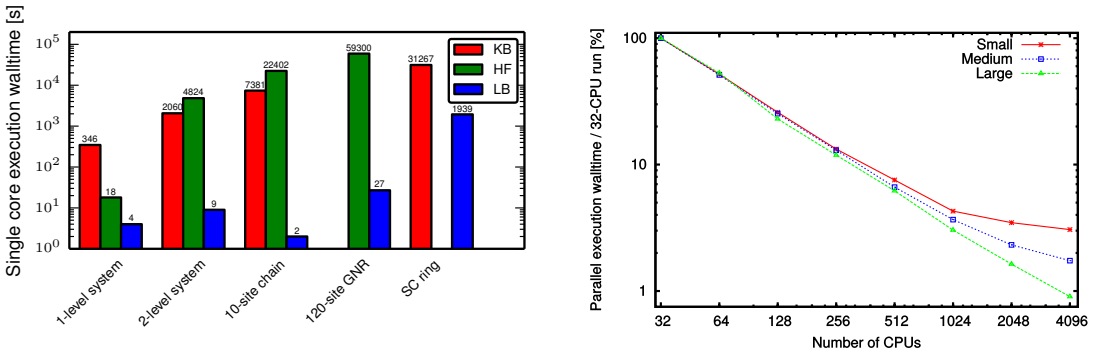

(a) Computational cost of different methods in the comparison simulations.

(b) Parallel scaling: Fixed amount of work, increasing number of CPUs

Fig. 3.5: Comparison of the computational cost for single core jobs (panel a) and parallel jobs (panel b).

the left to the right lead over the central molecule: the two left-most carbon atoms have an on-site potential $|t_C|/2$, the two carbon and the two hydrogen atoms in the middle are non-gated while the two right-most carbon atoms have an on-site potential $-|t_C|/2$. The molecule is coupled to the leads so that the resonance widths are $\Gamma_\alpha = 0.001$ eV for each lead, and the transport is set up at inverse temperature $\beta = 10/|t_C|$, hence, for the LB method we will be using the formulae in Eqs. (2.136), (2.137) and (2.138).

We only compare LB to KB because, as have been shown in the previous examples, the HF method only gives rise to finite-size effects which is seen as a deviation from the embedded methods (KB and LB). This simulation acts as a check for the parametrization of the superconducting central region and the overlaps between the unperturbed and perturbed bases of the central region in Eq. (2.127). In Fig. 3.4 we show the simulation of 500 time steps of length $\Delta t = 0.00002\Gamma^{-1}$, and we plot the time-dependent current through the molecule (panel a) and the Cooper pair density within the molecule (panel b). There is minor numerical discrepancy between KB and LB in the current computation due to the small absolute value ($\sim 10^{-5}$) of the current. However, for the Cooper pair density, which is naturally evaluated from the same density matrix, the match is perfect. We also notice the increased computational cost in LB compared to earlier simulations as we now have the central region perturbed by a potential profile, and the overlaps between the unperturbed and perturbed bases need to be evaluated as in Eq. (2.127).

3.1.7 Computational cost and parallelization

A general remark for the simulations presented in this section: The time-dependent Landauer–Büttiker formalism compares well with the existing methods of propagating the Kadanoff–Baym equations for the Green's function and the single-particle Hartree–Fock orbitals. When WBA can be assumed, the results are very congruent. Importantly, also, the computational cost is brought down considerably, see Fig. 3.5a, as the time-stepping in KB scales as N_t^2 [113, 114] and in HF as N_t [157] with N_t the number of time steps. In LB the cost depends only on numerical integration or on the evaluation of the special functions in the derived formulae.

Also, as time is only a parameter in LB, the implemented formulae parallelize trivially; separate time steps of the transient can be computed on separate processors as they operate without exchanging information. Only exceptions are the initialization of the studied structure and collecting the results in the end. As an example of the scaling of the parallelization we computed the time-dependent density matrix for armchair-oriented graphene nanoribbons connected to two-dimensional tight-binding leads, similar to one of the examples above but for bigger systems. Here we do not list a detailed description of the transport setup, as these comparisons were already presented, and for this simulation we only want to compare the computation times. In Fig. 3.5b we show the computation wall-times (in seconds) for small, medium and large graphene structures ($N_C = \{280, 384, 720\}$ sites in the central region, respectively). For small systems the overall computation time is small, and the initialization and collecting the results might take longer time to execute than the essential part of the calculation. Still, we see how the parallelization is rather trivial up to one thousand processes, and it gets even better for larger systems.

3.2 Electronic transport through a ring-shaped junction

Although the main result in Pub. [I] was the derivation of Eqs. (2.79) and (2.85), here we will review the numerical considerations presented in this article for a six-site tight-binding ring connected to two leads as shown schematically in Fig. 3.6. This could vaguely be understood as a study of transport through a benzene-like molecular ring with the wave function perfectly localized around the carbon atoms – also similar to one of the comparison examples presented in the previous section. The parameters in the setup were $t_C = -2.0$ for the hopping strength in the ring, $\mu = 0$ for the chemical potential and $\beta = 100$ for the zero-temperature limit (compared to other parameters it was as if $\beta \to \infty$). The hopping $t_L = t_R$ in the left/right lead

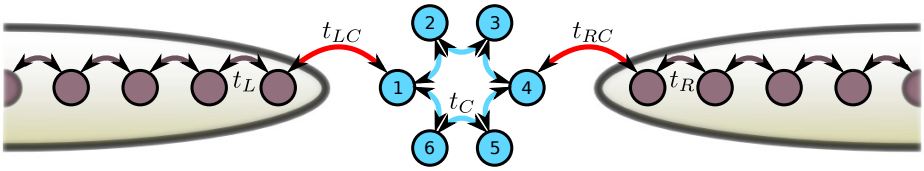

Fig. 3.6: Six-site ring coupled symmetrically to one-dimensional TB leads.

was chosen to be much larger than any other energy scale, so that the wide-band limit with $\Gamma_\alpha = 2t_{\alpha C}^2/t_\alpha$ was a good approximation; $\Sigma_\alpha^{\mathrm{A}}(\omega \sim \mu) = \mathrm{i}\, t_{\alpha C}^2/t_\alpha + O(1/t_\alpha^2)$ with $t_{\alpha C}$ being the hopping between the ring and the leads. The system was driven out of equilibrium by the sudden switch-on of a bias voltage, i.e., the energy levels of the leads were raised by $V_L = V = -V_R$. In order to study the system's response to the external bias voltage, we evaluated numerically the frequency integrals in Eq. (2.85).

In Pub. [I] there is a thorough analysis of the transient features captured by the derived formulae in Eqs. (2.79) and (2.85) with almost a plethora of graphs as evidence. Here we only review the main findings which include different transitions occurring during the transient given by the different terms of Eq. (2.85), and an underlying selection rule for the hexagonal structure. Indeed, the time-dependence in the second row of Eq. (2.85) (the term linear in the bias voltage) gave rise to molecule–lead transitions with oscillation frequencies $\omega_j = |\mu + V_\alpha - \mathrm{Re}[\epsilon_j]|$ with ϵ_j the complex eigenvalue of the effective Hamiltonian h_{eff}. On the other hand, the intramolecular transitions were captured by the third row of Eq. (2.85) (the term quadratic in the bias voltage) with the oscillation frequencies being $\omega_{jk} = |\mathrm{Re}[\epsilon_j] - \mathrm{Re}[\epsilon_k]|$. Interestingly, however, not all the possible transitions within the transport setup were visible in the transient behaviour; a selection rule was found for some of the levels which did not participate in the transport process. This was a special case caused by the symmetries of the molecule and the coupling to the leads. These *inert states* only affected the static part of the density matrix and did not contribute to the dynamics since the states were given by wave functions having nodal planes exactly at the sites coupled to the leads. If this symmetry was broken either by asymmetric coupling or by deforming the molecule (modified hopping parameter between some of the sites), also the remaining transitions became visible.

In Figs. 3.7 and 3.9 we display the transient current through the right interface of the transport setup, i.e., the bond between the ring and the right lead. In Figs. 3.8 and 3.10 we have the corresponding Fourier transforms of the transient currents. In Fig. 3.7 we varied the bias voltage and in Fig. 3.9 the coupling strength leading to different values for the broadening Γ. Also, in Fig. 3.7 we scaled the axes due to equal value for the coupling strength, so the transient scales could be compared better. In Fig. 3.9, on the other hand, the axes were not scaled due to varying Γ. Clearly, increasing the bias voltage (widening the bias window) opened up more

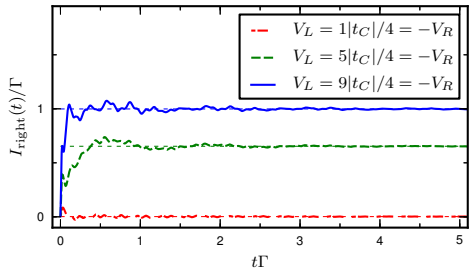

Fig. 3.7: Time-dependent current in units of Γ through the right interface with symmetric coupling ($\Gamma = 0.1$) and varying bias. (Dotted lines refer to steady-state values.)

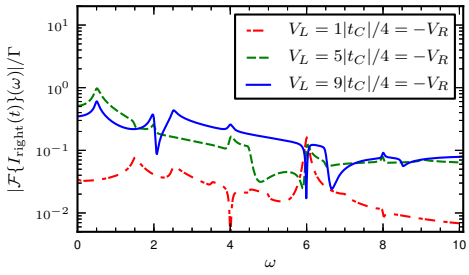

Fig. 3.8: Absolute value of the Fourier transformed right current in units of Γ.

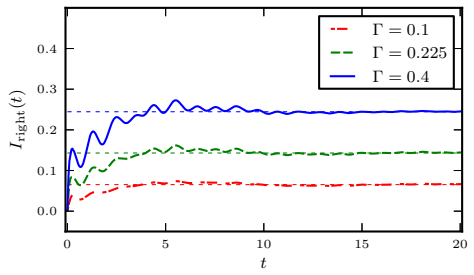

Fig. 3.9: Time-dependent current through the right interface with symmetric coupling (varying strength) and bias $V_L = -V_R = 2.5$. (Dotted lines refer to steady-state values.)

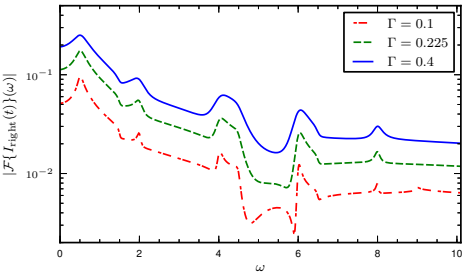

Fig. 3.10: Absolute value of the Fourier transformed right current.

levels as transport channels and the steady-state current grows. The oscillation frequencies corresponding to transitions between the molecular levels in the ring remained unchanged while the oscillation frequencies corresponding to transitions between the ring and the leads varied (some of the Fourier peaks moved while some did not), see Fig. 3.8. By increasing Γ, and hence by widening the resonances, electrons could flow even with intermediate bias voltages. Correspondingly, the steady-state value of the current increased, the relaxation times decreased whereas the oscillation frequencies remained invariant (peaks did not move), see Fig. 3.10.

3.3 Edge-state transitions in graphene nanoribbons

In Pub. [II] we presented an extension to the results in Eqs. (2.79) and (2.85). We expressed the frequency integrals in Eq. (2.79) in the eigenbasis of the effective Hamiltonian h_{eff}, and this way we were able to perform the integrations analytically in the zero-temperature limit. The results were expressed in terms of logarithms and special functions called the exponential integral in Eq. (2.92). This procedure allowed for even larger scale calculations in the time-dependent Landauer–Büttiker formalism since one bottleneck, the numerical integration of spiked spectral functions, was overcome.

3.3.1 Classification of the ribbons

We used this extended formalism in Pub. [II] to study local bond currents in graphene nanoribbons (GNR) of different geometries; the transport setup is shown in Fig. 3.11. The leads were semi-infinite with their terminal sites coupled to the

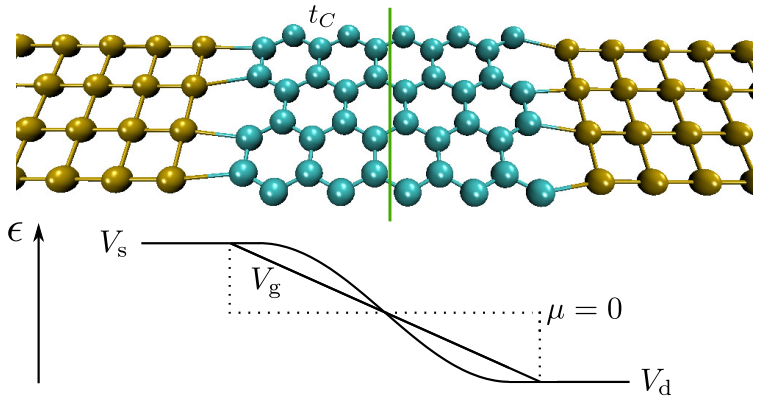

Fig. 3.11: Transport setup of a (zigzag) graphene nanoribbon connected to metallic leads: contacts to leads are between doubly-coloured bonds; bridge (explained in text) is shown by the green cutting line. The structure of the leads is shown for illustratory purposes. Voltage profile is shown below the structure.

GNR in the center. The GNR was modelled by a single-orbital π-electron network, parametrized by nearest neighbour hopping $t_C = -2.7$ eV [89]; second and third nearest neighbour hoppings [89] were neglected but they could trivially be included at the same computational cost. The size and the orientation [zigzag (zGNR) or armchair (aGNR)] of the central region was arbitrary as well as the structure of the leads. The level-width functions, Γ_α, depended on the couplings between the central region and the leads, and also on the internal properties of the leads. In

principle, Γ_α could be any positive semidefinite matrix [161, 162] but here it was taken simply as $\Gamma_{\alpha,mn} = \gamma_\alpha \Delta_{\alpha,mn}$ where $\Delta_{\alpha,mn} = \delta_{mn}$ when m, n labeled edge atoms contacted to lead α and $\Delta_{mn,\alpha} = 0$ otherwise. In the calculations we chose the coupling strengths so that $\gamma_\alpha = 0.1$ eV for each lead α. Also in this study, the system was driven out of equilibrium by a sudden symmetric bias voltage between source and drain electrodes, i.e., $V_\alpha = \pm V_{\mathrm{sd}}/2$. The bias voltage, or the level shift in the leads, was set with respect to the chemical potential $\mu = 0$ (i.e., we had a charge neutral GNR in equilibrium). The potential profile within the central region could be, e.g., linear or sinusoidal as illustrated in Fig. 3.11, or of any other shape. The strength of this potential was given by the parameter V_{g}. For the numerical simulations we considered a virtual interface in the middle of the studied structure by a cutting line or a *bridge* and calculated the sum of all bond currents for the bonds cut by the bridge, see Fig. 3.11. This sum of time-dependent bond currents was denoted simply by $I(t)$. The energies were evaluated in units of $\epsilon = 1$ eV giving the unit of time $t = \hbar/\epsilon \approx 6.58 \cdot 10^{-16}$ s and the unit of current $I = e\epsilon/\hbar \approx 2.43 \cdot 10^{-4}$ A.

3.3.2 Transient features depend on the length, width and orientation of the ribbon

First we investigated the dependence of the time-dependent current on the length of the GNR at fixed width and bias voltage. We show the current $I(t)$ in Fig. 3.12a-b and the corresponding Fourier transforms of the current, $|\mathcal{F}\{I(t)\}(\omega)|$, in Fig. 3.12c for aGNRs of width 1.4 nm and a zGNRs of width 1.6 nm. More specifically, the armchair structure was a 13-aGNR where 13 refers to the number of armchair dimer rows [160], and the zigzag structure was an 8-zGNR where 8 is the number of zigzag rows [160]. The Fourier transforms were calculated from the long-time simulations shown in the inset of Fig. 3.12c where the steady-state value was subtracted from the sample points. Also, Blackman-window filtering [163] was used and the absolute value of the result was plotted. In both cases the bias voltage was $V_{\mathrm{sd}} = 5.6$ eV and the potential profile was set to zero, $V_{\mathrm{g}} = 0$ eV. We saw that elongating the ribbon made the initial transient start with a delay, since the current was evaluated in the center (see Fig. 3.11), but the steady-state value remained roughly invariant. By increasing the length the overall number of states also increased, and hence, more states close to the Fermi level were available as transport channels. Consequently, smaller transition energies became possible and the peaks in the Fourier spectra shifted towards lower energies as they were more favourable. In zGNRs we also saw an amplified high-energy peak independent of the length of the ribbon; this frequency corresponded to the fast superimposed oscillations in the time domain that lasted throughout the transient. As the oscillation lasted for a long time, the strength of the Fourier peak was also amplified. This oscillation frequency was $\omega = V_{\mathrm{sd}}/2 = 2.8$ eV and therefore corresponded to transitions between the biased Fermi

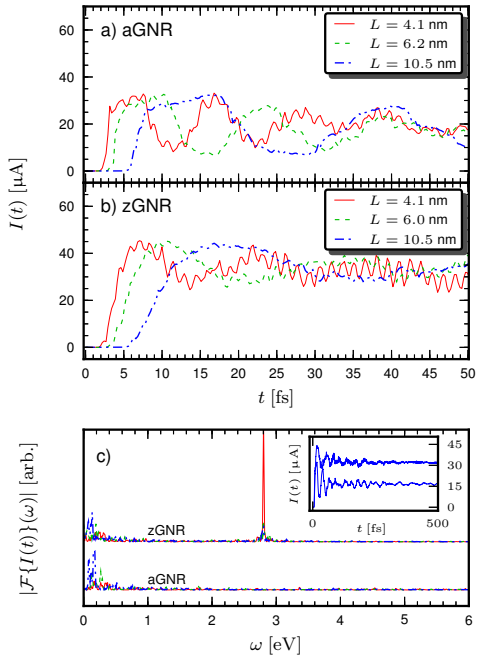

Fig. 3.12: Time-dependent bond currents through ribbons of *varying length*: a) aGNR: (fixed width W = 1.5 nm (13)), b) zGNR: (fixed width W = 1.6 nm (8)), and c) the corresponding Fourier transforms (zGNR is offset for clarity); the inset shows the long-time behaviour of the currents for L = 10.5 nm in a) and b). [The line colours and styles correspond to those in a) and b).]

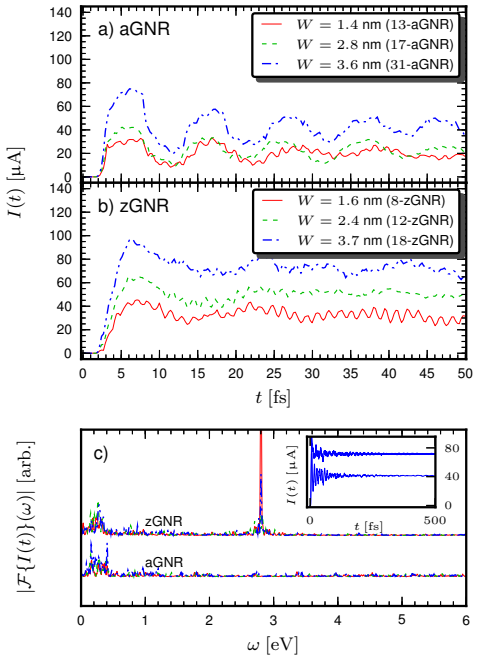

Fig. 3.13: Time-dependent bond currents through ribbons of *varying width*: a) aGNR: (fixed length L = 4.1 nm), b) zGNR: (fixed length L = 4.1 nm), and c) the corresponding Fourier transforms (zGNR is offset for clarity); the inset shows the long-time behaviour of the currents for W = 3.6 nm in a) and W = 3.7 nm in b), respectively. [The line colours and styles correspond to those in a) and b).]

level of the leads and the zero-energy states of the ribbon, i.e., the edge states. The edge states were weakly coupled to the leads and therefore these transitions were slowly damped. Also, similar high-frequency oscillations were visible in aGNRs as well, see panel a. Nevertheless, the Fourier transform did not show any high frequency peak in this case as the oscillation was damped in much faster time scale. In aGNRs we had zigzag edges at the lead interface, and hence, the edge states were strongly coupled to the leads, also dissipating faster.

Then, we varied the width of the ribbons while keeping the length and the bias voltage fixed. We also did not have a potential profile present in the central region, $V_g = 0$. In Fig. 3.13 we show the time-dependent currents and the dependency

on the width for aGNRs and zGNRs of length 4.1 nm. Compared to the previous study, changing the width of the ribbon might have lead to more involved transient behaviour because, depending on the width, the ribbons might have been either metallic or semiconducting [164]. Nevertheless, the semiconducting gap would have been much smaller than the applied bias window $V_{\mathrm{sd}} = 5.6$ eV, and therefore the conducting properties should not have been affected by the gap or further by the width. When increasing the width of the ribbon the length of the bridge, through which the overall bond current I was evaluated, also increased and so did the steady-state value of I. However, the transient features were mostly invariant as can be seen in the Fourier spectrum in panel c. Therefore, widening the ribbon did not shift the low-energy peaks towards smaller energies [cf. Fig. 3.12c]. This was also the case for the high-energy peak in zGNRs, which agreed with the edge-state energy being independent of the size of the ribbon. Recently, also the width of the graphene ribbons was considered in detail both computationally and experimentally [165] verifying "the $3n-1$ width-rule" (where n is an integer) that the electronic structure of the ribbon varies between semiconducting and metallic. This has considerable further implications in the transport studies such as the ones presented here.

As a third study, we investigated the dependence on the bias window but still had $V_{\mathrm{g}} = 0$. In Figs. 3.14a and 3.14c we show the results for a 13-aGNR of length 4.1 nm and width 1.4 nm, and in Figs. 3.14b and 3.14c the results for an 8-zGNR of length 4.1 nm and width 1.6 nm. The ribbons were chosen as comparable in size for better visualization of the dependence on the voltage. For zGNR the frequency of the oscillations associated to the edge-state transitions increased linearly with the bias, as it should have done. The transition energy between the biased Fermi level of the leads and the edge state of the ribbon increased with the voltage. It was also evident that for both ribbon geometries the transient regime lasted longer the larger was the bias, and that the steady-state was attained after several hundreds of femtoseconds. Increasing the bias window obviously enabled more states to take part in the transport dynamics.

We could conclude that the absolute values of the steady-state currents were higher through zGNRs than through aGNRs (of comparable sizes). An intuitive explanation for this observation was not straightforward to provide since we were considering rather large bias regime. The large bias regime enabled very many states to contribute to the absolute value of the steady-state current. We could still vaguely say that, as the zGNRs contain more states close to the zero energy, then this put more weight on the possible transport channels, at least for these bias windows. If we had chosen a bias window covering all the states for ribbons of comparable sizes, we could have naïvely expected the steady-state values to be equivalent. However, there might still have been room for possible selection rules depending on the ribbon orientation; whether some of the states would not have been participating to the dynamics at all due to wave function localization as was seen in Sec. 3.2. We

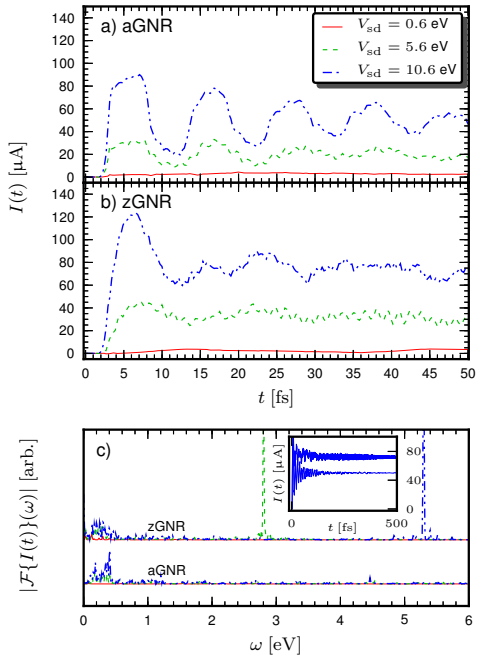

Fig. 3.14: Time-dependent bond currents through fixed-size ribbons with *varying bias voltage* a) aGNR: (W = 1.5 nm (13), L = 4.1 nm), b) zGNR: (W = 4.1 nm (8), L = 4.1 nm), and c) the corresponding Fourier transforms (zGNR is offset for clarity); the inset shows the long-time behaviour of the currents for V_{sd} = 10.6 eV in a) and b).

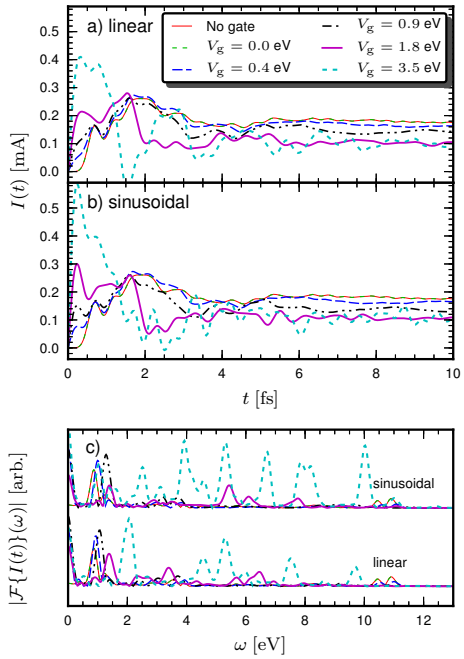

Fig. 3.15: Time-dependent bond currents through a 4-zGNR (length 0.7 nm and width 0.9 nm) with fixed bias voltage $V_{sd}/2$ = 3.5 eV and with *varying potentials*: a) linear potential profile, b) sinusoidal potential profile, c) the corresponding Fourier transforms (sinusoidal is offset for clarity).

also observed that the micro–milliampere range for the current with bias in the eV range agreed with the experimental results of Refs. [166–173].

3.4 Doped graphene flakes and controlling the transient current

In Pub. [II] we also considered extensions to perturbed central regions. This lead to illustrations of the formula in Eq. (2.127) where two different Hamiltonians were set for the central region: the equilibrium one only consisted of the plain

tight-binding lattice whereas the out-of-equilibrium one included a sudden switch-on of electric and/or magnetic fields. As the eigenbases of the unperturbed and perturbed Hamiltonians did not, in general, need to be equivalent, we were left with evaluating the overlaps between these bases in Eq. (2.127). This also increased the computational cost which was also discussed in Sec. 3.1.

We looked into the transient behaviour of a 4 hexagons-by-4 hexagons graphene flake exposed to both external bias voltage from the leads and an on-site potential profile within the flake. The potential profile could be understood as a self-consistent field inside the flake due to the modified charge profile, or due to charge injection or chemical doping. The system was composed of 32 carbon atoms with an on-site potential u_m being switched on at site m concurrently with the applied bias. We were interested in how the form of the potential profile within the flake affected the transient dynamics. We defined the distance of the m-th carbon atom from the left lead interface to be x_m, and then correspondingly defined the on-site potential as $u_m = u(x_m)$. For the linear and sinusoidal potential profiles (the function u of x) we used

$$u_{\text{lin.}}(x_m) = -\frac{2V_{\text{g}}}{L}\, x_m + V_{\text{g}}\,, \quad u_{\text{sin.}}(x_m) = \begin{cases} V_{\text{g}}\,, & x_m < L/10 \\ V_{\text{g}} \cos\left(\frac{5\pi}{4L} x_m - \frac{\pi}{8}\right), & L/10 \le x_m \le 9L/10 \\ -V_{\text{g}}\,, & x_m > 9L/10\,, \end{cases} \tag{3.1}$$

where L was the length of the flake.

The time-dependent currents through the flake with fixed bias voltage $V_{\text{sd}}/2 = 3.5$ eV are shown in In Fig. 3.15a for linear potential and in Fig. 3.15b for sinusoidal potential. A numerical check between Eqs. (2.92) and (2.127) was provided by looking at the data for non-perturbed (denoted in the figure by 'No gate' and '$V_{\text{g}} = 0.0$ eV') central regions. The equivalence was indeed found as the corresponding curves were on top of each other. For small voltages (< 1 eV) the transient was roughly similar to the non-perturbed one but, for stronger voltages, a rather non-trivial transient behaviour was observed. The Fourier spectrum (in panel c) shows a rich structure in several high-energy spectral windows. This was due to transitions involving levels of the *perturbed* central region, and these transitions could be mapped more thoroughly by looking at the nonequilibrium spectral function

$$A(\omega) = -\frac{1}{\pi} \operatorname{Im} \operatorname{Tr}\left[G^{\text{R}}(\omega)\right] \tag{3.2}$$

with the trace over the states of the central region. We show the spectral function in Fig. 3.16, and, as expected, the spectrum was widened when increasing the on-site potential strength V_{g}. The high energy peaks at $\omega \approx \pm 8$ eV (in the non-perturbed case: $V_{\text{g}} = 0$ eV) shifted to $\omega \approx \pm 10$ eV (when the perturbation was at its maximum: $V_{\text{g}} = 3.5$ eV). This was consistent with the Fourier peaks occurring at around

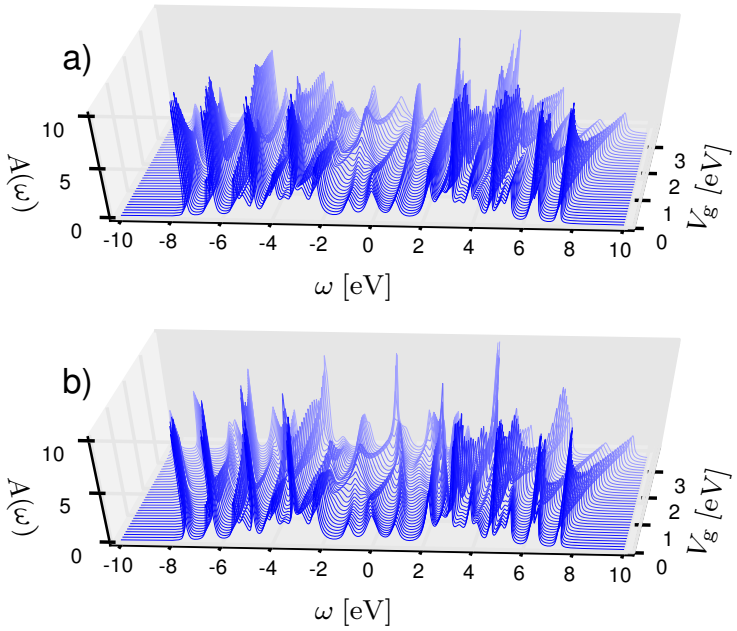

Fig. 3.16: Nonequilibrium spectral functions of the studied flake with *varying potential*: a) linear potential profile, and b) sinusoidal potential profile.

$\omega \approx 10$ eV in Fig. 3.15c. Similarly, all other main peaks in the Fourier spectrum could have been interpreted by inspecting the spectral function.

3.5 Curved graphene nanoribbons and focused transient currents

In Pub. [III] we further used the formalism developed in Pubs. [I, II] in a more applied study of transient response in curved graphene nanoribbons. As atomic precision fabrication and patterning is becoming routinely accessible in graphene based nanostructures [174, 175], it is interesting, and also important, to study the immediate applications of such tailored structures [174, 176–180]. In many experiments curved graphene structures have been realized [178, 181] but the more detailed transport properties have mainly been unexplored, apart from a few stationary transport studies [182–185]. For instance, in Ref. [186] a transmission electron microscopy (TEM) was used to probe the edge structure and widths of graphene structures in Ångström resolution, see Fig. 3.17. Electron irradiation was further used to manipulate the edge structures as shown in the snapshots.

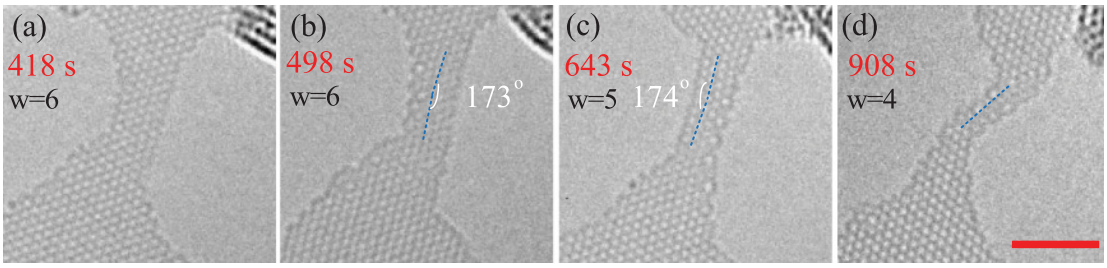

Fig. 3.17: Edge configurations of a GNR in a TEM study by Cheng et al. [186]. Snapshots at different times show the edge structures under electron irradiation. The scale bar is 2 nm.

3.5.1 Classification of the curved samples

Since TEM, as a procedure, is based on quantum transport, we investigated how the edge structures affected the transport properties of a GNR, and also how the mechanisms leading to these properties happened in the transient regime. Our study was based on four representative curved graphene nanoribbons (CGNR) in Fig. 3.18. The samples included two 60° arcs of different curvature (samples V_{short}

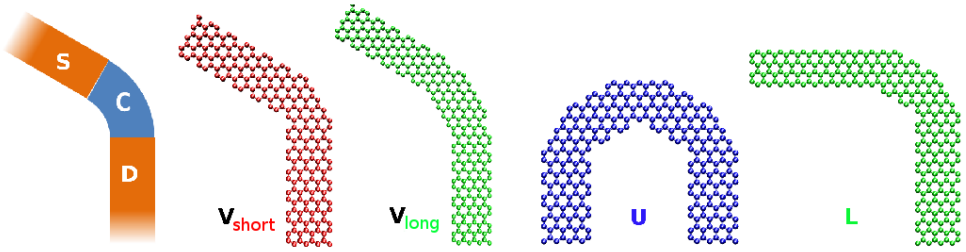

Fig. 3.18: Curved graphene nanoribbons in transport calculations. From left to right: schematics of curved ribbons attached to straight ribbons of the same width, forming a typical two-terminal transport device: source (S) and drain (D) electrodes connected via a central conducting device (C). Atomic structures of the samples used as a conducting device V_{short}, V_{long}, U, and L, i.e., these structures take the place of C in the schematic on the left. Hydrogen atoms are omitted from the figure for clarity.

and V_{long}. They both had 8-AGNR legs but in V_{short} the curved parts were shorter and only the outer edge contained a zigzag section; in V_{long} both the inner and the outer edge contained zigzag sections. The sample U contained a 180° arc and the sample L a 90° arc. For the transport setup, the arcs were coupled to straight, semi-infinite graphene nanoribbons. The leads were of armchair type (AGNR) or zigzag type (ZGNR), depending on the bisection angle [164]. The 60° and 180° arcs were coupled to two AGNRs and the 90° arcs to AGNR on one side and to ZGNR

on the other side. The atomic structures in Fig. 3.18 correspond to the central region in the transport setup, i.e., the curved part is extended by the straight ribbons (acting as leads) and the terminal of the straight part is then contacted to the biased electrode. In addition, the three-part systems were saturated by hydrogen to remove the dangling bonds. The systems had no in-plane stresses, i.e., the samples were simply cut out from pristine graphene planes without introducing any bending to the structure. In Pub. [III] we performed a rather systematic and extensive study on how the transport properties are affected by the curvature, but here we will only review a couple of the most important findings.

3.5.2 Transient currents through the curved sections

Similarly to the results presented in the previous sections, also here, in the transport setup, the bias voltage from the source to the drain electrode (over the central region) V_{SD} was switched on at $t = 0$ and the transient dynamics was calculated at zero temperature [using the formulae in terms of the logarithms and the exponential integrals in Eqs. (2.93), (2.94) and (2.95)] until the current saturated towards a steady state. The bias windows in this study were from $V_{\mathrm{SD}} = 0.2$ eV to 2.0 eV. The coupling strengths between the CGNR and the electrodes were chosen so that the resonance widths became $\gamma = 0.1$ eV, for both source and drain electrodes. For the studied samples these conditions lead to saturation times from few hundred femtoseconds up to 1 ns. The transient dynamics was analyzed similarly as in the previous section, as a sum over individual bond currents through virtual interfaces, *bridges*, B1 and B2 in the sample, see Fig. 3.19.

At the beginning of the transient, the current at B1 grew fast and then oscillated over hundreds of femtoseconds and then damped towards a steady state. For the wavecrest to reach the other bridge B2, it needed to travel roughly 30 Å, and, similarly to the findings in the previous section, this was seen as a short delay in the bridge current. The observed delay corresponded to a speed or mobility of the charge carriers of ~ 10 Å/fs, which roughly equals the Fermi velocity in graphene, $v_{\mathrm{F}} = 3|t_C|a/(2\hbar)$ with $|t_C| = 2.7$ eV and $a = 2.46$ Å, as was expected [83]. Both of the transients (at B1 and at B2) were characterized by slow oscillations superimposed by fast oscillations which could be associated with transitions happening inside the CGNR (intra-ribbon transition) or between the CGNR and the leads (ribbon-lead transition). The low-frequency oscillations came from the slow lead-to-lead reflections given by the overall charge-density wave after the bias voltage was switched on. In high-voltage regime we also saw another type of low-frequency oscillation which originated from multiple scatterings of the charge-density waves sloshing back-and-forth in the curved section of the CGNR.

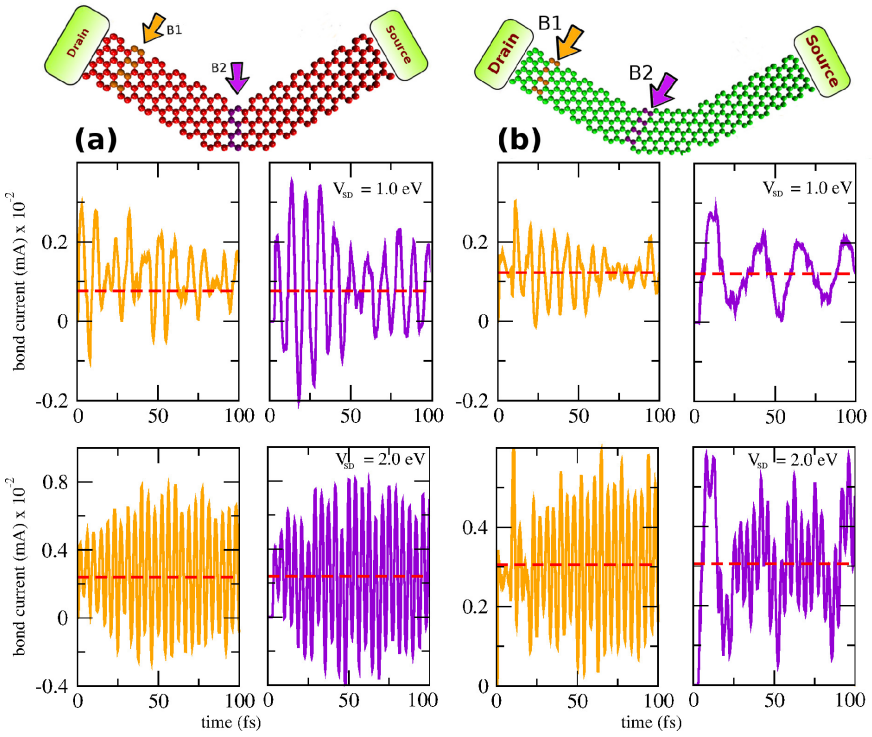

Fig. 3.19: Time-dependent currents in CGNRs. (a) Top figure shows the atomic structure of sample V_{short} with bridges B1 and B2. The four panels show time-dependent currents through B1 (left) and B2 (right) at $V_{SD} = 1.0$ eV (middle) and at $V_{SD} = 2.0$ eV (bottom). (b) Same as panels a for sample V_{long}. Dashed lines mark the steady-state currents.

In straight GNRs (without curvature) the currents were rather regular and flowed in the same direction, as was studied in Pub. [II], but in the CGNRs the current profiles were more complex. The curved section of the central region acted as a *deflection center* for the electronic current, and it could cause direction reversal, especially when the bias voltage was low. This lead to backscattering or backward currents which, in time domain, could be visualized nicely by animations, see the electronic supplemental information of Pub. [III]. The essential dynamics of the backscattering in the studied CGNRs boiled down to two variables: the lead-to-lead and the lead-to-curved part distance. The rich interference patterns upon multiple scatterings at the interfaces were governed by these length scales. The observed interference of the charge-density waves resulted in a rather complex Fourier spectrum of the currents, see Fig. 3.20.

We looked at one of the transitions in more detail. The time-dependent currents of the sample V_{long} at bias voltage $V_{SD} = 1.0$ eV showed well-defined oscillations of period $P = 30$ fs, and this oscillation was seen in the Fourier spectrum as an intense peak at the corresponding energy $\omega = 2\pi/P \approx 0.15$ eV. As all of the transitions, also

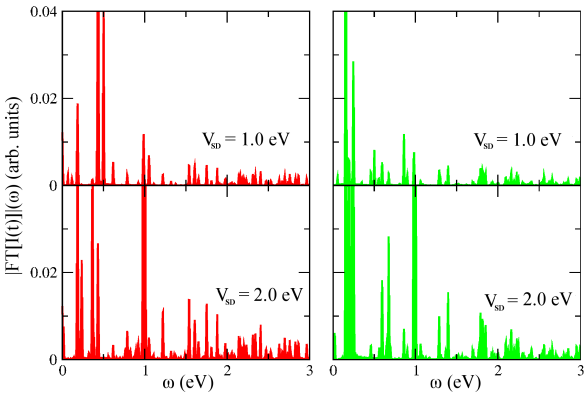

Fig. 3.20: Fourier transforms of time-dependent B2 currents of Fig. 3.19. Samples are V_{short} (left panels) and V_{long} (right panels) at the shown bias voltages.

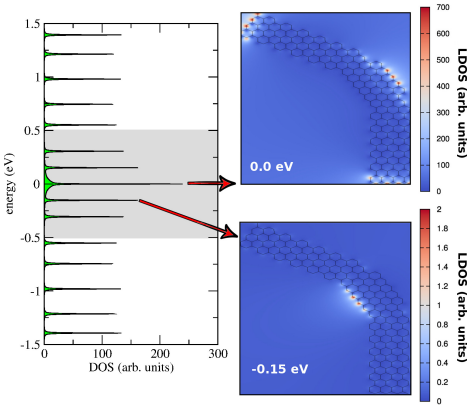

Fig. 3.21: Density of states (DOS) of sample V_{long}. Shaded region shows the 1.0 eV bias window. Right insets show the local density of states (colourmaps) for the selected DOS peaks at 0 eV and −0.15 eV.

this one could be further analyzed and identified by looking at the local density of states (LDOS) at energies given by the frequency of the oscillation. The LDOS at energies 0 eV and −0.15 eV (i.e., the difference in energy between these states was exactly the observed oscillation frequency) showed elongated edge states at inner and outer edges of the curved section, see Fig. 3.21. Therefore, we concluded that the electronic excitations at $\omega \approx 0.15$ eV corresponded to edge-state transitions taking place inside the CGNR between these two states. This oscillation, however, became masked when the bias voltage V_{SD} was increased because additional electronic transitions started taking place within the wider bias window.

In Pub. [III] we also compared the single π-orbital model used in the time-dependent Landauer–Büttiker formalism to a multi-orbital density-functional tight-binding model; both models yielded frontier orbitals of a similar edge-localized nature and a similar level structure. Even though we did not perform time-dependent transport calculations in the full multi-orbital framework, we argued that the qualitative features of the transients would not have been affected by the choice of the model.

3.5.3 Temporal and spatial focusing of the current

The Fourier transform, as seen by the above analysis, can provide some insight into identifying transitions occurring during the transients. However, it misses all the temporal information as it is unable to provide either the times or the durations

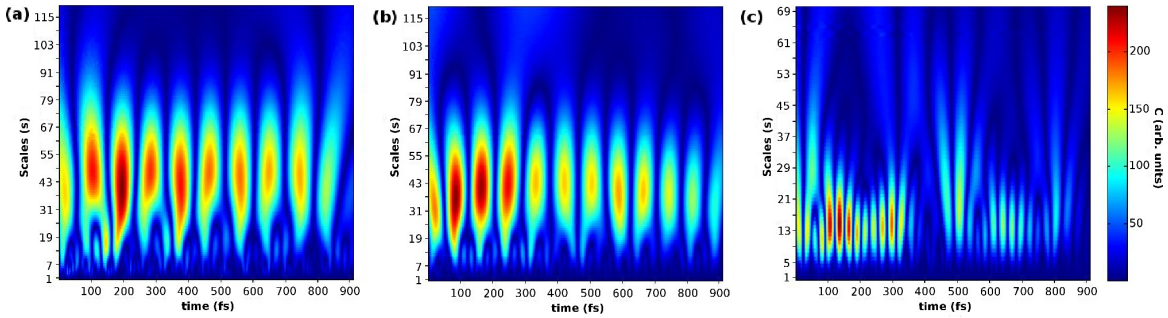

Fig. 3.22: Wavelet amplitudes (colourmaps) as a function of scale (s) and time (τ) for currents through the curved sections in (a) sample U, (b) sample L, and (c) sample V_{short} with an impurity site, all at $V_{\text{SD}} = 1.0$ eV.

when certain transitions are active. This is due to the averaging nature of the integral transformation; if certain oscillation in the time-dependent signal is present for a long time, it integrates to a large Fourier peak amplitude, although this oscillation does not need to be present all the time [187]. The peak intensities in the Fourier spectrum only give an averaged-out information about how long durations certain frequencies are present. For a more accurate temporal analysis, in Pub. [III], we consulted an alternative analysis tool – *the wavelet decomposition*. In this method, the signal is convolved with a set of basis functions called wavelets [187, 188]. The continuous wavelet transformation (CWT) for a signal $I(t)$ is defined as

$$\mathcal{I}(s,\tau) = \frac{1}{\sqrt{s}} \int_{-\infty}^{\infty} I(t)\, \psi^* \left(\frac{t-\tau}{s} \right) \mathrm{d}t, \tag{3.3}$$

where ψ^* is the complex conjugate of the wavelet shifted (in time) by τ and scaled by the dimensionless parameter s. This transformation maps the data into an (s,τ)-plane, where τ is related to time and s can be related to frequencies via $f_s = f_c/(s\Delta)$, where Δ is the sampling period and f_c is the center frequency of the wavelet. With 1 femtosecond as our unit of time, we used the Ricker wavelets (or the Mexican hat wavelet)

$$\psi(t) = \frac{2}{\sqrt{3}\pi^{1/4}} [1 - t^2] \mathrm{e}^{-t^2/2} \tag{3.4}$$

with a center frequency of $f_c = 0.25\ \mathrm{fs}^{-1}$ and sampling of $\Delta = 0.16$ fs. The advantage of wavelet analysis is that it allows for distinguishing between rapid and slow current fluctuations by choosing the scale s. This means that the transients can be analyzed simultaneously at different frequencies and at different times, although this increases the computational cost.

By looking carefully at the wavelet amplitudes in the (s,τ)-plane we could identify instants and frequencies for possibly interesting events. We calculated CWT on the currents by using the Wavelet Toolbox in Matlab [189] and scales large enough to

scan all the frequencies relevant to our transport setup. We present here the wavelet analysis for the transient signal in samples U and L (see Pub. [III] for more details). The transport setup was otherwise the same as in samples V_{short} and V_{long} above and we set the bias voltage to V_{SD} = 1.0 eV. In Fig. 3.22 we have the wavelet amplitudes as a colourmap in terms of time and scale for the sample U in panel (a) and for the sample L in panel (b). According to the colourmap we picked two instants for each structure: one when the wavelet amplitude showed rich fluctuation and another when it remained small. At these instants we plotted, from the full density matrix for the structure, the charge and current distributions along the whole sample, and we expected to see many transitions active in the first instant whereas for the second instant we expected to see a more uniform distribution. In Fig. 3.23 we show these selected snapshots of the two instants, and indeed, the behaviour was as expected: At the first instant the current distribution showed more fluctuations and backscattering compared to the second instant when the distribution was fairly uniform. The wavelet amplitudes and snapshots also showed *spatial and temporal focusing* of the current: At certain instants the current was spatially focused in certain bonds within the structure. (This was also particularly evident in the animations, see the supplementary information of Pub. [III].) Sample U captured strong currents along the armchair leads and along the inner edges of curved section. In sample L one of the leads was zigzag while the other lead was armchair, and this asymmetry became clearly visible in the charge and current distributions. The charge variations occurred along the sample irregularly, which happened because the zigzag lead supported more current paths than the armchair lead, at least for this type of CGNR. The difference in the wave propagation speeds in the different leads quickly created a non-uniform and irregular charge distributions across the sample.

We also used the wavelet analysis to investigate how impurities might have affected the transient behaviour and especially the time-dependent current distributions along the curved section. For this study, we took the sample V_{short} and placed an impurity atom adsorbed on top of a carbon atom located at the bridge B2 (through which the transient current was calculated, see Fig. 3.19). The impurity was modelled by an on-site energy of 0.2 eV and a modified hopping parameter to the nearest carbon atom −2.16 eV. This model for an impurity caused weaker bonding to its neighboring atoms [90]. We have the wavelet analysis for this system in Fig. 3.22c. (This can also be compared with the one of the pristine sample V_{short}, see Pub. [III].) By inspecting the timescales in the wavelet analysis we could again pinpoint certain instants when most oscillating modes were simultaneously present, and then view the corresponding charge and current distributions along the sample. We observed how the impurity atom within the curved section could affect the current paths. In Fig. 3.24 (and also in animations, see the supplementary information in Pub. [III]) we could direct (or control) the paths of the charge carriers to the outer edge of the curved section. It was evident that in CGNRs the electric currents were highly sensitive to even single impurities since entire current patterns could be rearranged

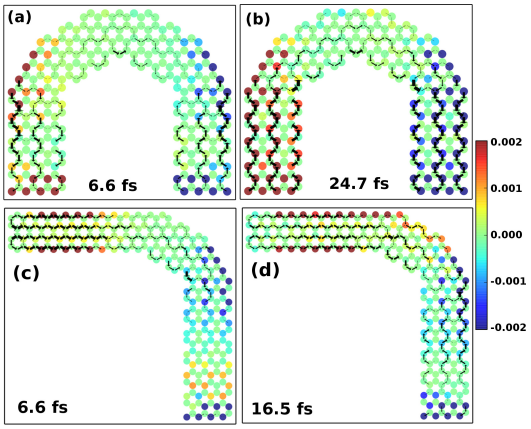

Fig. 3.23: Snapshots of the bond currents (black arrows) and the charge variations (colourmap; units of electron charge) for samples U (a and b) and samples L (c and d) at V_{SD} = 1.0 eV and at times shown in the panels.

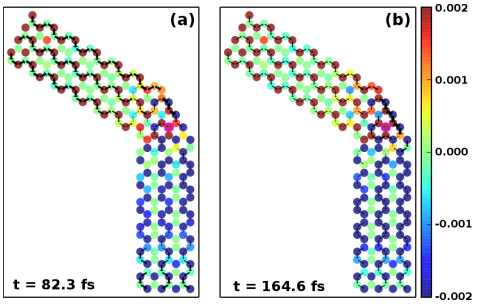

Fig. 3.24: Snapshots of bond currents (black arrows) and charge variations (colourmap; units of electron charge) for sample V_{short} with an impurity adsorbed on the top of the carbon atom enclosed by a bold line (magenta) located at the center of the curvature. V_{SD} = 1.0 eV and the respective instants are shown in the panels.

by them.

We also analyzed how strong the focusing effect of the bond currents can be, i.e., how much of the total current is dictated by individual bonds. When we looked at the time-dependent currents through samples V_{short}, U, and L at instants of the first peaks in the wavelet amplitudes, we could create a simple list of bond currents along the whole sample at those instants. For instance, in V_{short} the number of atoms is 216 and the number of individual bonds is 568. At a specific instant the currents through each of these bonds have certain values. By plotting these values with respect to the bond index we could compare how the bond current profile was distributed along the sample, see Fig. 3.25. We observed rather extreme focusing, depending on the structure, because already only few of the bonds could carry instantaneous currents exceeding even the overall steady-state current through the whole sample. This was our central result as such focusing is absent in straight GNRs, which showed temporally and spatially far more homogeneous currents, see Pub. [II]. This focusing effect could be used in graphene-based edge-detecting devices [190], but the extreme focusing might also lead to detrimental Joule heating and eventually burning the sample. However, this could be avoided by using low biases and ultra-fast time scales for the heat to dissipate. The operation of the device when heated could then be probed by resistive heating maps [191].

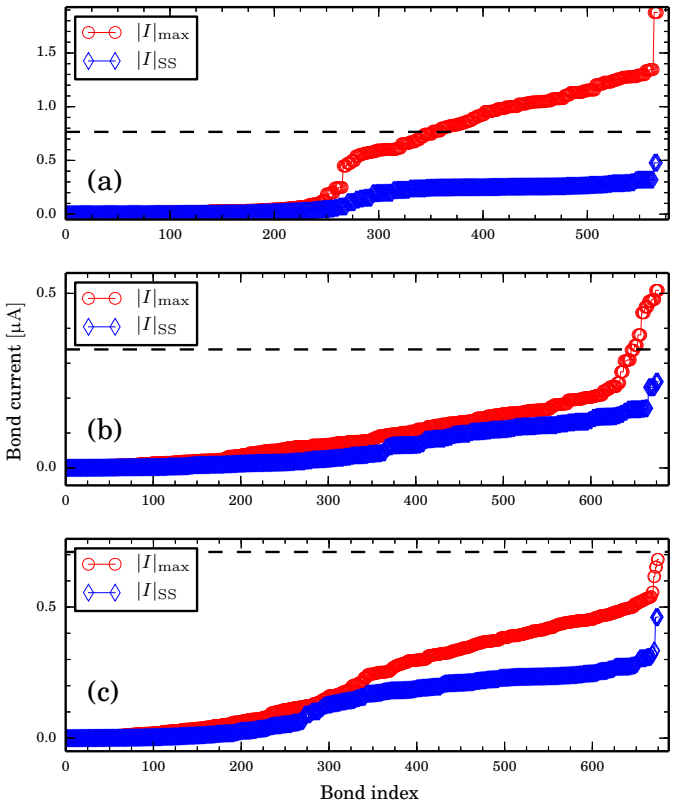

Fig. 3.25: Instantaneous bond currents for samples (a) V_{short} at $t = 12.6$ fs, (b) U at $t = 19.7$ fs and (c) L at $t = 16.5$ fs with bias voltage $V_{SD} = 1.0$ eV as a function of bond index (red circles). Panels also include the corresponding bond currents at the steady-state (blue diamonds) and the overall steady-state current through the sample (dashed line). Bonds are indexed wrt. increasing current.

3.6 Superconducting junctions

In Pub. [IV] we investigated transport in NSN junctions where a superconducting central region is coupled to two (normal) metallic leads. Here, an outline of the key results is presented.

The transport setup is exactly the same as in Fig. 3.1; the central region is a superconducting benzene-like molecule. In these type of samples the superconductivity could be induced, e.g., by charge injection, chemical doping or using the proximity effect leading to critical temperatures ranging from 1 to 10 K [192–195]. The benzene molecule is modelled in a single π-orbital tight-binding framework with the hopping parameter $t_C = -2.7$ eV [89], and then other energies are related to this scale. Also, the molecule's edges (longitudinally, in the transport direction) are saturated

by hydrogen with modified tight-binding parameters for hydrogen on-site energies and hydrogen–carbon hopping [90], respectively, so that there is no band gap in equilibrium. We set this condition because we want to isolate the effects from the superconducting gap Δ without complicating the spectrum with the semiconducting gap. We further choose the coupling strength between the molecule and the leads and the lead hopping so that we are in weak coupling regime $\Gamma = 0.2$ eV.

In this setup, it is possible to observe different transition mechanisms depending on the chosen parameters. When the bias voltage V_α is larger than the superconducting gap Δ, all the levels inside the bias window are available for transport, and transitions through the superconducting states are disrupted since the energy for the incoming electrons is high enough to break possible Cooper pairs (CP) in the central region; this is referred to as normal tunneling (NT). On the other hand, if the bias voltage is smaller than the superconducting gap, it is possible to form a CP in the central region. Then, it is further possible to observe Andreev reflection (AR) between an electron and a hole in the source (or drain) lead forming the CP in the center, or to observe a crossed Andreev reflection (CAR) where an electron from the source (drain) lead is coupled to a hole in the drain (source) lead through the CP in the center. In addition, direct tunneling of an electron via the CP, referred to as co-tunneling (CT), is a possible transmission channel.

We first simulate the NT. The temperature is fixed well below the critical temperature, $\beta = 100/|t_C|$, so that the gap can be approximated as the (constant) value at zero temperature $\Delta(T = 0)$ according to the self-consistent gap equation [196]. The bias window is symmetric around the chemical potential, $V_L = -V_R = 3|t_C|/2$, and the gap Δ is varied but kept smaller than the bias. The transient currents through the sample are calculated by Eq. (2.162); we sum the individual bond currents transversally in the middle of the molecule. The pair densities are calculated by summing the pair densities within the molecule: $P(t) = \sum_m P_m(t)$ from Eq. (2.163). These results are plotted in Fig. 3.26 with a Fourier transform of the current. When the gap Δ is increased, the overall current is decreased since the conducting states are moved away from the bias window. This can also be seen as shifts in the transient frequencies in the Fourier spectrum. The spectral function, plotted in Fig. 3.29, may be used to further identify the transitions. When $\Delta = 0$, we observe two intramolecular transitions (frequencies $\omega = |t_C|$ and $\omega = 2|t_C|$) which shift when the gap is varied corresponding to the shifted energy levels. We also notice two lead–molecule transitions (frequencies $\omega = |t_C|/2$ and $\omega = 5|t_C|/2$) when $\Delta = 0$. Also these transitions shift with the peaks in the spectral function corresponding to the fixed bias $V = 3|t_C|/2$. In addition, we observe the pair density going to zero from its equilibrium value when $\Delta < V$. Therefore, we do not see AR or CAR processes due to no out-of-equilibrium CPs forming in the central region. When the gap is set equal to the bias window, we notice that the steady-state current goes to zero since there are no transport channels within the bias window. However, some transient

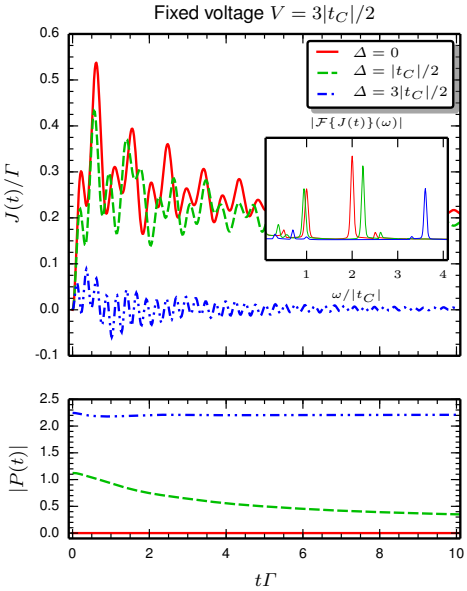

Fig. 3.26: Transient currents (top panel) and pair densities (bottom panel) in the molecule when varying Δ. The inset shows the absolute value of the Fourier-transformed current.

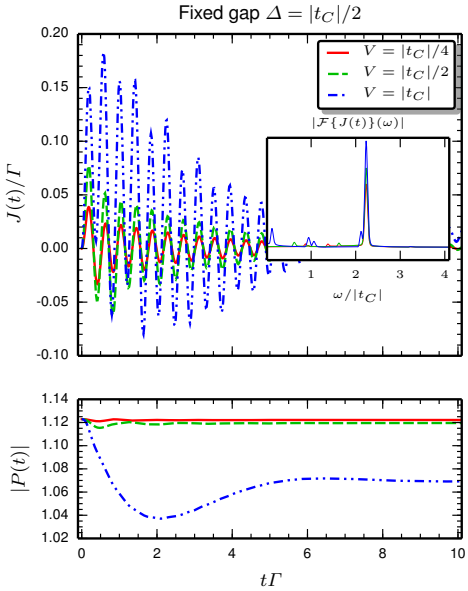

Fig. 3.27: Same as Fig. 3.26 but with varying V.

oscillations are still present due to the states in the vicinity of the resonant window, which is seen as an intramolecular transition at $\omega \sim 7|t_C|/2$.

Then we simulate the AR and CAR processes. We choose the gap in Fig. 3.27 as $\Delta = |t_C|/2$, and in Fig. 3.28 as $\Delta = 3|t_C|/2$. In both cases, when $V \leq \Delta$, the transient current oscillates towards a zero steady-state current with frequencies mainly corresponding to intramolecular transitions (around $\omega = |t_C|$ and $\omega = 2|t_C|$). When the gap is larger in Fig. 3.28 and for $V \leq \Delta$, we observe CP formation within the molecule. When the voltages are small, we mainly find the first intramolecular transition at around $\omega = 7|t_C|/2$. For larger voltages we also see the lead–molecule transitions at lower frequencies recovering again the NT regime.

3.7 Heat transport in atomic chains

Here the key results of Pub. [V] are reviewed. We studied the transient behaviour of the heat current in simple lattice models when coupled to reservoirs of different temperatures. We benchmarked the validity of the approximations made in the

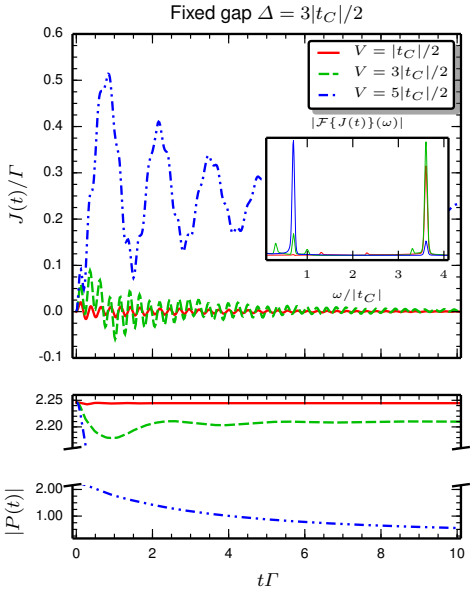

Fig. 3.28: Transient currents (top panel) and pair densities (bottom panel) in the molecule when varying V. The inset shows the absolute value of the Fourier-transformed current.

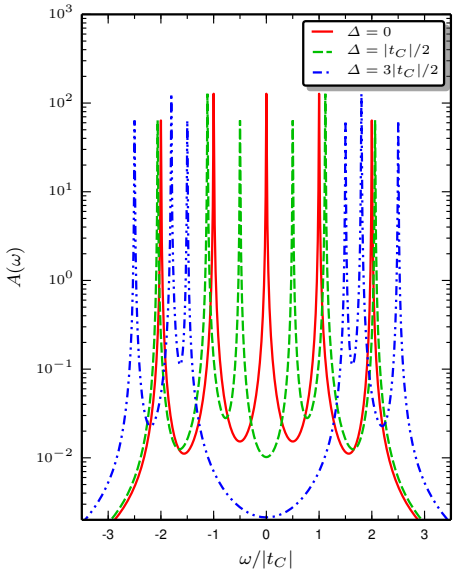

Fig. 3.29: Spectral functions of the coupled benzene molecule when varying Δ.

derivation of Eq. (2.209) by comparing to full numerical solution to the equation of motion (2.183) with the embedding self-energy in Eq. (2.194). The full numerical solution was obtained self-consistently in the full two-time plane [141, 142], and then the time-diagonal components were extracted for comparison with Eq. (2.209). In both full and approximate solutions we employ the partitioned approach with the subsystems being initially uncontacted at separate temperatures.

3.7.1 Validity of the analytical formula (2.209)

The derived result provided information about the one-particle density matrix in the central region, so we were interested in local quantities in this region. The local heat current between sites j and k in the central region could be calculated by Eq. (2.216). In our transport setup we had uniform one-dimensional (semi-infinite) systems of coupled springs as reservoirs, and we fixed the spring constant in the reservoirs as $k_\lambda = 1$ and then related the remaining parameters to this energy scale. Also, the central region, through which we studied the heat current transients, was similarly a uniform one-dimensional (but finite) system of coupled springs.

We could tune the embedding by choosing the coupling strength $k_{\lambda C}$. Also, for the levels of the central region to be inside the bandwidth (given by $\pm 2\sqrt{k_\lambda}$) we chose the spring constant in the central region k_C small enough. We also set the Boltzmann constant $k_B = 1$ so that the temperature differences between the reservoirs and the central region could be related to the order of the eigenmode energies in the central region for the heat transport to occur in the quantum regime. We considered this temperature scale as a difference $\Delta T = T_L - T_R$ and set the temperature for the central region as $T_C = (T_L + T_R)/2$. We fixed the temperature in the right reservoir $T_R = 1$ and related the remaining ones to this.

Compared to the full numerical solution of Eq. (2.183), we made many approximations when deriving the analytic solution in Eq. (2.209). We studied how much error each approximation caused when compared to the full numerical solution. First, we made the wide-band approximation for the self-energy in Eq. (2.194) but otherwise we still solved the equation of motion numerically, i.e., without approximating the time-convolutions. We denoted this level of approximation as 'WB'. Second, in addition to the wide-band approximation for the self-energy, we employed the approximation for the time-convolution $[\boldsymbol{D}^{\mathrm{R}} \cdot \boldsymbol{\Pi}^{<}]$ in Eq. (2.200) (and its conjugate) with the cut-off frequency being set to the phonon bandwidth, but we still evaluated numerically the other time-convolution $[\boldsymbol{D}^{<} \cdot \boldsymbol{\Pi}^{\mathrm{A}}]$ (and its conjugate). This level of approximation was denoted as 'WB-1'. Third approximation was the same as WB-1 but the other way around, i.e., approximating the time-convolution $[\boldsymbol{D}^{<} \cdot \boldsymbol{\Pi}^{\mathrm{A}}]$ as in Eq. (2.204) (and its conjugate) but evaluating numerically the other time-convolution $[\boldsymbol{D}^{\mathrm{R}} \cdot \boldsymbol{\Pi}^{<}]$ (and its conjugate). This we denoted as 'WB-2'. Ultimately, both time-convolutions were approximated as in Eqs. (2.200) and (2.204) with the cut-off frequency being set to the phonon bandwidth, and this procedure resulted in the analytic solution in Eq. (2.209).

We benchmarked the validity of these approximations by studying heat current through a dimer molecule as the central region. The parameters were chosen so that: (a) the energy levels of the dimer molecule were comparable with the reservoir bandwidth, i.e., the wide-band approximation was expected to fail; and (b) the energy levels of the dimer were in a narrow range compared to the reservoir bandwidth, i.e., the wide-band approximation should not have neglected the detail of the spectrum. In case (a) we took $k_{\lambda C} = 1/2$ and $k_C = 1$, and in case (b) we took $k_{\lambda C} = 1/4$ and $k_C = 1/3$. In both cases we had the temperature profile as $T_L = 5$, $\Delta T = 4$.

The heat current between the dimer atoms evaluated from Eq. (2.216) for the two above-mentioned cases is shown in Fig. 3.30. In case (a) we saw more deviation from the full solution (red, thick solid line) compared to case (b) as was expected from the parameter choice. By neglecting the frequency dependency of the phonon band we saw in both cases (green, long-dashed curve, WB) that the transient behaviour

was overestimated due to too crude an approximation for the band edges. This also affected the long-time behaviour as the current saturated faster than the full solution because the coupling strength (dissipation) was overestimated in WB. Also, the steady-state value for the heat current was overestimated. When we also added the approximation for the time-convolution $[\boldsymbol{D}^{\mathrm{R}} \cdot \boldsymbol{\Pi}^{<}]$ (blue, dash-dotted curve, WB-1) we did not, at least in this case, see any considerable difference to WB. This meant that approximating the retarded Green's function in Eqs. (A.100) and (A.101) as the embedded one only slightly modified the initial transient. When we considered the approximation only for the time-convolution $[\boldsymbol{D}^{<} \cdot \boldsymbol{\Pi}^{\mathrm{A}}]$ (magenta, short-dashed curve, WB-2) we saw a relatively good match with the full solution. However, individual density matrix elements could still differ considerably between the approximated and full solutions, see the details in Pub. [V]. When deriving $[\boldsymbol{D}^{\mathrm{R}} \cdot \boldsymbol{\Pi}^{<}]$ in Eq. (A.107) and $[\boldsymbol{D}^{<} \cdot \boldsymbol{\Pi}^{\mathrm{A}}]$ in Eq. (A.118) we implicitly assumed the limit $\omega_c \to \infty$. When the cut-off frequency was set to the phonon bandwidth, in Fig. 3.30(a) the approximations did not fully take into account the broader spectrum of the central region. In Fig. 3.30(b) the spectrum of the central region was more narrow, and all approximations gave a reasonable agreement. Even if the general trend of the transient was qualitatively captured in both cases, quantitative differences could still be considerable, see the insets in Fig. 3.30. When combining all the approximations, we got the derived result in Eq. (2.209) (cyan, thin solid line). This fully analytic result, which did not need any numerical evaluation of the Green's function, could still give a comparatively good description. For the validity of the approximations we concluded that the wide-band-like approximation overestimates the results obtained by integrating the spectral function, see also Fig. 2.6.

3.7.2 Relaxation times from low to high temperature gradients

We also used the time-dependent formalism to estimate relaxation time scales using a measure $\kappa = (J^{\mathrm{Q}}(t = \tau) - J^{\mathrm{Q}}_{\mathrm{SS}})/J^{\mathrm{Q}}_{\mathrm{SS}}$ and define the *relaxation time* τ (time from $t = 0$ to reach the steady state) as $\kappa = 10\%$ [53]. We considered similar atomic chains as in the previous example but we varied the length of the chain and the strength of the coupling between the chain and the reservoirs. We chose the model parameters in physical units as $k_\lambda = 1.0$ eV/(Å^{2}u), $k_C = 0.625$ eV/(Å^{2}u) where u is the atomic mass unit. (These are the mass-normalized spring constants, i.e., in SI units $[k] = 1/\mathrm{s}^2$.) In Fig. 3.31 we have the relaxation times (colourmap) for chains of varying length (horizontal axis) and with varying coupling strength (vertical axis) with a 10% temperature difference between the reservoirs. In panel a the baseline temperature is 10 K (leading to $T_L = 11$ K and $T_R = 9$ K), and in panel b the baseline temperature is 300 K (leading to $T_L = 330$ K and $T_R = 270$ K).

We observed that, for both low and high temperature regimes, the relaxation was

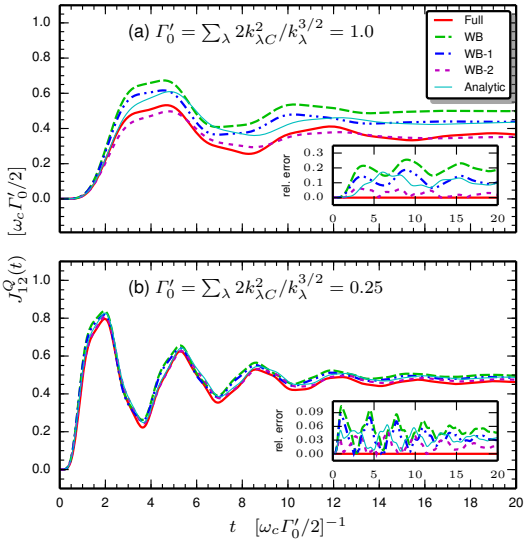

Fig. 3.30: Time-dependent heat current through a dimer molecule: (a) strong coupling and broad spectrum, and (b) weak coupling and narrow spectrum. The insets show the relative difference between the approximate and full solutions.

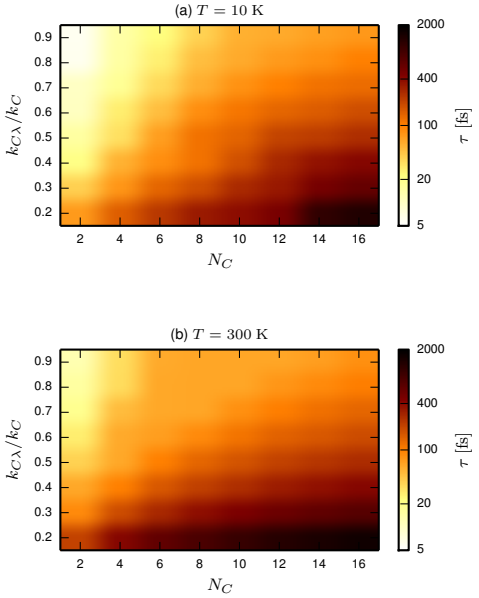

Fig. 3.31: Relaxation times (colourmap) for atomic chains of varying length (horizontal axis) and coupling strength to the reservoirs (vertical axis) at (a) low and (b) high temperature.

fastest in the shortest chain ($N_C = 2$) when the coupling strength between the central region and the reservoirs was the highest ($k_{C\lambda} = 0.9k_C$). It simply took longer time for the phonons to populate longer systems, and when the coupling strength between the central region and the reservoirs was increased the relaxation times decreased due to the stronger dissipation. Expectedly, the slowest relaxation, which could take up to picosecond scale, occurred in the longest chain ($N_C = 16$) when the coupling was the weakest ($k_{C\lambda} = 0.2k_C$). The overall dependency on the studied parameters was roughly similar in both low and high temperature regimes. However, we saw in high temperature and small coupling that even the mid-range chains could have a comparatively long relaxation time. On the other hand, increasing the coupling strength in the high-temperature regime resulted in comparatively faster relaxation. This was also partly due to the larger absolute difference in temperature in the high-temperature case.

4 Conclusion and outlook

In this thesis quantum transport in the transient regime was studied. In both electronic and phononic transport setups, a time-dependent extension to the traditional Landauer–Büttiker approach was derived from the point of view of nonequilibrium Green's functions. The derived results follow directly as analytical solutions to the equations of motion for the Green's function. The studied transport setups considered only noninteracting particles within wide-band approximation for the surrounding reservoirs. Lifting these assumptions would have required solving the equations of motion for the Green's function numerically using self-consistent and time-stepping algorithms as there is no closed solution for the general case. The Green's function method offered a natural framework for the description of quantum transport, and previously derived known results, e.g., Meir–Wingreen and Landauer–Büttiker formulae, were obtained as limiting cases of the present study.

More explicitly, the Kadanoff–Baym equations for the Green's function of an open noninteracting system were solved by properly taking into account the initial contacts between the system and the reservoirs. The results of the present study are closed integral expressions for the time-dependence of the electronic density matrix of a molecular junction after switch-on of a bias voltage in the leads or an electromagnetic perturbation in the junction. The molecular junction could further be described as superconducting. Also, similar closed integral expression for the current flowing into the leads was obtained. As these results were closed expressions they could be evaluated without the necessity of propagating individual single-particle orbitals or Green's functions. In addition, the integral expressions were written in terms of known functions (logarithms, exponential integrals, digamma and hypergeometric functions) to further speed up the computation of the transport properties of interest. Similar to the electronic case, also for the phonon transport equivalent closed integral expressions were derived for the time-dependent phonon density matrix.

Using the derived formulae for time-dependent density matrix and current transient dynamics in charge and thermal transport through molecular junctions was analyzed. Benchmark tests in various structures were performed for the validity of the obtained formulae where also the computational cost between existing methods was discussed. As applications tight-binding lattices such as ring-shaped junctions, zigzag and armchair graphene nanoribbons of different geometries and

atomic chains were considered by calculating the time-dependent charge and heat currents flowing through the structures. In all the simulations rich transient dynamics was found: After the switch-on long time oscillatory motion, related to multiple reflections of the charge and heat currents within the studied structures, was observed. This indicated the need for a fully time-dependent description of the quantum transport processes as the saturation times were not negligible or insignificant, to say the least.

When studying graphene nanoribbons pronounced quasi-steady states, which were explained by reflections of the density wave passing through the ribbon with the edge states located at the ribbon–lead interfaces, were found. Further, in the case of zigzag nanoribbons, there was a predominant oscillation frequency associated with virtual transitions between the edge states and the Fermi levels of the electrode. The observed transient dynamics provided detailed spectral information on the structure of the studied nanoribbons. Also stationary and time-dependent electronic transport properties of graphene nanoribbons with intrinsic curvature were studied. The curved parts greatly influenced the transport features of graphene nanoribbons. Conductance gaps were governed both by the electronic character of the leads and by the presence and the amount of curvature. The curvature also induced temporally and spatially focused electric currents that mostly flowed at the ribbons edges. This focusing enhanced the sensitivity to perturbations since the presence of a localized impurity could cause a complete rearrangement of the current profile. These findings could benefit the development of sensing devices that employ materials' edges for probing ultrafast modifications in the environment.

When analyzing transient heat currents in atomic chains it was possible to benchmark the derived result for the time-dependent phonon density matrix against a full numerical solution to the equations of motion for the Green's function, and furthermore test the validity of the approximations put forward when deriving the result. The approximations were found to be reasonable and the benchmark results congruent when the cut-off frequency was chosen large enough compared to the relevant energy scales of the studied systems, and when the coupling strength between the central region and the reservoirs was small enough for the wide-band-like approximation to hold.

When simulating transport in a superconducting benzene-like molecule attached to two-dimensional normal metal leads the formation of Cooper pairs within the central molecule was observed leading to Andreev reflection processes. As the transport setup for the derivation was very general, the same methodology may be used for more involved systems. For instance, adding a third normal metal lead or a gate potential would allow for controlling the transients [131, 197, 198]. Understanding the transient properties of such systems, possibly used as transistors or switches, is of great importance when designing prospective effective nanoscale

electronics.

The advantages of the derived results for transient dynamics are that the numerical effort in computing the transport properties of interest is drastically reduced and that the transient behavior can easily be interpreted in terms of virtual transitions and decay rates. Recently, measuring the ultrafast dynamics has been made possible due to the technical advances in laser sources [199, 200]. Experiments in individual atomic and molecular scale systems [201–204] and carbon nanotubes [205, 206] have been carried out reaching temporal resolutions corresponding to nuclear and even electronic motion. There are therefore important experimental developments that can, in the future, give access to the direct study of transient dynamics. Such transient spectroscopy can give important detailed information on the structure of molecular junctions out of equilibrium.

It remains to be investigated how the formalism for time-dependent perturbations, developed by Ridley et al. [101, 139] could be incorporated in further computational studies similar to the ones presented in this thesis for, e.g., carbon nanotube or graphene based junctions. Also, since the formulation is valid in the whole two-time plane for both lesser and greater Green's functions, Eq. (2.168), many physical quantities such as noise spectra could readily be computed. For the phonon transport methodology it could be studied if and how a partition-free approach, conventionally used in electronic transport [96], could be incorporated also in this context. A related issue, in the case of heat transport due to electrons, has recently been discussed in Refs. [207, 208]. Further computational advances could also be obtained by performing the frequency integrals in Eq. (2.209) analytically using a Padé expansion for the Bose function, making it possible to study transient phonon dynamics in systems of even larger spatial scale.

Appendix A: Technical details of the derivations

A.1 Details of the derivations in electronic transport

Here the details of the derivations presented in Sec. 2.3 are provided for completeness. We first discuss the form of the self-energy approximation and the corresponding Keldysh components for it. Then we use these expressions to obtain, accordingly, the Green's functions, and then we evaluate the time-convolutions between the self-energies and the Green's functions in Eq. (2.67). Finally, we insert the time-convolutions in the equation of motion and derive an analytic solution for the remaining differential equation.

A.1.1 Deriving the Keldysh components of the self-energies and Green's functions

Since the retarded/advanced component of the self-energy in WBA can be written in frequency domain as $\Sigma^{\mathrm{R/A}}_{\alpha,mn}(\omega) = \mp\frac{\mathrm{i}}{2}\Gamma_{\alpha,mn}$, we may perform an analytic continuation to complex frequencies to obtain the Matsubara component as $\Sigma^{\mathrm{M}}_{\alpha,mn}(\omega_q) = \mp\frac{\mathrm{i}}{2}\Gamma_{\alpha,mn}$ where the minus sign is taken when the Matsubara frequency is located on the upper-half plane (UHP): $\mathrm{Im}\,\omega_q > 0$ and the plus sign when the Matsubara frequency is located on the lower-half plane (LHP): $\mathrm{Im}\,\omega_q < 0$. Then, in time-domain (on the vertical track of the Keldysh contour) we have the self-energy as a Fourier-type transformation [73]

$$\Sigma^{\mathrm{M}}_{\alpha,mn}(\tau,\tau') = \frac{1}{-\mathrm{i}\beta}\sum_q \mathrm{e}^{\omega_q(\tau-\tau')}\Sigma^{\mathrm{M}}_{\alpha,mn}(\omega_q). \tag{A.1}$$

The advanced Green's function for isolated α-th lead satisfies the equation of motion in Eq. (2.6) with the lead Hamiltonian given simply as $\epsilon_{k\alpha} + V_\alpha$. The solution for the Green's function is then readily written as

$$g^{\mathrm{A}}_{k\alpha}(t_0,t) = \mathrm{i}\theta(t-t_0)\mathrm{e}^{\mathrm{i}(\epsilon_{k\alpha}+V_\alpha)(t-t_0)}. \tag{A.2}$$

Then, we can express the 'left' component of the isolated α-th lead's Green's function by separating the corresponding Green's functions on the horizontal and vertical branch of the Keldysh contour as

$$g^{\lceil}_{k\alpha}(\tau,t) = -\mathrm{i}g^{\mathrm{M}}_{k\alpha}(\tau,0)g^{\mathrm{A}}_{k\alpha}(0,t) = \mathrm{e}^{\mathrm{i}(\epsilon_{k\alpha}+V_\alpha)t}g^{\mathrm{M}}_{k\alpha}(\tau,0), \tag{A.3}$$

where, without loss of generality, we could choose $t_0 = 0$ for simplicity (as the time when the bias voltage is switched on). The Matsubara Green's functions in time-domain can also be expressed from the corresponding Green's function in terms of the Matsubara frequency as a Fourier-type series

$$g^{\mathrm{M}}_{k\alpha}(\tau,\tau') = \frac{1}{-\mathrm{i}\beta}\sum_q \mathrm{e}^{-\omega_q(\tau-\tau')}g^{\mathrm{M}}(\omega_q) = \frac{1}{-\mathrm{i}\beta}\sum_q \frac{\mathrm{e}^{-\omega_q(\tau-\tau')}}{\omega_q-\epsilon_{k\alpha}+\mu}, \tag{A.4}$$

where we inserted a general form for the Green's function in frequency domain from Eq. (2.11) and using an analytic continuation. By using Eq. (A.3) we can calculate the corresponding component for the self-energy in Eq. (2.63)

$$\begin{aligned}
\Sigma^{\lceil}_{\alpha,mn}(\tau,t) &= \frac{1}{-\mathrm{i}\beta}\sum_q \mathrm{e}^{-\omega_q\tau}\sum_k T_{m,k\alpha}\frac{\mathrm{e}^{\mathrm{i}(\epsilon_{k\alpha}+V_\alpha)t}}{\omega_q-\epsilon_{k\alpha}+\mu}T_{k\alpha,n} \\
&= \frac{1}{-\mathrm{i}\beta}\sum_q \mathrm{e}^{-\omega_q\tau}\sum_k T_{m,k\alpha}\left[\int \mathrm{d}\omega\delta(\omega-\epsilon_{k\alpha})\frac{\mathrm{e}^{\mathrm{i}(\omega+V_\alpha)t}}{\omega_q-\omega+\mu}\right]T_{k\alpha,n} \\
&= \frac{1}{-\mathrm{i}\beta}\sum_q \mathrm{e}^{-\omega_q\tau}\int\frac{\mathrm{d}\omega}{2\pi}2\pi\sum_k T_{m,k\alpha}\delta(\omega-\epsilon_{k\alpha})T_{k\alpha,n}\frac{\mathrm{e}^{\mathrm{i}(\omega+V_\alpha)t}}{\omega_q-\omega+\mu},
\end{aligned} \tag{A.5}$$

where we notice the definition of the level-width functions in Eq. (2.62) as $\Gamma_{\alpha,mn} = 2\pi\sum_k T_{m,k\alpha}\delta(\omega-\epsilon_{k\alpha})T_{k\alpha,n}$. Inserting this gives

$$\Sigma^{\lceil}_{\alpha,mn}(\tau,t) = \Gamma_\alpha\frac{1}{-\mathrm{i}\beta}\sum_q \mathrm{e}^{-\omega_q\tau}\int\frac{\mathrm{d}\omega}{2\pi}\frac{\mathrm{e}^{\mathrm{i}(\omega+V_\alpha)t}}{\omega_q-\omega+\mu}. \tag{A.6}$$

Similarly, the 'right' component becomes

$$\Sigma^{\rceil}_{\alpha,mn}(t,\tau) = \Gamma_\alpha\frac{1}{-\mathrm{i}\beta}\sum_q \mathrm{e}^{\omega_q\tau}\int\frac{\mathrm{d}\omega}{2\pi}\frac{\mathrm{e}^{-\mathrm{i}(\omega+V_\alpha)t}}{\omega_q-\omega+\mu}. \tag{A.7}$$

The remaining calculation for the self-energy is for the 'lesser' component which we can get by using the lesser Green's function $g^{<}_{k\alpha}(t,t') = \mathrm{i}f(\epsilon_{k\alpha}-\mu)\mathrm{e}^{-\mathrm{i}(\epsilon_{k\alpha}+V_\alpha)(t-t')}$ in Eq. (2.63) as

$$\Sigma^{<}_{\alpha,mn}(t,t') = \sum_k T_{m,k\alpha}\mathrm{i}f(\epsilon_{k\alpha}-\mu)\mathrm{e}^{-\mathrm{i}(\epsilon_{k\alpha}+V_\alpha)(t-t')}T_{k\alpha,n}. \tag{A.8}$$

We may convert the sum over k to an integral over ω by introducing a delta function

$$\begin{aligned}\Sigma^{<}_{\alpha,mn}(t,t') &= \sum_{k\alpha} T_{m,k\alpha}\int\frac{\mathrm{d}\omega}{2\pi}2\pi\delta(\omega-\epsilon_{k\alpha})\mathrm{i}f(\omega-\mu)\mathrm{e}^{-\mathrm{i}(\omega+V_\alpha)(t-t')}T_{k\alpha,n}\\ &= \int\frac{\mathrm{d}\omega}{2\pi}2\pi\sum_{k} T_{m,k\alpha}\delta(\omega-\epsilon_{k\alpha})T_{k\alpha,n}\mathrm{i}f(\omega-\mu)\mathrm{e}^{-\mathrm{i}(w+V_\alpha)(t-t')}\\ &= \mathrm{i}\Gamma_{\alpha,mn}\int\frac{\mathrm{d}\omega}{2\pi}f(\omega-\mu)\mathrm{e}^{-\mathrm{i}(\omega+V_\alpha)(t-t')}, \end{aligned} \tag{A.9}$$

where we also used Eq. (2.62) on the last line.

With the self-energies calculated above, we can now derive expressions for the Green's functions (on the central molecule). Using the general form for the Green's function in frequency domain in Eq. (2.17) the Matsubara component is readily written as

$$G^{\mathrm{M}}(\omega_q) = \frac{1}{\omega_q - h - \Sigma^{\mathrm{M}}(\omega_q)+\mu} = \begin{cases}\frac{1}{\omega_q-h+\frac{\mathrm{i}}{2}\Gamma+\mu}\\ \frac{1}{\omega_q-h-\frac{\mathrm{i}}{2}\Gamma+\mu}\end{cases} = \begin{cases}\frac{1}{\omega_q-h_{\mathrm{eff}}+\mu}, & \mathrm{Im}[\omega_q]>0\\ \frac{1}{\omega_q-h^{+}_{\mathrm{eff}}+\mu}, & \mathrm{Im}[\omega_q]<0,\end{cases} \tag{A.10}$$

where we inserted the definition for the effective Hamiltonian from Eq. (2.68). The 'right' component of the Green's function can be obtained directly from its equation of motion

$$\Big[\mathrm{i}\frac{\mathrm{d}}{\mathrm{d}t}-h\Big]G^{\rceil}(t,\tau) = \int_0^\infty \mathrm{d}\bar{t}\Sigma^{\mathrm{R}}(t,\bar{t})G^{\rceil}(\bar{t},\tau) - \mathrm{i}\int_0^\beta \mathrm{d}\bar{\tau}\Sigma^{\rceil}(t,\bar{\tau})G^{\mathrm{M}}(\bar{\tau},\tau), \tag{A.11}$$

where the integration on the Keldysh contour was split in two contributions. Then we may insert the self-energy in WBA, $\Sigma^{\mathrm{R}}(t,\bar{t}) = -\frac{\mathrm{i}}{2}\Gamma\delta(\bar{t}-t)$, into Eq. (A.11) to find

$$\Big[\mathrm{i}\frac{\mathrm{d}}{\mathrm{d}t}-h\Big]G^{\rceil}(t,\tau) = -\int_0^\infty \mathrm{d}\bar{t}\frac{\mathrm{i}}{2}\Gamma\delta(\bar{t}-t)G^{\rceil}(\bar{t},\tau) - \mathrm{i}\int_0^\beta \mathrm{d}\bar{\tau}\Sigma^{\rceil}(t,\bar{\tau})G^{\mathrm{M}}(\bar{\tau},\tau), \tag{A.12}$$

where the first integral on the right-hand side gives simply $\frac{\mathrm{i}}{2}\Gamma G^{\rceil}(t,\tau)$, and we can combine the terms with Γ and h to form a non-homogeneous differential equation

$$\Big[\mathrm{i}\frac{\mathrm{d}}{\mathrm{d}t}-(h-\frac{\mathrm{i}}{2}\Gamma)\Big]G^{\rceil}(t,\tau) = -\mathrm{i}\int_0^\beta \mathrm{d}\bar{\tau}\Sigma^{\rceil}(t,\bar{\tau})G^{\mathrm{M}}(\bar{\tau},\tau), \tag{A.13}$$

where on the left-hand side we find the definition for h_{eff}. For this differential equation we can write the solution, by noticing the boundary condition $G^{\rceil}(0,\tau) = G^{\mathrm{M}}(0,\tau)$, as

$$G^{\rceil}(t,\tau) = \mathrm{e}^{-\mathrm{i}h_{\mathrm{eff}}t}\Big[G^{\mathrm{M}}(0,\tau) - \int_0^t \mathrm{d}t'\mathrm{e}^{\mathrm{i}h_{\mathrm{eff}}t'}\int_0^\beta \mathrm{d}\bar{\tau}\Sigma^{\rceil}(t',\bar{\tau})G^{\mathrm{M}}(\bar{\tau},\tau)\Big]. \tag{A.14}$$

For the retarded Green's function, for which we have $G^{\mathrm{R}}(t,t') = G^{\mathrm{R}}(t-t')$, we may write a Fourier transformation

$$G^{\mathrm{R}}(t-t') = \int \frac{\mathrm{d}\omega}{2\pi} \mathrm{e}^{\mathrm{i}\omega(t-t')} G^{\mathrm{R}}(\omega), \tag{A.15}$$

and then use the expression on frequency domain from Eq. (2.17) as

$$G^{\mathrm{R}}(\omega) = \frac{1}{\omega - h_{\mathrm{eff}}}. \tag{A.16}$$

This way we get by integrating

$$G^{\mathrm{R}}(t-t') = \int \frac{\mathrm{d}\omega}{2\pi} \frac{\mathrm{e}^{-\mathrm{i}\omega(t-t')}}{\omega - h_{\mathrm{eff}}} = -\mathrm{i}\theta(t-t')\mathrm{e}^{-\mathrm{i}h_{\mathrm{eff}}(t-t')}. \tag{A.17}$$

Here, in Eq. (A.17), for the Fourier integral to be defined correctly, the analytic structure of $(\omega - h_{\mathrm{eff}})^{-1}$ is such that the complex eigenvalues of h_{eff} lie on the LHP. Correspondingly, for the advanced Green's function, G^{A}, the complex eigenvalues of $h_{\mathrm{eff}}^{\dagger}$ are located on the UHP. This leads to $G^{\mathrm{A}}(t-t') = \mathrm{i}\theta(t'-t)\mathrm{e}^{-\mathrm{i}h_{\mathrm{eff}}^{\dagger}(t'-t)}$. It is, however, also possible to have such a transport setup that h_{eff} has zero eigenvalues; in this case it becomes important to take into account the infinitesimal $\pm\mathrm{i}\eta$ in the retarded/advanced Green's functions, i.e., the Green's function operator acting on the corresponding states has the effective form $G^{\mathrm{R/A}}(\omega) = (\omega - h \pm \mathrm{i}\eta)^{-1}$, see Pub. [II].

A.1.2 Calculating the time-convolutions of different Keldysh components of the self-energies and Green's functions

In this subsection, we only insert the derived forms for the different Keldysh components of the Green's functions and self-energies (from the previous subsection) into the definitions of time-convolutions along the Keldysh contour, and derive accordingly expressions for the time-convolutions to be inserted into the equation of motion (2.67).

Inserting from Eqs. (A.17) and (A.9) we may calculate straightforwardly (it is still important to keep in mind that $[h_{\mathrm{eff}}, \Gamma] \neq 0$, in general)

$$\begin{aligned}
\left[G^{\mathrm{R}} \cdot \Sigma^{<}\right](t,t) &= \int_0^{\infty} \mathrm{d}\bar{t}\, G^{\mathrm{R}}(t,\bar{t})\Sigma^{<}(\bar{t},t) \\
&= \int_0^{\infty} \mathrm{d}\bar{t} \left[-\mathrm{i}\theta(t-\bar{t})\mathrm{e}^{-\mathrm{i}h_{\mathrm{eff}}(t-\bar{t})}\right] \sum_{\alpha} \mathrm{i}\Gamma_{\alpha} \int \frac{\mathrm{d}\omega}{2\pi} f(\omega-\mu)\mathrm{e}^{-\mathrm{i}(\omega+V_{\alpha})(\bar{t}-t)}.
\end{aligned} \tag{A.18}$$

We may couple the $\bar{t}$-independent terms outside the time integral as

$$\begin{aligned}\left[G^{\mathrm{R}}\cdot\Sigma^{<}\right](t,t) &= \mathrm{i}\sum_{\alpha}\int\frac{\mathrm{d}\omega}{2\pi}f(\omega-\mu)(-\mathrm{i})\mathrm{e}^{-\mathrm{i}h_{\mathrm{eff}}t}\mathrm{e}^{\mathrm{i}(\omega+V_\alpha)t}\int_0^t\mathrm{d}\bar{t}\mathrm{e}^{\mathrm{i}h_{\mathrm{eff}}\bar{t}}\mathrm{e}^{-\mathrm{i}(\omega+V_\alpha)\bar{t}}\Gamma_\alpha \\ &= \mathrm{i}\sum_{\alpha}\int\frac{\mathrm{d}\omega}{2\pi}(-\mathrm{i})\mathrm{e}^{\mathrm{i}(\omega+V_\alpha-h_{\mathrm{eff}})t}\int_0^t\mathrm{d}\bar{t}\mathrm{e}^{-\mathrm{i}(\omega+V_\alpha-h_{\mathrm{eff}})\bar{t}}f(\omega-\mu)\Gamma_\alpha\,, \qquad (A.19)\end{aligned}$$

where on the right-hand side we may perform the integration over $\bar{t}$ to give $\int_0^t\mathrm{d}\bar{t}\mathrm{e}^{-\mathrm{i}(\omega+V_\alpha-h_{\mathrm{eff}})\bar{t}} = \frac{1}{-\mathrm{i}(\omega+V_\alpha-h_{\mathrm{eff}})}\left[\mathrm{e}^{-\mathrm{i}(\omega+V_\alpha-h_{\mathrm{eff}})t}-1\right]$. This can be written in terms of the retarded Green's function in Eq. (A.16) and combining with the exponential factor in front of the whole expression to give

$$\begin{aligned}\left[G^{\mathrm{R}}\cdot\Sigma^{<}\right](t,t) &= \mathrm{i}\sum_{\alpha}\int\frac{\mathrm{d}\omega}{2\pi}f(\omega-\mu)\mathrm{e}^{\mathrm{i}(\omega+V_\alpha-h_{\mathrm{eff}})t}G^{\mathrm{R}}(\omega+V_\alpha)\left[\mathrm{e}^{-\mathrm{i}(\omega+V_\alpha-h_{\mathrm{eff}})t}-1\right]\Gamma_\alpha \\ &= \mathrm{i}\sum_{\alpha}\int\frac{\mathrm{d}\omega}{2\pi}f(\omega-\mu)\left[1-\mathrm{e}^{\mathrm{i}(\omega+V_\alpha-h_{\mathrm{eff}})t}\right]G^{\mathrm{R}}(\omega+V_\alpha)\Gamma_\alpha. \qquad (A.20)\end{aligned}$$

The second time-convolution includes $G^{<}$, i.e., the function we are solving from the equation of motion. Thus, inserting from Eq. (2.64) this is readily calculated

$$\left[G^{<}\cdot\Sigma^{\mathrm{A}}\right](t,t) = \int_0^\infty\mathrm{d}\bar{t}G^{<}(t,\bar{t})\Sigma^{\mathrm{A}}(\bar{t},t) = \int_0^\infty G^{<}(t,\bar{t})\frac{\mathrm{i}}{2}\Gamma\delta(\bar{t}-t) = \frac{\mathrm{i}}{2}G^{<}(t,t)\Gamma. \qquad (A.21)$$

The third time-convolution involves somewhat more trickery as it cannot be integrated right away into known expressions due to a more complicated form for the 'right' Green's function. However, inserting the expressions from Eqs. (A.12) and (A.5) gives as an intermediate result

$$\begin{aligned}&\left[G^{\rceil}\star\Sigma^{\lceil}\right](t,t) \\ &= -\mathrm{i}\int_0^\beta\mathrm{d}\tau G^{\rceil}(t,\tau)\Sigma^{\lceil}(\tau,t) \\ &= -\mathrm{i}\int_0^\beta\mathrm{d}\tau\mathrm{e}^{-\mathrm{i}h_{\mathrm{eff}}t}\left[G^{\mathrm{M}}(0,\tau)-\int_0^t\mathrm{d}t'\mathrm{e}^{\mathrm{i}h_{\mathrm{eff}}t'}\int_0^\beta\mathrm{d}\bar{\tau}\Sigma^{\rceil}(t',\bar{\tau})G^{\mathrm{M}}(\bar{\tau},\tau)\right]\Sigma^{\lceil}(\tau,t) \\ &= \mathrm{e}^{-\mathrm{i}h_{\mathrm{eff}}t}\left\{-\mathrm{i}\int_0^\beta\mathrm{d}\tau G^{\mathrm{M}}(0,\tau)\Sigma^{\lceil}(\tau,t)\right. \\ &\qquad\left.+\mathrm{i}\int_0^\beta\mathrm{d}\tau\int_0^t\mathrm{d}t'\mathrm{e}^{\mathrm{i}h_{\mathrm{eff}}t'}\int_0^\beta\mathrm{d}\bar{\tau}\Sigma^{\rceil}(t',\bar{\tau})G^{\mathrm{M}}(\bar{\tau},\tau)\Sigma^{\lceil}(\tau,t)\right\} \\ &= \mathrm{e}^{-\mathrm{i}h_{\mathrm{eff}}t}\left\{\left[G^{\mathrm{M}}\star\Sigma^{\lceil}\right](0,t)-\mathrm{i}\int_0^t\mathrm{d}t'\mathrm{e}^{\mathrm{i}h_{\mathrm{eff}}t'}\left[\Sigma^{\rceil}\star G^{\mathrm{M}}\star\Sigma^{\lceil}\right](t',t)\right\}. \qquad (A.22)\end{aligned}$$

Before going further, let us obtain a useful result regarding Matsubara frequencies $\omega_q = \frac{2\pi}{-\mathrm{i}\beta}(2q+1)$:

$$\begin{aligned}\int_0^\beta \mathrm{d}\tau \mathrm{e}^{(\omega_q-\omega_{q'})\tau} &= \int_0^\beta \mathrm{d}\tau \mathrm{e}^{\frac{2\pi}{-\mathrm{i}\beta}(q+1-q'-1)\tau} = \int_0^\beta \mathrm{d}\tau \mathrm{e}^{\frac{2\pi\mathrm{i}}{\beta}(q-q')\tau} = \frac{\beta}{2\pi\mathrm{i}(q-q')}\left[\mathrm{e}^{2\pi\mathrm{i}(q-q')}-1\right] \\ &= \begin{cases}\beta & \text{when } q=q' \\ 0 & \text{when } q\neq q'\end{cases} = \beta\delta_{qq'}. \end{aligned} \tag{A.23}$$

Then, let us calculate Eq. (A.22) further. Inserting from Eqs. (A.5), (A.7) and (A.10) we obtain for the double convolution

$$\begin{aligned}&\left[\Sigma^\rceil \star G^\mathrm{M} \star \Sigma^\lceil\right](t',t) \\ =\ & -\mathrm{i}\int_0^\beta \mathrm{d}\tau(-\mathrm{i})\int_0^\beta \mathrm{d}\bar\tau \Sigma^\rceil(t',\bar\tau)G^\mathrm{M}(\bar\tau,\tau)\Sigma^\lceil(\tau,t) \\ =\ & -\sum_{\alpha,\alpha'}\int_0^\beta \mathrm{d}\tau\int_0^\beta \mathrm{d}\bar\tau \Gamma_\alpha \frac{1}{-\mathrm{i}\beta}\sum_q \mathrm{e}^{\omega_q\bar\tau}\int\frac{\mathrm{d}\omega}{2\pi}\frac{\mathrm{e}^{-\mathrm{i}(\omega+V_\alpha)t'}}{\omega_q-\omega+\mu}G^\mathrm{M}(\bar\tau,\tau) \\ &\qquad \times\Gamma_{\alpha'}\frac{1}{-\mathrm{i}\beta}\sum_{q'}\mathrm{e}^{-\omega_{q'}\tau}\int\frac{\mathrm{d}\omega'}{2\pi}\frac{\mathrm{e}^{\mathrm{i}(\omega'+V_{\alpha'})t}}{\omega_{q'}-\omega'+\mu} \\ =\ & -\int\frac{\mathrm{d}\omega}{2\pi}\int\frac{\mathrm{d}\omega'}{2\pi}\sum_{\alpha,\alpha'}\sum_{q,q'}\int_0^\beta \mathrm{d}\tau\int_0^\beta \mathrm{d}\bar\tau\Gamma_\alpha\left(\frac{1}{-\mathrm{i}\beta}\right)^2\mathrm{e}^{\omega_q\bar\tau}\frac{\mathrm{e}^{-\mathrm{i}(\omega+V_\alpha)t'}}{\omega_q-\omega+\mu} \\ &\qquad \times\mathrm{e}^{-\omega_{q'}\bar\tau}\mathrm{e}^{\omega_{q'}\bar\tau}G^\mathrm{M}(\bar\tau,\tau)\Gamma_{\alpha'}\mathrm{e}^{-\omega_{q'}\tau}\frac{\mathrm{e}^{\mathrm{i}(\omega'+V_{\alpha'})t}}{\omega_{q'}-\omega'+\mu}, \end{aligned} \tag{A.24}$$

where we wrote a simple product of exponentials $\mathrm{e}^{-\omega_{q'}\bar\tau}\mathrm{e}^{\omega_{q'}\bar\tau} = 1$, and we may manipulate the expression further

$$\begin{aligned}&\left[\Sigma^\rceil \star G^\mathrm{M} \star \Sigma^\lceil\right](t',t) \\ =\ & \frac{1}{\beta^2}\int\frac{\mathrm{d}\omega}{2\pi}\int\frac{\mathrm{d}\omega'}{2\pi}\sum_{\alpha,\alpha'}\sum_{q,q'}\int_0^\beta \mathrm{d}\tau\int_0^\beta \mathrm{d}\bar\tau\Gamma_\alpha\frac{\mathrm{e}^{-\mathrm{i}(\omega+V_\alpha)t'}}{\omega_q-\omega+\mu}\mathrm{e}^{(\omega_q-\omega_{q'})\bar\tau}\mathrm{e}^{\omega_{q'}(\bar\tau-\tau)} \\ &\qquad \times G^\mathrm{M}(\bar\tau,\tau)\Gamma_{\alpha'}\frac{\mathrm{e}^{\mathrm{i}(\omega'+V_{\alpha'})t}}{\omega_{q'}-\omega'+\mu}. \end{aligned} \tag{A.25}$$

Now, Eq. (A.23) can be used

$$\begin{aligned}
&\left[\Sigma^{\rceil} \star G^{\mathrm{M}} \star \Sigma^{\lceil}\right](t',t) \\
&= \frac{1}{-\mathrm{i}\beta^2}\int\frac{\mathrm{d}\omega}{2\pi}\int\frac{\mathrm{d}\omega'}{2\pi}\sum_{\alpha,\alpha'}\sum_{q,q'}\beta\delta_{qq'}\Gamma_\alpha\frac{\mathrm{e}^{-\mathrm{i}(\omega+V_\alpha)t'}}{\omega_q-\omega+\mu} \\
&\qquad\times(-\mathrm{i})\int_0^\beta \mathrm{d}\tau \mathrm{e}^{\omega_{q'}(\bar{\tau}-\tau)}G^{\mathrm{M}}(\bar{\tau},\tau)\Gamma_{\alpha'}\frac{\mathrm{e}^{\mathrm{i}(\omega'+V_{\alpha'})t}}{\omega_{q'}-\omega'+\mu} \\
&= \int\frac{\mathrm{d}\omega}{2\pi}\int\frac{\mathrm{d}\omega'}{2\pi}\sum_{\alpha,\alpha'}\Gamma_\alpha\frac{1}{-\mathrm{i}\beta}\sum_q\frac{\mathrm{e}^{-\mathrm{i}(\omega+V_\alpha)t'}}{\omega_q-\omega+\mu}G^{\mathrm{M}}(\omega_q)\frac{\mathrm{e}^{\mathrm{i}(\omega'+V_{\alpha'})t}}{\omega_q-\omega'+\mu}\Gamma_{\alpha'}\,, \qquad \text{(A.26)}
\end{aligned}$$

where on the last line we noticed the Fourier transformation of the Matsubara Green's function as $G^{\mathrm{M}}(\omega_{q'}) = -\mathrm{i}\int_0^\beta \mathrm{d}\tau \mathrm{e}^{\omega_{q'}(\bar{\tau}-\tau)}G^{\mathrm{M}}(\bar{\tau},\tau)$. Looking at Eq. (A.26) more closely reveals that the integration with respect to ω must be done via LHP whereas the integration with respect to ω' must be done via UHP, because of the exponentials $\mathrm{e}^{-\mathrm{i}(\omega+V_\alpha)t'}$ and $\mathrm{e}^{\mathrm{i}(\omega'+V_\alpha)t}$. However, the corresponding poles are on the opposite half planes, and this makes the double integral to vanish for every ω_q. Hence,

$$\left[\Sigma^{\rceil} \star G^{\mathrm{M}} \star \Sigma^{\lceil}\right](t',t) = 0. \qquad \text{(A.27)}$$

Then in Eq. (A.22) we are left with

$$\begin{aligned}
\left[G^{\mathrm{M}} \star \Sigma^{\lceil}\right](0,t) &= -\mathrm{i}\int_0^\beta \mathrm{d}\tau G^{\mathrm{M}}(0,\tau)\Sigma^{\lceil}(\tau,t) \\
&= -\mathrm{i}\int_0^\beta \mathrm{d}\tau G^{\mathrm{M}}(0,\tau)\sum_\alpha\Gamma_\alpha\frac{1}{-\mathrm{i}\beta}\sum_q\mathrm{e}^{-\omega_q\tau}\int\frac{\mathrm{d}\omega}{2\pi}\frac{\mathrm{e}^{\mathrm{i}(\omega+V_\alpha)t}}{\omega_q-\omega+\mu} \\
&= \sum_{q,\alpha}\int\frac{\mathrm{d}\omega}{2\pi}(-\mathrm{i})\int_0^\beta \mathrm{d}\tau \mathrm{e}^{\omega_q(0-\tau)}G^{\mathrm{M}}(0,\tau)\Gamma_\alpha\frac{1}{-\mathrm{i}\beta}\frac{\mathrm{e}^{\mathrm{i}(\omega+V_\alpha)t}}{\omega_q-\omega+\mu} \\
&= \int\frac{\mathrm{d}\omega}{2\pi}\frac{1}{-\mathrm{i}\beta}\sum_q\frac{G^{\mathrm{M}}(\omega_q)\mathrm{e}^{\eta\omega_q}}{\omega_q-\omega+\mu}\sum_\alpha\Gamma_\alpha\mathrm{e}^{\mathrm{i}(\omega+V_\alpha)t}, \qquad \text{(A.28)}
\end{aligned}$$

where on the last line we added a convergence factor $\mathrm{e}^{\eta\omega_q}$ to account for correct limiting behaviour when $t \to 0$; it must be $\left[G^{\mathrm{M}} \star \Sigma^{\lceil}\right](0,0^+) = \left[G^{\mathrm{M}} \star \Sigma^{\mathrm{M}}\right](0,0^+)$. This also defines the correct analytic structure for the Fourier transformation for complex time variable τ on the last but one line $G^{\mathrm{M}}(\omega_q) = -\mathrm{i}\int_0^\beta \mathrm{d}\tau \mathrm{e}^{\omega_q(0-\tau)}G^{\mathrm{M}}(0,\tau)$. In Eq. (A.28) we have a sum of Matsubara frequencies. This can be calculated with some complex-analytic methods [209]. First, we notice that for a piecewise smooth and closed contour γ, encircling counter-clockwise all the poles in the UHP,

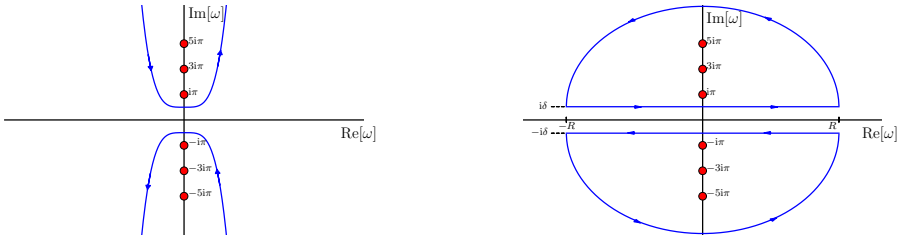

(a) Original contour encircling all the Matsubara frequencies.

(b) Deformed contour spanning the whole complex plane when $R \to \infty$ and $\delta \to 0$.

Fig. A.1: Contour deformation for evaluating the sum over Matsubara frequencies in Eq. (A.28).

corresponding to the Matsubara frequencies,

$$\int_\gamma \mathrm{d}\omega' \underbrace{\frac{1}{\mathrm{e}^{\beta\omega'}+1}}_{=f(\omega')} \mathrm{e}^{\eta\omega'} \frac{G^{\mathrm{M}}(\omega')}{\omega'-\omega+\mu} \overset{\beta\omega'\to\omega''}{=} \frac{1}{\beta}\int_\gamma \mathrm{d}\omega'' \frac{\mathrm{e}^{\eta\omega''/\beta} G^{\mathrm{M}}(\omega''/\beta)/(\omega''/\beta-\omega+\mu)}{\underbrace{\mathrm{e}^{\omega''}+1}_{=0 \text{ when } \omega''=\mathrm{i}(2q+1)\pi}}$$

$$\begin{aligned} &= \frac{2\pi\mathrm{i}}{\beta}\sum_q \mathrm{e}^{\eta\left(\frac{2(q+1)\pi}{-\mathrm{i}\beta}\right)} \frac{G^{\mathrm{M}}\left(\frac{2(q+1)\pi}{-\mathrm{i}\beta}\right)}{\frac{2(q+1)\pi}{-\mathrm{i}\beta}-\omega+\mu} \\ &= \frac{2\pi\mathrm{i}}{\beta}\sum_q \mathrm{e}^{\eta\omega_q} \frac{G^{\mathrm{M}}(\omega_q)}{\omega_q-\omega+\mu}, \end{aligned} \tag{A.29}$$

due to Cauchy's integral formula. Second, we may also deform the contour γ as in Fig. A.1, and then calculate

$$\begin{aligned} &\frac{1}{-\mathrm{i}\beta}\sum_q \frac{G^{\mathrm{M}}(\omega_q)\mathrm{e}^{\eta\omega_q}}{\omega_q-\omega+\mu} = \int_\gamma \frac{\mathrm{d}\omega'}{2\pi} f(\omega')\mathrm{e}^{\eta\omega'} \frac{G^{\mathrm{M}}(\omega')}{\omega'-\omega+\mu} \\ &= \int_{\gamma_{\mathrm{LHP}}} \frac{\mathrm{d}\omega'}{2\pi} f(\omega')\mathrm{e}^{\eta\omega'} \frac{G^{\mathrm{M}}(\omega'-\mathrm{i}\delta)}{\omega'-\mathrm{i}\delta-\omega+\mu} + \int_{\gamma_{\mathrm{UHP}}} \frac{\mathrm{d}\omega'}{2\pi} f(\omega')\mathrm{e}^{\eta\omega'} \frac{G^{\mathrm{M}}(\omega'+\mathrm{i}\delta)}{\omega'+\mathrm{i}\delta-\omega+\mu} \\ &= \int_{\infty}^{-\infty} \frac{\mathrm{d}\omega'}{2\pi} f(\omega')\mathrm{e}^{\eta\omega'} \frac{G^{\mathrm{M}}(\omega'-\mathrm{i}\delta)}{\omega'-\mathrm{i}\delta-\omega+\mu} + \int_{-\infty}^{\infty} \frac{\mathrm{d}\omega'}{2\pi} f(\omega')\mathrm{e}^{\eta\omega'} \frac{G^{\mathrm{M}}(\omega'+\mathrm{i}\delta)}{\omega'+\mathrm{i}\delta-\omega+\mu} \\ &= -\int_{-\infty}^{\infty} \frac{\mathrm{d}\omega'}{2\pi} f(\omega')\mathrm{e}^{\eta\omega'} \left[\frac{G^{\mathrm{M}}(\omega'-\mathrm{i}\delta)}{\omega'-\omega+\mu-\mathrm{i}\delta} - \frac{G^{\mathrm{M}}(\omega'+\mathrm{i}\delta)}{\omega'-\omega+\mu+\mathrm{i}\delta}\right]. \end{aligned} \tag{A.30}$$

By inserting Eq. (A.30) into Eq. (A.28) we get

$$\begin{aligned}&\left[G^{\mathrm{M}} \star \Sigma^{\lceil}\right](0,t)\\ =\ & -\int \frac{\mathrm{d}\omega}{2\pi}\int \frac{\mathrm{d}\omega'}{2\pi} f(\omega')\mathrm{e}^{\eta\omega'}\left[\frac{G^{\mathrm{M}}(\omega'-\mathrm{i}\delta)}{\omega'-\omega+\mu-\mathrm{i}\delta}-\frac{G^{\mathrm{M}}(\omega'+\mathrm{i}\delta)}{\omega'-\omega+\mu+\mathrm{i}\delta}\right]\sum_\alpha \Gamma_\alpha \mathrm{e}^{\mathrm{i}(\omega+V_\alpha)t}.\end{aligned} \tag{A.31}$$

Now, the integral over ω can be closed in the UHP because of the exponential $\mathrm{e}^{\mathrm{i}(\omega+V_\alpha)t}$ since $t > 0$. Then, the first term in the square brackets integrates to zero because of the pole in the LHP. The pole of the second term occurs at $\omega = \omega' + \mu + \mathrm{i}\delta$, and then we have

$$\begin{aligned}\left[G^{\mathrm{M}} \star \Sigma^{\lceil}\right](0,t) &= \mathrm{i}\int \frac{\mathrm{d}\omega'}{2\pi} f(\omega')\mathrm{e}^{\eta\omega'} G^{\mathrm{M}}(\omega'+\mathrm{i}\delta)\sum_\alpha \Gamma_\alpha \mathrm{e}^{\mathrm{i}(\omega'+\mu+\mathrm{i}\delta+V_\alpha)t}\\ &= \mathrm{i}\int \frac{\mathrm{d}\omega}{2\pi} f(\omega-\mu) G^{\mathrm{M}}(\omega-\mu)\sum_\alpha \Gamma_\alpha \mathrm{e}^{\mathrm{i}(\omega-\mu+\mu+V_\alpha)t}\\ &= \mathrm{i}\int \frac{\mathrm{d}\omega}{2\pi} f(\omega-\mu) G^{\mathrm{R}}(\omega)\sum_\alpha \Gamma_\alpha \mathrm{e}^{\mathrm{i}(\omega+V_\alpha)t},\end{aligned} \tag{A.32}$$

where we also noticed a boundary condition $G^{\mathrm{R}}(\omega) = G^{\mathrm{M}}(\omega-\mu)$ on the last but one line. Also, the limits $\eta \to 0^+$ and $\delta \to 0^+$, and a change of variables $\omega' = \omega - \mu$ should be understood. The expression in Eq. (A.32) we may finally insert into Eq. (A.22) to obtain

$$\begin{aligned}\left[G^{\rceil} \star \Sigma^{\lceil}\right](t,t) &= \mathrm{i}\mathrm{e}^{-\mathrm{i}h_{\mathrm{eff}}t}\int \frac{\mathrm{d}\omega}{2\pi} f(\omega-\mu) G^{\mathrm{R}}(\omega)\sum_\alpha \Gamma_\alpha \mathrm{e}^{\mathrm{i}(\omega+V_\alpha)t}\\ &= \mathrm{i}\int \frac{\mathrm{d}\omega}{2\pi} f(\omega-\mu)\sum_\alpha \mathrm{e}^{\mathrm{i}(\omega+V_\alpha-h_{\mathrm{eff}})t} G^{\mathrm{R}}(\omega)\Gamma_\alpha.\end{aligned} \tag{A.33}$$

Now, we have derived all the needed expressions for the equation of motion (2.67), and we may start solving the remaining differential equation.

A.1.3 Details on solving the equation of motion for the Green's function

Before inserting Eqs. (A.19), (A.21) and (A.33) into Eq. (2.67) we notice a useful 'Dyson'-like identity for the retarded Green's function which can be manipulated

as follows

$$\begin{aligned} G^{\mathrm{R}}(\omega) &= \frac{1}{\omega - h_{\mathrm{eff}}} = (\omega + V_\alpha - h_{\mathrm{eff}} - V_\alpha)^{-1} \\ &= \left[\left(\frac{1}{\omega + V_\alpha - h_{\mathrm{eff}}}\right)^{-1} - V_\alpha\right]^{-1} = \left\{\left[G^{\mathrm{R}}(\omega + V_\alpha)\right]^{-1} - V_\alpha\right\}^{-1}. \end{aligned} \tag{A.34}$$

Here, we may multiply (from right) by the inverse of the expression on the right-hand side to obtain

$$\mathbb{1} = G^{\mathrm{R}}(\omega)\left\{\left[G^{\mathrm{R}}(\omega + V_\alpha)\right]^{-1} - V_\alpha\right\} = G^{\mathrm{R}}(\omega)\left[G^{\mathrm{R}}(\omega + V_\alpha)\right]^{-1} - V_\alpha G^{\mathrm{R}}(\omega) \tag{A.35}$$

which we may again multiply (from right) by the inverted term on the right-hand side. This way we obtain a 'Dyson'-type relation between equilibrium and nonequilibrium retarded Green's functions

$$G^{\mathrm{R}}(\omega + V_\alpha) = G^{\mathrm{R}}(\omega) - V_\alpha G^{\mathrm{R}}(\omega) G^{\mathrm{R}}(\omega + V_\alpha). \tag{A.36}$$

Similar consideration may also be extended to second order in the external perturbation (bias voltage) by including also the advanced Green's functions

$$V_\alpha^2 G^{\mathrm{R}}(\omega) G^{\mathrm{A}}(\omega) G^{\mathrm{R}}(\omega + V_\alpha) G^{\mathrm{A}}(\omega + V_\alpha) = [G^{\mathrm{R}}(\omega) - G^{\mathrm{R}}(\omega + V_\alpha)][G^{\mathrm{A}}(\omega) - G^{\mathrm{A}}(\omega + V_\alpha)]. \tag{A.37}$$

Then, let us look at Eq. (2.67); by inserting the expressions derived in the previous section we have

$$\begin{aligned} & \mathrm{i}\frac{\mathrm{d}}{\mathrm{d}t} G^<(t,t) - [h, G^<(t,t)] \\ = & -\left\{ \mathrm{i} \sum_\alpha \int \frac{\mathrm{d}\omega}{2\pi} f(\omega - \mu) \left[1 - \mathrm{e}^{\mathrm{i}(\omega + V_\alpha - h_{\mathrm{eff}})t}\right] G^{\mathrm{R}}(\omega + V_\alpha) \Gamma_\alpha + \frac{\mathrm{i}}{2} \Gamma G^<(t,t) \right. \\ & \left. + \mathrm{i} \int \frac{\mathrm{d}\omega}{2\pi} f(\omega - \mu) \sum_\alpha \mathrm{e}^{\mathrm{i}(\omega + V_\alpha - h_{\mathrm{eff}})t} G^{\mathrm{R}}(\omega) \Gamma_\alpha \right\} + \mathrm{h.c.}, \end{aligned} \tag{A.38}$$

where we also assume the explicit time-independence in the Hamiltonian for the central molecule on the left-hand side. In Eq. (A.38) we have a nonhomogeneous, first order, linear differential equation for $G^<(t,t)$, and this may be solved explicitly. By simply organizing terms we get

$$\begin{aligned} & \mathrm{i}\frac{\mathrm{d}}{\mathrm{d}t} G^<(t,t) - h G^<(t,t) + G^<(t,t) h + \frac{\mathrm{i}}{2} \Gamma G^<(t,t) + \left[\frac{\mathrm{i}}{2} \Gamma G^<(t,t)\right]^\dagger \\ = & -\left\{ \mathrm{i} \sum_\alpha \int \frac{\mathrm{d}\omega}{2\pi} f(\omega - \mu) \left[1 - \mathrm{e}^{\mathrm{i}(\omega + V_\alpha - h_{\mathrm{eff}})t}\right] G^{\mathrm{R}}(\omega + V_\alpha) \Gamma_\alpha \right. \\ & \left. + \mathrm{i} \int \frac{\mathrm{d}\omega}{2\pi} f(\omega - \mu) \sum_\alpha \mathrm{e}^{\mathrm{i}(\omega + V_\alpha - h_{\mathrm{eff}})t} G^{\mathrm{R}}(\omega) \Gamma_\alpha \right\} + \mathrm{h.c.}, \end{aligned} \tag{A.39}$$

where we may use the property in Eq (2.42) to get $\left[\frac{\mathrm{i}}{2}\Gamma G^<(t,t)\right]^\dagger = \frac{-\mathrm{i}}{2}\Big[-G^<(t,t)\Big]\Gamma$. By coupling the terms with Hamiltonians h and level-width functions Γ we find the definitions of the effective Hamiltonian h_{eff}, and we may write

$$\begin{aligned} & \mathrm{i}\frac{\mathrm{d}}{\mathrm{d}t}G^<(t,t) - h_{\mathrm{eff}}G^<(t,t) + G^<(t,t)h_{\mathrm{eff}}^\dagger \\ = \; & -\mathrm{i}\int\frac{\mathrm{d}\omega}{2\pi}f(\omega-\mu)\sum_\alpha\Big\{\mathrm{e}^{\mathrm{i}(\omega+V_\alpha-h_{\mathrm{eff}})t}\Big[G^{\mathrm{R}}(\omega)-G^{\mathrm{R}}(\omega+V_\alpha)\Big]+G^{\mathrm{R}}(\omega+V_\alpha)\Big\}\Gamma_\alpha + \mathrm{h.c.}. \end{aligned} \tag{A.40}$$

Here we can employ the identity from Eq. (A.36) for the difference inside the square brackets to write the final expanded form

$$\begin{aligned} & \mathrm{i}\frac{\mathrm{d}}{\mathrm{d}t}G^<(t,t) - h_{\mathrm{eff}}G^<(t,t) + G^<(t,t)h_{\mathrm{eff}}^\dagger \\ = \; & -\mathrm{i}\int\frac{\mathrm{d}\omega}{2\pi}f(\omega-\mu)\sum_\alpha\Big\{\mathrm{e}^{\mathrm{i}(\omega+V_\alpha-h_{\mathrm{eff}})t}V_\alpha G^{\mathrm{R}}(\omega)G^{\mathrm{R}}(\omega+V_\alpha)+G^{\mathrm{R}}(\omega+V_\alpha)\Big\}\Gamma_\alpha \\ + \; & \mathrm{i}\int\frac{\mathrm{d}\omega}{2\pi}f(\omega-\mu)\sum_\alpha\Gamma_\alpha\Big\{G^{\mathrm{A}}(\omega+V_\alpha)G^{\mathrm{A}}(\omega)V_\alpha\mathrm{e}^{-\mathrm{i}(\omega+V_\alpha-h_{\mathrm{eff}}^\dagger)t}+G^{\mathrm{A}}(\omega+V_\alpha)\Big\}. \end{aligned} \tag{A.41}$$

Now, the equation is split such that the function $G^<(t,t)$ is on the left-hand side and the nonhomogeneous part is on the right-hand side. Because there appears terms like $\mathrm{e}^{-\mathrm{i}h_{\mathrm{eff}}t}$ and $\mathrm{e}^{\mathrm{i}h_{\mathrm{eff}}^\dagger t}$, it is convenient to transform the Green's function as $G^<(t,t) = \mathrm{e}^{-\mathrm{i}h_{\mathrm{eff}}t}\widetilde{G}^<(t,t)\mathrm{e}^{\mathrm{i}h_{\mathrm{eff}}^\dagger t}$. This way the left-hand side of Eq. (A.38) becomes

$$\begin{aligned} & \mathrm{i}\frac{\mathrm{d}}{\mathrm{d}t}\Big[\mathrm{e}^{-\mathrm{i}h_{\mathrm{eff}}t}\widetilde{G}^<(t,t)\mathrm{e}^{\mathrm{i}h_{\mathrm{eff}}^\dagger t}\Big] - h_{\mathrm{eff}}\mathrm{e}^{-\mathrm{i}h_{\mathrm{eff}}t}\widetilde{G}^<(t,t)\mathrm{e}^{\mathrm{i}h_{\mathrm{eff}}^\dagger t} + \mathrm{e}^{-\mathrm{i}h_{\mathrm{eff}}t}\widetilde{G}^<(t,t)\mathrm{e}^{\mathrm{i}h_{\mathrm{eff}}^\dagger t}h_{\mathrm{eff}}^\dagger \\ = \; & \mathrm{i}\Big[-\mathrm{i}h_{\mathrm{eff}}\mathrm{e}^{-\mathrm{i}h_{\mathrm{eff}}t}\widetilde{G}^<(t,t)\mathrm{e}^{\mathrm{i}h_{\mathrm{eff}}^\dagger t} + \mathrm{e}^{-\mathrm{i}h_{\mathrm{eff}}t}\frac{\mathrm{d}}{\mathrm{d}t}\widetilde{G}^<(t,t)\mathrm{e}^{\mathrm{i}h_{\mathrm{eff}}^\dagger t} + \mathrm{e}^{-\mathrm{i}h_{\mathrm{eff}}t}\widetilde{G}^<(t,t)\mathrm{i}h_{\mathrm{eff}}^\dagger\mathrm{e}^{\mathrm{i}h_{\mathrm{eff}}^\dagger t}\Big] \\ & -h_{\mathrm{eff}}\mathrm{e}^{-\mathrm{i}h_{\mathrm{eff}}t}\widetilde{G}^<(t,t)\mathrm{e}^{\mathrm{i}h_{\mathrm{eff}}^\dagger t} + \mathrm{e}^{-\mathrm{i}h_{\mathrm{eff}}t}\widetilde{G}^<(t,t)\mathrm{e}^{\mathrm{i}h_{\mathrm{eff}}^\dagger t}h_{\mathrm{eff}}^\dagger \\ = \; & \mathrm{e}^{-\mathrm{i}h_{\mathrm{eff}}t}\mathrm{i}\frac{\mathrm{d}}{\mathrm{d}t}\widetilde{G}^<(t,t)\mathrm{e}^{\mathrm{i}h_{\mathrm{eff}}^\dagger t}. \end{aligned} \tag{A.42}$$

Then, we can multiply the right-hand side of Eq. (A.38) from left by $\mathrm{e}^{\mathrm{i}h_{\mathrm{eff}}t}$ and from

right by $\mathrm{e}^{-\mathrm{i}h_{\mathrm{eff}}^{\dagger}t}$ to obtain

$$\begin{aligned}
&\mathrm{i}\frac{\mathrm{d}}{\mathrm{d}t}\widetilde{G}^{<}(t,t) \\
= \;& -\mathrm{i}\int\frac{\mathrm{d}\omega}{2\pi}f(\omega-\mu)\sum_{\alpha}\mathrm{e}^{\mathrm{i}h_{\mathrm{eff}}t}\Big\{\mathrm{e}^{\mathrm{i}(\omega+V_\alpha-h_{\mathrm{eff}})t}V_\alpha G^{\mathrm{R}}(\omega)G^{\mathrm{R}}(\omega+V_\alpha) \\
&\qquad + G^{\mathrm{R}}(\omega+V_\alpha)\Big\}\Gamma_\alpha\mathrm{e}^{-\mathrm{i}h_{\mathrm{eff}}^{\dagger}t} \\
&+\mathrm{i}\int\frac{\mathrm{d}\omega}{2\pi}f(\omega-\mu)\sum_{\alpha}\mathrm{e}^{\mathrm{i}h_{\mathrm{eff}}t}\Gamma_\alpha\Big\{G^{\mathrm{A}}(\omega+V_\alpha)G^{\mathrm{A}}(\omega)V_\alpha\mathrm{e}^{-\mathrm{i}(\omega+V_\alpha-h_{\mathrm{eff}}^{\dagger})t} \\
&\qquad + G^{\mathrm{A}}(\omega+V_\alpha)\Big\}\mathrm{e}^{-\mathrm{i}h_{\mathrm{eff}}^{\dagger}t}, \qquad \text{(A.43)}
\end{aligned}$$

where also the dependency on the bias voltage V_α may be separated to a 'zeroth' and 'first' order terms

$$\begin{aligned}
&\mathrm{i}\frac{\mathrm{d}}{\mathrm{d}t}\widetilde{G}^{<}(t,t) \\
= \;& -\mathrm{i}\int\frac{\mathrm{d}\omega}{2\pi}f(\omega-\mu)\sum_{\alpha}\mathrm{e}^{\mathrm{i}h_{\mathrm{eff}}t}\Big[G^{\mathrm{R}}(\omega+V_\alpha)\Gamma_\alpha-\Gamma_\alpha G^{\mathrm{A}}(\omega+V_\alpha)\Big]\mathrm{e}^{\mathrm{i}h_{\mathrm{eff}}^{\dagger}t} \\
&-\mathrm{i}\int\frac{\mathrm{d}\omega}{2\pi}f(\omega-\mu)\sum_{\alpha}V_\alpha\Big[G^{\mathrm{R}}(\omega)G^{\mathrm{R}}(\omega+V_\alpha)\Gamma_\alpha\mathrm{e}^{\mathrm{i}(\omega+V_\alpha-h_{\mathrm{eff}}^{\dagger})t} \\
&\qquad -\mathrm{e}^{-\mathrm{i}(\omega+V_\alpha-h_{\mathrm{eff}})t}\Gamma_\alpha G^{\mathrm{A}}(\omega+V_\alpha)G^{\mathrm{A}}(\omega)\Big]. \qquad \text{(A.44)}
\end{aligned}$$

Now we are ready to integrate both sides over t to obtain (note that 'i' cancels from both sides)

$$\begin{aligned}
&\widetilde{G}^{<}(t,t)-\widetilde{G}^{<}(0,0^{+}) \\
= \;& -\int\frac{\mathrm{d}\omega}{2\pi}f(\omega-\mu)\sum_{\alpha}\int_0^t\mathrm{d}t'\mathrm{e}^{\mathrm{i}h_{\mathrm{eff}}t'}\Big[G^{\mathrm{R}}(\omega+V_\alpha)\Gamma_\alpha-\Gamma_\alpha G^{\mathrm{A}}(\omega+V_\alpha)\Big]\mathrm{e}^{-\mathrm{i}h_{\mathrm{eff}}^{\dagger}t'} \\
&-\int\frac{\mathrm{d}\omega}{2\pi}f(\omega-\mu)\sum_{\alpha}V_\alpha\int_0^t\mathrm{d}t'\Big[G^{\mathrm{R}}(\omega)G^{\mathrm{R}}(\omega+V_\alpha)\Gamma_\alpha\mathrm{e}^{\mathrm{i}(\omega+V_\alpha-h_{\mathrm{eff}}^{\dagger})t'} \\
&\qquad -\mathrm{e}^{-\mathrm{i}(\omega+V_\alpha-h_{\mathrm{eff}})t'}\Gamma_\alpha G^{\mathrm{A}}(\omega+V_\alpha)G^{\mathrm{A}}(\omega)\Big], \qquad \text{(A.45)}
\end{aligned}$$

where the initial condition on the left-hand side can also be written as $\widetilde{G}^{<}(0,0^{+}) = G^{<}(0,0^{+}) = G^{\mathrm{M}}(0,0^{+})$. The integration over t' for the second term in Eq (A.45) can be done easily since the only dependence on t' is inside the single exponentials. For the first term we need to do something different because of the product of exponentials. The following calculation explains the idea for the first line in Eq. (A.45): For arbitrary matrices A and B, and for a matrix x proportional to a unit matrix, we

have

$$\begin{aligned}
&\frac{\partial}{\partial t'}\left[\mathrm{e}^{\mathrm{i}At'}\frac{1}{x-A}B\frac{1}{x-A^\dagger}\mathrm{e}^{-\mathrm{i}A^\dagger t'}\right]\\
=\;&\frac{\partial}{\partial t'}\left[\mathrm{e}^{-\mathrm{i}(x-A)t'}\frac{1}{x-A}B\frac{1}{x-A^\dagger}\mathrm{e}^{\mathrm{i}(x-A^\dagger)t'}\right]\\
=\;&-\mathrm{i}(x-A)\mathrm{e}^{-\mathrm{i}(x-A)t'}\frac{1}{x-A}B\frac{1}{x-A^\dagger}\mathrm{e}^{\mathrm{i}(x-A^\dagger)t'}+\mathrm{e}^{-\mathrm{i}(x-A)t'}\frac{1}{x-A}B\frac{1}{x-A^\dagger}\mathrm{i}(x-A^\dagger)\mathrm{e}^{\mathrm{i}(x-A^\dagger)t'}\\
=\;&\mathrm{i}\mathrm{e}^{-\mathrm{i}(x-A)t'}\left[\frac{1}{x-A}B-B\frac{1}{x-A^\dagger}\right]\mathrm{e}^{\mathrm{i}(x-A^\dagger)t'}=\mathrm{i}\mathrm{e}^{\mathrm{i}At'}\left[\frac{1}{x-A}B-B\frac{1}{x-A^\dagger}\right]\mathrm{e}^{-\mathrm{i}A^\dagger t'}. \quad \text{(A.46)}
\end{aligned}$$

Therefore, in the other way around, we may write

$$\int_0^t \mathrm{d}t'\mathrm{e}^{\mathrm{i}At'}\left[\frac{1}{x-A}B-B\frac{1}{x-A^\dagger}\right]\mathrm{e}^{-\mathrm{i}A^\dagger t'}=-\mathrm{i}\mathrm{e}^{\mathrm{i}At'}\frac{1}{x-A}B\frac{1}{x-A^\dagger}\mathrm{e}^{-\mathrm{i}A^\dagger t'}\Big|_0^t. \quad \text{(A.47)}$$

Applying the result in Eq. (A.47) to Eq. (A.45) we find

$$\begin{aligned}
&\widetilde{G}^<(t,t)-G^{\mathrm{M}}(0,0^+)\\
=\;&-\int\frac{\mathrm{d}\omega}{2\pi}f(\omega-\mu)\sum_\alpha\left[-\mathrm{i}\mathrm{e}^{\mathrm{i}h_{\mathrm{eff}}t'}\frac{1}{\omega+V_\alpha-h_{\mathrm{eff}}}\Gamma_\alpha\frac{1}{\omega+V_\alpha-h_{\mathrm{eff}}^\dagger}\mathrm{e}^{-\mathrm{i}h_{\mathrm{eff}}^\dagger t'}\right]_0^t\\
&-\int\frac{\mathrm{d}\omega}{2\pi}f(\omega-\mu)\sum_\alpha V_\alpha\left\{G^{\mathrm{R}}(\omega)G^{\mathrm{R}}(\omega+V_\alpha)\Gamma_\alpha\left[\frac{-\mathrm{i}}{\omega+V_\alpha-h_{\mathrm{eff}}^\dagger}\mathrm{e}^{\mathrm{i}(\omega+V_\alpha-h_{\mathrm{eff}}^\dagger)t'}\right]_0^t\right.\\
&\qquad\left.+\left[\frac{-\mathrm{i}}{\omega+V_\alpha-h_{\mathrm{eff}}}\mathrm{e}^{-\mathrm{i}(\omega+V_\alpha-h_{\mathrm{eff}})t'}\right]_0^t\Gamma_\alpha G^{\mathrm{A}}(\omega+V_\alpha)G^{\mathrm{A}}(\omega)\right\}. \quad \text{(A.48)}
\end{aligned}$$

For the zero-time Matsubara Green's function we may use its Fourier decomposition similar to Eq. (A.30)

$$\begin{aligned}
G^{\mathrm{M}}(0,0^+)&=\frac{1}{-\mathrm{i}\beta}\sum_q\mathrm{e}^{\eta\omega_q}G^{\mathrm{M}}(\omega_q)=-\int\frac{\mathrm{d}\omega}{2\pi}f(\omega)\left[G^{\mathrm{M}}(\omega-\mathrm{i}\delta)-G^{\mathrm{M}}(\omega+\mathrm{i}\delta)\right]\\
&=-\int\frac{\mathrm{d}\omega}{2\pi}f(\omega-\mu)\left[G^{\mathrm{A}}(\omega)-G^{\mathrm{R}}(\omega)\right]=\mathrm{i}\int\frac{\mathrm{d}\omega}{2\pi}f(\omega-\mu)G^{\mathrm{R}}(\omega)\Gamma G^{\mathrm{A}}(\omega).
\end{aligned} \quad \text{(A.49)}$$

By expanding the other terms on the right-hand side as well we find

$$\begin{aligned}
\widetilde{G}^<(t,t) &= \mathrm{i}\int\frac{\mathrm{d}\omega}{2\pi}f(\omega-\mu)G^\mathrm{R}(\omega)\Gamma G^\mathrm{A}(\omega)\\
&+ \mathrm{i}\int\frac{\mathrm{d}\omega}{2\pi}f(\omega-\mu)\sum_\alpha\Big[\mathrm{e}^{\mathrm{i}h_\mathrm{eff}t}G^\mathrm{R}(\omega+V_\alpha)\Gamma_\alpha G^\mathrm{A}(\omega+V_\alpha)\mathrm{e}^{-\mathrm{i}h_\mathrm{eff}^\dagger t}\\
&\quad -G^\mathrm{R}(\omega+V_\alpha)\Gamma_\alpha G^\mathrm{A}(\omega+V_\alpha)\Big]\\
&+ \mathrm{i}\int\frac{\mathrm{d}\omega}{2\pi}f(\omega-\mu)\sum_\alpha V_\alpha\Big\{G^\mathrm{R}(\omega)G^\mathrm{R}(\omega+V_\alpha)\Gamma_\alpha G^\mathrm{A}(\omega+V_\alpha)\mathrm{e}^{\mathrm{i}(\omega+V_\alpha-h_\mathrm{eff}^\dagger)t}\\
&\quad -G^\mathrm{R}(\omega)G^\mathrm{R}(\omega+V_\alpha)\Gamma_\alpha G^\mathrm{A}(\omega+V_\alpha)\\
&\quad +G^\mathrm{R}(\omega+V_\alpha)\mathrm{e}^{-\mathrm{i}(\omega+V_\alpha-h_\mathrm{eff})t}\Gamma_\alpha G^\mathrm{A}(\omega+V_\alpha)G^\mathrm{A}(\omega)\\
&\quad -G^\mathrm{R}(\omega+V_\alpha)\Gamma_\alpha G^\mathrm{A}(\omega+V_\alpha)G^\mathrm{A}(\omega)\Big\}. \qquad \text{(A.50)}
\end{aligned}$$

The integrals and sums can also be coupled together to give

$$\begin{aligned}
\widetilde{G}^<(t,t) &= \mathrm{i}\int\frac{\mathrm{d}\omega}{2\pi}f(\omega-\mu)\sum_\alpha\Big\{G^\mathrm{R}(\omega)\Gamma_\alpha G^\mathrm{A}(\omega)\\
&\quad +\mathrm{e}^{\mathrm{i}h_\mathrm{eff}t}G^\mathrm{R}(\omega+V_\alpha)\Gamma_\alpha G^\mathrm{A}(\omega+V_\alpha)\mathrm{e}^{-\mathrm{i}h_\mathrm{eff}^\dagger t}\\
&\quad -G^\mathrm{R}(\omega+V_\alpha)\Gamma_\alpha G^\mathrm{A}(\omega+V_\alpha)\\
&\quad +V_\alpha G^\mathrm{R}(\omega)G^\mathrm{R}(\omega+V_\alpha)\Gamma_\alpha G^\mathrm{A}(\omega+V_\alpha)\mathrm{e}^{\mathrm{i}(\omega+V_\alpha-h_\mathrm{eff}^\dagger)t}\\
&\quad -V_\alpha G^\mathrm{R}(\omega)G^\mathrm{R}(\omega+V_\alpha)\Gamma_\alpha G^\mathrm{A}(\omega+V_\alpha)\\
&\quad +V_\alpha G^\mathrm{R}(\omega+V_\alpha)\mathrm{e}^{-\mathrm{i}(\omega+V_\alpha-h_\mathrm{eff})t}\Gamma_\alpha G^\mathrm{A}(\omega+V_\alpha)G^\mathrm{A}(\omega)\\
&\quad -V_\alpha G^\mathrm{R}(\omega+V_\alpha)\Gamma_\alpha G^\mathrm{A}(\omega+V_\alpha)G^\mathrm{A}(\omega)\Big\}. \qquad \text{(A.51)}
\end{aligned}$$

Then, let us insert the definition for $\widetilde{G}$ into the left-hand side, and multiply accordingly by $\mathrm{e}^{-\mathrm{i}h_\mathrm{eff}t}$ from left and by $\mathrm{e}^{\mathrm{i}h_\mathrm{eff}^\dagger t}$ from right. This way we obtain

$$\begin{aligned}
-\mathrm{i}G^<(t,t) &= \int\frac{\mathrm{d}\omega}{2\pi}f(\omega-\mu)\sum_\alpha\Big\{\mathrm{e}^{-\mathrm{i}h_\mathrm{eff}t}G^\mathrm{R}(\omega)\Gamma_\alpha G^\mathrm{A}(\omega)\mathrm{e}^{\mathrm{i}h_\mathrm{eff}^\dagger t}\\
&\quad +\underline{G^\mathrm{R}(\omega+V_\alpha)\Gamma_\alpha G^\mathrm{A}(\omega+V_\alpha)}\\
&\quad -\mathrm{e}^{-\mathrm{i}h_\mathrm{eff}t}G^\mathrm{R}(\omega+V_\alpha)\Gamma_\alpha G^\mathrm{A}(\omega+V_\alpha)\mathrm{e}^{\mathrm{i}h_\mathrm{eff}^\dagger t}\\
&\quad +V_\alpha\underline{\mathrm{e}^{-\mathrm{i}h_\mathrm{eff}t}}G^\mathrm{R}(\omega)G^\mathrm{R}(\omega+V_\alpha)\Gamma_\alpha G^\mathrm{A}(\omega+V_\alpha)\underline{\mathrm{e}^{\mathrm{i}(\omega+V_\alpha)t}}\\
&\quad -V_\alpha\mathrm{e}^{-\mathrm{i}h_\mathrm{eff}t}G^\mathrm{R}(\omega)G^\mathrm{R}(\omega+V_\alpha)\Gamma_\alpha G^\mathrm{A}(\omega+V_\alpha)\mathrm{e}^{\mathrm{i}h_\mathrm{eff}^\dagger t}\\
&\quad +V_\alpha G^\mathrm{R}(\omega+V_\alpha)\underline{\mathrm{e}^{-\mathrm{i}(\omega+V_\alpha)t}}\Gamma_\alpha G^\mathrm{A}(\omega+V_\alpha)G^\mathrm{A}(\omega)\underline{\mathrm{e}^{\mathrm{i}h_\mathrm{eff}^\dagger t}}\\
&\quad -V_\alpha\mathrm{e}^{-\mathrm{i}h_\mathrm{eff}t}G^\mathrm{R}(\omega+V_\alpha)\Gamma_\alpha G^\mathrm{A}(\omega+V_\alpha)G^\mathrm{A}(\omega)\mathrm{e}^{\mathrm{i}h_\mathrm{eff}^\dagger t}\Big\}, \qquad \text{(A.52)}
\end{aligned}$$

where the underlined parts refer to coupling the corresponding exponentials, and we also define the *partial spectral functions*

$$A_\alpha(\omega) = G^\mathrm{R}(\omega)\Gamma_\alpha G^\mathrm{A}(\omega). \qquad \text{(A.53)}$$

The full spectral function is obtained by summing over all the leads $A(\omega) = \sum_\alpha A_\alpha(\omega)$. By combining terms and simplifying further we find

$$\begin{aligned}
&-\mathrm{i}G^<(t,t)\\
=\ &\int\frac{\mathrm{d}\omega}{2\pi}f(\omega-\mu)\sum_\alpha\Big\{A_\alpha(\omega+V_\alpha)+V_\alpha\Big[\mathrm{e}^{\mathrm{i}(\omega+V_\alpha-h_{\mathrm{eff}})t}G^{\mathrm{R}}(\omega)A_\alpha(\omega+V_\alpha)+\mathrm{h.c.}\Big]\\
&+\mathrm{e}^{-\mathrm{i}h_{\mathrm{eff}}t}\Big[G^{\mathrm{R}}(\omega)\Gamma_\alpha G^{\mathrm{A}}(\omega)-G^{\mathrm{R}}(\omega+V_\alpha)\Gamma_\alpha G^{\mathrm{A}}(\omega+V_\alpha)\\
&-\underline{V_\alpha G^{\mathrm{R}}(\omega)G^{\mathrm{R}}(\omega+V_\alpha)}\Gamma_\alpha G^{\mathrm{A}}(\omega+V_\alpha)-\underline{V_\alpha}G^{\mathrm{R}}(\omega+V_\alpha)\Gamma_\alpha\underline{G^{\mathrm{A}}(\omega+V_\alpha)G^{\mathrm{A}}(\omega)}\Big]\mathrm{e}^{\mathrm{i}h_{\mathrm{eff}}^\dagger t}\Big\}.
\end{aligned}\tag{A.54}$$

Here the underlined parts may be combined by using Eq. (A.36) which leads to

$$\begin{aligned}
-\mathrm{i}G^<(t,t) \ =\ &\int\frac{\mathrm{d}\omega}{2\pi}f(\omega-\mu)\sum_\alpha\Big\{A_\alpha(\omega+V_\alpha)\\
&+V_\alpha\Big[\mathrm{e}^{\mathrm{i}(\omega+V_\alpha-h_{\mathrm{eff}})t}G^{\mathrm{R}}(\omega)A_\alpha(\omega+V_\alpha)+\mathrm{h.c.}\Big]\\
&+\mathrm{e}^{-\mathrm{i}h_{\mathrm{eff}}t}\Big[G^{\mathrm{R}}(\omega)\Gamma_\alpha G^{\mathrm{A}}(\omega)-G^{\mathrm{R}}(\omega+V_\alpha)\Gamma_\alpha G^{\mathrm{A}}(\omega+V_\alpha)\\
&-G^{\mathrm{R}}(\omega)\Gamma_\alpha G^{\mathrm{A}}(\omega+V_\alpha)+G^{\mathrm{R}}(\omega+V_\alpha)\Gamma_\alpha G^{\mathrm{A}}(\omega+V_\alpha)\\
&-G^{\mathrm{R}}(\omega+V_\alpha)\Gamma_\alpha G^{\mathrm{A}}(\omega)+G^{\mathrm{R}}(\omega+V_\alpha)\Gamma_\alpha G^{\mathrm{A}}(\omega+V_\alpha)\Big]\mathrm{e}^{\mathrm{i}h_{\mathrm{eff}}^\dagger t}\Big\},
\end{aligned}\tag{A.55}$$

where we may further combine terms so that Eq. (A.37) may be used (marked again with underlining)

$$\begin{aligned}
-\mathrm{i}G^<(t,t) \ =\ &\int\frac{\mathrm{d}\omega}{2\pi}f(\omega-\mu)\sum_\alpha\Big\{A_\alpha(\omega+V_\alpha)\\
&+V_\alpha\Big[\mathrm{e}^{\mathrm{i}(\omega+V_\alpha-h_{\mathrm{eff}})t}G^{\mathrm{R}}(\omega)A_\alpha(\omega+V_\alpha)+\mathrm{h.c.}\Big]\\
&+\mathrm{e}^{-\mathrm{i}h_{\mathrm{eff}}t}\Big[\underline{\big(G^{\mathrm{R}}(\omega)-G^{\mathrm{R}}(\omega+V_\alpha)\big)}\Gamma_\alpha\underline{\big(G^{\mathrm{A}}(\omega)-G^{\mathrm{A}}(\omega+V_\alpha)\big)}\Big]\mathrm{e}^{\mathrm{i}h_{\mathrm{eff}}^\dagger t}\Big\}\\
=\ &\int\frac{\mathrm{d}\omega}{2\pi}f(\omega-\mu)\sum_\alpha\Big\{\,A_\alpha(\omega+V_\alpha)\\
&+V_\alpha\Big[\mathrm{e}^{\mathrm{i}(\omega+V_\alpha-h_{\mathrm{eff}})t}G^{\mathrm{R}}(\omega)A_\alpha(\omega+V_\alpha)+\mathrm{h.c.}\Big]\\
&+V_\alpha^2\mathrm{e}^{-\mathrm{i}h_{\mathrm{eff}}t}G^{\mathrm{R}}(\omega)G^{\mathrm{R}}(\omega+V_\alpha)\Gamma_\alpha G^{\mathrm{A}}(\omega+V_\alpha)G^{\mathrm{A}}(\omega)\mathrm{e}^{\mathrm{i}h_{\mathrm{eff}}^\dagger t}\,\Big\}.
\end{aligned}\tag{A.56}$$

The result in Eq. (A.56) is now the solved Green's function at equal time limit, giving the time-dependent density matrix.

A.1.4 Time-dependent Landauer–Büttiker formula

Here we go through the main steps in obtaining the time-dependent extension to the Landauer–Büttiker formula in Eq. (2.85). Now, we can put the expressions for

the time-convolutions into Eq. (2.81) and calculate further (also expand the trace as $\mathrm{Re}\{\mathrm{Tr}[A]\} = \mathrm{Tr}\{A + A^\dagger\}/2$ and put the electron charge to -1)

$$\begin{aligned} I_\alpha(t) &= -2\mathrm{Tr}\Big\{\mathrm{i}\int\frac{\mathrm{d}\omega}{2\pi}f(\omega-\mu)\Gamma_\alpha G^{\mathrm{A}}(\omega+V_\alpha)\Big[1-\mathrm{e}^{-\mathrm{i}(\omega+V_\alpha-h_{\mathrm{eff}}^\dagger)t}\Big] \\ &\quad -\mathrm{i}\int\frac{\mathrm{d}\omega}{2\pi}f(\omega-\mu)\Big[1-\mathrm{e}^{\mathrm{i}(\omega+V_\alpha-h_{\mathrm{eff}})t}\Big]G^{\mathrm{R}}(\omega+V_\alpha)\Gamma_\alpha \\ &\quad -\frac{\mathrm{i}}{2}\Gamma_\alpha G^<(t,t)-\frac{\mathrm{i}}{2}G^<(t,t)\Gamma_\alpha \\ &\quad +\mathrm{i}\int\frac{\mathrm{d}\omega}{2\pi}f(\omega-\mu)\Gamma_\alpha G^{\mathrm{A}}(\omega)\mathrm{e}^{-\mathrm{i}(\omega+V_\alpha-h_{\mathrm{eff}}^\dagger)t} \\ &\quad -\mathrm{i}\int\frac{\mathrm{d}\omega}{2\pi}f(\omega-\mu)\mathrm{e}^{\mathrm{i}(\omega+V_\alpha-h_{\mathrm{eff}})t}G^{\mathrm{R}}(\omega)\Gamma_\alpha\Big\}, \end{aligned} \tag{A.57}$$

where we may use the cyclic property of the trace $\mathrm{Tr}(AB) = \mathrm{Tr}(BA)$ and write

$$\begin{aligned} I_\alpha(t) &= -2\int\frac{\mathrm{d}\omega}{2\pi}f(\omega-\mu)\mathrm{Tr}\Big\{\mathrm{i}\Gamma_\alpha G^{\mathrm{A}}(\omega+V_\alpha)-\mathrm{i}G^{\mathrm{R}}(\omega+V_\alpha)\Gamma_\alpha \\ &\quad +\mathrm{i}\Big[\underline{G^{\mathrm{A}}(\omega)-G^{\mathrm{A}}(\omega+V_\alpha)}\Big]\mathrm{e}^{-\mathrm{i}(\omega+V_\alpha-h_{\mathrm{eff}}^\dagger)t}\Gamma_\alpha \\ &\quad -\mathrm{i}\Gamma_\alpha\mathrm{e}^{-\mathrm{i}(\omega+V_\alpha-h_{\mathrm{eff}})t}\Big[\underline{G^{\mathrm{R}}(\omega)-G^{\mathrm{R}}(\omega+V_\alpha)}\Big]-\mathrm{i}\Gamma_\alpha G^<(t,t)\Big\}. \end{aligned} \tag{A.58}$$

Here, again, the underlined parts refer to the identity in Eq. (A.36), and we may also insert the final result for the lesser Green's function from Eq. (2.79) to find

$$\begin{aligned} I_\alpha(t) &= -2\int\frac{\mathrm{d}\omega}{2\pi}f(\omega-\mu)\sum_\beta\mathrm{Tr}\Big\{ \\ &\quad \Gamma_\alpha G^{\mathrm{R}}(\omega+V_\alpha)\Gamma_\beta G^{\mathrm{A}}(\omega+V_\alpha)-\Gamma_\alpha\underline{\mathrm{i}\Big[G^{\mathrm{R}}(\omega+V_\alpha)-G^{\mathrm{A}}(\omega+V_\alpha)\Big]} \\ &\quad +V_\beta\Big\{\Gamma_\alpha\mathrm{e}^{\mathrm{i}(\omega+V_\beta-h_{\mathrm{eff}})t}G^{\mathrm{R}}(\omega)\Big[-\mathrm{i}\delta_{\alpha\beta}G^{\mathrm{R}}(\omega+V_\beta)+A_\beta(\omega+V_\beta)\Big]+\mathrm{h.c.}\Big\} \\ &\quad +V_\beta^2\Gamma_\alpha\mathrm{e}^{-\mathrm{i}h_{\mathrm{eff}}t}G^{\mathrm{R}}(\omega)A_\beta(\omega+V_\beta)G^{\mathrm{A}}(\omega)\mathrm{e}^{\mathrm{i}h_{\mathrm{eff}}^\dagger t}\Big\}, \end{aligned} \tag{A.59}$$

where we use the relation for the difference of the retarded and advanced Green's functions (the underlined part) in Eq. (2.21) to find our final result for the current through the interface between the central region and the α-th lead

$$\begin{aligned} I_\alpha(t) &= -2\int\frac{\mathrm{d}\omega}{2\pi}f(\omega-\mu)\sum_\beta\mathrm{Tr}\Big\{ \\ &\quad \Gamma_\alpha G^{\mathrm{R}}(\omega+V_\beta)\Gamma_\beta G^{\mathrm{A}}(\omega+V_\beta)-\Gamma_\alpha G^{\mathrm{R}}(\omega+V_\alpha)\Gamma_\beta G^{\mathrm{A}}(\omega+V_\alpha) \\ &\quad +V_\beta\Big\{\Gamma_\alpha\mathrm{e}^{\mathrm{i}(\omega+V_\beta-h_{\mathrm{eff}})t}G^{\mathrm{R}}(\omega)\Big[-\mathrm{i}\delta_{\alpha\beta}G^{\mathrm{R}}(\omega+V_\beta)+A_\beta(\omega+V_\beta)\Big]+\mathrm{h.c.}\Big\} \\ &\quad +V_\beta^2\Gamma_\alpha\mathrm{e}^{-\mathrm{i}h_{\mathrm{eff}}t}G^{\mathrm{R}}(\omega)A_\beta(\omega+V_\beta)G^{\mathrm{A}}(\omega)\mathrm{e}^{\mathrm{i}h_{\mathrm{eff}}^\dagger t}\Big\}. \end{aligned} \tag{A.60}$$

A.1.5 Solving the equation of motion with perturbed central region

When trying to solve Eq. (2.125) we notice that also a relation between the unperturbed and perturbed Green's functions is needed; this can be obtained as a Dyson-like equation [similar to Eq. (A.36)]

$$\begin{aligned} G^{\mathrm{R}}(\omega) &= (\omega - h_{\mathrm{eff}})^{-1} = (\omega - h_{\mathrm{eff}} - u + V_\alpha + u - V_\alpha)^{-1} \\ &= \left[\left(\frac{1}{\omega - h_{\mathrm{eff}} - u + V_\alpha}\right)^{-1} + u - V_\alpha\right]^{-1} = \left[\left(\frac{1}{\omega - \widetilde{h}_{\mathrm{eff}} + V_\alpha}\right)^{-1} - \widetilde{V}_\alpha\right]^{-1} \\ &= \left\{\left[\widetilde{G}^{\mathrm{R}}(\omega + V_\alpha)\right]^{-1} - \widetilde{V}_\alpha\right\}^{-1}, \end{aligned} \tag{A.61}$$

where we defined $\widetilde{V}_\alpha = V_\alpha \mathbb{1} - u$ which is now to be understood as an arbitrary matrix (before it was proportional to a unit matrix). Inverting the above equation gives

$$\mathbb{1} = G^{\mathrm{R}}(\omega)\left\{\left[\widetilde{G}^{\mathrm{R}}(\omega + V_\alpha)\right]^{-1} - \widetilde{V}_\alpha\right\} = G^{\mathrm{R}}(\omega)\left[\widetilde{G}^{\mathrm{R}}(\omega + V_\alpha)\right]^{-1} - G^{\mathrm{R}}(\omega)\widetilde{V}_\alpha \tag{A.62}$$

which can further be written in the following form

$$G^{\mathrm{R}}(\omega) - \widetilde{G}^{\mathrm{R}}(\omega + V_\alpha) = G^{\mathrm{R}}(\omega)\widetilde{V}_\alpha\widetilde{G}^{\mathrm{R}}(\omega + V_\alpha). \tag{A.63}$$

Similarly, a second order relation reads

$$[G^{\mathrm{R}}(\omega) - \widetilde{G}^{\mathrm{R}}(\omega + V_\alpha)][G^{\mathrm{A}}(\omega) - \widetilde{G}^{\mathrm{A}}(\omega + V_\alpha)] = G^{\mathrm{R}}(\omega)\widetilde{V}_\alpha\widetilde{G}^{\mathrm{R}}(\omega + V_\alpha)\widetilde{G}^{\mathrm{A}}(\omega + V_\alpha)\widetilde{V}_\alpha^\dagger G^{\mathrm{A}}(\omega). \tag{A.64}$$

Compared to the earlier derivation, special care must now be taken for the order of multiplication of the matrices. Now, we may go on with Eq. (2.125)

$$\begin{aligned} & \mathrm{i}\frac{\mathrm{d}}{\mathrm{d}t}G^<(t,t) - \widetilde{h}_{\mathrm{eff}}G^<(t,t) + G^<(t,t)\widetilde{h}_{\mathrm{eff}}^\dagger \\ = \; & -\mathrm{i}\int \frac{\mathrm{d}\omega}{2\pi} f(\omega - \mu)\sum_a \left\{\mathrm{e}^{\mathrm{i}(\omega + V_\alpha - \widetilde{h}_{\mathrm{eff}})t}G^{\mathrm{R}}(\omega)\widetilde{V}_\alpha\widetilde{G}^{\mathrm{R}}(\omega + V_\alpha) + \widetilde{G}^{\mathrm{R}}(\omega + V_\alpha)\right\}\Gamma_\alpha \\ + \; & \mathrm{i}\int \frac{\mathrm{d}\omega}{2\pi} f(\omega - \mu)\sum_\alpha \Gamma_\alpha \left\{\widetilde{G}^{\mathrm{A}}(\omega + V_\alpha)\widetilde{V}_\alpha^\dagger G^{\mathrm{A}}(\omega)\mathrm{e}^{-\mathrm{i}(\omega + V_\alpha - \widetilde{h}_{\mathrm{eff}}^\dagger)t} + \widetilde{G}^{\mathrm{A}}\omega + V_\alpha)\right\}. \end{aligned} \tag{A.65}$$

Then, we introduce a similar transformation for the Green's function as in Eq. (A.42)

$$G^<(t,t) = \mathrm{e}^{-\mathrm{i}\widetilde{h}_{\mathrm{eff}}t}\mathcal{G}^<(t,t)\mathrm{e}^{\mathrm{i}\widetilde{h}_{\mathrm{eff}}^\dagger t} \tag{A.66}$$

but now we denote the transformed Green's function by a calligraphic symbol since the tildes already denote the functions evaluated with the perturbed Hamiltonian. Evaluating the derivative on the left-hand side and then multiplying both sides with the corresponding exponentials leads to

$$\begin{aligned}\frac{\mathrm{d}}{\mathrm{d}t}\mathcal{G}^<(t,t) &= -\int\frac{\mathrm{d}\omega}{2\pi}f(\omega-\mu)\sum_\alpha \mathrm{e}^{\mathrm{i}\widetilde{h}_{\mathrm{eff}}t}\left[\widetilde{G}^{\mathrm{R}}(\omega+V_\alpha)\Gamma_\alpha-\Gamma_\alpha\widetilde{G}^{\mathrm{A}}(\omega+V_\alpha)\right]\mathrm{e}^{-\mathrm{i}\widetilde{h}^\dagger_{\mathrm{eff}}t}\\ &- \int\frac{\mathrm{d}\omega}{2\pi}f(\omega-\mu)\sum_\alpha\Big[G^{\mathrm{R}}(\omega)\widetilde{V}_\alpha\widetilde{G}^{\mathrm{R}}(\omega+V_\alpha)\Gamma_\alpha\mathrm{e}^{\mathrm{i}(\omega+V_\alpha-\widetilde{h}^\dagger_{\mathrm{eff}})t}\\ &\quad -\mathrm{e}^{-\mathrm{i}(\omega+V_\alpha-\widetilde{h}_{\mathrm{eff}})t}\Gamma_\alpha\widetilde{G}^{\mathrm{A}}(\omega+V_\alpha)\widetilde{V}^\dagger_\alpha G^{\mathrm{A}}(\omega)\Big]. \end{aligned}\tag{A.67}$$

Here, we may integrate both sides over t using the result in Eq. (A.47)

$$\begin{aligned}&\mathcal{G}^<(t,t)-\mathcal{G}^<(0,0^+)\\ =\;&\mathrm{i}\int\frac{\mathrm{d}\omega}{2\pi}f(\omega-\mu)\sum_\alpha\Big\{\mathrm{e}^{\mathrm{i}\widetilde{h}_{\mathrm{eff}}t}\widetilde{G}^{\mathrm{R}}(\omega+V_\alpha)\Gamma_\alpha\widetilde{G}^{\mathrm{A}}(\omega+V_\alpha)\mathrm{e}^{-\mathrm{i}\widetilde{h}^\dagger_{\mathrm{eff}}t}\\ &-\widetilde{G}^{\mathrm{R}}(\omega+V_\alpha)\Gamma_\alpha\widetilde{G}^{\mathrm{A}}(\omega+V_\alpha)\Big\}\\ +\;&\mathrm{i}\int\frac{\mathrm{d}\omega}{2\pi}f(\omega-\mu)\sum_\alpha\Big\{G^{\mathrm{R}}(\omega)\widetilde{V}_\alpha\widetilde{G}^{\mathrm{R}}(\omega+V_\alpha)\Gamma_\alpha\widetilde{G}^{\mathrm{A}}(\omega+V_\alpha)\left[\mathrm{e}^{\mathrm{i}(\omega+V_\alpha-\widetilde{h}^\dagger_{\mathrm{eff}})t}-1\right]\\ &+\widetilde{G}^{\mathrm{R}}(\omega+V_\alpha)\left[\mathrm{e}^{-\mathrm{i}(\omega+V_\alpha-\widetilde{h}_{\mathrm{eff}})t}-1\right]\Gamma_\alpha\widetilde{G}^{\mathrm{A}}(\omega+V_\alpha)\widetilde{V}^\dagger_\alpha G^{\mathrm{A}}(\omega)\Big\}. \end{aligned}\tag{A.68}$$

The initial condition on the left-hand side $\mathcal{G}^<(0,0^+)=G^<(0,0^+)$ is then (naturally) evaluated from the unperturbed Hamiltonian, and for this we may use the same Matsubara Green's function as in Eq. (A.49). Inserting this and combining the terms on the right-hand side gives

$$\begin{aligned}&\mathcal{G}^<(t,t)\\ =\;&\mathrm{i}\int\frac{\mathrm{d}\omega}{2\pi}f(\omega-\mu)\sum_\alpha\Big\{G^{\mathrm{R}}(\omega)\Gamma_\alpha G^{\mathrm{A}}(\omega)+\mathrm{e}^{\mathrm{i}\widetilde{h}_{\mathrm{eff}}t}\widetilde{G}^{\mathrm{R}}(\omega+V_\alpha)\Gamma_\alpha\widetilde{G}^{\mathrm{A}}(\omega+V_\alpha)\mathrm{e}^{-\mathrm{i}\widetilde{h}^\dagger_{\mathrm{eff}}t}\\ -\;&\widetilde{G}^{\mathrm{R}}(\omega+V_\alpha)\Gamma_\alpha\widetilde{G}^{\mathrm{A}}(\omega+V_\alpha)+G^{\mathrm{R}}(\omega)\widetilde{V}_\alpha\widetilde{G}^{\mathrm{R}}(\omega+V_\alpha)\Gamma_\alpha\widetilde{G}^{\mathrm{A}}(\omega+V_\alpha)\mathrm{e}^{\mathrm{i}(\omega+V_\alpha-\widetilde{h}^\dagger_{\mathrm{eff}})t}\\ -\;&G^{\mathrm{R}}(\omega)\widetilde{V}_\alpha\widetilde{G}^{\mathrm{R}}(\omega+V_\alpha)\Gamma_\alpha\widetilde{G}^{\mathrm{A}}(\omega+V_\alpha)-\widetilde{G}^{\mathrm{R}}(\omega+V_\alpha)\Gamma_\alpha\widetilde{G}^{\mathrm{A}}(\omega+V_\alpha)\widetilde{V}^\dagger_\alpha G^{\mathrm{A}}(\omega)\\ +\;&\widetilde{G}^{\mathrm{R}}(\omega+V_\alpha)\mathrm{e}^{-\mathrm{i}(\omega+V_\alpha-\widetilde{h}_{\mathrm{eff}})t}\Gamma_\alpha\widetilde{G}^{\mathrm{A}}(\omega+V_\alpha)\widetilde{V}^\dagger_\alpha G^{\mathrm{A}}(\omega)\Big\}. \end{aligned}\tag{A.69}$$

Then, we are left with transforming back from $\mathcal{G}^<$ to $G^<$ by multiplying with the corresponding exponentials. We may combine the terms on the right-hand side according to Eqs. (A.63) and (A.64) and have as the final result

$$\begin{aligned}-\mathrm{i}G^<(t,t) &= \int\frac{\mathrm{d}\omega}{2\pi}f(\omega-\mu)\sum_\alpha\Big\{\widetilde{G}^{\mathrm{R}}(\omega+V_\alpha)\Gamma_\alpha\widetilde{G}^{\mathrm{A}}(\omega+V_\alpha)\\ &\quad+\left[\mathrm{e}^{\mathrm{i}(\omega+V_\alpha-\widetilde{h}_{\mathrm{eff}})t}G^{\mathrm{R}}(\omega)\widetilde{V}_\alpha\widetilde{G}^{\mathrm{R}}(\omega+V_\alpha)\Gamma_\alpha\widetilde{G}^{\mathrm{A}}(\omega+V_\alpha)+\mathrm{h.c.}\right]\\ &\quad+\mathrm{e}^{-\mathrm{i}\widetilde{h}_{\mathrm{eff}}t}G^{\mathrm{R}}(\omega)\widetilde{V}_\alpha\widetilde{G}^{\mathrm{R}}(\omega+V_\alpha)\Gamma_\alpha\widetilde{G}^{\mathrm{A}}(\omega+V_\alpha)\widetilde{V}^\dagger_\alpha G^{\mathrm{A}}(\omega)\mathrm{e}^{\mathrm{i}\widetilde{h}^\dagger_{\mathrm{eff}}t}\Big\} \end{aligned}\tag{A.70}$$

which applies in the case of perturbed central regions.

By careful bookkeeping of labels and indices we end up with the following expansion of Eq. (2.126) (the density matrix is now expanded in the perturbed 'left–left' eigenbasis of the effective Hamiltonian $\widetilde{h}_{\text{eff}}$)

$$\begin{aligned}
\rho_{jk}(t) &= \langle\widetilde{\Psi}_j^{\text{L}}|\rho(t)|\widetilde{\Psi}_k^{\text{L}}\rangle \\
&= \int\frac{\mathrm{d}\omega}{2\pi}f(\omega-\mu)\sum_\alpha\Big\{\langle\widetilde{\Psi}_j^{\text{L}}|\widetilde{G}^{\text{R}}(\omega+V_\alpha)\Gamma_\alpha\widetilde{G}^{\text{A}}(\omega+V_\alpha)|\widetilde{\Psi}_j^{\text{L}}\rangle \\
&+ \sum_{mn}\Big[\langle\widetilde{\Psi}_j^{\text{L}}|\mathrm{e}^{\mathrm{i}(\omega+V_\alpha-\widetilde{h}_{\text{eff}})t}\frac{|\Psi_m^{\text{R}}\rangle\langle\Psi_m^{\text{L}}|}{\langle\Psi_m^{\text{L}}|\Psi_m^{\text{R}}\rangle}G^{\text{R}}(\omega) \\
&\quad\times\widetilde{V}_\alpha\frac{|\widetilde{\Psi}_n^{\text{R}}\rangle\langle\widetilde{\Psi}_n^{\text{L}}|}{\langle\widetilde{\Psi}_n^{\text{L}}|\widetilde{\Psi}_n^{\text{R}}\rangle}\widetilde{G}^{\text{R}}(\omega+V_\alpha)\Gamma_\alpha\widetilde{G}^{\text{A}}(\omega+V_\alpha)|\widetilde{\Psi}_j^{\text{L}}\rangle+\text{h.c.}\Big] \\
&+ \sum_{mnpq}\langle\widetilde{\Psi}_j^{\text{L}}|\mathrm{e}^{-\mathrm{i}\widetilde{h}_{\text{eff}}t}\frac{|\Psi_m^{\text{R}}\rangle\langle\Psi_m^{\text{L}}|}{\langle\Psi_m^{\text{L}}|\Psi_m^{\text{R}}\rangle}G^{\text{R}}(\omega)\widetilde{V}_\alpha\frac{|\widetilde{\Psi}_n^{\text{R}}\rangle\langle\widetilde{\Psi}_n^{\text{L}}|}{\langle\widetilde{\Psi}_n^{\text{L}}|\widetilde{\Psi}_n^{\text{R}}\rangle}\widetilde{G}^{\text{R}}(\omega+V_\alpha) \\
&\quad\times\Gamma_\alpha\widetilde{G}^{\text{A}}(\omega+V_\alpha)\frac{|\widetilde{\Psi}_p^{\text{L}}\rangle\langle\widetilde{\Psi}_p^{\text{R}}|}{\langle\widetilde{\Psi}_p^{\text{R}}|\widetilde{\Psi}_p^{\text{L}}\rangle}\widetilde{V}_\alpha^\dagger G^{\text{A}}(\omega)\frac{|\Psi_q^{\text{L}}\rangle\langle\Psi_q^{\text{R}}|}{\langle\Psi_q^{\text{R}}|\Psi_q^{\text{L}}\rangle}\mathrm{e}^{\mathrm{i}\widetilde{h}_{\text{eff}}^\dagger t}|\widetilde{\Psi}_j^{\text{L}}\rangle\Big\}. \qquad \text{(A.71)}
\end{aligned}$$

Looking at how the non-hermitian matrices operate on the corresponding eigenstates (see Eq. (2.69)) we may write

$$\begin{aligned}
\rho_{jk}(t) &= \sum_\alpha\langle\widetilde{\Psi}_j^{\text{L}}|\Gamma_\alpha|\widetilde{\Psi}_k^{\text{L}}\rangle\int\frac{\mathrm{d}\omega}{2\pi}\frac{f(\omega-\mu)}{(\omega+V_\alpha-\widetilde{\epsilon}_j)(\omega+V_\alpha-\widetilde{\epsilon}_k^*)} \\
&+ \sum_\alpha\Bigg[\sum_{mn}\frac{\langle\widetilde{\Psi}_j^{\text{L}}|\Psi_m^{\text{R}}\rangle\langle\Psi_m^{\text{L}}|\widetilde{V}_\alpha|\widetilde{\Psi}_n^{\text{R}}\rangle\langle\widetilde{\Psi}_n^{\text{L}}|\Gamma_\alpha|\widetilde{\Psi}_k^{\text{L}}\rangle}{\langle\Psi_m^{\text{L}}|\Psi_m^{\text{R}}\rangle\langle\widetilde{\Psi}_n^{\text{L}}|\widetilde{\Psi}_n^{\text{R}}\rangle} \\
&\quad\times\int\frac{\mathrm{d}\omega}{2\pi}\frac{f(\omega-\mu)\mathrm{e}^{\mathrm{i}(\omega+V_\alpha-\widetilde{\epsilon}_j)t}}{(\omega-\epsilon_m)(\omega+V_\alpha-\widetilde{\epsilon}_n)(\omega+V_\alpha-\widetilde{\epsilon}_k^*)}+\text{h.c.}\Bigg] \\
&+ \sum_\alpha\sum_{mnpq}\frac{\langle\widetilde{\Psi}_j^{\text{L}}|\Psi_m^{\text{R}}\rangle\langle\Psi_m^{\text{L}}|\widetilde{V}_\alpha|\widetilde{\Psi}_n^{\text{R}}\rangle\langle\widetilde{\Psi}_n^{\text{L}}|\Gamma_\alpha|\widetilde{\Psi}_p^{\text{L}}\rangle\langle\widetilde{\Psi}_p^{\text{R}}|\widetilde{V}_\alpha^\dagger|\Psi_q^{\text{L}}\rangle\langle\Psi_q^{\text{R}}|\widetilde{\Psi}_k^{\text{L}}\rangle}{\langle\Psi_m^{\text{L}}|\Psi_m^{\text{R}}\rangle\langle\widetilde{\Psi}_n^{\text{L}}|\widetilde{\Psi}_n^{\text{R}}\rangle\langle\widetilde{\Psi}_p^{\text{R}}|\widetilde{\Psi}_p^{\text{L}}\rangle\langle\Psi_q^{\text{R}}|\Psi_q^{\text{L}}\rangle} \\
&\quad\times\mathrm{e}^{-\mathrm{i}(\widetilde{\epsilon}_j-\widetilde{\epsilon}_k^*)t}\int\frac{\mathrm{d}\omega}{2\pi}\frac{f(\omega-\mu)}{(\omega-\epsilon_m)(\omega+V_\alpha-\widetilde{\epsilon}_n)(\omega+V_\alpha-\widetilde{\epsilon}_p^*)(\omega-\epsilon_q^*)}, \qquad \text{(A.72)}
\end{aligned}$$

where ϵ and $\widetilde{\epsilon}$ are the complex eigenvalues of h_{eff} and $\widetilde{h}_{\text{eff}}$, respectively.

A.2 Details of the derivations in phononic transport

Here the details of the derivations presented in Sec. 2.5 are provided for completeness. We start with deriving the equations of motion for the Green's function in the combined 'u, p'-operator representation in terms of the spinor operators $\hat{\phi}$. After we know what the equations of motions consist of, we discuss an approximation for the self-energy, similar to the wide-band approximation in the electronic case. With the stated approximation, we may derive expressions for the time-convolutions in the equation of motion; this also involves introducing to the concept of a cut-off frequency. Finally, we insert all the expressions into the equation of motion, simplify the equation by noticing some reductions in the matrix forms, and solve the remaining differential equation analytically. The solution is almost equivalent to the case of electronic transport.

A.2.1 Deriving the equations of motion for the phonon Green's functions

Since the phonon Green's function is defined on the contour γ as in Eq. (2.177), we may simply evaluate the derivative with respect to the first contour-time coordinate z as

$$\begin{aligned} \mathrm{i}\partial_z D^{\mu\nu}_{jk}(z,z') &= \partial_z \left[\theta(z,z')\langle\hat{\phi}^\mu_j(z)\hat{\phi}^\nu_k(z') + \theta(z',z)\langle\hat{\phi}^\nu_k(z')\hat{\phi}^\mu_j(z)\rangle\right] \\ &= \delta(z,z')\langle\hat{\phi}^\mu_j(z)\hat{\phi}^\nu_k(z') - \hat{\phi}^\nu_k(z')\hat{\phi}^\mu_j(z)\rangle - \mathrm{i}\langle\mathcal{T}_\gamma[\mathrm{i}\partial_z\hat{\phi}^\mu_j(z)\hat{\phi}^\nu_k(z')]\rangle \\ &= \delta(z,z')[\hat{\phi}^\mu_j(z),\hat{\phi}^\nu_k(z')] - \mathrm{i}\langle\mathcal{T}_\gamma[\mathrm{i}\partial_z\hat{\phi}^\mu_j(z)\hat{\phi}^\nu_k(z')]\rangle, \end{aligned} \tag{A.73}$$

where the commutator gives $\alpha^{\mu\nu}\delta_{jk}$, see Eq. (2.176), and the time-evolution of the field operator in the second term on the right-hand side may be derived from its equation of motion. By inserting the Hamiltonian from Eq. (2.173) we get

$$\begin{aligned} \mathrm{i}\partial_z\hat{\phi}^\mu_j &= [\hat{\phi}^\mu_j,\hat{H}] = \frac{1}{2}\sum_{kl,\sigma\rho}(\hat{\phi}^\mu_j\hat{\phi}^\sigma_k\Omega^{\sigma\rho}_{kl}\hat{\phi}^\rho_l - \hat{\phi}^\sigma_k\Omega^{\sigma\rho}_{kl}\hat{\phi}^\rho_l\hat{\phi}^\mu_j) = \frac{1}{2}\sum_{kl,\sigma\rho}\Omega^{\sigma\rho}_{kl}[\hat{\phi}^\mu_j,\hat{\phi}^\sigma_k\hat{\phi}^\rho_l] \\ &= \frac{1}{2}\sum_{kl,\sigma\rho}\Omega^{\sigma\rho}_{kl}\left([\hat{\phi}^\mu_j,\hat{\phi}^\sigma_k]\hat{\phi}^\rho_l + \hat{\phi}^\sigma_k[\hat{\phi}^\mu_j,\hat{\phi}^\rho_l]\right), \end{aligned} \tag{A.74}$$

where we used a relation for the commutator $[A,BC] = [A,B]C + B[A,C]$. Now, the commutators between the field operators $\hat{\phi}$ give, according to Eq. (2.176), matrix elements of α and Kronecker deltas. These can be simplified to the following form

$$\mathrm{i}\partial_z\hat{\phi}^\mu_j = \frac{1}{2}\sum_{l,\sigma\rho}\left[\alpha^{\mu\sigma}\Omega^{\sigma\rho}_{jl}\hat{\phi}^\rho_l + \alpha^{\mu\rho}(\Omega^{\mathrm{T}})^{\rho\sigma}_{jl}\hat{\phi}^\sigma_l\right], \tag{A.75}$$

and inserting this, further, back into Eq. (A.73) gives

$$\mathrm{i}\partial_z D^{\mu\nu}_{jk}(z,z') = \delta_{jk}\alpha^{\mu\nu}\delta(z,z') - \mathrm{i}\Big\langle \mathcal{T}_\gamma\Big[\frac{1}{2}\sum_{l,\sigma\rho}\Big(\alpha^{\mu\sigma}\Omega^{\sigma\rho}_{jl}\hat{\phi}^\rho_l(z) + \alpha^{\mu\rho}(\Omega^{\mathrm{T}})^{\rho\sigma}_{jl}\hat{\phi}^\sigma_l(z)\Big)\hat{\phi}^\nu_k(z')\Big]\Big\rangle, \tag{A.76}$$

where the superscript 'T' refers to a matrix transpose. This can be simplified by relabeling dummy indices and using the definition for the Green's function in Eq. (2.177), and the final equation is

$$\mathrm{i}\partial_z D^{\mu\nu}_{jk}(z,z') = \delta_{jk}\alpha^{\mu\nu}\delta(z,z') + \sum_{q,\gamma\delta}\alpha^{\mu\gamma}\frac{1}{2}(\Omega+\Omega^{\mathrm{T}})^{\gamma\delta}_{jq}D^{\delta\nu}_{qk}(z,z'). \tag{A.77}$$

The Hamiltonian matrix Ω is symmetric, so the term inside the sum $(\Omega+\Omega^{\mathrm{T}})/2 = \Omega$, and this equation can be written in the $\boldsymbol{\alpha}$-matrix representation as in Eq. (2.178). The adjoint equation is derived similarly and it reads

$$-\mathrm{i}\partial_{z'} D^{\mu\nu}_{jk}(z,z') = \alpha^{\mu\nu}\delta_{jk}\delta(z,z') + \sum_{q,\gamma\delta} D^{\mu\gamma}_{jq}(z,z')\frac{1}{2}(\Omega+\Omega^{\mathrm{T}})^{\gamma\delta}_{qk}\alpha^{\delta\nu}. \tag{A.78}$$

Then we may perform a similar projection procedure as in Sec. 2.2. We extract the 'CC' and 'λC' components from the equation of motion (2.178), and they read

$$\mathrm{i}\partial_z \boldsymbol{D}_{CC}(z,z') = \boldsymbol{\alpha}\delta(z,z') + \boldsymbol{\alpha}\boldsymbol{\Omega}_{CC}\boldsymbol{D}_{CC}(z,z') + \sum_\lambda \boldsymbol{\alpha}\boldsymbol{\Omega}_{C\lambda}\boldsymbol{D}_{\lambda C}(z,z'), \tag{A.79}$$

$$\mathrm{i}\partial_z \boldsymbol{D}_{\lambda C}(z,z') = \boldsymbol{\alpha}\boldsymbol{\Omega}_{\lambda C}\boldsymbol{\Omega}_{CC} + \sum_\lambda \boldsymbol{\alpha}\boldsymbol{\Omega}_{\lambda\lambda}\boldsymbol{D}_{\lambda C}(z,z') \tag{A.80}$$

with $\boldsymbol{\alpha}$ being a matrix $\mathbf{1}\otimes\alpha$ of appropriate dimension. For the isolated reservoir λ we have a Green's function $\boldsymbol{d}_{\lambda\lambda}$ satisfying the equation of motion

$$(\mathrm{i}\partial_z - \boldsymbol{\alpha}\boldsymbol{\Omega}_{\lambda\lambda})\boldsymbol{d}_{\lambda\lambda}(z,z') = \boldsymbol{\alpha}\delta_{\lambda\lambda}(z,z') \tag{A.81}$$

which we may use to derive an expression for $\boldsymbol{D}_{\lambda C}$ from Eq. (A.80) by multiplying both sides of the equation from left by $\boldsymbol{d}_{\lambda\lambda}$ and then integrating over the contour γ. This gives

$$\boldsymbol{D}_{\lambda C}(z,z') = \int_\gamma \mathrm{d}\bar{z}\,\boldsymbol{d}_{\lambda\lambda}(z,\bar{z})\boldsymbol{\Omega}_{\lambda C}\boldsymbol{D}_{CC}(\bar{z},z') \tag{A.82}$$

which we may insert into the right-hand side of Eq. (A.79). By introducing the *phononic embedding self-energy* as

$$\boldsymbol{\Pi}_{CC}(z,z') = \sum_\lambda \boldsymbol{\Omega}_{C\lambda}\boldsymbol{d}_{\lambda\lambda}(z,z')\boldsymbol{\Omega}_{\lambda C} \tag{A.83}$$

we may write the equation of motion for the '*CC*' component as

$$(\mathrm{i}\partial_z - \boldsymbol{\alpha}\boldsymbol{\Omega}_{CC})\boldsymbol{D}_{CC}(z,z') = \boldsymbol{\alpha}\delta(z,z') + \boldsymbol{\alpha}\int_\gamma \mathrm{d}\bar{z}\boldsymbol{\Pi}_{CC}(z,\bar{z})\boldsymbol{D}_{CC}(\bar{z},z'). \tag{A.84}$$

Exactly in the same way, we could derive the adjoint equation

$$\boldsymbol{D}_{CC}(z,z')(-\mathrm{i}\overleftarrow{\partial}_{z'} - \boldsymbol{\Omega}_{CC}\boldsymbol{\alpha}) = \boldsymbol{\alpha}\delta(z,z') + \Big[\int_\gamma \mathrm{d}\bar{z}\boldsymbol{D}_{CC}(z,\bar{z})\boldsymbol{\Pi}_{CC}(\bar{z},z')\Big]\boldsymbol{\alpha}. \tag{A.85}$$

A.2.2 Deriving the self-energy approximation

From Eq. (2.190) we may deduce the greater and lesser components for the uncoupled Green's function to be

$$\boldsymbol{d}^{>}_{\lambda\lambda}(t,t') = -\mathrm{i}\boldsymbol{\alpha}\bar{f}_\lambda(\boldsymbol{\Omega}_{\lambda\lambda}\boldsymbol{\alpha})\mathrm{e}^{-\mathrm{i}\boldsymbol{\Omega}_{\lambda\lambda}\boldsymbol{\alpha}(t-t')}, \tag{A.86}$$

$$\boldsymbol{d}^{<}_{\lambda\lambda}(t,t') = -\mathrm{i}\boldsymbol{\alpha}f_\lambda(\boldsymbol{\Omega}_{\lambda\lambda}\boldsymbol{\alpha})\mathrm{e}^{-\mathrm{i}\boldsymbol{\Omega}_{\lambda\lambda}\boldsymbol{\alpha}(t-t')}, \tag{A.87}$$

and further, the retarded component to read as

$$\boldsymbol{d}^{\mathrm{R}}_{\lambda\lambda}(t,t') = \theta(t-t')\left[\boldsymbol{d}^{>}_{\lambda\lambda}(t,t') - \boldsymbol{d}^{<}_{\lambda\lambda}(t,t')\right] = -\mathrm{i}\boldsymbol{\alpha}\theta(t-t')\mathrm{e}^{-\mathrm{i}\boldsymbol{\Omega}_{\lambda\lambda}\boldsymbol{\alpha}(t-t')}. \tag{A.88}$$

Since the retarded Green's function is a function of $t-t'$, we find by Fourier transforming

$$\boldsymbol{d}^{\mathrm{R}}_{\lambda\lambda}(\omega) = \boldsymbol{\alpha}\frac{1}{\omega - \boldsymbol{\Omega}_{\lambda\lambda}\boldsymbol{\alpha} + \mathrm{i}\eta} = \frac{1}{\boldsymbol{\alpha}(\omega+\mathrm{i}\eta) - \boldsymbol{\Omega}_{\lambda\lambda}}, \tag{A.89}$$

where, for the second equality, we used the idempotency of $\boldsymbol{\alpha}$. The parameter η is a positive infinitesimal accounting for correct causal structure. We can then insert Eq. (A.89) into Eq. (2.187) and derive an expression for the retarded self-energy for the central region embedded in the environment. We may evaluate the retarded Green's function by performing a matrix inversion for a block matrix

$$\boldsymbol{d}^{\mathrm{R}}_{\lambda\lambda}(\omega) = \begin{pmatrix} \left((\omega+\mathrm{i}\eta)^2 - K'_{\lambda\lambda}\right)^{-1} & \mathrm{i}(\omega+\mathrm{i}\eta)\left((\omega+\mathrm{i}\eta)^2 - K'_{\lambda\lambda}\right)^{-1} \\ -\mathrm{i}(\omega+\mathrm{i}\eta)\left((\omega+\mathrm{i}\eta)^2 - K'_{\lambda\lambda}\right)^{-1} & K'_{\lambda\lambda}\left((\omega+\mathrm{i}\eta)^2 - K'_{\lambda\lambda}\right)^{-1} \end{pmatrix}. \tag{A.90}$$

If we know the eigen decomposition of $K'_{\lambda\lambda}$ as $K'_{\lambda\lambda}X = X\omega^2_\lambda$, we can then also diagonalize the full reservoir Hamiltonian with $\mathcal{X} \coloneqq \mathrm{diag}(X, X)$ as

$$\widetilde{\boldsymbol{\Omega}}_{\lambda\lambda} = \mathcal{X}^\dagger\boldsymbol{\Omega}_{\lambda\lambda}\mathcal{X} = \begin{pmatrix} \omega^2_\lambda & 0 \\ 0 & 1 \end{pmatrix} =: \boldsymbol{\omega}^2_\lambda. \tag{A.91}$$

Further, we may write the retarded embedding self-energy in terms of the eigenmodes when inserting Eq. (A.90) into Eq. (2.187)

$$\boldsymbol{\Pi}_\lambda^{\mathrm{R}}(\omega) = \sum_{q_\lambda} \widetilde{\boldsymbol{\Omega}}_{Cq_\lambda} \frac{1}{(\omega+\mathrm{i}\eta)^2-\omega_{q_\lambda}^2} \begin{pmatrix} 1 & \mathrm{i}(\omega+\mathrm{i}\eta) \\ -\mathrm{i}(\omega+\mathrm{i}\eta) & \omega_{q_\lambda}^2 \end{pmatrix} \widetilde{\boldsymbol{\Omega}}_{q_\lambda C} \tag{A.92}$$

where we wrote explicitly a sum over q_λ labeling the q-th basis element of reservoir λ. Also, $\widetilde{\boldsymbol{\Omega}}_{Cq_\lambda} \coloneqq \boldsymbol{\Omega}_{Cq_\lambda} X$. Since the coupling Hamiltonians only have nonzero elements in the uu block, this gives

$$\begin{aligned} (\boldsymbol{\Pi}_\lambda^{\mathrm{R}})^{11}(\omega) =: \Pi_\lambda^{\mathrm{R}}(\omega) &= \sum_{q_\lambda} \frac{\widetilde{K}_{Cq_\lambda}\widetilde{K}_{q_\lambda C}}{(\omega+\mathrm{i}\eta)^2-\omega_{q_\lambda}^2} \\ &= \sum_{q_\lambda} \frac{\widetilde{K}_{Cq_\lambda}\widetilde{K}_{q_\lambda C}}{2\omega_{q_\lambda}} \left(\frac{1}{\omega-\omega_{q_\lambda}+\mathrm{i}\eta} - \frac{1}{\omega+\omega_{q_\lambda}+\mathrm{i}\eta} \right), \end{aligned} \tag{A.93}$$

where $\widetilde{K}_{Cq_\lambda} \coloneqq K_{Cq_\lambda} X$. The advanced embedding self-energy Π_λ^{A} is simply given by complex conjugating Eq. (A.93). Then, we may evaluate the level-width function Γ_λ defined as

$$\begin{aligned} \Gamma_\lambda(\omega) &\coloneqq \mathrm{i}\left[\Pi_\lambda^{\mathrm{R}} - \Pi_\lambda^{\mathrm{A}}\right](\omega) \\ &= \mathrm{i}\sum_{q_\lambda} \frac{\widetilde{K}_{Cq_\lambda}\widetilde{K}_{q_\lambda C}}{2\omega_{q_\lambda}} \left(\frac{1}{\omega-\omega_{q_\lambda}+\mathrm{i}\eta} - \frac{1}{\omega+\omega_{q_\lambda}+\mathrm{i}\eta} \right. \\ &\qquad\qquad \left. - \frac{1}{\omega-\omega_{q_\lambda}-\mathrm{i}\eta} + \frac{1}{\omega+\omega_{q_\lambda}-\mathrm{i}\eta} \right) \\ &= \sum_{q_\lambda} \frac{\widetilde{K}_{Cq_\lambda}\widetilde{K}_{q_\lambda C}}{\omega_{q_\lambda}} \left(\frac{\eta}{(\omega-\omega_{q_\lambda})^2+\eta^2} - \frac{\eta}{(\omega+\omega_{q_\lambda})^2+\eta^2} \right) \\ &= \sum_{q_\lambda} \pi\widetilde{K}_{Cq_\lambda} \frac{1}{\omega_{q_\lambda}} \left[\delta(\omega-\omega_{q_\lambda}) - \delta(\omega+\omega_{q_\lambda})\right] \widetilde{K}_{q_\lambda C}\,, \end{aligned} \tag{A.94}$$

where we used the lorentzian representation for the delta function $\pi\delta(x-a) = \lim_{\eta\to 0} \eta/[(x-a)^2+\eta^2]$. Since $\Pi^{\mathrm{A}} = (\Pi^{\mathrm{R}})^\dagger$, we have that

$$\Pi_\lambda^{\mathrm{R}}(\omega) = \Lambda_\lambda(\omega) - \frac{\mathrm{i}}{2}\Gamma_\lambda(\omega), \tag{A.95}$$

where Λ and Γ are real functions related by the Hilbert transform

$$\Lambda_\lambda(\omega) = \frac{1}{\pi}\mathcal{P}\int_{-\infty}^{\infty} \mathrm{d}\omega' \frac{\Gamma_\lambda(\omega')}{\omega-\omega'} = \sum_{q_\lambda} \frac{\widetilde{K}_{Cq_\lambda}\widetilde{K}_{q_\lambda C}}{\omega_{q_\lambda}} \left(\frac{1}{\omega-\omega_{q_\lambda}} - \frac{1}{\omega+\omega_{q_\lambda}} \right). \tag{A.96}$$

From Eqs. (A.94) and (A.96) we notice that Λ_λ is an even function and Γ_λ is an odd function, see Fig. A.2.

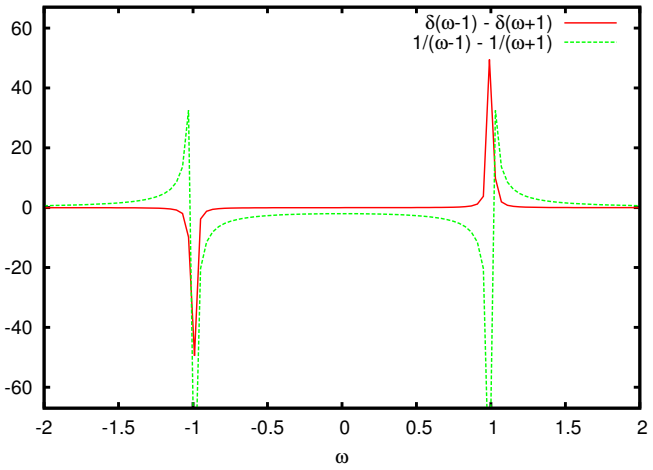

Fig. A.2: Schematic of the frequency dependency of the embedding self-energy in Eqs. (A.94) and (A.96).

A.2.3 Calculating the time-convolutions of different Keldysh components of the self-energies and Green's functions

Here we calculate the convolutions $[\boldsymbol{\Pi}^< \cdot \boldsymbol{D}^{\mathrm{A}}]$, $[\boldsymbol{D}^{\mathrm{R}} \cdot \boldsymbol{\Pi}^<]$, $[\boldsymbol{\Pi}^{\mathrm{R}} \cdot \boldsymbol{D}^<]$ and $[\boldsymbol{D}^< \cdot \boldsymbol{\Pi}^{\mathrm{A}}]$ in Eq. (2.189).

We keep $\boldsymbol{D}^{\mathrm{R}}$ so far unspecified and we calculate the time convolution

$$\begin{aligned}\left[\boldsymbol{D}^{\mathrm{R}} \cdot \boldsymbol{\Pi}^<\right](t,t) &= \int_0^\infty \mathrm{d}\bar{t}\boldsymbol{D}^{\mathrm{R}}(t,\bar{t})\boldsymbol{\Pi}^<(\bar{t},t) = \int_0^\infty \mathrm{d}\bar{t}\boldsymbol{D}^{\mathrm{R}}(t-\bar{t})\int_{-\infty}^\infty \frac{\mathrm{d}\omega}{2\pi}\boldsymbol{\Pi}^<(\omega)\mathrm{e}^{-\mathrm{i}\omega(\bar{t}-t)} \\ &= \int_{-\infty}^\infty \frac{\mathrm{d}\omega}{2\pi}\int_{-\infty}^\infty \mathrm{d}t'\boldsymbol{D}^{\mathrm{R}}(t')\mathrm{e}^{\mathrm{i}\omega t'}\boldsymbol{\Pi}^<(\omega)\theta(t-t'), \qquad \text{(A.97)}\end{aligned}$$

where we inserted the Fourier transform of $\boldsymbol{\Pi}^<$, changed the integration variable as $t - \bar{t} = t'$ and inserted a step function for extending the time interval to minus infinity. For the step function we may use the expression

$$\theta(t-t') = \lim_{\eta\to 0^+}\int_{-\infty}^\infty \frac{\mathrm{d}\omega'}{2\pi\mathrm{i}}\frac{\mathrm{e}^{\mathrm{i}\omega'(t-t')}}{\omega' - \mathrm{i}\eta} \qquad \text{(A.98)}$$

and evaluate further

$$\begin{aligned}\left[\boldsymbol{D}^{\mathrm{R}} \cdot \boldsymbol{\Pi}^<\right](t,t) &= \int_{-\infty}^\infty \frac{\mathrm{d}\omega}{2\pi}\int_{-\infty}^\infty \mathrm{d}t'\int_{-\infty}^\infty \frac{\mathrm{d}\omega'}{2\pi\mathrm{i}}\boldsymbol{D}^{\mathrm{R}}(t')\mathrm{e}^{\mathrm{i}\omega t'}\boldsymbol{\Pi}^<(\omega)\frac{\mathrm{e}^{\mathrm{i}\omega'(t-t')}}{\omega' - \mathrm{i}\eta} \\ &= \int_{-\infty}^\infty \frac{\mathrm{d}\omega}{2\pi}\int_{-\infty}^\infty \frac{\mathrm{d}\omega'}{2\pi\mathrm{i}}\frac{\mathrm{e}^{\mathrm{i}\omega' t}}{\omega' - \mathrm{i}\eta}\int_{-\infty}^\infty \mathrm{d}t'\boldsymbol{D}^{\mathrm{R}}(t')\mathrm{e}^{\mathrm{i}(\omega-\omega')t'}\boldsymbol{\Pi}^<(\omega) \\ &= \int_{-\infty}^\infty \frac{\mathrm{d}\omega}{2\pi}\int_{-\infty}^\infty \frac{\mathrm{d}\bar{\omega}}{2\pi\mathrm{i}}\frac{\mathrm{e}^{\mathrm{i}(\omega-\bar{\omega})t}\boldsymbol{D}^{\mathrm{R}}(\bar{\omega})}{\omega - \bar{\omega} - \mathrm{i}\eta}\boldsymbol{\Pi}^<(\omega), \qquad \text{(A.99)}\end{aligned}$$

where we used the Fourier transform of $\boldsymbol{D}^{\mathrm{R}}(t)$ and changed the integration variable to $\omega - \omega' = \bar{\omega}$. The exponential involving both frequencies can be split up, and we may also insert the approximation for the embedding self-energy

$$\left[\boldsymbol{D}^{\mathrm{R}} \cdot \boldsymbol{\Pi}^{<}\right](t,t) = \sum_{\lambda=L,R} \int_{-\infty}^{\infty} \frac{\mathrm{d}\omega}{2\pi} \mathrm{e}^{\mathrm{i}\omega t} \left[\int_{-\infty}^{\infty} \frac{\mathrm{d}\omega'}{2\pi\mathrm{i}} \frac{\mathrm{e}^{-\mathrm{i}\omega' t} \boldsymbol{D}^{\mathrm{R}}(\omega')}{\omega - \omega' - \mathrm{i}\eta}\right] \theta(\omega_c - |\omega|) \left[-\mathrm{i} f_\lambda(\omega) \omega \boldsymbol{\Gamma}'_{0,\lambda}\right]. \tag{A.100}$$

The cut-off frequency ω_c is now explicitly in this expression without specifying $\boldsymbol{D}^{\mathrm{R}}$. As we argued earlier, the expression for the retarded Green's function should then only be valid in the cut-off regime and we simply use the embedded retarded Green's function for all frequencies ω' (in the inner integral)

$$\boldsymbol{D}^{\mathrm{R}}(\omega) = \frac{1}{\boldsymbol{\alpha}\omega - \boldsymbol{\Omega} - \boldsymbol{\Pi}^{\mathrm{R}}(\omega)} \approx \frac{1}{\omega - \boldsymbol{\Omega}_{\mathrm{eff}}} \frac{1}{\boldsymbol{\alpha} + \frac{\mathrm{i}}{2}\boldsymbol{\Gamma}'_0}, \tag{A.101}$$

where we inserted the approximation for the embedding self-energy and defined an effective (non-hermitian) Hamiltonian

$$\boldsymbol{\Omega}_{\mathrm{eff}} = \frac{1}{\boldsymbol{\alpha} + \frac{\mathrm{i}}{2}\boldsymbol{\Gamma}'_0} (\boldsymbol{\Omega} + \boldsymbol{\Lambda}_0). \tag{A.102}$$

Now the retarded Green's function is specified, and $\boldsymbol{D}^{\mathrm{R}}$ and $\boldsymbol{\Pi}^{\mathrm{R}}$ satisfy the Dyson equation in the limits of $|\omega| < \omega_c$. In Eq. (A.100), also the analytical structure is correct: $\boldsymbol{D}^{\mathrm{R}}(\omega')$ has poles in the lower-half plane, and also the denominator goes to zero when $\omega' = \omega - \mathrm{i}\eta$ (in LHP). The key for evaluating the time-convolution was the approximation for $\boldsymbol{D}^{\mathrm{R}}$ in Eq. (A.100). As we approximate the retarded Green's function for all frequencies ω as in Eq. (A.101), this implicitly means the limit $\omega_c \to \infty$. On the other hand, when we specify the cut-off frequency directly to the self-energy approximation in Eq. (2.198), this would amount to

$$\boldsymbol{D}^{\mathrm{R}}_{\theta}(\omega) \coloneqq \frac{1}{\boldsymbol{\alpha}\omega - \boldsymbol{\Omega} - \boldsymbol{\Pi}^{\mathrm{R}}(\omega)} = \frac{1}{\boldsymbol{\alpha}\omega - \boldsymbol{\Omega} - \theta(\omega_c - |\omega|)(\boldsymbol{\Lambda}_0 + \frac{\mathrm{i}\omega}{2}\boldsymbol{\Gamma}'_0)}. \tag{A.103}$$

As we discuss only the region $|\omega| < \omega_c$ when evaluating the time-convolution in Eq. (A.100), we may compare how much the approximated Green's function deviates from that in Eq. (A.103) (outside the cut-off window)

$$\begin{aligned} \frac{\boldsymbol{D}^{\mathrm{R}}(\omega)}{\boldsymbol{D}^{\mathrm{R}}_{\theta}(\omega)} &= \frac{\boldsymbol{\alpha}\omega - \boldsymbol{\Omega} - \theta(\omega_c - |\omega|)(\boldsymbol{\Lambda}_0 + \frac{\mathrm{i}\omega}{2}\boldsymbol{\Gamma}'_0)}{\boldsymbol{\alpha}\omega - \boldsymbol{\Omega} - \boldsymbol{\Lambda}_0 + \frac{\mathrm{i}\omega}{2}\boldsymbol{\Gamma}'_0} \\ &\overset{\omega>\omega_c}{=} \frac{\boldsymbol{\alpha}\omega - \boldsymbol{\Omega}}{\boldsymbol{\alpha}\omega - \boldsymbol{\Omega} - \boldsymbol{\Lambda}_0 + \frac{\mathrm{i}\omega}{2}\boldsymbol{\Gamma}'_0} \xrightarrow{\omega \gg \mathrm{Re}[\omega_{\mathrm{eff}}]} \frac{\boldsymbol{\alpha}}{\boldsymbol{\alpha} + \frac{\mathrm{i}}{2}\boldsymbol{\Gamma}'_0}, \end{aligned} \tag{A.104}$$

where ω_{eff} are the eigenvalues of the effective Hamiltonian $\boldsymbol{\Omega}_{\mathrm{eff}}$. This limit means: (1) we choose the cut-off frequency high enough so that the physical frequencies of

the central region fall well inside this window; (2) if the frequency in the retarded Green's function still was higher than ω_c, we would have, in the limit $\boldsymbol{\Gamma}'_0 \to 0$ (weak coupling), that the difference in the retarded Green's functions approaches unity.

By using the eigenbasis of the effective Hamiltonian $\boldsymbol{\Omega}_{\text{eff}}$ we can evaluate the integral in Eq. (A.100) over ω' by closing the contour in the lower-half plane (t is a positive number):

$$\int_{-\infty}^{\infty} \frac{\mathrm{d}\omega'}{2\pi\mathrm{i}} \frac{\mathrm{e}^{-\mathrm{i}\omega' t}}{\omega - \omega' - \mathrm{i}\eta} \frac{1}{\omega' - \boldsymbol{\Omega}_{\text{eff}}} \frac{1}{\boldsymbol{\alpha} + \frac{\mathrm{i}}{2}\boldsymbol{\Gamma}'_0} = -\left[\frac{\mathrm{e}^{-\mathrm{i}\boldsymbol{\Omega}_{\text{eff}} t}}{\omega - \boldsymbol{\Omega}_{\text{eff}} - \mathrm{i}\eta} - \frac{\mathrm{e}^{-\mathrm{i}(\omega - \mathrm{i}\eta)t}}{\omega - \mathrm{i}\eta - \boldsymbol{\Omega}_{\text{eff}}} \right] \frac{1}{\boldsymbol{\alpha} + \frac{\mathrm{i}}{2}\boldsymbol{\Gamma}'_0}, \tag{A.105}$$

where the overall minus sign, when applying the Cauchy formula, comes from the clock-wise orientation of the contour. Then we can take the limit $\eta \to 0$ and write

$$\int_{-\infty}^{\infty} \frac{\mathrm{d}\omega'}{2\pi\mathrm{i}} \frac{\mathrm{e}^{-\mathrm{i}\omega' t} \boldsymbol{D}^{\mathrm{R}}(\omega')}{\omega - \omega' - \mathrm{i}\eta} = \frac{\mathrm{e}^{-\mathrm{i}\omega t} - \mathrm{e}^{-\mathrm{i}\boldsymbol{\Omega}_{\text{eff}} t}}{\omega - \boldsymbol{\Omega}_{\text{eff}}} \frac{1}{\boldsymbol{\alpha} + \frac{\mathrm{i}}{2}\boldsymbol{\Gamma}'_0} = \left(\mathrm{e}^{-\mathrm{i}\omega t} - \mathrm{e}^{-\mathrm{i}\boldsymbol{\Omega}_{\text{eff}} t} \right) \boldsymbol{D}^{\mathrm{R}}(\omega). \tag{A.106}$$

Inserting this into Eq. (A.100) we get

$$\begin{aligned} \left[\boldsymbol{D}^{\mathrm{R}} \cdot \boldsymbol{\Pi}^{<} \right](t,t) &= \sum_{\lambda=L,R} \int_{-\infty}^{\infty} \frac{\mathrm{d}\omega}{2\pi} \mathrm{e}^{\mathrm{i}\omega t} \left(\mathrm{e}^{-\mathrm{i}\omega t} - \mathrm{e}^{-\mathrm{i}\boldsymbol{\Omega}_{\text{eff}} t} \right) \boldsymbol{D}^{\mathrm{R}}(\omega) \theta(\omega_c - |\omega|) \left[-\mathrm{i} f_\lambda(\omega) \omega \boldsymbol{\Gamma}'_{0,\lambda} \right] \\ &= \sum_{\lambda=L,R} \int_{-\infty}^{\infty} \frac{\mathrm{d}\omega}{2\pi} \left[\mathbf{1} - \mathrm{e}^{\mathrm{i}(\omega - \boldsymbol{\Omega}_{\text{eff}})t} \right] \boldsymbol{D}^{\mathrm{R}}(\omega) \theta(\omega_c - |\omega|) \left[-\mathrm{i} f_\lambda(\omega) \omega \boldsymbol{\Gamma}'_{0,\lambda} \right]. \end{aligned} \tag{A.107}$$

It is worth noticing that this result could also be derived by Fourier transforming $\boldsymbol{D}^{\mathrm{R}}(\omega)$ from Eq. (A.101) and then inserting the resulting $\boldsymbol{D}^{\mathrm{R}}(t,t')$ directly into Eq. (A.97). $[\boldsymbol{\Pi}^{<} \cdot \boldsymbol{D}^{\mathrm{A}}]$ is found by conjugating Eq. (A.107).

Let us briefly investigate what would happen if we did not take the cut-off frequency into account. As said above, we could simply calculate the retarded Green's function by Fourier transforming

$$\begin{aligned} \boldsymbol{D}^{\mathrm{R}}(t,t') &= \boldsymbol{D}^{\mathrm{R}}(t-t') = \int \frac{\mathrm{d}\omega}{2\pi} \boldsymbol{D}^{\mathrm{R}}(\omega) \mathrm{e}^{-\mathrm{i}\omega(t-t')} \\ &= \int \frac{\mathrm{d}\omega}{2\pi} \frac{1}{\boldsymbol{\alpha}(\omega + \mathrm{i}\eta) - \boldsymbol{\Omega} - \boldsymbol{\Pi}^{\mathrm{R}}(\omega)} \mathrm{e}^{-\mathrm{i}\omega(t-t')} \\ &= \int \frac{\mathrm{d}\omega}{2\pi} \frac{1}{\boldsymbol{\alpha}(\omega + \mathrm{i}\eta) - \boldsymbol{\Omega} - \boldsymbol{\Lambda}_0 + \frac{\mathrm{i}\omega}{2}\boldsymbol{\Gamma}'_0} \mathrm{e}^{-\mathrm{i}\omega(t-t')}, \end{aligned} \tag{A.108}$$

where we inserted the approximatiaon for the retarded self-energy. Now, the ω-

dependent terms may be coupled to give (the infinitesimal η is not needed anymore)

$$\begin{aligned}
\boldsymbol{D}^{\mathrm{R}}(t,t') &= \int \frac{\mathrm{d}\omega}{2\pi} \frac{1}{\omega(\boldsymbol{\alpha}+\frac{\mathrm{i}}{2}\boldsymbol{\Gamma}_0') - \boldsymbol{\Omega} - \boldsymbol{\Lambda}_0} \mathrm{e}^{-\mathrm{i}\omega(t-t')} \\
&= \int \frac{\mathrm{d}\omega}{2\pi} \frac{1}{(\boldsymbol{\alpha}+\frac{\mathrm{i}}{2}\boldsymbol{\Gamma}_0')\left[\omega - \frac{1}{\boldsymbol{\alpha}+\frac{\mathrm{i}}{2}\boldsymbol{\Gamma}_0'}(\boldsymbol{\Omega}+\boldsymbol{\Lambda}_0)\right]} \mathrm{e}^{-\mathrm{i}\omega(t-t')} \\
&= \left[\int \frac{\mathrm{d}\omega}{2\pi} \frac{1}{\omega - \boldsymbol{\Omega}_{\mathrm{eff}}} \mathrm{e}^{-\mathrm{i}\omega(t-t')}\right] \frac{1}{\boldsymbol{\alpha}+\frac{\mathrm{i}}{2}\boldsymbol{\Gamma}_0'} \\
&= \left[-\mathrm{i}\theta(t-t')\mathrm{e}^{-\mathrm{i}\boldsymbol{\Omega}_{\mathrm{eff}}(t-t')}\right] \frac{1}{\boldsymbol{\alpha}+\frac{\mathrm{i}}{2}\boldsymbol{\Gamma}_0'}.
\end{aligned} \tag{A.109}$$

Evaluating a simple matrix inverse gives

$$\frac{1}{\boldsymbol{\alpha}+\frac{\mathrm{i}}{2}\boldsymbol{\Gamma}_0'} = \frac{1}{\mathrm{i}} \begin{pmatrix} 0 & -1 \\ 1 & \frac{\Gamma_0'}{2} \end{pmatrix} \tag{A.110}$$

and further

$$\boldsymbol{\Omega}_{\mathrm{eff}} = \frac{1}{\boldsymbol{\alpha}+\frac{\mathrm{i}}{2}\boldsymbol{\Gamma}_0'}(\boldsymbol{\Omega}+\boldsymbol{\Lambda}_0) = \frac{1}{\mathrm{i}} \begin{pmatrix} 0 & -1 \\ 1 & \frac{\Gamma_0'}{2} \end{pmatrix} \left[\begin{pmatrix} K & 0 \\ 0 & 1 \end{pmatrix} + \begin{pmatrix} \Lambda_0 & 0 \\ 0 & 0 \end{pmatrix} \right] = \frac{1}{\mathrm{i}} \begin{pmatrix} 0 & -1 \\ K+\Lambda_0 & \frac{\Gamma_0'}{2} \end{pmatrix}. \tag{A.111}$$

Inserting Eqs. (A.110) and (A.111) into Eq. (A.109) finally gives for the phonon propagator

$$\begin{aligned}
\boldsymbol{D}^{\mathrm{R}}(t,t') &= -\mathrm{i}\theta(t-t') \exp\left[-\mathrm{i}\frac{1}{\mathrm{i}} \begin{pmatrix} 0 & -1 \\ K+\Lambda_0 & \frac{\Gamma_0'}{2} \end{pmatrix} (t-t')\right] \frac{1}{\mathrm{i}} \begin{pmatrix} 0 & -1 \\ 1 & \frac{\Gamma_0'}{2} \end{pmatrix} \\
&= -\theta(t-t') \exp\left[-\begin{pmatrix} 0 & -1 \\ K+\Lambda_0 & \frac{\Gamma_0'}{2} \end{pmatrix} (t-t')\right] \begin{pmatrix} 0 & -1 \\ 1 & \frac{\Gamma_0'}{2} \end{pmatrix}.
\end{aligned} \tag{A.112}$$

On the other hand, we know the limiting behaviour for the propagator

$$\lim_{t\to t'^{+}} \boldsymbol{D}^{\mathrm{R}}(t,t') = -\mathrm{i}[\hat{\boldsymbol{\phi}}, \hat{\boldsymbol{\phi}}] = -\mathrm{i}\boldsymbol{\alpha} = -\begin{pmatrix} 0 & -1 \\ 1 & 0 \end{pmatrix}, \tag{A.113}$$

but now, based on our derivation, we get

$$\lim_{t\to t'^{+}} \boldsymbol{D}^{\mathrm{R}}(t,t') = -\begin{pmatrix} 0 & -1 \\ 1 & \frac{\Gamma_0'}{2} \end{pmatrix} \tag{A.114}$$

which would agree only with $\Gamma_0' = 0$. This problem originates from the approximation stated for the self-energy: the linear imaginary part does not satisfy the Kramers–Kronig relation as integrating this gives divergent behaviour. And, on the

other hand, constant real part should lead to zero imaginary part if the Kramers–Kronig relation was obeyed. For this reason, it is important to regulate the diverging behaviour in the self-energy approximation by a cut-off frequency. In the electronic case we did not have this problem because there our wide-band approximation (that the imaginary part is simply a constant) lead to zero real part according to the Kramers–Kronig relations. This issue is discussed more in detail with further visualizations in Pub. [V].

Then we will calculate the other time convolution in Eq. (2.189), $[\boldsymbol{D}^< \cdot \boldsymbol{\Pi}^\mathrm{A}]$. From Eq. (2.198) we get $\boldsymbol{\Pi}^\mathrm{A}(\omega) = \left[\boldsymbol{\Pi}^\mathrm{R}(\omega)\right]^\dagger$ and further in time domain

$$\begin{aligned}
\boldsymbol{\Pi}^\mathrm{A}(t,t') &= \int \frac{\mathrm{d}\omega}{2\pi}\boldsymbol{\Pi}^\mathrm{A}(\omega)\mathrm{e}^{-\mathrm{i}\omega(t-t')} = \int \frac{\mathrm{d}\omega}{2\pi}\theta(\omega_c - |\omega|)\left[\boldsymbol{\Lambda}_0 + \frac{\mathrm{i}\omega}{2}\boldsymbol{\Gamma}_0'\right]\mathrm{e}^{-\mathrm{i}\omega(t-t')} \\
&= \boldsymbol{\Lambda}_0 \int_{-\omega_c}^{\omega_c} \frac{\mathrm{d}\omega}{2\pi}\mathrm{e}^{-\mathrm{i}\omega(t-t')} + \frac{\mathrm{i}\boldsymbol{\Gamma}_0'}{2}\int_{-\omega_c}^{\omega_c}\frac{\mathrm{d}\omega}{2\pi}\omega\mathrm{e}^{-\mathrm{i}\omega(t-t')} \\
&= \boldsymbol{\Lambda}_0 \frac{1}{2\pi(-\mathrm{i}(t-t'))}\left[\mathrm{e}^{-\mathrm{i}\omega_c(t-t')} - \mathrm{e}^{\mathrm{i}\omega_c(t-t')}\right] \\
&- \frac{\boldsymbol{\Gamma}_0'}{2}\frac{\partial}{\partial t}\left\{\frac{1}{2\pi(-\mathrm{i}(t-t'))}\left[\mathrm{e}^{-\mathrm{i}\omega_c(t-t')} - \mathrm{e}^{\mathrm{i}\omega_c(t-t')}\right]\right\} \\
&= \boldsymbol{\Lambda}_0 \frac{1}{\pi(t-t')}\sin\left(\frac{t-t'}{1/\omega_c}\right) - \frac{\boldsymbol{\Gamma}_0'}{2}\frac{\partial}{\partial t}\left[\frac{1}{\pi(t-t')}\sin\left(\frac{t-t'}{1/\omega_c}\right)\right].
\end{aligned} \tag{A.115}$$

In the limit $\omega_c \to \infty$ the sinc functions become delta functions, i.e., $\lim_{\epsilon\to 0}\frac{1}{\pi x}\sin\left(\frac{x}{\epsilon}\right) = \delta(x)$ and we obtain

$$\boldsymbol{\Pi}^\mathrm{A}(t,t') \to \boldsymbol{\Lambda}_0\delta(t-t') - \frac{\boldsymbol{\Gamma}_0'}{2}\frac{\partial}{\partial t}\delta(t-t'). \tag{A.116}$$

This is naturally the same result as if we put the limits of the integration in the derivation of Eq. (A.115) to $\pm\infty$. Based on the above expression for the advanced embedding self-energy we aim to calculate the time convolution in the equation of motion

$$\left[\boldsymbol{D}^< \cdot \boldsymbol{\Pi}^\mathrm{A}\right](t,t) = \int_0^\infty \mathrm{d}\bar{t}\boldsymbol{D}^<(t,\bar{t})\boldsymbol{\Pi}^\mathrm{A}(\bar{t},t) \tag{A.117}$$

and the corresponding hermitian-conjugated one. The higher cut-off frequency ω_c we choose for the advanced embedding self-energy, the faster will the oscillations (in time) be in $\boldsymbol{\Pi}^\mathrm{A}(\bar{t},t)$. On the other hand, the fastest oscillations for $\boldsymbol{D}^<(t,\bar{t})$ correspond to transitions of highest energy differences in our central region of interest. If we choose the cut-off frequency ω_c to be considerably higher than the typical energy scales in the central region, then in time-domain, $\boldsymbol{\Pi}^\mathrm{A}(\bar{t},t)$ appears *almost as* Eq. (A.116) compared to $\boldsymbol{D}^<(t,\bar{t})$. Following this line of thought would allow us to

calculate

$$\begin{aligned}\left[\boldsymbol{D}^{<}\cdot\boldsymbol{\Pi}^{\mathrm{A}}\right](t,t) &= \int_0^\infty \mathrm{d}\bar{t}\boldsymbol{D}^{<}(t,\bar{t})\sum_{\lambda}\left[\boldsymbol{\Lambda}_{0,\lambda}\delta(\bar{t}-t)-\frac{\boldsymbol{\Gamma}'_{0,\lambda}}{2}\frac{\partial}{\partial\bar{t}}\delta(\bar{t}-t)\right]\\ &= \sum_{\lambda=L,R}\left[\boldsymbol{D}^{<}(t,t)\boldsymbol{\Lambda}_{0,\lambda}-\int_0^\infty \mathrm{d}\bar{t}\boldsymbol{D}^{<}(t,\bar{t})\frac{\partial}{\partial\bar{t}}\delta(\bar{t}-t)\frac{\boldsymbol{\Gamma}'_{0,\lambda}}{2}\right]\\ &= \sum_{\lambda=L,R}\left[\boldsymbol{D}^{<}(t,t)\boldsymbol{\Lambda}_{0,\lambda}+\left.\frac{\partial\boldsymbol{D}^{<}(t,t')}{\partial t'}\right|_{t'=t}\frac{\boldsymbol{\Gamma}'_{0,\lambda}}{2}\right]\\ &= \boldsymbol{D}^{<}(t,t)\boldsymbol{\Lambda}_0+\left.\frac{\partial\boldsymbol{D}^{<}(t,t')}{\partial t'}\right|_{t'=t}\frac{\boldsymbol{\Gamma}'_0}{2},\end{aligned}\tag{A.118}$$

where we integrated by parts and noticed that the boundary term vanishes. By conjugating Eq. (A.118) we also find

$$\left[\boldsymbol{\Pi}^{\mathrm{R}}\cdot\boldsymbol{D}^{<}\right](t,t)=-\left[\boldsymbol{D}^{<}\cdot\boldsymbol{\Pi}^{\mathrm{A}}\right]^{\dagger}(t,t)=\boldsymbol{\Lambda}_0\boldsymbol{D}^{<}(t,t)+\frac{\boldsymbol{\Gamma}'_0}{2}\left.\frac{\partial\boldsymbol{D}^{<}(t,t')}{\partial t}\right|_{t=t'}.\tag{A.119}$$

The result in Eq. (A.118), however, implicitly assumes the limit $\omega_c\to\infty$ as we motivated its derivation by comparison of energy scales in $\boldsymbol{\Pi}^{\mathrm{A}}$ and $\boldsymbol{D}^{<}$ exactly this way: $\omega_c\gg\omega$ for frequencies ω in the central region. Let us try to validate this by evaluating the time convolution of $\boldsymbol{\Pi}^{\mathrm{A}}$ and $\boldsymbol{D}^{<}$ also by using the explicit expression in Eq. (A.115) and performing an asymptotic expansion in ω_c in

$$\begin{aligned}&\left[\boldsymbol{D}^{<}\cdot\boldsymbol{\Pi}^{\mathrm{A}}\right](t,t)=\int_0^\infty \mathrm{d}\bar{t}\boldsymbol{D}^{<}(t,\bar{t})\boldsymbol{\Pi}^{\mathrm{A}}(\bar{t},t)\\ =&\int_0^\infty \mathrm{d}\bar{t}\boldsymbol{D}^{<}(t,\bar{t})\left\{\boldsymbol{\Lambda}_0\frac{1}{\pi(\bar{t}-t)}\sin\left(\frac{\bar{t}-t}{1/\omega_c}\right)-\frac{\boldsymbol{\Gamma}'}{2}\frac{\partial}{\partial\bar{t}}\left[\frac{1}{\pi(\bar{t}-t)}\sin\left(\frac{\bar{t}-t}{1/\omega_c}\right)\right]\right\}\theta(t-\bar{t})\\ =&\int_0^t \mathrm{d}\bar{t}\boldsymbol{D}^{<}(t,\bar{t})\boldsymbol{\Lambda}_0\frac{1}{\pi(\bar{t}-t)}\sin\left(\frac{\bar{t}-t}{1/\omega_c}\right)+\int_0^t \mathrm{d}\bar{t}\boldsymbol{D}^{<}(t,\bar{t})\frac{\boldsymbol{\Gamma}'}{2}\frac{\partial}{\partial\bar{t}}\left[\frac{1}{\pi(\bar{t}-t)}\sin\left(\frac{\bar{t}-t}{1/\omega_c}\right)\right],\end{aligned}\tag{A.120}$$

where the upper limit of the integration follows from the advanced nature of $\boldsymbol{\Pi}^{\mathrm{A}}(\bar{t},t)\sim\theta(t-\bar{t})$. Using Leibniz' rule we may write the second term as

$$\begin{aligned}&\int_0^t \mathrm{d}\bar{t}\boldsymbol{D}^{<}(t,\bar{t})\frac{\boldsymbol{\Gamma}'}{2}\frac{\partial}{\partial\bar{t}}\left[\frac{1}{\pi(\bar{t}-t)}\sin\left(\frac{\bar{t}-t}{1/\omega_c}\right)\right]\\ =&\int_0^t \mathrm{d}\bar{t}\frac{\partial\boldsymbol{D}^{<}(t,\bar{t})}{\partial t}\frac{\boldsymbol{\Gamma}'}{2}\frac{1}{\pi(\bar{t}-t)}\sin\left(\frac{\bar{t}-t}{1/\omega_c}\right)-\frac{\mathrm{d}}{\mathrm{d}t}\left[\int_0^t \mathrm{d}\bar{t}\boldsymbol{D}^{<}(t,\bar{t})\frac{\boldsymbol{\Gamma}'}{2}\frac{1}{\pi(\bar{t}-t)}\sin\left(\frac{\bar{t}-t}{1/\omega_c}\right)\right]\end{aligned}\tag{A.121}$$

which tells us we only need to consider "the first line"-like terms in Eq. (A.120)

$$F(t)=\int_0^t \mathrm{d}\bar{t}f(t,\bar{t})\frac{1}{\pi(\bar{t}-t)}\sin\left(\frac{\bar{t}-t}{1/\omega_c}\right),\tag{A.122}$$

and then we get the second line by inserting $\partial_t \boldsymbol{D}^<(t,\bar{t})\boldsymbol{\Gamma}'/2$ and $\boldsymbol{D}^<(t,\bar{t})\boldsymbol{\Gamma}'/2$ as $f(t,\bar{t})$ and using Eq. (A.121). Assuming we are allowed to differentiate under the integral sign (the functions are well-behaving in our case) we get

$$\frac{\mathrm{d}F(t)}{\mathrm{d}\omega_c} = \pi^{-1}\int_0^t \mathrm{d}\bar{t} f(t,\bar{t})\cos[\omega_c(\bar{t}-t)] \tag{A.123}$$

for which we may perform a sequential integration by parts (we know all the anti-derivatives of a cosine function)

$$\begin{aligned}\frac{\mathrm{d}F(t)}{\mathrm{d}\omega_c} &= \pi^{-1}\left\{f(t,\bar{t})\frac{1}{\omega_c}\sin[\omega_c(\bar{t}-t)] + \frac{\partial f(t,\bar{t})}{\partial\bar{t}}\frac{1}{\omega_c^2}\cos[\omega_c(\bar{t}-t)]\right.\\ &- \left.\frac{\partial^2 f(t,\bar{t})}{\partial\bar{t}^2}\frac{1}{\omega_c^3}\sin[\omega_c(\bar{t}-t)] - \frac{\partial^3 f(t,\bar{t})}{\partial\bar{t}^3}\frac{1}{\omega_c^4}\cos[\omega_c(\bar{t}-t)] + \ldots\right\}_0^t,\end{aligned} \tag{A.124}$$

where the remainder will only be higher order in $1/\omega_c$, and since we are interested in the large ω_c limit, we may simply drop them. Integrating once over ω_c we obtain

$$F(t) = \pi^{-1}\left\{f(t,\bar{t})\mathrm{Si}[\omega_c(\bar{t}-t)] + \mathcal{O}\left(\frac{1}{\omega_c^2}\right)\right\}_0^t, \tag{A.125}$$

where $\mathrm{Si}(x)$ is the *sine integral function*. By using an asymptotic expansion for the sine integral [210] and using Eq. (A.121) we may conclude that the terms neglected by approximating Eq. (A.120) by Eq. (A.118) are of the order $\mathcal{O}[(\omega_c t)^{-1}]$. Therefore, for long times the approximation is reasonable but even if we choose a large cut-off frequency ω_c, for short times $t \lesssim 1/\omega_c$ the approximation fails. However, as argumented earlier, the cut-off frequency, is still explicitly included in the other term involving $\boldsymbol{\Pi}^<$ and $\boldsymbol{D}^{\mathrm{R}}$.

Let us also investigate a concrete example, and assume that the central region of interest would have a characteristic frequency ω_0, and let us for simplification assume an oscillatory behaviour for $\boldsymbol{D}_0^<(t,\bar{t}) = \mathrm{e}^{-\mathrm{i}\omega_0(t+\bar{t})}$. (We are not after anything rigorous but simply want to see how the sinc functions turn out for large ω_c.) The integral we wish to evaluate

$$I = \int_0^t \mathrm{d}\bar{t}\boldsymbol{D}_0^<(t,\bar{t})\boldsymbol{\Lambda}_0\frac{1}{\pi(\bar{t}-t)}\sin\left(\frac{\bar{t}-t}{1/\omega_c}\right) = \int_0^t \mathrm{d}\bar{t}\mathrm{e}^{-\mathrm{i}\omega_0(t+\bar{t})}\boldsymbol{\Lambda}_0\frac{1}{\pi(\bar{t}-t)}\sin\left(\frac{\bar{t}-t}{1/\omega_c}\right) \tag{A.126}$$

can be written in terms of the exponential integral function as

$$I = \frac{\mathrm{i}}{\pi}\mathrm{e}^{-2\mathrm{i}\omega_0 t}\boldsymbol{\Lambda}_0\left\{\mathrm{E}_1[-\mathrm{i}(\omega_0+\omega_c)t] - \mathrm{E}_1[-\mathrm{i}(\omega_0-\omega_c)t] - \mathrm{Log}\left(\frac{\omega_0-\omega_c}{\omega_0+\omega_c}\right)\right\}. \tag{A.127}$$

We know the asymptotic expansion of the exponential integral as $\mathrm{E}_1(z) \sim \mathrm{e}^{-z}/z$ [119], so we get as an asymptotic behaviour (the Logarithm can also be expanded)

$$\begin{aligned} I &\sim \frac{\mathrm{i}}{\pi}\mathrm{e}^{-2\mathrm{i}\omega_0 t}\boldsymbol{\Lambda}_0\left[\frac{\mathrm{e}^{\mathrm{i}(\omega_0+\omega_c)t}}{-\mathrm{i}(\omega_0+\omega_c)t} - \frac{\mathrm{e}^{\mathrm{i}(\omega_0-\omega_c)t}}{-\mathrm{i}(\omega_0-\omega_c)t} - \mathrm{i}\pi + \frac{2\omega_0}{\omega_c}\right] \\ &\to \mathrm{e}^{-2\mathrm{i}\omega_0 t}\boldsymbol{\Lambda}_0 \quad \text{when } \omega_c \to \infty. \end{aligned} \tag{A.128}$$

This means that the result, in the limit $\omega_c \to \infty$, is the same as if $\boldsymbol{D}^<$ was integrated with a delta function.

We could also have done the asymptotic expansion directly to the integral using `Mathematica` by

```
Dlss[t_, tb_] := Exp[-I*w0*(t + tb)];
Series[Integrate[
  Dlss[t, tb]*L0*(1/(Pi*(tb - t)))*Sin[(tb - t)/(1/ww)], {tb, 0, t},
  Assumptions -> {Im[w0] == 0 & Re[w0] > 0 && Im[t] == 0 &&
     Re[t] > 0 && Im[L0] == 0 && Re[L0] > 0}], {ww, Infinity, 2}]
```

which will expand to second order in ω_c at $\omega_c \to \infty$. This will give (after some simplification)

$$\begin{aligned} &\int_0^t \mathrm{d}\bar{t}\boldsymbol{D}_0^<(t,\bar{t})\boldsymbol{\Lambda}_0\frac{1}{\pi(\bar{t}-t)}\sin\left(\frac{1}{1/\omega_c}\right) \\ &\sim \frac{\boldsymbol{\Lambda}_0}{\pi}\left\{\mathrm{e}^{-2\mathrm{i}\omega_0 t}\left(\frac{\omega_0}{\omega_c}+\pi\right) - \mathrm{e}^{-\mathrm{i}\omega_0 t}\left[\frac{\cos(\omega_c t)}{\omega_c t} + \frac{\sin(\omega_c t)}{(\omega_c t)^2}\right]\right\}. \end{aligned} \tag{A.129}$$

However, we can also evaluate

$$\int_0^\infty \mathrm{d}\bar{t}\boldsymbol{D}_0^<(t,\bar{t})\boldsymbol{\Lambda}_0\delta(\bar{t}-t) = \boldsymbol{D}_0^<(t,t)\boldsymbol{\Lambda}_0 = \mathrm{e}^{-2\mathrm{i}\omega_0 t}\boldsymbol{\Lambda}_0 \tag{A.130}$$

and then plot the difference between the asymptotic expansion and the above expression with different values of ω_c. This is shown in Fig. A.3. Looking at the expressions, also the limit $\omega_c \to \infty$ goes correctly. We see that if ω_c is the same as the oscillation frequencies in the central region, the approximation with delta function is poor. However, already when $\omega_c = 10\omega_0$ the difference is only few percent. In all cases the limit $t \to 0$ is problematic because the expressions blow up but finally this will not be a problem because in the limit $t \to 0$ the final expressions give zero.

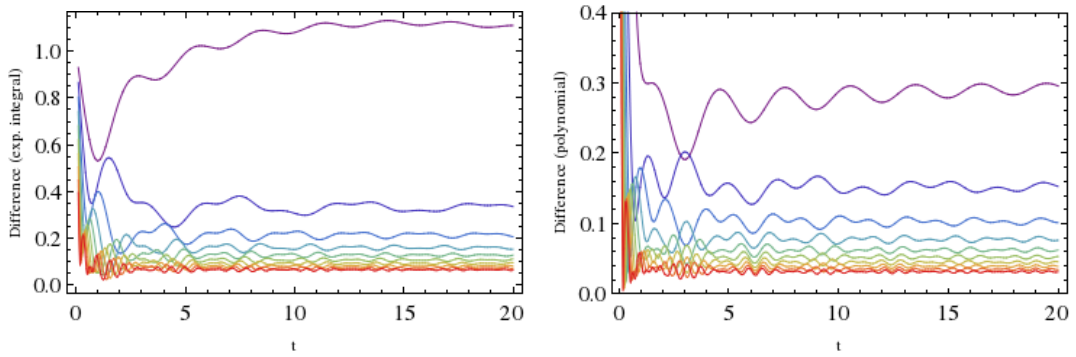

Fig. A.3: Asymptotic expansions of the integral in Eq. (A.126) with different values of ω_c; the rainbow colours go from $\omega_c = \omega_0 =$ purple to $\omega_c = 10\omega_0 =$ red. Left panel is the difference between Eqs. (A.127) and (A.130), and the right panel is the difference between Eqs. (A.129) and (A.130).

A.2.4 Details on solving the equation of motion for the Green's function

Looking at Eq. (2.206) we need to insert the expressions for $\partial \boldsymbol{D}(t,t')/\partial t$ and $\partial \boldsymbol{D}(t,t')/\partial t'$ from Eqs. (2.183) and (2.184). Also, since we now have the step functions involving the cut-off frequency, let us denote the integrals as $\int \widetilde{\frac{\mathrm{d}\omega}{2\pi}}$ where the range is suppressed to $[-\omega_c\,,\omega_c]$

$$
\begin{aligned}
&\mathrm{i}\frac{\mathrm{d}}{\mathrm{d}t}\boldsymbol{D}^<(t,t) - [\boldsymbol{\alpha}\boldsymbol{\Omega}\boldsymbol{D}^<(t,t) - \boldsymbol{D}^<(t,t)\boldsymbol{\Omega}\boldsymbol{\alpha}] \\
= \;& \boldsymbol{\alpha}\left[-\mathrm{i}\sum_\lambda \int \widetilde{\frac{\mathrm{d}\omega}{2\pi}}\omega f_\lambda(\omega)\boldsymbol{\Gamma}'_\lambda \boldsymbol{D}^{\mathrm{A}}(\omega)\left[1-\mathrm{e}^{-\mathrm{i}(\omega-\boldsymbol{\Omega}^\dagger_{\mathrm{eff}})t}\right] + \boldsymbol{\Lambda}_0\boldsymbol{D}^<(t,t)\right. \\
&\left. +\frac{\boldsymbol{\Gamma}'_0}{2}\left\{-\mathrm{i}\boldsymbol{\alpha}\boldsymbol{\Omega}\boldsymbol{D}^<(t,t) - \mathrm{i}\boldsymbol{\alpha}\left[\int_0^\infty \mathrm{d}\bar{t}\boldsymbol{\Pi}^<(t,\bar{t})\boldsymbol{D}^{\mathrm{A}}(\bar{t},t') + \int_0^\infty \mathrm{d}\bar{t}\boldsymbol{\Pi}^{\mathrm{R}}(t,\bar{t})\boldsymbol{D}^<(\bar{t},t')\right]_{t'=t}\right\}\right] \\
- \;& \left[\boldsymbol{D}^<(t,t)\boldsymbol{\Lambda}_0\right. \\
&\left. +\left\{\mathrm{i}\boldsymbol{D}^<(t,t)\boldsymbol{\Omega}\boldsymbol{\alpha} + \mathrm{i}\left[\int_0^\infty \mathrm{d}\bar{t}\boldsymbol{D}^<(t,\bar{t})\boldsymbol{\Pi}^{\mathrm{A}}(\bar{t},t') + \int_0^\infty \mathrm{d}\bar{t}\boldsymbol{D}^{\mathrm{R}}(t,\bar{t})\boldsymbol{\Pi}^<(\bar{t},t')\right]_{t'=t}\boldsymbol{\alpha}\right\}\frac{\boldsymbol{\Gamma}'_0}{2}\right. \\
&\left. -\mathrm{i}\sum_\lambda \int \widetilde{\frac{\mathrm{d}\omega}{2\pi}}\omega f_\lambda(\omega)\left[1-\mathrm{e}^{\mathrm{i}(\omega-\boldsymbol{\Omega}_{\mathrm{eff}})t}\right]\boldsymbol{D}^{\mathrm{R}}(\omega)\boldsymbol{\Gamma}'_\lambda\right]\boldsymbol{\alpha}. \qquad \text{(A.131)}
\end{aligned}
$$

And then, insert the remaining convolutions

$$
\begin{aligned}
& \mathrm{i}\frac{\mathrm{d}}{\mathrm{d}t}\boldsymbol{D}^<(t,t) - [\boldsymbol{\alpha}\boldsymbol{\Omega}\boldsymbol{D}^<(t,t) - \boldsymbol{D}^<(t,t)\boldsymbol{\Omega}\boldsymbol{\alpha}] \\
= \; & \boldsymbol{\alpha}\Bigg[-\mathrm{i}\sum_\lambda \int \widetilde{\frac{\mathrm{d}\omega}{2\pi}}\omega f_\lambda(\omega)\boldsymbol{\Gamma}'_\lambda \boldsymbol{D}^{\mathrm{A}}(\omega)\left[1-\mathrm{e}^{-\mathrm{i}(\omega-\boldsymbol{\Omega}^\dagger_{\mathrm{eff}})t}\right] + \boldsymbol{\Lambda}_0\boldsymbol{D}^<(t,t) \\
& + \frac{\boldsymbol{\Gamma}'_0}{2}\Bigg\{-\mathrm{i}\boldsymbol{\alpha}\boldsymbol{\Omega}\boldsymbol{D}^<(t,t) - \mathrm{i}\boldsymbol{\alpha}\Bigg[-\mathrm{i}\sum_\lambda \int \widetilde{\frac{\mathrm{d}\omega}{2\pi}}\omega f_\lambda(\omega)\boldsymbol{\Gamma}'_\lambda \boldsymbol{D}^{\mathrm{A}}(\omega)\left[1-\mathrm{e}^{-\mathrm{i}(\omega-\boldsymbol{\Omega}^\dagger_{\mathrm{eff}})t}\right] \\
& + \boldsymbol{\Lambda}_0\boldsymbol{D}^<(t,t) + \frac{\boldsymbol{\Gamma}'_0}{2}\left.\frac{\partial \boldsymbol{D}^<(t,t')}{\partial t}\right|_{t=t'}\Bigg]\Bigg\}\Bigg] \\
- \; & \Big[\boldsymbol{D}^<(t,t)\boldsymbol{\Lambda}_0 \\
& + \Bigg\{\mathrm{i}\boldsymbol{D}^<(t,t)\boldsymbol{\Omega}\boldsymbol{\alpha} + \mathrm{i}\Bigg[\boldsymbol{D}^<(t,t)\boldsymbol{\Lambda}_0 + \left.\frac{\partial \boldsymbol{D}^<(t,t')}{\partial t'}\right|_{t'=t}\frac{\boldsymbol{\Gamma}'_0}{2} \\
& -\mathrm{i}\sum_\lambda \int \widetilde{\frac{\mathrm{d}\omega}{2\pi}}\omega f_\lambda(\omega)\left[1-\mathrm{e}^{\mathrm{i}(\omega-\boldsymbol{\Omega}_{\mathrm{eff}})t}\right]\boldsymbol{D}^{\mathrm{R}}(\omega)\boldsymbol{\Gamma}'_\lambda\Bigg]\alpha\Bigg\}\frac{\boldsymbol{\Gamma}'_0}{2} \\
& -\mathrm{i}\sum_\lambda \int \widetilde{\frac{\mathrm{d}\omega}{2\pi}}\omega f_\lambda(\omega)\left[1-\mathrm{e}^{\mathrm{i}(\omega-\boldsymbol{\Omega}_{\mathrm{eff}})t}\right]\boldsymbol{D}^{\mathrm{R}}(\omega)\boldsymbol{\Gamma}'_\lambda\Big]\alpha. \qquad \text{(A.132)}
\end{aligned}
$$

As there are a lot of terms, the equations start to get longer and longer, but let us still expand the parentheses so that we can more easily see the terms that can be coupled together

$$
\begin{aligned}
& \mathrm{i}\frac{\mathrm{d}\boldsymbol{D}^<(t,t)}{\mathrm{d}t} - \boldsymbol{\alpha}\boldsymbol{\Omega}\boldsymbol{D}^<(t,t) + \boldsymbol{D}^<(t,t)\boldsymbol{\Omega}\boldsymbol{\alpha} \\
= \; & -\mathrm{i}\boldsymbol{\alpha}\sum_\lambda \int \widetilde{\frac{\mathrm{d}\omega}{2\pi}}\omega f_\lambda(\omega)\boldsymbol{\Gamma}'_\lambda \boldsymbol{D}^{\mathrm{A}}(\omega)\left[1-\mathrm{e}^{-\mathrm{i}(\omega-\boldsymbol{\Omega}^\dagger_{\mathrm{eff}})t}\right] + \boldsymbol{\alpha}\boldsymbol{\Lambda}_0\boldsymbol{D}^<(t,t) - \mathrm{i}\boldsymbol{\alpha}\frac{\boldsymbol{\Gamma}'_0}{2}\boldsymbol{\alpha}\boldsymbol{\Omega}\boldsymbol{D}^<(t,t) \\
- \; & \boldsymbol{\alpha}\frac{\boldsymbol{\Gamma}'_0}{2}\boldsymbol{\alpha}\sum_\lambda \int \widetilde{\frac{\mathrm{d}\omega}{2\pi}}\omega f_\lambda(\omega)\boldsymbol{\Gamma}'_\lambda \boldsymbol{D}^{\mathrm{A}}(\omega)\left[1-\mathrm{e}^{-\mathrm{i}(\omega-\boldsymbol{\Omega}^\dagger_{\mathrm{eff}})t}\right] - \mathrm{i}\boldsymbol{\alpha}\frac{\boldsymbol{\Gamma}'_0}{2}\boldsymbol{\alpha}\boldsymbol{\Lambda}_0\boldsymbol{D}^<(t,t) \\
- \; & \mathrm{i}\boldsymbol{\alpha}\frac{\boldsymbol{\Gamma}'_0}{2}\boldsymbol{\alpha}\frac{\boldsymbol{\Gamma}'_0}{2}\left.\frac{\partial \boldsymbol{D}^<(t,t')}{\partial t}\right|_{t=t'} - \boldsymbol{D}^<(t,t)\boldsymbol{\Lambda}_0\boldsymbol{\alpha} - \mathrm{i}\boldsymbol{D}^<(t,t)\boldsymbol{\Omega}\boldsymbol{\alpha}\frac{\boldsymbol{\Gamma}'_0}{2}\boldsymbol{\alpha} - \mathrm{i}\boldsymbol{D}^<(t,t)\boldsymbol{\Lambda}_0\boldsymbol{\alpha}\frac{\boldsymbol{\Gamma}'_0}{2}\boldsymbol{\alpha} \\
- \; & \mathrm{i}\left.\frac{\partial \boldsymbol{D}^<(t,t')}{\partial t'}\right|_{t'=t}\frac{\boldsymbol{\Gamma}'_0}{2}\boldsymbol{\alpha}\frac{\boldsymbol{\Gamma}'_0}{2}\boldsymbol{\alpha} - \sum_\lambda \int \widetilde{\frac{\mathrm{d}\omega}{2\pi}}\omega f_\lambda(\omega)\left[1-\mathrm{e}^{\mathrm{i}(\omega-\boldsymbol{\Omega}_{\mathrm{eff}})t}\right]\boldsymbol{D}^{\mathrm{R}}(\omega)\boldsymbol{\Gamma}'_\lambda\boldsymbol{\alpha}\frac{\boldsymbol{\Gamma}'_0}{2}\boldsymbol{\alpha} \\
+ \; & \mathrm{i}\sum_\lambda \int \widetilde{\frac{\mathrm{d}\omega}{2\pi}}\omega f_\lambda(\omega)\left[1-\mathrm{e}^{\mathrm{i}(\omega-\boldsymbol{\Omega}_{\mathrm{eff}})t}\right]\boldsymbol{D}^{\mathrm{R}}(\omega)\boldsymbol{\Gamma}'_\lambda\boldsymbol{\alpha}. \qquad \text{(A.133)}
\end{aligned}
$$

Then, let us think about the matrix forms more carefully, and see if we can get rid of some of the terms. Recall, that the important matrix structures appearing in the

expressions are

$$\boldsymbol{\alpha} = \begin{pmatrix} 0 & \mathrm{i} \\ -\mathrm{i} & 0 \end{pmatrix}; \qquad \boldsymbol{\Lambda}_0 = \begin{pmatrix} \Lambda_0 & 0 \\ 0 & 0 \end{pmatrix}; \qquad \boldsymbol{\Gamma}'_{(\lambda)} = \begin{pmatrix} \Gamma'_{(\lambda)} & 0 \\ 0 & 0 \end{pmatrix}. \tag{A.134}$$

By evaluating simple matrix products we can conclude that

$$\boldsymbol{\alpha}\frac{\boldsymbol{\Gamma}'_{(\lambda)}}{2}\boldsymbol{\alpha}\boldsymbol{\Lambda}_0 = 0\,; \quad \boldsymbol{\alpha}\frac{\boldsymbol{\Gamma}'_{(\lambda)}}{2}\boldsymbol{\alpha}\frac{\boldsymbol{\Gamma}'_{(\lambda)}}{2} = 0\,; \quad \boldsymbol{\Lambda}_0\boldsymbol{\alpha}\frac{\boldsymbol{\Gamma}'_{(\lambda)}}{2}\boldsymbol{\alpha} = 0\,; \quad \frac{\boldsymbol{\Gamma}'_{(\lambda)}}{2}\boldsymbol{\alpha}\frac{\boldsymbol{\Gamma}'_{(\lambda)}}{2}\boldsymbol{\alpha} = 0. \tag{A.135}$$

Then, using these reductions in Eq. (A.133) gives

$$\begin{aligned} &\mathrm{i}\frac{\mathrm{d}\boldsymbol{D}^<(t,t)}{\mathrm{d}t} - \boldsymbol{\alpha}\boldsymbol{\Omega}\boldsymbol{D}^<(t,t) + \boldsymbol{D}^<(t,t)\boldsymbol{\Omega}\boldsymbol{\alpha} - \boldsymbol{\alpha}\boldsymbol{\Lambda}_0\boldsymbol{D}^<(t,t) \\ &+\mathrm{i}\boldsymbol{\alpha}\frac{\boldsymbol{\Gamma}'_0}{2}\boldsymbol{\alpha}\boldsymbol{\Omega}\boldsymbol{D}^<(t,t) + \boldsymbol{D}^<(t,t)\boldsymbol{\Lambda}_0\boldsymbol{\alpha} + \mathrm{i}\boldsymbol{D}^<(t,t)\boldsymbol{\Omega}\boldsymbol{\alpha}\frac{\boldsymbol{\Gamma}'_0}{2}\boldsymbol{\alpha} \\ = \;& -\mathrm{i}\sum_\lambda \widetilde{\int \frac{\mathrm{d}\omega}{2\pi}} \omega f_\lambda(\omega)\left\{\boldsymbol{\alpha}\boldsymbol{\Gamma}'_\lambda\boldsymbol{D}^{\mathrm{A}}(\omega)\left[1 - \mathrm{e}^{-\mathrm{i}(\omega-\boldsymbol{\Omega}^\dagger_{\mathrm{eff}})t}\right] - \left[1 - \mathrm{e}^{\mathrm{i}(\omega-\boldsymbol{\Omega}_{\mathrm{eff}})t}\right]\boldsymbol{D}^{\mathrm{R}}(\omega)\boldsymbol{\Gamma}'_\lambda\boldsymbol{\alpha}\right\}. \end{aligned} \tag{A.136}$$

We may couple the terms on the left-hand side involving a lesser Green's function in a little far-fetched form as

$$\begin{aligned} &\mathrm{i}\frac{\mathrm{d}\boldsymbol{D}^<(t,t)}{\mathrm{d}t} - \left[\left(1 - \mathrm{i}\boldsymbol{\alpha}\frac{\boldsymbol{\Gamma}'_0}{2}\right)\boldsymbol{\alpha}\boldsymbol{\Omega} + \boldsymbol{\alpha}\boldsymbol{\Lambda}_0\right]\boldsymbol{D}^<(t,t) \\ &+\boldsymbol{D}^<(t,t)\left[\boldsymbol{\Omega}\boldsymbol{\alpha}\left(1 + \mathrm{i}\frac{\boldsymbol{\Gamma}'_0}{2}\boldsymbol{\alpha}\right) + \boldsymbol{\Lambda}_0\boldsymbol{\alpha}\right] \\ = \;& -\mathrm{i}\sum_\lambda \widetilde{\int \frac{\mathrm{d}\omega}{2\pi}} \omega f_\lambda(\omega)\left\{\boldsymbol{\alpha}\boldsymbol{\Gamma}'_\lambda\boldsymbol{D}^{\mathrm{A}}(\omega)\left[1 - \mathrm{e}^{-\mathrm{i}(\omega-\boldsymbol{\Omega}^\dagger_{\mathrm{eff}})t}\right] - \left[1 - \mathrm{e}^{\mathrm{i}(\omega-\boldsymbol{\Omega}_{\mathrm{eff}})t}\right]\boldsymbol{D}^{\mathrm{R}}(\omega)\boldsymbol{\Gamma}'_\lambda\boldsymbol{\alpha}\right\}. \end{aligned} \tag{A.137}$$

The reason for this is that

$$\begin{aligned} \left(1 - \mathrm{i}\boldsymbol{\alpha}\frac{\boldsymbol{\Gamma}'_0}{2}\right)\boldsymbol{\alpha}\boldsymbol{\Omega} + \boldsymbol{\alpha}\boldsymbol{\Lambda}_0 &= \frac{1}{\boldsymbol{\alpha} + \frac{\mathrm{i}}{2}\boldsymbol{\Gamma}'_0}\left(\boldsymbol{\Omega} + \boldsymbol{\Lambda}_0\right) = \boldsymbol{\Omega}_{\mathrm{eff}}, \\ \boldsymbol{\Omega}\boldsymbol{\alpha}\left(1 + \mathrm{i}\frac{\boldsymbol{\Gamma}'_0}{2}\boldsymbol{\alpha}\right) + \boldsymbol{\Lambda}_0\boldsymbol{\alpha} &= \left(\boldsymbol{\Omega} + \boldsymbol{\Lambda}_0\right)\frac{1}{\boldsymbol{\alpha} - \frac{\mathrm{i}}{2}\boldsymbol{\Gamma}'_0} = \boldsymbol{\Omega}^\dagger_{\mathrm{eff}} \end{aligned} \tag{A.138}$$

which can be checked by calculating the matrix products and inverses. Then, the remaining differential equation takes the final form

$$\begin{aligned} &\mathrm{i}\frac{\mathrm{d}\boldsymbol{D}^<(t,t)}{\mathrm{d}t} - \boldsymbol{\Omega}_{\mathrm{eff}}\boldsymbol{D}^<(t,t) + \boldsymbol{D}^<(t,t)\boldsymbol{\Omega}^\dagger_{\mathrm{eff}} \\ = \;& -\mathrm{i}\sum_\lambda \widetilde{\int \frac{\mathrm{d}\omega}{2\pi}} \omega f_\lambda(\omega)\left\{\boldsymbol{\alpha}\boldsymbol{\Gamma}'_\lambda\boldsymbol{D}^{\mathrm{A}}(\omega)\left[1 - \mathrm{e}^{-\mathrm{i}(\omega-\boldsymbol{\Omega}^\dagger_{\mathrm{eff}})t}\right] - \left[1 - \mathrm{e}^{\mathrm{i}(\omega-\boldsymbol{\Omega}_{\mathrm{eff}})t}\right]\boldsymbol{D}^{\mathrm{R}}(\omega)\boldsymbol{\Gamma}'_\lambda\boldsymbol{\alpha}\right\}. \end{aligned} \tag{A.139}$$

This takes exactly the same form as in the derivation of the electronic case, see Eq. (A.41).

Now, for solving the remaining differential equation, it is convenient to start by making a transformation

$$\boldsymbol{D}^<(t,t) = \mathrm{e}^{-\mathrm{i}\boldsymbol{\Omega}_{\mathrm{eff}}t}\widetilde{\boldsymbol{D}}^<(t,t)\mathrm{e}^{\mathrm{i}\boldsymbol{\Omega}_{\mathrm{eff}}^\dagger t}. \tag{A.140}$$

When evaluating the derivative of this product and canceling terms, the left-hand side of Eq. (2.207) simply becomes $\mathrm{e}^{-\mathrm{i}\boldsymbol{\Omega}_{\mathrm{eff}}t}\mathrm{i}\frac{\mathrm{d}\widetilde{\boldsymbol{D}}^<(t,t)}{\mathrm{d}t}\mathrm{e}^{\mathrm{i}\boldsymbol{\Omega}_{\mathrm{eff}}^\dagger t}$. We can then, accordingly, multiply both sides of the equation from left and right with the exponentials to get

$$\begin{aligned}
&\frac{\mathrm{d}\widetilde{\boldsymbol{D}}^<(t,t)}{\mathrm{d}t} \\
&= \sum_{\lambda=L,R}\int\frac{\mathrm{d}\omega}{2\pi}\theta(\omega_c-|\omega|)\omega f_\lambda(\omega)\mathrm{e}^{\mathrm{i}\boldsymbol{\Omega}_{\mathrm{eff}}t}\left[\boldsymbol{D}^{\mathrm{R}}(\omega)\boldsymbol{\Gamma}'_{0,\lambda}\boldsymbol{\alpha}-\boldsymbol{\alpha}\boldsymbol{\Gamma}'_{0,\lambda}\boldsymbol{D}^{\mathrm{A}}(\omega)\right]\mathrm{e}^{-\mathrm{i}\boldsymbol{\Omega}_{\mathrm{eff}}^\dagger t} \\
&- \sum_{\lambda=L,R}\int\frac{\mathrm{d}\omega}{2\pi}\theta(\omega_c-|\omega|)\omega f_\lambda(\omega)\left[\boldsymbol{D}^{\mathrm{R}}(\omega)\boldsymbol{\Gamma}'_{0,\lambda}\boldsymbol{\alpha}\mathrm{e}^{\mathrm{i}(\omega-\boldsymbol{\Omega}_{\mathrm{eff}}^\dagger)t}-\mathrm{e}^{-\mathrm{i}(\omega-\boldsymbol{\Omega}_{\mathrm{eff}})t}\boldsymbol{\alpha}\boldsymbol{\Gamma}'_{0,\lambda}\boldsymbol{D}^{\mathrm{A}}(\omega)\right].
\end{aligned} \tag{A.141}$$

Before we start integrating over t, recall the matrix structures

$$\boldsymbol{D}^{\mathrm{R}}(\omega) = \frac{1}{\omega-\boldsymbol{\Omega}_{\mathrm{eff}}}\frac{1}{\boldsymbol{\alpha}+\frac{\mathrm{i}}{2}\boldsymbol{\Gamma}'_0}\,;\quad \boldsymbol{D}^{\mathrm{A}}(\omega) = \frac{1}{\boldsymbol{\alpha}-\frac{\mathrm{i}}{2}\boldsymbol{\Gamma}'_0}\frac{1}{\omega-\boldsymbol{\Omega}_{\mathrm{eff}}^\dagger}. \tag{A.142}$$

In Eq. (A.141) we have terms such as

$$\boldsymbol{D}^{\mathrm{R}}(\omega)\boldsymbol{\Gamma}'_{0,\lambda}\boldsymbol{\alpha} = \frac{1}{\omega-\boldsymbol{\Omega}_{\mathrm{eff}}}\frac{1}{\boldsymbol{\alpha}+\frac{\mathrm{i}}{2}\boldsymbol{\Gamma}'_0}\boldsymbol{\Gamma}'_{0,\lambda}\boldsymbol{\alpha}\,;\quad \boldsymbol{\alpha}\boldsymbol{\Gamma}'_{0,\lambda}\boldsymbol{D}^{\mathrm{A}}(\omega) = \boldsymbol{\alpha}\boldsymbol{\Gamma}'_{0,\lambda}\frac{1}{\boldsymbol{\alpha}-\frac{\mathrm{i}}{2}\boldsymbol{\Gamma}'_0}\frac{1}{\omega-\boldsymbol{\Omega}_{\mathrm{eff}}^\dagger}, \tag{A.143}$$

where, conveniently,

$$\boldsymbol{\alpha}\boldsymbol{\Gamma}'_{0,\lambda}\frac{1}{\boldsymbol{\alpha}-\frac{\mathrm{i}}{2}\boldsymbol{\Gamma}'_0} = \frac{1}{\boldsymbol{\alpha}+\frac{\mathrm{i}}{2}\boldsymbol{\Gamma}'_0}\boldsymbol{\Gamma}'_{0,\lambda}\boldsymbol{\alpha} \tag{A.144}$$

which can be checked by simply evaluating the matrix products and inverses. Then, looking at the first row of Eq. (A.141), we can perform the integration over t by using the formula in Eq. (A.47). The second row of Eq. (A.141) is simple to integrate over t since there is only one exponential depending on time in each term.

After integration we arrive at

$$\begin{aligned}\widetilde{\boldsymbol{D}}^{<}(t,t)-\widetilde{\boldsymbol{D}}^{<}(0,0^{+}) &= -\mathrm{i}\sum_{\lambda=L,R}\int\frac{\mathrm{d}\omega}{2\pi}\theta(\omega_c-|\omega|)\omega f_\lambda(\omega)\Big\{\\ &\quad \mathrm{e}^{\mathrm{i}\boldsymbol{\Omega}_{\mathrm{eff}}t}\frac{1}{\omega-\boldsymbol{\Omega}_{\mathrm{eff}}}\frac{1}{\boldsymbol{\alpha}+\frac{\mathrm{i}}{2}\boldsymbol{\Gamma}'_0}\boldsymbol{\Gamma}'_{0,\lambda}\frac{1}{\boldsymbol{\alpha}-\frac{\mathrm{i}}{2}\boldsymbol{\Gamma}'_0}\frac{1}{\omega-\boldsymbol{\Omega}^{\dagger}_{\mathrm{eff}}}\mathrm{e}^{-\mathrm{i}\boldsymbol{\Omega}^{\dagger}_{\mathrm{eff}}t}\\ &\quad +\frac{1}{\omega-\boldsymbol{\Omega}_{\mathrm{eff}}}\frac{1}{\boldsymbol{\alpha}+\frac{\mathrm{i}}{2}\boldsymbol{\Gamma}'_0}\boldsymbol{\Gamma}'_{0,\lambda}\frac{1}{\boldsymbol{\alpha}-\frac{\mathrm{i}}{2}\boldsymbol{\Gamma}'_0}\frac{1}{\omega-\boldsymbol{\Omega}^{\dagger}_{\mathrm{eff}}}\\ &\quad -\frac{1}{\omega-\boldsymbol{\Omega}_{\mathrm{eff}}}\frac{1}{\boldsymbol{\alpha}+\frac{\mathrm{i}}{2}\boldsymbol{\Gamma}'_0}\boldsymbol{\Gamma}'_{0,\lambda}\frac{1}{\boldsymbol{\alpha}-\frac{\mathrm{i}}{2}\boldsymbol{\Gamma}'_0}\frac{1}{\omega-\boldsymbol{\Omega}^{\dagger}_{\mathrm{eff}}}\mathrm{e}^{\mathrm{i}(\omega-\boldsymbol{\Omega}^{\dagger}_{\mathrm{eff}})t}\\ &\quad -\mathrm{e}^{-\mathrm{i}(\omega-\boldsymbol{\Omega}_{\mathrm{eff}})t}\frac{1}{\omega-\boldsymbol{\Omega}_{\mathrm{eff}}}\frac{1}{\boldsymbol{\alpha}+\frac{\mathrm{i}}{2}\boldsymbol{\Gamma}'_0}\boldsymbol{\Gamma}'_{0,\lambda}\frac{1}{\boldsymbol{\alpha}-\frac{\mathrm{i}}{2}\boldsymbol{\Gamma}'_0}\frac{1}{\omega-\boldsymbol{\Omega}^{\dagger}_{\mathrm{eff}}}\Big\}.\end{aligned} \tag{A.145}$$

On the left-hand side we have the initial-state Green's function (at $t = 0$). We are working in the partitioned scheme, i.e., the systems of different temperatures are coupled at $t = 0$, so the initial condition should be equal to the uncoupled Green's function as in Eq. (A.87) but for the indices in the central region:

$$\widetilde{\boldsymbol{D}}^{<}(0,0^{+}) = \boldsymbol{D}^{<}(0,0^{+}) = -\mathrm{i}\boldsymbol{\alpha}f_C(\boldsymbol{\Omega}\boldsymbol{\alpha}). \tag{A.146}$$

Here f_C gives the thermal distribution according to which the central system is prepared before it is connected to the reservoirs, and $\boldsymbol{\Omega}\boldsymbol{\alpha}$ is correspondingly the uncoupled Hamiltonian. Now, in Eq. (A.145) we may transform back from $\widetilde{\boldsymbol{D}}^{<}(t,t)$ to $\boldsymbol{D}^{<}(t,t)$ by multiplying with the exponentials from left and right and obtain our final result

$$\begin{aligned}\mathrm{i}\boldsymbol{D}^{<}(t,t) &= \mathrm{e}^{-\mathrm{i}\boldsymbol{\Omega}_{\mathrm{eff}}t}\boldsymbol{\alpha}f_C(\boldsymbol{\Omega}\boldsymbol{\alpha})\mathrm{e}^{\mathrm{i}\boldsymbol{\Omega}^{\dagger}_{\mathrm{eff}}t}\\ &\quad +\sum_{\lambda=L,R}\int\frac{\mathrm{d}\omega}{2\pi}\theta(\omega_c-|\omega|)\omega f_\lambda(\omega)\left[\mathbf{1}-\mathrm{e}^{\mathrm{i}(\omega-\boldsymbol{\Omega}_{\mathrm{eff}})t}\right]\\ &\quad \times\frac{1}{\omega-\boldsymbol{\Omega}_{\mathrm{eff}}}\frac{1}{\boldsymbol{\alpha}+\frac{\mathrm{i}}{2}\boldsymbol{\Gamma}'_0}\boldsymbol{\Gamma}'_{0,\lambda}\frac{1}{\boldsymbol{\alpha}-\frac{\mathrm{i}}{2}\boldsymbol{\Gamma}'_0}\frac{1}{\omega-\boldsymbol{\Omega}^{\dagger}_{\mathrm{eff}}}\left[\mathbf{1}-\mathrm{e}^{-\mathrm{i}(\omega-\boldsymbol{\Omega}^{\dagger}_{\mathrm{eff}})t}\right]\end{aligned} \tag{A.147}$$

which can be written as Eq. (2.209) in main text by introducing the spectral function $\boldsymbol{B}_\lambda(\omega)$ in Eq. (2.211).

Bibliography

[I] R. Tuovinen, R. van Leeuwen, E. Perfetto, and G. Stefanucci, "Time-dependent Landauer–Büttiker formula for transient dynamics", J. Phys.: Conf. Ser. **427**, 012014 (2013).

[II] R. Tuovinen, E. Perfetto, G. Stefanucci, and R. van Leeuwen, "Time-dependent Landauer–Büttiker formula: Application to transient dynamics in graphene nanoribbons", Phys. Rev. B **89**, 085131 (2014).

[III] C. G. Rocha, R. Tuovinen, R. van Leeuwen, and P. Koskinen, "Curvature in graphene nanoribbons generates temporally and spatially focused electric currents", Nanoscale **7**, 8627 (2015).

[IV] R. Tuovinen, R. van Leeuwen, E. Perfetto, and G. Stefanucci, "Time-dependent Landauer–Büttiker formalism for superconducting junctions at arbitrary temperatures", J. Phys.: Conf. Ser. **696**, 012016 (2016).

[V] R. Tuovinen, N. Säkkinen, D. Karlsson, G. Stefanucci, and R. van Leeuwen, "Phononic heat transport in the transient regime: An analytic solution", Phys. Rev. B, *accepted* (2016), arXiv:1604.02298.

[6] A. Aviram and M. A. Ratner, "Molecular rectifiers", Chem. Phys. Lett. **29**, 277 (1974).

[7] C. Joachim, J. K. Gimzewski, R. R. Schlittler, and C. Chavy, "Electronic Transparence of a Single C60 Molecule", Phys. Rev. Lett. **74**, 2102 (1995).

[8] M. A. Reed, C. Zhou, C. J. Muller, T. P. Burgin, and J. M. Tour, "Conductance of a Molecular Junction", Science **278**, 252 (1997).

[9] M. Elbing et al., "A single-molecule diode", Proc. Natl. Acad. Sci. **102**, 8815 (2005).

[10] G. Binnig and H. Rohrer, "Scanning tunneling microscopy", IBM J. Res. Des. **30**, 355 (1986).

[11] G. Binnig, "Scanning Tunneling Microscopy – From Birth to Adolescence", in *Nobel Lectures, Physics 1981-1990* (World Scientific Publishing Co, Singapore, 1993).

[12] G. Binnig, C. F. Quate, and C. Gerber, "Atomic Force Microscope", Phys. Rev. Lett. **56**, 930 (1986).

[13] I. K. Yanson, "Nonlinear effects in the electric conductivity of point junctions and electron-phonon interaction in normal metals", Sov. Phys. JETP **39**, 506 (1974).

[14] J. Langan and P. Hansma, "Can the concentration of surface species be measured with inelastic electron tunneling?", Surf. Sci. **52**, 211 (1975).

[15] M. A. Reed, "Inelastic electron tunneling spectroscopy", Mater. Today **11**, 46 (2008).

[16] W. B. Shockley, "Transistor Technology Evokes New Physics", in *Nobel Lectures, Physics 1942-1962* (Elsevier Publishing Company, Amsterdam, 1964).

[17] G. E. Moore, "Cramming More Components onto Integrated Circuits", Electronics **38**, 114 (1965).

[18] T. A. Edison, "Electrical indicator", Patent US307031 (Oct. 21, 1884).

[19] J. A. Fleming, "Instrument for converting alternating electric currents into continuous currents", Patent US803684 (Nov. 7, 1905).

[20] W. Jacobi, "Halbleiterverstaerker", (Siemens AG) Patent DE833366 (June 30, 1952).

[21] G. Boone, "Computing systems CPU", (Texas Instruments) Patent US3757306 (Aug. 31, 1971).

[22] F. Faggin, "Power supply settable bi-stable circuit", (Intel) Patent US3753011 (Aug. 14, 1973).

[23] F. Faggin, M. Hoff, and S. Mazor, "Memory system for a multi chip digital computer", (Intel) Patent US3821715 (June 28, 1974).

[24] G. P. Hyatt, "Single chip integrated circuit computer architecture", Patent US4942516 (June 17, 1988).

[25] R. Kurzweil, *The age of spiritual machines* (Viking, 1999).

[26] K. E. Drexler, *Engines of Creation: The Coming Era of Nanotechnology* (Fourth Estate, 1986).

[27] K. E. Drexler, *Nanosystems: Molecular Machinery, Manufacturing, and Computation* (Wiley, 1992).

[28] M. E. Vance et al., "Nanotechnology in the real world: Redeveloping the nanomaterial consumer products inventory", Beilstein J. Nanotechnol. **6**, 1769 (2015).

[29] N. J. Tao, "Electron transport in molecular junctions", Nat. Nanotechnol. **1**, 173 (2006).

[30] Y.-M. Lin et al., "Operation of Graphene Transistors at Gigahertz Frequencies", Nano Lett. **9**, 422 (2009).

[31] A. D. Franklin and Z. Chen, "Length scaling of carbon nanotube transistors", Nat. Nanotechnol. **5**, 858 (2010).

[32] P. Hohenberg and W. Kohn, "Inhomogeneous Electron Gas", Phys. Rev. **136**, B864 (1964).

[33] W. Kohn and L. J. Sham, "Self-Consistent Equations Including Exchange and Correlation Effects", Phys. Rev. **140**, A1133 (1965).

[34] E. Runge and E. K. U. Gross, "Density-Functional Theory for Time-Dependent Systems", Phys. Rev. Lett. **52**, 997 (1984).

[35] J. Schwinger, "Brownian Motion of a Quantum Oscillator", J. Math. Phys. **2**, 407 (1961).

[36] G. Baym and L. P. Kadanoff, "Conservation Laws and Correlation Functions", Phys. Rev. **124**, 287 (1961).

[37] G. Baym, "Self-Consistent Approximations in Many-Body Systems", Phys. Rev. **127**, 1391 (1962).

[38] L. P. Kadanoff and G. Baym, *Quantum Statistical Mechanics* (Benjamin, 1962).

[39] L. V. Keldysh, "Diagram Technique for Nonequilibrium Processes", Sov. Phys. JETP **20**, 1018 (1965).

[40] L. Hedin, "New Method for Calculating the One-Particle Green's Function with Application to the Electron-Gas Problem", Phys. Rev. **139**, A796 (1965).

[41] D. C. Langreth and J. W. Wilkins, "Theory of Spin Resonance in Dilute Magnetic Alloys", Phys. Rev. B **6**, 3189 (1972).

[42] P. Danielewicz, "Quantum theory of nonequilibrium processes, I", Ann. Phys. **152**, 239 (1984).

[43] S. R. White, "Density matrix formulation for quantum renormalization groups", Phys. Rev. Lett. **69**, 2863 (1992).

[44] T. Tokuyasu, M. Kamal, and G. Murthy, "Numerical renormalization group for finite Fermi systems", Phys. Rev. Lett. **71**, 4202 (1993).

[45] A. Georges and G. Kotliar, "Hubbard model in infinite dimensions", Phys. Rev. B **45**, 6479 (1992).

[46] J. K. Freericks, M. Jarrell, and D. J. Scalapino, "Holstein model in infinite dimensions", Phys. Rev. B **48**, 6302 (1993).

[47] A. Georges, G. Kotliar, W. Krauth, and M. J. Rozenberg, "Dynamical mean-field theory of strongly correlated fermion systems and the limit of infinite dimensions", Rev. Mod. Phys. **68**, 13 (1996).

[48] M. Caffarel and P. Claverie, "Development of a pure diffusion quantum Monte Carlo method using a full generalized Feynman–Kac formula. I. Formalism", J. Chem. Phys. **88**, 1088 (1988).

[49] A. Korzeniowski, J. L. Fry, D. E. Orr, and N. G. Fazleev, "Feynman–Kac path-integral calculation of the ground-state energies of atoms", Phys. Rev. Lett. **69**, 893 (1992).

[50] E. Khosravi, G. Stefanucci, S. Kurth, and E. Gross, "Bound states in time-dependent quantum transport: oscillations and memory effects in current and density", Phys. Chem. Chem. Phys. **11**, 4535 (2009).

[51] E. Perfetto, G. Stefanucci, and M. Cini, "Time-dependent transport in graphene nanoribbons", Phys. Rev. B **82**, 035446 (2010).

[52] D. Vieira, K. Capelle, and C. A. Ullrich, "Physical signatures of discontinuities of the time-dependent exchange-correlation potential", Phys. Chem. Chem. Phys. **11**, 4647 (2009).

[53] B. Wang et al., "Transient dynamics of magnetic Co-graphene systems", Nanoscale **7**, 10030 (2015).

[54] S. Kurth, G. Stefanucci, E. Khosravi, C. Verdozzi, and E. K. U. Gross, "Dynamical Coulomb Blockade and the Derivative Discontinuity of Time-Dependent Density Functional Theory", Phys. Rev. Lett. **104**, 236801 (2010).

[55] F. Foieri and L. Arrachea, "Ac-dc voltage profile and four point impedance of a quantum driven system", Phys. Rev. B **82**, 125434 (2010).

[56] L. Arrachea, E. R. Mucciolo, C. Chamon, and R. B. Capaz, "Microscopic model of a phononic refrigerator", Phys. Rev. B **86**, 125424 (2012).

[57] H. Ness and L. K. Dash, "Nonequilibrium quantum transport in fully interacting single-molecule junctions", Phys. Rev. B **84**, 235428 (2011).

[58] H. O. Wijewardane and C. A. Ullrich, "Time-Dependent Kohn-Sham Theory with Memory", Phys. Rev. Lett. **95**, 086401 (2005).

[59] P. Myöhänen, A. Stan, G. Stefanucci, and R. van Leeuwen, "A many-body approach to quantum transport dynamics: Initial correlations and memory effects", EPL **84**, 67001 (2008).

[60] A.-M. Uimonen et al., "Comparative study of many-body perturbation theory and time-dependent density functional theory in the out-of-equilibrium Anderson model", Phys. Rev. B **84**, 115103 (2011).

[61] P. Myöhänen, R. Tuovinen, T. Korhonen, G. Stefanucci, and R. van Leeuwen, "Image charge dynamics in time-dependent quantum transport", Phys. Rev. B **85**, 075105 (2012).

[62] S. Latini, E. Perfetto, A.-M. Uimonen, R. van Leeuwen, and G. Stefanucci, "Charge dynamics in molecular junctions: Nonequilibrium Green's function approach made fast", Phys. Rev. B **89**, 075306 (2014).

[63] C. Verdozzi, G. Stefanucci, and C.-O. Almbladh, "Classical Nuclear Motion in Quantum Transport", Phys. Rev. Lett. **97**, 046603 (2006).

[64] D. Segal, A. Nitzan, and P. Hänggi, "Thermal conductance through molecular wires", J. Chem. Phys. **119**, 6840 (2003).

[65] M. Galperin, M. A. Ratner, and A. Nitzan, "Molecular transport junctions: vibrational effects", J. Phys. Condens. Matter **19**, 103201 (2007).

[66] Y. Dubi and M. Di Ventra, "*Colloquium*: Heat flow and thermoelectricity in atomic and molecular junctions", Rev. Mod. Phys. **83**, 131 (2011).

[67] I. Söllner et al., "Deterministic photon–emitter coupling in chiral photonic circuits", Nat. Nanotechnol. **10**, 775 (2015).

[68] A. Liddle, *Introduction to Modern Cosmology*, 2nd ed. (Wiley, 2003).

[69] J. M. Cline, M. Joyce, and K. Kainulainen, "Supersymmetric electroweak baryogenesis in the WKB approximation", Phys. Lett. B **417**, 79 (1998).

[70] J. M. Cline and K. Kainulainen, "New Source for Electroweak Baryogenesis in the Minimal Supersymmetric Standard Model", Phys. Rev. Lett. **85**, 5519 (2000).

[71] R. Shankar, *Principles of Quantum Mechanics*, 2nd ed. (Springer, 1994).

[72] E. Schrödinger, "An Undulatory Theory of the Mechanics of Atoms and Molecules", Phys. Rev. **28**, 1049 (1926).

[73] G. Stefanucci and R. van Leeuwen, *Nonequilibrium Many-Body Theory of Quantum Systems: A Modern Introduction* (Cambridge University Press, 2013).

[74] I. Mäkinen and K. Tuominen, *Lecture notes in Quantum Mechanics I* (University of Jyväskylä, Department of Physics, 2012).

[75] N. E. Dahlen and R. van Leeuwen, "Solving the Kadanoff-Baym Equations for Inhomogeneous Systems: Application to Atoms and Molecules", Phys. Rev. Lett. **98**, 153004 (2007).

[76] R. van Leeuwen, "Causality and Symmetry in Time-Dependent Density-Functional Theory", Phys. Rev. Lett. **80**, 1280 (1998).

[77] R. van Leeuwen, N. E. Dahlen, G. Stefanucci, C.-O. Almbladh, and U. von Barth, "Introcution to the Keldysh Formalism", in *Time-dependent Density Functional Theory*, edited by M. A. L. Marques et al. (Springer, Berlin, 2006).

[78] W. Pauli, "The Connection Between Spin and Statistics", Phys. Rev. **58**, 716 (1940).

[79] R. Pariser and R. G. Parr, "A Semi-Empirical Theory of the Electronic Spectra and Electronic Structure of Complex Unsaturated Molecules. I.", J. Chem. Phys. **21**, 466 (1953).

[80] J. A. Pople, "Electron interaction in unsaturated hydrocarbons", Trans. Faraday Soc. **49**, 1375 (1953).

[81] W. Liang et al., "Fabry-Perot interference in a nanotube electron waveguide", Nature **411**, 665 (2001).

[82] J. Baringhaus et al., "Exceptional ballistic transport in epitaxial graphene nanoribbons", Nature **506**, 349 (2014).

[83] A. H. Castro Neto, F. Guinea, N. M. R. Peres, K. S. Novoselov, and A. K. Geim, "The electronic properties of graphene", Rev. Mod. Phys. **81**, 109 (2009).

[84] I. Bloch, J. Dalibard, and W. Zwerger, "Many-body physics with ultracold gases", Rev. Mod. Phys. **80**, 885 (2008).

[85] U. Schneider et al., "Fermionic transport and out-of-equilibrium dynamics in a homogeneous Hubbard model with ultracold atoms", Nat. Phys. **8**, 213 (2012).

[86] J. Ibañez-Azpiroz, A. Eiguren, A. Bergara, G. Pettini, and M. Modugno, "Tight-binding models for ultracold atoms in honeycomb optical lattices", Phys. Rev. A **87**, 011602 (2013).

[87] M. I. Katsnelson, *Graphene: carbon in two dimensions* (Cambridge University Press, 2012).

[88] S. R. Bahn and K. W. Jacobsen, "An object-oriented scripting interface to a legacy electronic structure code", Comput. Sci. Eng. **4**, 56 (2002).

[89] Y. Hancock, A. Uppstu, K. Saloriutta, A. Harju, and M. J. Puska, "Generalized tight-binding transport model for graphene nanoribbon-based systems", Phys. Rev. B **81**, 245402 (2010).

[90] J. P. Robinson, H. Schomerus, L. Oroszlány, and V. I. Fal'ko, "Adsorbate-Limited Conductivity of Graphene", Phys. Rev. Lett. **101**, 196803 (2008).

[91] R. Landauer, "Spatial Variation of Currents and Fields Due to Localized Scatterers in Metallic Conduction", IBM J. Res. Dev. **1**, 233 (1957).

[92] M. Büttiker, "Four-Terminal Phase-Coherent Conductance", Phys. Rev. Lett. **57**, 1761 (1986).

[93] C. Caroli, R. Combescot, P. Nozieres, and D. Saint-James, "Direct calculation of the tunneling current", J. Phys. C **4**, 916 (1971).

[94] C. Caroli, R. Combescot, D. Lederer, P. Nozieres, and D. Saint-James, "A direct calculation of the tunnelling current. II. Free electron description", J. Phys. C **4**, 2598 (1971).

[95] M. Cini, "Time-dependent approach to electron transport through junctions: General theory and simple applications", Phys. Rev. B **22**, 5887 (1980).

[96] G. Stefanucci and C.-O. Almbladh, "Time-dependent partition-free approach in resonant tunneling systems", Phys. Rev. B **69**, 195318 (2004).

[97] Y. Meir and N. S. Wingreen, "Landauer formula for the current through an interacting electron region", Phys. Rev. Lett. **68**, 2512 (1992).

[98] H. M. Pastawski, "Classical and quantum transport from generalized Landauer-Büttiker equations", Phys. Rev. B **44**, 6329 (1991).

[99] A.-P. Jauho, N. S. Wingreen, and Y. Meir, "Time-dependent transport in interacting and noninteracting resonant-tunneling systems", Phys. Rev. B **50**, 5528 (1994).

[100] E. Perfetto, G. Stefanucci, and M. Cini, "Spin-flip scattering in time-dependent transport through a quantum dot: Enhanced spin-current and inverse tunneling magnetoresistance", Phys. Rev. B **78**, 155301 (2008).

[101] M. Ridley, A. MacKinnon, and L. Kantorovich, "Current through a multilead nanojunction in response to an arbitrary time-dependent bias", Phys. Rev. B **91**, 125433 (2015).

[102] G. Stefanucci and C.-O. Almbladh, "Time-dependent quantum transport: An exact formulation based on TDDFT", EPL **67**, 14 (2004).

[103] S. Kurth, G. Stefanucci, C.-O. Almbladh, A. Rubio, and E. K. U. Gross, "Time-dependent quantum transport: A practical scheme using density functional theory", Phys. Rev. B **72**, 035308 (2005).

[104] Y. Kwok, Y. Zhang, and G. Chen, "Time-dependent density functional theory for quantum transport", Front. Phys. **9**, 698 (2014).

[105] P. Schmitteckert, "Nonequilibrium electron transport using the density matrix renormalization group method", Phys. Rev. B **70**, 121302 (2004).

[106] S. R. White and A. E. Feiguin, "Real-Time Evolution Using the Density Matrix Renormalization Group", Phys. Rev. Lett. **93**, 076401 (2004).

[107] A. J. Daley, C. Kollath, U. Schollwöck, and G. Vidal, "Time-dependent density-matrix renormalization-group using adaptive effective Hilbert spaces", J. Stat. Mech. Theor. Exp. **2004**, P04005 (2004).

[108] P. Schmitteckert, M. Dzierzawa, and P. Schwab, "Exact time-dependent density functional theory for impurity models", Phys. Chem. Chem. Phys. **15**, 5477 (2013).

[109] G. Vidal, "Classical Simulation of Infinite-Size Quantum Lattice Systems in One Spatial Dimension", Phys. Rev. Lett. **98**, 070201 (2007).

[110] R. Orús and G. Vidal, "Infinite time-evolving block decimation algorithm beyond unitary evolution", Phys. Rev. B **78**, 155117 (2008).

[111] M. Hyrkäs, V. Apaja, and M. Manninen, "Many-particle dynamics of bosons and fermions in quasi-one-dimensional flat-band lattices", Phys. Rev. A **87**, 023614 (2013).

[112] P. Myöhänen, A. Stan, G. Stefanucci, and R. van Leeuwen, "Kadanoff-Baym approach to quantum transport through interacting nanoscale systems: From the transient to the steady-state regime", Phys. Rev. B **80**, 115107 (2009).

[113] P. Myöhänen, "Many-particle theory for time-dependent quantum transport in nanostructures", JYFL Research Report 4/2012, PhD thesis (Department of Physics, University of Jyväskylä, 2012).

[114] A.-M. Uimonen, "Developments in Many-body Theory of Quantum Transport and Spectroscopy with Non-equilibrium Green's Functions and Time-dependent Density Functional Theory", JYFL Research Report 3/2015, PhD thesis (Department of Physics, University of Jyväskylä, 2015).

[115] A. Stan, N. E. Dahlen, and R. van Leeuwen, "Time propagation of the Kadanoff–Baym equations for inhomogeneous systems", J. Chem. Phys. **130**, 224101 (2009).

[116] D. C. Langreth, "Linear and Nonlinear Response Theory with Applications", in *Linear and Nonlinear Electron Transport in Solids*, edited by J. T. Devreese (Springer, 1976).

[117] J. C. Cuevas and E. Scheer, *Molecular Electronics: An Introduction to Theory and Experiment* (World Scientific, 2010).

[118] J. S. Toll, "Causality and the Dispersion Relation: Logical Foundations", Phys. Rev. **104**, 1760 (1956).

[119] V. Pegoraro and P. Slusallek, "On the Evaluation of the Complex-Valued Exponential Integral", J. Graphics, GPU, Game Tools **15**, 183 (2011).

[120] R. Tuovinen, E. Perfetto, G. Stefanucci, and R. van Leeuwen, *in preparation*.

[121] E. W. Weisstein, *Digamma function. From MathWorld—A Wolfram Web Resource*.

[122] E. W. Weisstein, *Hypergeometric function. From MathWorld—A Wolfram Web Resource*.

[123] R. Peierls, "Zur Theorie des Diamagnetismus von Leitungselektronen", Z. Phys. **80**, 763 (1933).

[124] J. M. Luttinger, "The Effect of a Magnetic Field on Electrons in a Periodic Potential", Phys. Rev. **84**, 814 (1951).

[125] K. Jiménez-García et al., "Peierls Substitution in an Engineered Lattice Potential", Phys. Rev. Lett. **108**, 225303 (2012).

[126] M. Graf and P. Vogl, "Electromagnetic fields and dielectric response in empirical tight-binding theory", Phys. Rev. B **51**, 4940 (1995).

[127] M. Cini, E. Perfetto, and G. Stefanucci, "Magnetic moments in biased quantum circuits", Phys. Rev. B **81**, 165202 (2010).

[128] Y. Nambu, "Quasi-Particles and Gauge Invariance in the Theory of Superconductivity", Phys. Rev. **117**, 648 (1960).

[129] J. C. Cuevas, A. Martín-Rodero, and A. L. Yeyati, "Hamiltonian approach to the transport properties of superconducting quantum point contacts", Phys. Rev. B **54**, 7366 (1996).

[130] A. P. Jauho, "Time-dependent transport in interacting mesoscopic systems", in *Progress in Nonequilibrium Green's Functions*, edited by M. Bonitz, R. Nareyka, and D. Semkat (World Scientific, 2000).

[131] G. Stefanucci, E. Perfetto, and M. Cini, "Time-dependent quantum transport with superconducting leads: a discrete-basis Kohn-Sham formulation and propagation scheme", Phys. Rev. B **81**, 115446 (2010).

[132] Z. Y. Zeng, B. Li, and F. Claro, "Electronic transport in hybrid mesoscopic structures: A nonequilibrium Green function approach", Phys. Rev. B **68**, 115319 (2003).

[133] Y. Xing, Q.-f. Sun, and J. Wang, "Response time of a normal-metal/superconductor hybrid system under a step-like pulse bias", Phys. Rev. B **75**, 125308 (2007).

[134] N. N. Bogoliubov, "A New Method in the Theory of Superconductivity. I", Sov. Phys. JETP **34**, 58 (1958).

[135] P. G. de Gennes, *Superconductivity of Metals and Alloys* (Benjamin, New York, 1966).

[136] G. Stefanucci, E. Perfetto, and M. Cini, "Time-dependent quantum transport with superconducting leads", J. Phys.: Conf. Ser. **220**, 012012 (2010).

[137] S. Kohler, J. Lehmann, and P. Hänggi, "Driven quantum transport on the nanoscale", Phys. Rep. **406**, 379 (2005).

[138] M. Moskalets, *Scattering Matrix Approach to Non-Stationary Quantum Transport* (Imperial College Press, 2012).

[139] M. Ridley, A. MacKinnon, and L. Kantorovich, "Fluctuating-bias controlled electron transport in molecular junctions", Phys. Rev. B **93**, 205408 (2016).

[140] E. C. Cuansing, H. Li, and J.-S. Wang, "Role of the on-site pinning potential in establishing quasi-steady-state conditions of heat transport in finite quantum systems", Phys. Rev. E **86**, 031132 (2012).

[141] N. Säkkinen, Y. Peng, H. Appel, and R. van Leeuwen, "Many-body Green's function theory for electron-phonon interactions: Ground state properties of the Holstein dimer", J. Chem. Phys. **143**, 234101 (2015).

[142] N. Säkkinen, Y. Peng, H. Appel, and R. van Leeuwen, "Many-body Green's function theory for electron-phonon interactions: The Kadanoff-Baym approach to spectral properties of the Holstein dimer", J. Chem. Phys. **143**, 234102 (2015).

[143] L. Arrachea and B. Rizzo, "Nonequilibrium Green's functions in the study of heat transport of driven nanomechanical systems", J. Phys.: Conf. Ser. **427**, 012012 (2013).

[144] M. Galperin, M. A. Ratner, and A. Nitzan, "On the Line Widths of Vibrational Features in Inelastic Electron Tunneling Spectroscopy", Nano Lett. **4**, 1605 (2004).

[145] M. Galperin, M. A. Ratner, and A. Nitzan, "Inelastic electron tunneling spectroscopy in molecular junctions: Peaks and dips", J. Chem. Phys. **121**, 11965 (2004).

[146] J.-S. Wang, B. K. Agarwalla, H. Li, and J. Thingna, "Nonequilibrium Green's function method for quantum thermal transport", Front. Phys. **9**, 673 (2014).

[147] K. Sääskilahti, J. Oksanen, and J. Tulkki, "Thermal balance and quantum heat transport in nanostructures thermalized by local Langevin heat baths", Phys. Rev. E **88**, 012128 (2013).

[148] A. Dhar, K. Saito, and P. Hänggi, "Nonequilibrium density-matrix description of steady-state quantum transport", Phys. Rev. E **85**, 011126 (2012).

[149] J. Hu, R.-X. Xu, and Y. Yan, "Communication: Padé spectrum decomposition of Fermi function and Bose function", J. Chem. Phys. **133**, 101106 (2010).

[150] J. Hu, M. Luo, F. Jiang, R.-X. Xu, and Y. Yan, "Padé spectrum decompositions of quantum distribution functions and optimal hierarchical equations of motion construction for quantum open systems", J. Chem. Phys. **134**, 244106 (2011).

[151] R. J. Hardy, "Energy-Flux Operator for a Lattice", Phys. Rev. **132**, 168 (1963).

[152] K. Sääskilahti, J. Oksanen, R. P. Linna, and J. Tulkki, "Thermal conduction and interface effects in nanoscale Fermi-Pasta-Ulam conductors", Phys. Rev. E **86**, 031107 (2012).

[153] K. Sääskilahti, J. Oksanen, and J. Tulkki, "Thermal balance and quantum heat transport in nanostructures thermalized by local Langevin heat baths", Phys. Rev. E **88**, 012128 (2013).

[154] T. Yamamoto and K. Watanabe, "Nonequilibrium Green's Function Approach to Phonon Transport in Defective Carbon Nanotubes", Phys. Rev. Lett. **96**, 255503 (2006).

[155] C. Froese Fischer, *The Hartree–Fock Method for Atoms: A Numerical Approach* (John Wiley and Sons, New York, 1977).

[156] J. Blaizot and G. Ripka, *Quantum Theory of Finite Systems* (The MIT Press, Cambridge, 1986).

[157] A. Castro and M. A. L. Marques, "Propagators for the Time-dependent Kohn–Sham Equations", in *Time-dependent Density Functional Theory*, edited by M. A. L. Marques et al. (Springer, Berlin, 2006).

[158] R. Tuovinen, *QPORT*, `www.bitbucket.org/rtuovine/qport`, code repository, 2016.

[159] R. Tuovinen, *WBPhonon*, `www.bitbucket.org/rtuovine/wbphonon`, code repository, 2016.

[160] K. Wakabayashi, Y. Takane, M. Yamamoto, and M. Sigrist, "Electronic transport properties of graphene nanoribbons", New J. Phys. **11**, 095016 (2009).

[161] H. Schomerus, "Effective contact model for transport through weakly-doped graphene", Phys. Rev. B **76**, 045433 (2007).

[162] Y. M. Blanter and I. Martin, "Transport through normal-metal–graphene contacts", Phys. Rev. B **76**, 155433 (2007).

[163] R. B. Blackman and J. W. Tukey, *Particular Pairs of Windows: In The Measurement of Power Spectra, From the Point of View of Communications Engineering* (Dover, 1959).

[164] K. Wakabayashi, K. Sasaki, T. Nakanishi, and T. Enoki, "Electronic states of graphene nanoribbons and analytical solutions", Sci. Tech. Adv. Mater. **11**, 054504 (2010).

[165] A. Kimouche et al., "Ultra-narrow metallic armchair graphene nanoribbons", Nat. Commun. **6**, 10177 (2015).

[166] X. Wang et al., "Room-Temperature All-Semiconducting Sub-10-nm Graphene Nanoribbon Field-Effect Transistors", Phys. Rev. Lett. **100**, 206803 (2008).

[167] M.-W. Lin et al., "Room-temperature high on/off ratio in suspended graphene nanoribbon field-effect transistors", Nanotechnology **22**, 265201 (2011).

[168] X. Li, X. Wang, L. Zhang, S. Lee, and H. Dai, "Chemically Derived, Ultrasmooth Graphene Nanoribbon Semiconductors", Science **319**, 1229 (2008).

[169] Y. Lu, C. A. Merchant, M. Drndić, and A. T. C. Johnson, "In Situ Electronic Characterization of Graphene Nanoconstrictions Fabricated in a Transmission Electron Microscope", Nano Lett. **11**, 5184 (2011).

[170] Q. Yan et al., "Intrinsic Current–Voltage Characteristics of Graphene Nanoribbon Transistors and Effect of Edge Doping", Nano Lett. **7**, 1469 (2007).

[171] G. Liang, "Performance Projections for Ballistic Graphene Nanoribbon Field-Effect Transistors", IEEE Trans. Electron Dev. **54**, 677 (2007).

[172] I. Meric et al., "Current saturation in zero-bandgap, top-gated graphene field-effect transistors", Nat. Nanotechnol. **3**, 654 (2008).

[173] Z. Li, H. Qian, J. Wu, B.-L. Gu, and W. Duan, "Role of Symmetry in the Transport Properties of Graphene Nanoribbons under Bias", Phys. Rev. Lett. **100**, 206802 (2008).

[174] J. Cai et al., "Atomically precise bottom-up fabrication of graphene nanoribbons", Nature **466**, 470 (2010).

[175] C.-A. Palma and P. Samori, "Blueprinting macromolecular electronics", Nat. Chem. **3**, 431 (2011).

[176] V. Barone, O. Hod, and G. E. Scuseria, "Electronic Structure and Stability of Semiconducting Graphene Nanoribbons", Nano Lett. **6**, 2748 (2006).

[177] Y.-W. Son, M. L. Cohen, and S. G. Louie, "Half-metallic graphene nanoribbons", Nature **444**, 347 (2006).

[178] X. Li, X. Wang, L. Zhang, S. Lee, and H. Dai, "Chemically Derived, Ultrasmooth Graphene Nanoribbon Semiconductors", Science **319**, 1229 (2008).

[179] P. Koskinen, S. Malola, and H. Häkkinen, "Self-Passivating Edge Reconstructions of Graphene", Phys. Rev. Lett. **101**, 115502 (2008).

[180] X. Wang et al., "Graphene nanoribbons with smooth edges behave as quantum wires", Nat. Nanotechnol. **6**, 563 (2011).

[181] M. Sprinkle et al., "Scalable templated growth of graphene nanoribbons on SiC", Nat. Nanotech. **5**, 727 (2010).

[182] J. Wurm, M. Wimmer, İ. Adagideli, K. Richter, and H. U. Baranger, "Interfaces within graphene nanoribbons", New J. Phys. **11**, 095022 (2009).

[183] H. Yin, W. Li, X. Hu, and R. Tao, "Coherent transport of armchair graphene constrictions", J. Appl. Phys. **107**, 103706 (2010).

[184] W. Qiu and E. Skafidas, "Quantum conductance of armchair graphene nanopores with edge impurities", J. Appl. Phys. **114**, 073703 (2013).

[185] W. Qiu, P. Nguyen, and E. Skafidas, "Graphene nanopores: electronic transport properties and design methodology", Phys. Chem. Chem. Phys. **16**, 1451 (2014).

[186] Y. C. Cheng et al., "Strain-activated edge reconstruction of graphene nanoribbons", Phys. Rev. B **85**, 073406 (2012).

[187] G. Kaiser, *A Friendly Guide to Wavelets* (Birkhäuser Boston, 1994).

[188] C. H. Baker, D. A. Jordan, and P. M. Norris, "Application of the wavelet transform to nanoscale thermal transport", Phys. Rev. B **86**, 104306 (2012).

[189] *Matlab and Wavelet Toolbox Release R2013b, The MathWorks, Inc., Natick, Massachusetts, United States.* Tech. rep. (2013).

[190] G. F. Schneider et al., "DNA Translocation through Graphene Nanopores", Nano Lett. **10**, 3163 (2010).

[191] K. L. Grosse et al., "Direct observation of resistive heating at graphene wrinkles and grain boundaries", Appl. Phys. Lett. **105**, 143109 (2014).

[192] C. Ojeda-Aristizabal, M. Ferrier, S. Guéron, and H. Bouchiat, "Tuning the proximity effect in a superconductor-graphene-superconductor junction", Phys. Rev. B **79**, 165436 (2009).

[193] K. Komatsu, C. Li, S. Autier-Laurent, H. Bouchiat, and S. Guéron, "Superconducting proximity effect in long superconductor/graphene/superconductor junctions: From specular Andreev reflection at zero field to the quantum Hall regime", Phys. Rev. B **86**, 115412 (2012).

[194] D. Haberer et al., "Anisotropic Eliashberg function and electron-phonon coupling in doped graphene", Phys. Rev. B **88**, 081401 (2013).

[195] S.-L. Yang et al., "Superconducting graphene sheets in CaC6 enabled by phonon-mediated interband interactions", Nat. Commun. **5**, 3493 (2014).

[196] J. Bardeen, L. N. Cooper, and J. R. Schrieffer, "Theory of Superconductivity", Phys. Rev. **108**, 1175 (1957).

[197] F. K. Wilhelm, G. Schön, and A. D. Zaikin, "Mesoscopic Superconducting–Normal Metal–Superconducting Transistor", Phys. Rev. Lett. **81**, 1682 (1998).

[198] P. Samuelsson, J. Lantz, V. S. Shumeiko, and G. Wendin, "Nonequilibrium Josephson effect in mesoscopic ballistic multiterminal SNS junctions", Phys. Rev. B **62**, 1319 (2000).

[199] Z.-H. Loh and S. R. Leone, "Capturing Ultrafast Quantum Dynamics with Femtosecond and Attosecond X-ray Core-Level Absorption Spectroscopy", J. Phys. Chem. Lett. **4**, 292 (2013).

[200] A. R. Beck, D. M. Neumark, and S. R. Leone, "Probing ultrafast dynamics with attosecond transient absorption", Chem. Phys. Lett. **624**, 119 (2015).

[201] K. Klünder et al., "Probing Single-Photon Ionization on the Attosecond Time Scale", Phys. Rev. Lett. **106**, 143002 (2011).

[202] A. Kotiaho, P. Myllyperkiö, and M. Pettersson, "Chemically Selective Imaging of Overlapping C-H Stretching Vibrations with Time-Resolved Coherent Anti-Stokes Raman Scattering (CARS) Microscopy", J. Phys. Chem. B **118**, 4363 (2014).

[203] Z. Q. Yang, D. F. Ye, T. Ding, T. Pfeifer, and L. B. Fu, "Attosecond XUV absorption spectroscopy of doubly excited states in helium atoms dressed by a time-delayed femtosecond infrared laser", Phys. Rev. A **91**, 013414 (2015).

[204] M. Kowalewski, K. Bennett, K. E. Dorfman, and S. Mukamel, "Catching Conical Intersections in the Act: Monitoring Transient Electronic Coherences by Attosecond Stimulated X-Ray Raman Signals", Phys. Rev. Lett. **115**, 193003 (2015).

[205] P. Myllyperkiö et al., "Femtosecond Four-Wave-Mixing Spectroscopy of Suspended Individual Semiconducting Single-Walled Carbon Nanotubes", ACS Nano **4**, 6780 (2010).

[206] M. J. Huttunen et al., "Measurement of optical second-harmonic generation from an individual single-walled carbon nanotube", New J. Phys. **15**, 083043 (2013).

[207] F. G. Eich, A. Principi, M. Di Ventra, and G. Vignale, "Luttinger-field approach to thermoelectric transport in nanoscale conductors", Phys. Rev. B **90**, 115116 (2014).

[208] F. G. Eich, M. Di Ventra, and G. Vignale, "Temperature-driven transient charge and heat currents in nanoscale conductors", Phys. Rev. B **93**, 134309 (2016).

[209] J. M. Luttinger and J. C. Ward, "Ground-State Energy of a Many-Fermion System. II", Phys. Rev. **118**, 1417 (1960).

[210] *NIST Digital Library of Mathematical Functions*, Release 1.0.9 of 2014-08-29, Online companion to [211].

[211] F. W. Olver, D. W. Lozier, R. F. Boisvert, and C. W. Clark, eds., *NIST Handbook of Mathematical Functions*, Print companion to [210] (Cambridge University Press, 2010).